



<https://theses.gla.ac.uk/>

Theses Digitisation:

<https://www.gla.ac.uk/myglasgow/research/enlighten/theses/digitisation/>

This is a digitised version of the original print thesis.

Copyright and moral rights for this work are retained by the author

A copy can be downloaded for personal non-commercial research or study, without prior permission or charge

This work cannot be reproduced or quoted extensively from without first obtaining permission in writing from the author

The content must not be changed in any way or sold commercially in any format or medium without the formal permission of the author

When referring to this work, full bibliographic details including the author, title, awarding institution and date of the thesis must be given

Enlighten: Theses

<https://theses.gla.ac.uk/>  
[research-enlighten@glasgow.ac.uk](mailto:research-enlighten@glasgow.ac.uk)

FUNCTIONAL CONSEQUENCES

OF

PROTEIN DYNAMICS

BY DAVID T.F. DRYDEN

A thesis submitted for the degree of Doctor of  
Philosophy at the University of Glasgow, U.K.

April, 1988.

ProQuest Number: 10997941

All rights reserved

INFORMATION TO ALL USERS

The quality of this reproduction is dependent upon the quality of the copy submitted.

In the unlikely event that the author did not send a complete manuscript and there are missing pages, these will be noted. Also, if material had to be removed, a note will indicate the deletion.



ProQuest 10997941

Published by ProQuest LLC (2018). Copyright of the Dissertation is held by the Author.

All rights reserved.

This work is protected against unauthorized copying under Title 17, United States Code  
Microform Edition © ProQuest LLC.

ProQuest LLC.  
789 East Eisenhower Parkway  
P.O. Box 1346  
Ann Arbor, MI 48106 – 1346

## ABSTRACT

This thesis explores the possible uses of dynamical fluctuations in protein structure for ligand binding and catalysis. Particular emphasis is placed on the dynamic interpretation of allosteric interactions and a statistical mechanical model of dynamic allostery is presented. This model shows that changes in either low frequency collective motions or random uncorrelated atomic fluctuations of the protein induced by the binding of a ligand can alter the binding properties of other remote ligand binding sites giving rise to allostery. Increases in the frequency of vibrational modes and reductions in uncorrelated motions gives rise to positive cooperativity and is equivalent to a stiffening of the protein structure. Small changes in the dynamics can be treated classically with many changes being required to give observed cooperative free energies. Large shifts in low frequency vibrational modes give much larger contributions to the cooperativity and the use of quantum mechanics is required. The dynamic allostery model predicts that cooperativity arising from dynamic changes is predominantly entropic in origin and complements the more conventional models of allostery which invoke changes in the static conformation of the protein involving domain movement, bond rearrangements and electrostatic effects with consequent effects on the enthalpy.

The predictions of this model are tested using laser Raman spectroscopy of solid samples to study low frequency modes in proteins and an allosteric model compound. The small organic

molecule which displays positive cooperativity between its two binding sites, shows sizeable shifts to higher frequencies in the low frequency spectrum in agreement with the model. The vibrational shifts seen require only the classical version of the model which when combined with changes in the uncorrelated motions of the atoms in the molecule can account for the observed cooperative free energy. The cooperativity is solely entropic in origin in agreement with published results. High frequency spectra of the molecule in various states of ligation are presented and analysed in terms of localised vibrations of atoms and groups of atoms.

The low frequency Raman spectra of lysozyme and its complex with the small inhibitor tri-N-acetyl glucosamine, and of trypsin and its complex with pancreatic trypsin inhibitor all displayed a broad band at  $20\text{cm}^{-1}$ . This band is a superposition of a large number of low frequency modes of the protein and the expected shift in frequency of some modes on inhibitor binding is not visible within such a broad band. The allosteric enzyme glyceraldehyde 3-phosphate dehydrogenase and its complex with the cofactor NAD also shows no changes in its low frequency spectrum. These results and their implications are discussed. High frequency Raman spectra of these enzymes are also presented and analysed.

## ACKNOWLEDGEMENTS

I would like to thank my supervisor Dr. Alan Cooper for all his guidance and advice while working at Glasgow. I also thank Prof. L.D. Barron for the use of his Raman spectrometer, and his explanation of the Raman effect, Mrs. Margaret Nutley for her technical assistance and Mr. Geoff Baxter and his staff in the mechanical workshop for turning my sketches into functioning apparatus.

I would also like to thank my friends, my family and especially Alison McInnes for their support while working on this thesis.

## CONTENTS

	Page no.
1. Introduction to Protein Dynamics	1
2. Allosterity without Conformational Change	24
2.1 Introduction to allosteric effects	24
2.2 Protein dynamics and equilibrium allosteric interactions. A general theory	34
2.2.1 The vibrational contribution to dynamic allosterity	40
2.2.2 The dynamic conformational contribution	47
2.2.3 Discussion of the theory	51
2.2.4 A simple model of allosterity using low frequency vibrations of proteins	52
3. Review of the structure and dynamics of an allosteric model compound, lysozyme, trypsin and glyceraldehyde 3-phosphate dehydrogenase	69
3.1 The structure and dynamics of an allosteric model compound	69
3.2 Introduction to the structure and dynamics of lysozyme	77
3.3 Introduction to the structure and dynamics of trypsin	85

3.4	Introduction to the structure and dynamics of glyceraldehyde-3-phosphate dehydrogenase	96
4.	Experimental Methods	104
4.1	Introduction	104
4.2	Theory of the Raman effect	105
4.3	Protein sample preparation	117
4.3.1	Lysozyme and Lysozyme-tri-NAG preparation	117
4.3.2	Trypsin and trypsin-BPTI preparation	122
4.3.3	Glyceraldehyde 3-phosphate dehydrogenase and GADPH-NAD preparation	125
4.3.4	Preparation of partially liganded allosteric bicyclic crown ethers	128
5.	Raman and infra-red spectroscopy of the allosteric model compound	130
5.1	General notes on the spectra of the unliganded and fully liganded compound	130
5.2	Assignments of Raman and I.R. bands of the 0/1 and 2/1 compounds	137
5.3	Raman spectra of partially liganded macrobicyclic compounds	147
6.	Raman spectroscopy of lysozyme, trypsin and glyceraldehyde-3-phosphate dehydrogenase	155
6.1	High frequency spectra	155
6.2	Low frequency Raman spectra	160

6.3	Summary of low frequency results	167
7.	Conclusions	172
Appendix 1	Details of the scissors dynamic allostery model	177
Appendix 2	Raman spectroscopy at room temperature and 77K of a urethane prepared from cycloundecanone and 4-phenylsemicarbazide	186
Appendix 3	Allostery without conformational change: A plausible model Published paper	
References		197

## FIGURES

Figure 1.1	Time scales and amplitudes of motions in protein dynamics	3
Figure 1.2	Temperature variation of the energy probability distribution for proteins undergoing cooperative thermal unfolding	6
Figure 1.3	Time-dependant probability distribution for the decay of systems initially at energy $E_0$	8
Figure 1.4	Hierarchical arrangement of the conformational substates in myoglobin	12
Figure 1.5	The residue variation in the r.m.s. positional fluctuations calculated from crystallographic temperature factors and from the 101 picosecond dynamic simulation of lysozyme	17
Figure 2.1	Comparison of binding curves for non-cooperative and cooperative binding in an enzyme system with two binding sites	25
Figure 2.2	Typical Gibbs free energy changes involved in positive cooperativity	36
Figure 2.3	The "scissors model"	53
Table 2.4	A typical set of results for the scissors model	60
Figure 2.5	A graph of the scissors frequency of the enzyme-ligand complexes versus unliganded scissor frequency	61
Figure 2.6	Free energy changes in ground vibrational states on binding ligands against unliganded scissor frequency	62
Figure 2.7	Free energy changes in excited vibrational states against unliganded scissor frequency	63
Figure 2.8	Enthalpy changes in excited vibrational states against unliganded scissor frequency	64
Figure 2.9	Entropy changes in excited vibrational states against unliganded scissor frequency	65
Figure 3.1	Molecular structure of Rebek's compound	63

Figure 3.2	The fraction of the ether with 0,1 or 2 ligands bound as a function of ligand concentration	71
Figure 3.3	The X-ray structure of the macrobicyclic ether with two ligands bound	72
Figure 3.4	The X-ray structure of a monocyclic ether	72
Figure 3.5	The X-ray temperature factors for the molecules in figures 3.3 and 3.4	75
Figure 3.6	The structure of the polysaccharide typically found in bacterial cell walls and hydrolysed by lysozyme	77
Figure 3.7	The backbone structure of lysozyme and the hinge bending mode	81
Table 3.8	Thermodynamics of lysozyme-tri-NAG binding	84
Figure 3.9	The reaction catalysed by trypsin	85
Figure 3.10	The backbone X-ray structure of trypsin	87
Figure 3.11	The backbone X-ray structure of BPTI	87
Table 3.12	Association constants for trypsin and BPTI	88
Figure 3.13	One of the low frequency normal modes of BPTI	91
Figure 3.14	The reaction catalysed by GAPDH and the structure of the cofactor NADH	96
Figure 3.15	A sketch of the structure of the NAD binding domain of one of the monomers of GAPDH	98
Figure 3.16	A sketch of the structure of the catalytic domain of one of the monomers of GAPDH	98
Figure 4.1	A block diagram of the apparatus used for recording Raman spectra	111
Figure 4.2	A diagram of the lightpath through the Coderg T800 spectrometer	114
Figure 4.3	U.V. absorption spectra of dilute lysozyme solutions	119
Figure 4.4	Absorption changes in a dilute suspension of <i>Micrococcus Lysodeikticus</i> cells on addition of lysozyme	120
Table 4.5	Lysozyme Assay Results	121

Figure 4.6	Absorption changes caused by the addition of NPGB to trypsin solutions	124
Table 4.7	Trypsin Assay Results	125
Figure 4.8	U.V. Absorption spectra of GAPDH	127
Figure 5.1	Low frequency ( $10-100\text{cm}^{-1}$ ) Raman spectra of the 0/1, 0.5/1, 1/1, 1.5/1 and 2/1 macrobicyclic ether compounds	132
Figure 5.2	High frequency ( $200-1650\text{cm}^{-1}$ ) Raman spectra of the 0/1 and 2/1 compounds	133
Figure 5.3	High frequency ( $200-1650\text{cm}^{-1}$ ) Raman spectra of the 0.5/1, 1/1 and 1.5/1 compound	136
Figure 5.4	The infra-red spectra of the 0/1 and 2/1 compounds from $200$ to $1800\text{cm}^{-1}$	135
Table 5.5	Vibrational frequencies for the 0/1 2/1 compounds	136
Figure 5.6	Ligand-crown ether low frequency vibrations for various sizes of ligand	140
Table 5.7	Scaling factors for low frequency Raman spectra	151
Figure 5.8	Change in scaled low frequency Raman bands as a function of ligand concentration	152
Figure 6.1	High frequency ( $200-1750\text{cm}^{-1}$ ) Raman spectra of lysozyme	156
Figure 6.2	High frequency ( $200-1750\text{cm}^{-1}$ ) Raman spectra of trypsin	157
Figure 6.3	High frequency ( $200-1750\text{cm}^{-1}$ ) Raman spectra of GAPDH	158
Figure 6.4	Low frequency ( $-10$ to $-200\text{cm}^{-1}$ ) anti-Stokes Raman spectra of lysozyme	162
Figure 6.5	The density of low frequency normal modes of lysozyme	163
Figure 6.6	Low frequency ( $-10$ to $-200\text{cm}^{-1}$ ) anti-Stokes Raman spectra of trypsin	164
Figure 6.7	Low frequency ( $-10$ to $-200\text{cm}^{-1}$ ) anti-Stokes Raman spectra of GAPDH	166

Figure A2.1	X-ray structure of the cycloundecanone-phenylsemicarbazide compound at room temperature	187
Figure A2.2	X-ray structure of the compound at 77K	187
Figure A2.3	High frequency (200-1750cm <sup>-1</sup> ) Raman spectra of the compound	188
Figure A2.4	Low frequency (-200 to +200cm <sup>-1</sup> ) Raman spectra of the compound	191
Figure A2.5	Expanded portion of Fig A2.3 showing the C-C-C skeletal deformation and CH <sub>2</sub> rocks and twists	194
Figure A2.6	Expanded portion of Fig. A2.3 showing the in-phase CH <sub>2</sub> rocks, out-of-phase twists and C-C stretches	195
Figure A2.7	Expanded portion of Fig. A2.3 showing the CH <sub>2</sub> out-of-phase rocks, in-phase twists and scissor-like deformations	196

## CHAPTER 1

### Introduction to protein dynamics

The importance of protein dynamics covering a large range of times and magnitudes to the proper functioning of proteins is now widely recognised. Haemoglobin and myoglobin for instance would be unable to bind oxygen if the structure revealed by crystallography could not open up slightly to allow the oxygen to reach the heme group. The structural changes caused by ligand binding are transmitted to other binding sites in a dynamic way giving rise to cooperativity not just in haemoglobin but also in dehydrogenases for example. Binding of the substrate and the cofactor causes large domain movements which close off the active site from the solvent and give rise to cooperative effects in the other subunits of the protein. Muscle contraction also requires great flexibility in the myosin proteins and the flexible arms of the Y shaped immunoglobulins may assist in antibody binding. Motions on a smaller scale of amino acid residues in the active sites of enzymes allow favourable configurations for the catalytic reactions to be achieved. The opening and closing of channels in transmembrane proteins to allow the directed passage of ions through the membranes will require numerous conformational changes in the protein.

This thesis is concerned with the dynamics of proteins with particular attention being given to the possibility that changes in dynamics may be a source of allosteric interactions vital to so many physiological processes.

Protein dynamics studies a whole range of movements within a protein or enzyme with a wide variety of experimental and theoretical techniques. The time scales involved have been reviewed by Careri et al., (1975,1979), range from seconds or longer for gross conformational changes to picoseconds for small individual atomic motions. Figure 1.1 summarises the motions involved.

The motions can be harmonic or anharmonic vibrations, random diffusional motions, infrequent but fast highly correlated motions, or rigid body movements changing the gross structure. Examples of these motions would be accordion-like vibrations of  $\alpha$ -helices, motion of loops of protein causing openings in the structure, aromatic ring flips occurring within the protein structure, and motion of whole domains or subunits, respectively.

The movements of small segments and loops of the protein structure required to explain early H exchange experiments performed either by I.R. (Linderstrom-Lang et al., 1959) or nmr (Wagner, G. 1983) and by <sup>0</sup> fluorescence quenching of buried tryptophan residues (Lakowicz et al., 1973; Eftink & Ghiron, 1976), led to the proposal of the mobile defect model (Lumry & Rosenberg, 1975), penetration model (Woodward & Hilton, 1979) and the local unfolding model (Englander & Kallenbach, 1984) which allowed the solvent molecules to move into the protein matrix by the transient appearance of holes or the localised unfolding of the structure. This picture of dynamics was initially at odds with the well defined structures of proteins revealed by X-ray crystallography which could, for example, show changes in the time averaged structure due to ligand binding (Blake et al., 1967),

## INTERNAL MOTIONS IN GLOBULAR PROTEINS

Types of motions	Spatial extent (nm)	Amplitude (nm)	Logarithm of characteristic time scale
Relative vibration of bonded atoms	0.2-0.5	0.001-0.01	-14 to -13
Elastic vibration of globular regions	1-2	0.005-0.05	-12 to -11
Rotation of side chains of surface	0.5-1	0.5-1	-11 to -10
Torsional vibration of buried groups	0.5-1	0.05	-11 to -9
Relative motion of different globular regions ("hinge bending")	1-2	0.1-0.5	-11 to -7
Rotation of medium-sized side chains in interior	0.5	0.5	-4 to 0
Allosteric transitions	0.5-4	0.1-0.5	-5 to 0
Local denaturation	0.5-1	0.5-1	-5 to +1

Fig. 1.1 Time scales and amplitudes of motions in protein dynamics. (from McCammon, 1984)

or surface regions of high mobility which could be inferred by a lack of electron density in the X-ray data. The H exchange experiments are observing motions taking microseconds or longer and the  $^2$  fluorescent quenching observes nanoseconds motions which are rare from the view point of x-ray crystallography resulting in a lack of electron density.

Nuclear magnetic resonance (nmr) has revealed several sorts of motion in proteins:-

- i. flipping of aromatic side chains of amino acids seemingly buried in tightly packed regions of structure at a rate of  $350 \text{ sec}^{-1}$  (Wagner, 1983), with the motion being rare but occurring rapidly.
- ii. the differing rates of hydrogen exchange for individual proteins in the protein can be measured from the proton nmr spectra on the microsecond to second scale (Wagner & Wuthrich, 1979a,b )
- iii. saturation transfer measuring the rate of exchange of proton in the solvent with those of the protein revealing differences in the rates for different parts of the protein (Wemmer et al., 1981)
- iv. magnetisation transfer measures gross conformational changes of the structure. Saturation of a particular resonance in one state of the protein can effect the corresponding resonance in the other states of the protein revealing for example partially unfolded states in equilibrium with the "native" state (Fox et al., 1986).

Nmr studies on other nuclei such as  $^{13}\text{C}$  also reveal dynamic

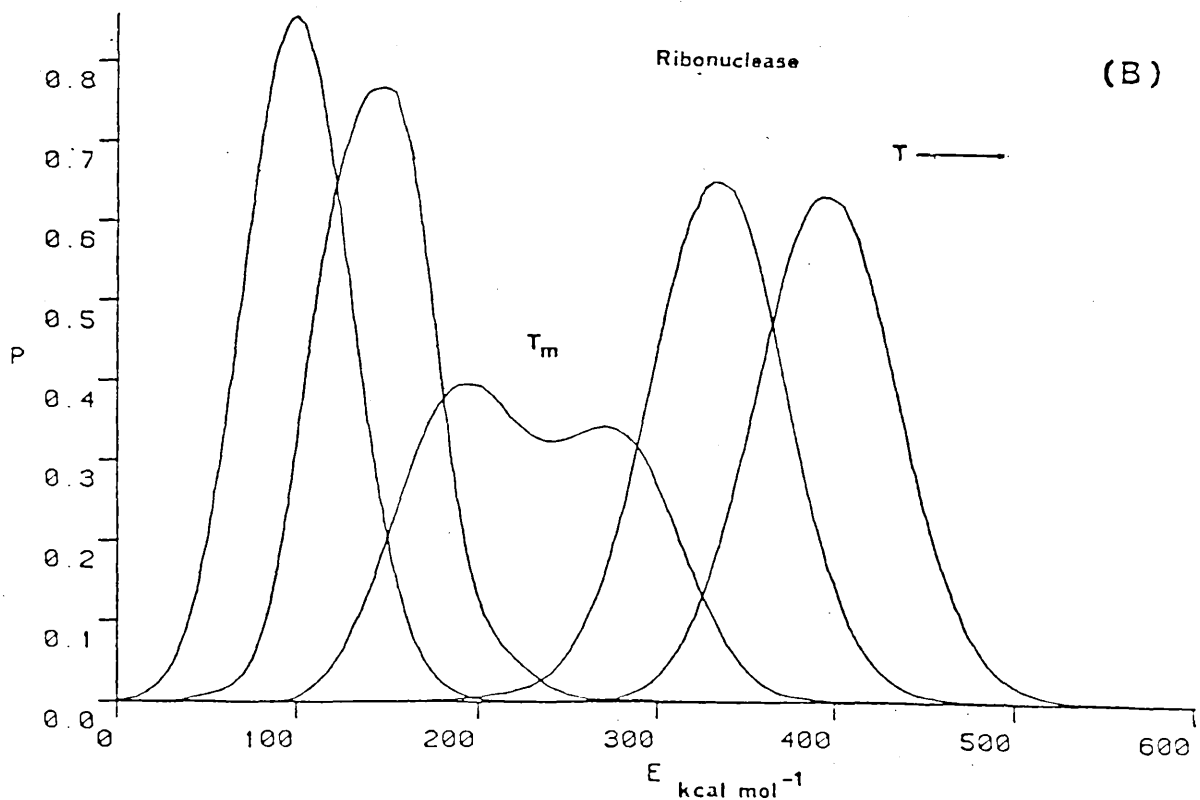
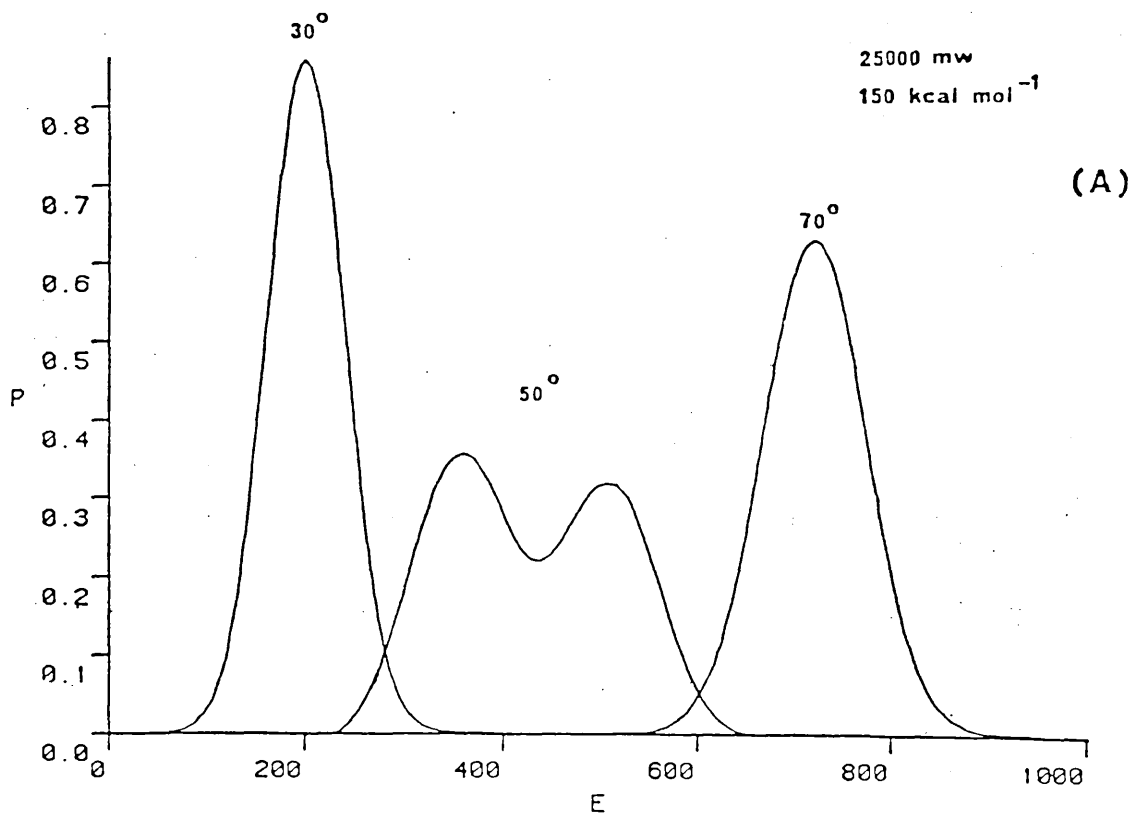
information particularly about the rotation of the protein in solution (Richarz et al., 1980).

The rest of this introduction surveys various theories and models of protein dynamics and their experimental basis.

The most general model independent information about protein dynamics comes from statistical thermodynamics. The thermodynamic properties of macroscopic systems such as a bulk protein solution, are well defined, however when small systems, such as a single protein are considered, the fluctuations of these properties around their average values becomes very large. Cooper (1976) has shown that the root mean square fluctuations in energy and volume for a 25,000 dalton protein at 25 °C are  $2.7 \times 10^{-19}$  Joules and  $5 \times 10^{-23}$  cm<sup>3</sup> per molecule. If all the molecules in one mole of this protein fluctuated in synchrony the fluctuations would amount to  $\sim 159$  kJmol<sup>-1</sup> and 30 cm<sup>3</sup> mol<sup>-1</sup>. The calculation of higher fluctuation moments of proteins is possible using the detailed calorimetric measurements of heat capacities made by Privalov (1979) from which the energy distribution function for the protein can be calculated (Cooper, 1984). This is shown in Figure 1.2 as a function of temperature.

This function shows the broad range of energy states easily accessible to any protein molecule and is slightly skewed to higher energies when compared with a Gaussian distribution. It spends 1/3 of its time more than 160 kJ away from its average energy at room temperature. As the temperature is increased the distribution becomes bimodal as the molecule denatures indicating that the unfolding is not a simple 2 state process. A two state denaturation process would show two separate distributions, one

Fig. 1.2 Temperature variation of the energy probability distribution for proteins undergoing cooperative thermal unfolding. (A) for a hypothetical 25000 dalton molecule with  $T_m = 50^\circ\text{C}$ ,  $\Delta H_m = 150 \text{ kcal mol}^{-1}$  and  $\Delta C_p = 0.1 \text{ cal K}^{-1}\text{g}^{-1}$ . (B) for a real protein (ribonuclease, 1400 dalton) in solution under conditions where it undergoes a 2-state transition at  $T_m = 50^\circ\text{C}$  with  $\Delta H_m = 88 \text{ kcal mol}^{-1}$ . (Experimental data estimated from Privalov, 1979.) Probability curves are plotted for  $10^\circ$  intervals. In both cases the energy origin is arbitrary, but the relative positions of the mean and the shapes of each distribution are to scale. (from Cooper, 1984)

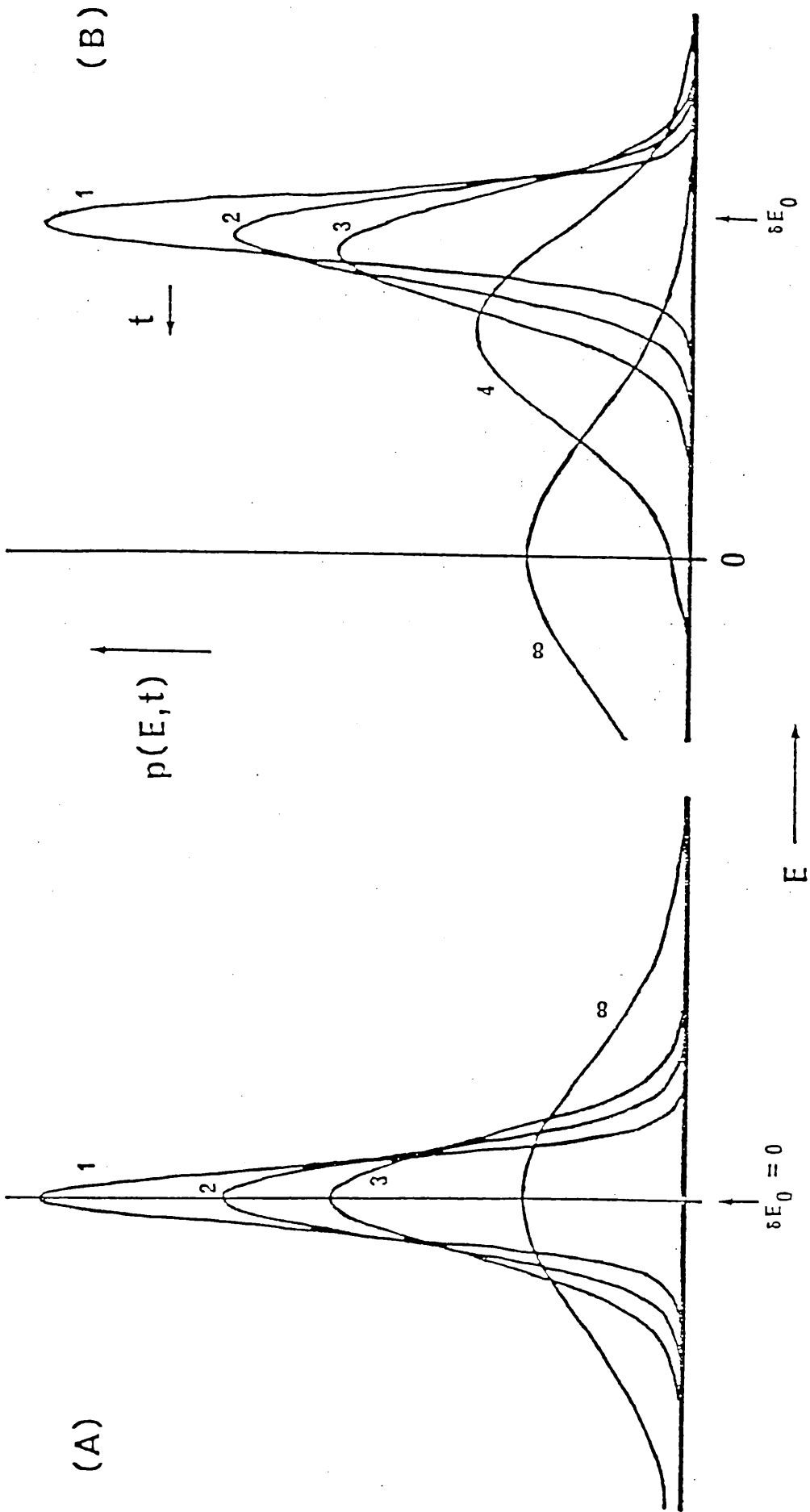


representing the folded state, the other the denatured state (Ikegami, 1977). Multi-domain proteins which have more complex heat capacity curves for temperature denaturation will have more complex energy distributions (Privalov,1982). Fluctuations in volume calculated from compressibility data (Gekko & Hasegawa,1986; Gavish et al., 1983) are found to be highly correlated with energy fluctuations. Energy increases are usually accompanied by volume increases and decreases in energy by volume decreases, which implies that the protein is not at a potential energy minimum <sup>h</sup> were any volume change would increase the energy. These fluctuations in volume only apply to the solvent excluded volume of the protein and not to cavities which fill up with solvent molecules when a particular fluctuation occurs.

This correlation can be understood if the solvent around the protein acts as a restrictive cage. Lee (1983) developed a model indicating that volume fluctuations were affected by the solvent surroundings. The time dependence of protein energy fluctuations can be calculated if the energy distribution is assumed to be Gaussian (Cooper, 1984). The Langevin equation for a damped harmonic oscillator subject to a random force (see Chandrasekhar 1943 for a review of stochastic processes) can be applied to this distribution and indicates that an ensemble of protein molecules all at some energy away from the mean would relax to a final Gaussian distribution about the mean via a succession of Gaussian distributions as shown in Figure 1.3.

A similar result for a simple harmonic oscillator in a heat bath was obtained, in which a Boltzmann distribution was maintained as the system relaxed to equilibrium (Montroll &

Fig. 1.3 Time-dependent probability distributions for the decay of systems initially at energy  $\delta E_0$ . (A)  $E_0 = 0$ , i.e. a system initially at the thermodynamic mean energy. (B) for a large positive initial fluctuation  $\delta E_0$  (the time dependence of low energy fluctuations, with negative  $\delta E_0$ , is the mirror-image of this). Note that in both cases after a sufficient length of time ( $t \rightarrow \infty$ ) the distributions become time-independent Gaussians centred about the thermodynamic mean. (from Cooper, 1984)



Shuler, 1957). The rate of both fluctuations away from the mean energy and towards it depend on phenomenological linear dissipation rates which will depend on the scale of the fluctuation involved. The smallest fluctuations will occur rapidly (picoseconds) and most frequently, while large changes will take longer and be rarer (minutes). Since the protein energy distribution is not quite Gaussian not all of these energy dissipation mechanisms will be linear, implying that some energy states accessible to the protein would be more difficult to "leave" for instance than to "enter". Barriers and bottlenecks in the relaxation pathways could possibly give rise to hysteretic effects such as the pressure induced dissociation of oligomeric proteins (Silva et al., 1986), which showed different rates for the recovery of structure and affinity, and the dependence of oligomer association rates on the extent of ligand binding (Xu & Weber, 1982). Membrane proteins involved in the pumping of ions across the membrane can also show similar large fluctuations and stochastic behaviour of a thermodynamically small system (Lauger, 1984; Hill & Chen, 1985; Westerhoff & Chen, 1985). During thermal denaturation of the protein the relaxation rates will be even more non-linear giving rise to the concerted cooperative effects leading to unfolding.

The phenomenological rates for the variety of motions which occur in proteins are sensitive to experimental variables such as temperature, solvent viscosity and pressure which if varied carefully can reveal the different scales of motion in proteins.

The work of Frauenfelder and his associates over the past few years has particularly exemplified this approach. They have

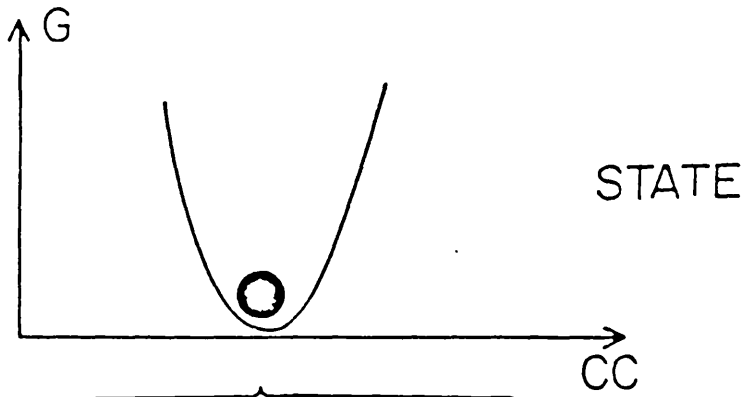
studied the rebinding kinetics of O<sub>2</sub> and CO to haemoglobin and myoglobin after flash photolysis using Kramer's equation (Kramers, 1940) which takes into account the solvent viscosity and the shape of the energy barriers to be surmounted on rebinding. Their results obtained by varying temperature from 1K to 300K (Austin et al., 1975), pressure from atmospheric to 2k bar (Frauenfelder, 1984) and viscosity from liquids to glass like solids (Beece et al., 1980), have shown that rebinding occurs by several consecutive steps each of which can be studied by varying the experimental conditions. To rebind, the ligand has to surmount several barriers which decrease in size as the ligand approaches the heme iron. As the temperature was raised it was found that the ligand could move further from the heme group crossing more barriers before rebinding. Some of the rebinding steps were nonexponential in character indicating that a distribution of barrier heights was required. These barriers were also found to be dynamic rather than static because of their viscosity dependence. These results combined with those obtained by Mossbauer spectroscopy (Krupyanskii et al., 1982; Parak & Knapp, 1984), low temperature heat capacity measurements on heme proteins (Singh et al., 1984), and viscosity dependent studies of kinetics using Kramers equation on other enzyme systems (Gavish & Werber, 1979) have led to the concept of protein conformational substates and the hierarchical model, derived from glass theories (Mezard et al., 1984), describing the range of substates available to a protein (Ansari et al., 1985; Frauenfelder, 1984; Stein, 1985). The protein is assumed to be able to exist in many different states, each slightly different, around its average

structure. The barriers between substates depend on how much change is required to go from one state to another. For instance movement of an amino acid side chain from one position to another is easier than moving a whole loop of protein. Further evidence for the hierarchical model in myoglobin has recently been obtained by following changes in several infra-red vibrational bands (Ansari et al., 1987). The bands change on rebinding at different, non-exponential rates representing different substates.

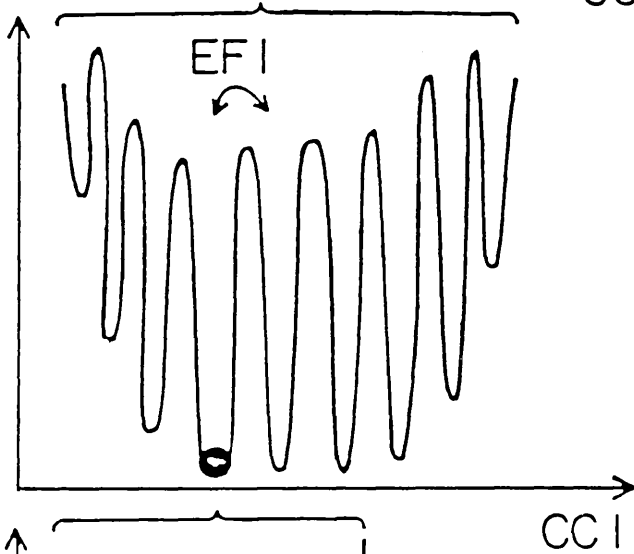
Four tiers of substates have been postulated for myoglobin (Figure 1.4). Each substate of a particular level contains many substates of the lower levels. At the lowest temperatures motion is only possible between substates on the lowest level corresponding to small atomic motions and quantum mechanical tunnelling (Alben et al., 1980 ; Alberding et al., 1978). The barriers between substates are less than  $1 \text{ kJmol}^{-1}$  and, in the flash photolysis experiment, the barrier seen is due to the breaking of the iron-ligand bond.

At about 20K the second level substates corresponding to motions of larger groups of atoms can interchange. The activation energies for this process are between 1 and 5 kJ/mol and for the photo dissociation of CO are postulated to represent relaxation of the heme group. Between 30K and 200K a distribution of energy barriers from 10 to 40kJ/mol define the motion in the third tier of whole amino acid residues around the heme group. Finally above 200K, motion of the whole protein and its hydration shell occurs with barriers between states of  $\sim 70 \text{ kJ/mol}$ . Relaxation of the protein after photodissociation to the deoxy structure involves the dissipation of energy by

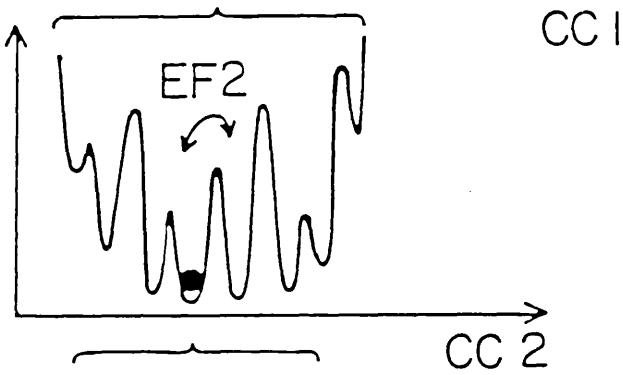
Fig. 1.4 Hierarchical arrangement of the conformational substates (CS) in myoglobin. (A) schematic energy surfaces showing equilibrium fluctuations (EF). (B) tree diagram.  $G$  denotes Gibbs energy of the protein,  $CC$  denotes conformational coordinate. (from Ansari et al, 1985)



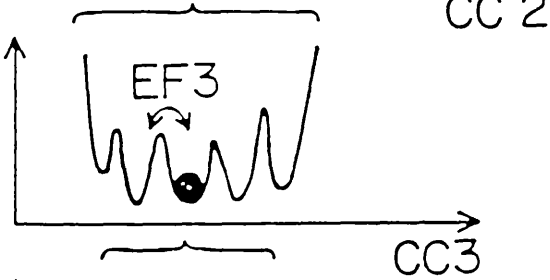
STATE



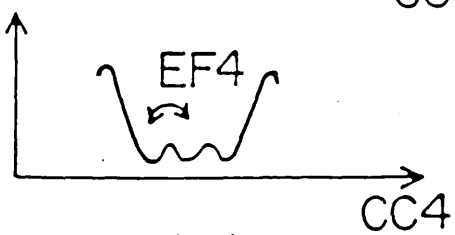
$CS^1$



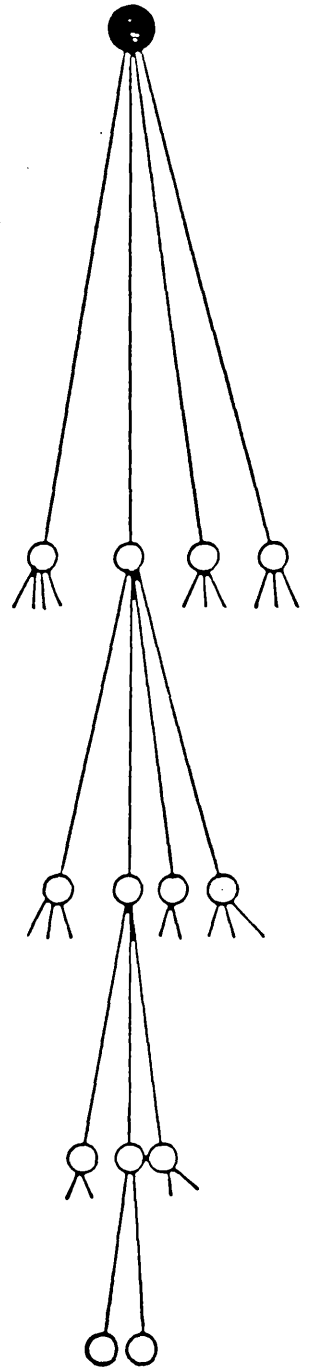
$CS^2$



$CS^3$



(a)



(b)

progressively larger fluctuations radiating out from the heme group through the tiers of substates.

The model of protein conformational substates for heme proteins which is based on information from many different experimental techniques is most likely applicable to many other proteins and enzymes and serves as a useful framework on which to place experimental observations. The proposed link between protein substates and the structure of glasses has been investigated by using photochemical and photophysical hole burning low temperature experiments (Avarmace & Rebane, 1985; Boxer et al., 1986; Cartier & Small, 1985; Friedrich et al., 1981a; Friedrich et al., 1981b; Friedrich & Haarer, 1984; Meech et al., 1985) where a chromophore with an inhomogenously broadened absorption band, which implies a distribution of chromophore states each with slightly different absorption characteristics, is trapped in a glass and forced into a non-equilibrium distribution of its substates by a laser pulse. The term photochemical indicates that the chromophore is chemically changed by the hole burning while photophysical implies that the chromophore has moved to another part of the equilibrium distribution with no chemical change. This non-equilibrium distribution can be seen as "holes" in the absorption band which then disappear as the temperature is raised and equilibrium is re-established. If holes could be burnt in the chromophore absorption bands of proteins this would be evidence for glass like properties. This hole burning mechanism has also been proposed (Cooper, 1983) as an explanation of the excitation wavelength dependence of the photochemical reaction of rhodopsin at very low temperatures

where unusual shifted absorption spectra of photoproducts are obtained by exciting the rhodopsin at the red, low energy side of its absorption band. Hole burning of biological pigments such as bile pigments and chlorophyll embedded in low temperature glasses and in their protein bound environments has been clearly observed indicating an inhomogeneous environment around the chromophores.

The inhomogeneity of the protein structure can also be seen directly by red edge excitation of fluorescence of tryptophan residues (Demchenko, 1986). Only those tryptophan residues in low energy substates can absorb the excitation light. If relaxation of the excited tryptophan environment occurs before it emits then normal fluorescence is observed but if relaxation is slow then the fluorescence is shifted to longer wavelengths than normal. This effect increases as the temperature is lowered and relaxation of the conformational substates slows down, until presumably the relaxation process responsible is frozen out and the protein distribution on the relevant tier of the substate heirarchy becomes fixed.

The lowest tier of protein substates involving atomic motions of less than  $1\text{\AA}$  on the  $10^{-15}$  sec to  $10^{-11}$  sec time scale is the only region at present amenable to computer simulations of protein dynamics by molecular mechanics or normal mode calculations. This means that most dynamic processes in proteins are missed or only hinted at by the simulations (Ansari et al., 1985; Parak & Knapp, 1984) and that the magnitudes of fluctuations are too small (Cooper, 1984) because the energy of the system is constrained to a constant value in these calculations. However if interpreted correctly they can be very

useful and as computer technology improves longer time scales may become accessible.

Molecular mechanics applies Newton's equations of motion to the atoms of a protein molecule which can move within the constraints of an arbitrary potential. The atomic motions are integrated over very short time periods (typically  $\sim 10^{-15}$  sec) so that the simulation does not become unstable. The initial x-ray structure is subject to energy minimisation to relieve any strain in the structure before the simulation is started. Typical simulations are around 100 picoseconds long. Levitt (1983a,b) describes the method in considerable detail. Detailed simulations of bovine pancreatic trypsin inhibitor (Levitt 1983a; Levitt 1983b; McCammon et al., 1977; McCammon & Karplus, 1983), cytochrome C (Northrup et al., 1980; Mao et al., 1982; Morgan et al., 1983), myoglobin (Levy et al., 1985) and lysozyme (Post et al., 1986) have been performed. The structures remain close (usually  $< 2\text{\AA}$ ) to the x-ray structure though hydrophilic residue side-chains, which project into the solvent in the x-ray structure, are often drawn closer to the surface of the protein while exposed hydrophobic residues project further out from the protein (Levitt, 1983b; Post et al., 1986) because the simulations are of a protein molecule in vacuo. The inclusion of water molecules or an approximate solvent potential around the protein can counteract this effect (van Gunsteren & Berendsen, 1984). Despite the short time scales studied, some simulations show fairly large correlated changes. Levitt's simulation of BPTI (1983b) shows a cooperative breaking of 6 H bonds at the two ends

of the  $\beta$  hairpin involving nearby water molecules which lasts about 40 picoseconds and which would allow H exchange to occur quite easily. Collective low frequency ( $3 \times 10^{-1}$  cm<sup>-1</sup>) damped oscillations have also been seen in another BPTI simulation (Swaminathan et al., 1982).

Most large correlated motions of proteins will be missed by molecular mechanics simulations but if the simulations are long enough the most common ones (given the assumptions involved) become visible. These motions will represent only a fraction of the substates of an intermediate tier in Frauenfelder's hierarchical model, whilst most of the small fast atomic motions will be equivalent to substates on the lowest tier with the smallest energy barriers (Elber & Karplus, 1987).

These small atomic motions correlate very closely with the temperature factors representing thermal motion determined by x-ray crystallography, though it should be noted that the x-ray data contains a general background contribution due to lattice disorder making comparison of the magnitudes of motion difficult (see Figure 1.5).

An approximate measure of the lattice disorder term in myoglobin crystals can be obtained by comparing the extent of motion of the iron atom as measured by Mossbauer spectroscopy which is not dependent on the crystal structure, with the x-ray temperature factor (Frauenfelder et al., 1979). This correction is then assumed to be applicable to the rest of the structure and brings the magnitudes of the motions as determined by molecular mechanics and crystallography into good agreement. Ringe & Petsko (1985) give an excellent review of all aspects of

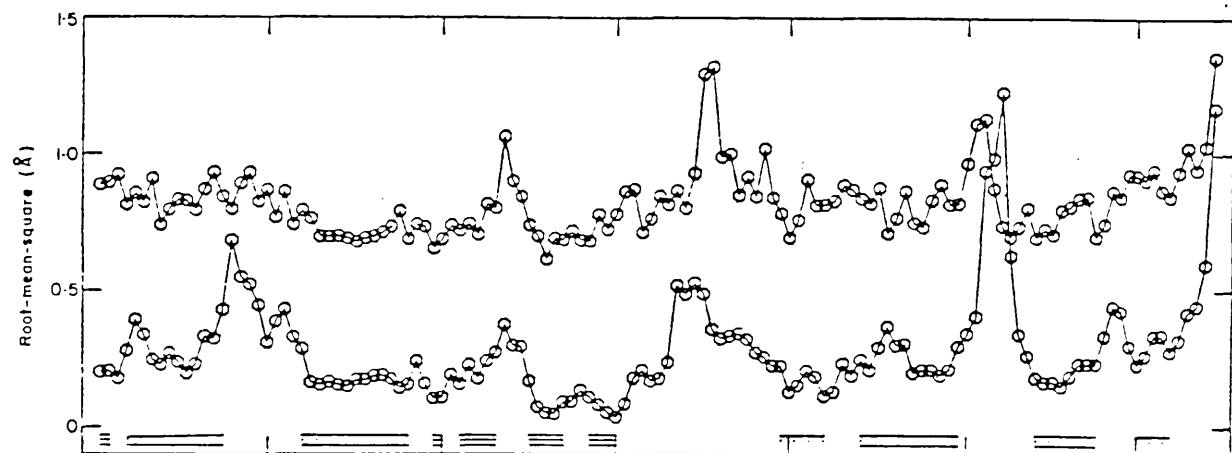


Fig. 1.5 The residue variation in the r.m.s. positional fluctuations calculated from crystallographic temperature factors (upper curve to scale) and from the 101 picosecond dynamic simulation (lower curve, displaced by  $-0.25\text{\AA}$ ) for lysozyme main chain atoms. (from Post et al, 1986)

protein dynamics as determined by x-ray crystallography. The relationship between molecular mechanics simulations and x-ray crystallography, to a certain extent due to shared methodology, is certain to become closer as molecular modelling of, for instance, drug binding to proteins becomes more sophisticated.

Another computer simulation method which correlates with spectroscopic, H exchange, and thermodynamic measurements rather than with crystallography is normal mode calculations for proteins. The calculation of high frequency ( $> 10^{12}$  Hz) normal modes for small molecules is a standard technique in spectroscopy (Wilson, Decius & Cross, 1955), but is much more difficult for proteins and other macromolecules because of the much larger number of degrees of freedom required. Assumptions which restrict this number such as fixing bond lengths simplify the problem with no noticeable loss of information. Three calculations for BPTI have been performed, one of which has all (1740) degrees of freedom and two which fix all bond lengths (Brooks & Karplus, 1983; Go et al., 1983; Levitt et al., 1983; Levitt et al., 1985). The histograms of frequencies below about  $300\text{cm}^{-1}$  are very similar showing a broad band of modes with the lowest at about  $3\text{cm}^{-1}$ , a maximum density of modes at about  $30\text{cm}^{-1}$  and a gradual decay of the density of modes to approximately zero at  $200\text{cm}^{-1}$ . Modes with frequencies above  $200\text{cm}^{-1}$  are increasingly localised and can be identified with group modes similar to those found in small molecules. All the simulations found that the magnitudes of the atomic motions were dominated by the highly delocalised modes below  $30\text{cm}^{-1}$  and are very close to those found by molecular mechanics simulations. These modes contribute

significantly to the entropy of the system and changes in their frequency, by for instance ligand binding can cause large thermodynamic stability changes (Brooks & Karplus, 1983). See Chapter 2 for a further discussion of this. It is also now possible to calculate the form of any low frequency mode of interest as has been done for the hinge bending mode of lysozyme (Brooks & Karplus, 1985) though this has the disadvantage that a preconceived notion of what an important mode may be is required. The calculated density of low frequency modes can, if transformed to the correct experimental observables, be compared with low frequency infra-red (Ataka & Tanaka, 1979), Raman (Brown et al., 1972, Genzel et al., 1976; Painter & Mosher, 1979; Painter et al., 1981; Painter et al., 1982) and inelastic neutron scattering spectra (Cusack, 1984; Jacrot et al., 1982; Middendorf, 1984; Cusack et al., 1986; Smith et al., 1986). Reasonable agreement is found for the I.R. and Raman spectra but not for the inelastic neutron scattering spectra.

Low frequency collective motions of proteins have been postulated as having important biological functions on numerous occasions (e.g. Chou, 1984; Sturtevant, 1977; Cooper, 1980; Peticolas, 1979) even if they are severely damped in solution. Peticolas (1979) showed that even overdamped vibrations subject to random forces from the solvent are still constrained to follow the trajectories of the normal modes, though in a diffusive manner.

If the low frequency modes are changed by ligand binding, subunit association, partial unfolding etc., then the stability of the protein can be affected (Sturtevant, 1977). For the case

of ligand binding one can imagine the protein being stiffened and the low frequency normal modes increasing in frequency. This can explain the large negative heat capacity changes seen in many ligand binding reactions. The possibility of allosteric communication between remote binding sites on proteins could also be affected by low frequency fluctuations and a theory for this is given in Chapter 2 (Cooper, 1980; Cooper & Dryden, 1984). Chou (1984,1985) has developed a simple classical model of  $\alpha$  helix and  $\beta$  sheet vibrations giving vibrational frequencies of these structures around  $30\text{cm}^{-1}$ . A change in frequency of vibration of the  $\alpha$  helix connected to the iron atom of the haem group in haemoglobin could be an important step in the cooperativity of this protein.

Low frequency vibrations of  $\alpha$  helices and  $\beta$  sheets will only form a fraction of the low frequency normal mode spectrum, and they cannot at present, be isolated from the broad spectrum of modes seen by Raman spectroscopy due to less structured regions of the protein.

The harmonic approximation necessary for a discussion of normal modes of proteins has been shown to be fairly accurate in many instances. For instance the size of atomic fluctuations if summed over all the modes agrees closely with those calculated by molecular mechanics and those found by x-ray crystallography. The general density of the low frequency modes agrees fairly well with the Raman spectra. However some studies have shown that motion of some parts of enzymes can be better described using nonparabolic potentials such as a square well potential. Metmyoglobin crystals studied by x-ray diffraction and Mossbauer

spectroscopy (Frauenfelder et al., 1979; Krupyanski et al., 1982) showed that many interior residues moved in very narrow deep wells with limits determined by the structure packed around the residue, while surface residues moved in broad square wells within the limits determined by bond lengths. Molecular mechanics simulations of ferrocycochrome C (Northrup et al., 1980) have also shown that buried residues are nearly as rigid as the molecules in a solid while surface residues move more like molecules in an organic liquid. Asymmetric wells indicating a substantial spread of the distribution of atomic positions from the average (Mao et al., 1982) have also been found. The harmonic approximation would give misleading results in this case. However as a method for simplifying large protein dynamics problems to obtain qualitative results, the harmonic approximation is invaluable and is used in chapter 2.

A recently proposed model of protein dynamics (Bialek & Goldstein, 1985) which uses a quasiharmonic potential for vibrational "modes" of a protein provides a reasonable vibrational alternative to Frauenfelders conformational substate model discussed earlier. This fits the CO rebinding myoglobin data very well using a few parameters derived solely from spectroscopic data. The use of a quasi-harmonic potential has many advantages over the harmonic potential since it allows energy relaxation of stress in the protein structure by multiphonon decay paths between high frequency localised modes and low frequency global modes. Energy can also be easily exchanged between the solvent and the protein interior by these modes.

A combined model using harmonic or quasi-harmonic vibrations and conformational substates is probably required to describe protein dynamics. The relative importance of the two models would depend on the motions being considered and different experimental techniques would be biased towards one or the other. The simplest route to combining the two models would perhaps be to consider the barriers between substates to be dynamic (Beece et al., 1980) with a harmonic or quasi-harmonic time dependence. The barriers between substates would then be more like gates which opened and closed at rates related to the vibrational frequencies of the protein structure forming the barrier between states. Gated reactions for the binding of ligands to proteins (Szabo et al., 1982; Northrup & McCammon, 1984), though concerned with transitions between gross conformational states rather than between closely related substates, implies that such a relationship between dynamic barriers and global vibrations is feasible. A computer simulation of tyrosine ring flipping in BPTI (McCammon et al., 1983), showed that the flip, a transition from one substate to another, occurred only after an adjacent section of backbone structure had moved. The motion of this backbone could be described by the harmonic or quasi-harmonic model.

This survey of protein dynamics has, I hope, mentioned most of the quantifiable models and their experimental basis. The dynamics of lysozyme, trypsin and glyceraldehyde 3-phosphate dehydrogenase studied in this thesis are reviewed in Chapter 3.

The amount of dynamic information available on biological systems has grown enormously in the past few years. Some reviews

of protein dynamics and related subjects are Cooper (1980,1984, Welch et al., (1982), McCammon (1984), Karplus & McCammon (1983), Debrunner & Frauenfelder (1982), Lauger (1984), Gurd & Rothgeb (1979), Careri et al., (1975, 1979), and Vergoten et al., (1978).

This introduction has also demonstrated that protein dynamics plays a significant part in protein functions particularly those involved in ligand binding. Changes in the protein dynamics, since they are virtually inevitable, are almost certainly utilised by the protein to help its function. If the binding of one ligand, such as O<sub>2</sub> to myoglobin, causes many changes in the dynamics then the binding of further ligands or the performance of some other function will be affected. This thesis is primarily concerned with the effect of protein dynamics on allosteric proteins. In Chapter 2 a statistical mechanical theory is given, which accounts for allosteric interactions using only the changes in dynamics induced by ligand binding, rather than the more commonly postulated "conformational change". An experimental study of the possible uses of low frequency Raman spectroscopy of several proteins and an organic allosteric model compound to verify the theoretical model is then given in Chapter 5.

## CHAPTER 2

### Allostery without Conformational Change

#### 2.1 Introduction to Allosteric Effects

An allosteric protein is one which binds more than one ligand at different binding sites with binding constants that depend on whether other ligands are already bound or not. In other words there is an interaction between binding sites which communicates the state, bound or unbound, of a site to the other sites, so modifying their affinities for binding a ligand. The cooperativity between sites is said to be positive if the affinity of a site for a ligand is increased by binding at another site and negative if the affinity is decreased. An extreme case of negative cooperativity is "half of the sites" cooperativity where binding of the first ligand prevents binding at other sites. Several excellent reviews of allostery have been published including Koshland (1970), Weber (1975) and Perlmutter-Hayman (1984) which, between them, cover all aspects of equilibrium allosteric interactions.

Positive cooperativity is most easily recognised because it changes a graph of binding site saturation versus ligand concentration, showing a hyperbolic curve obeying Michaelis-Menten kinetics for independent binding sites, to a sigmoidal curve characteristic of positive cooperativity. A sketch of this for an arbitrary system with two sites is shown in Figure 2.1.

No. of  
Ligands  
Bound

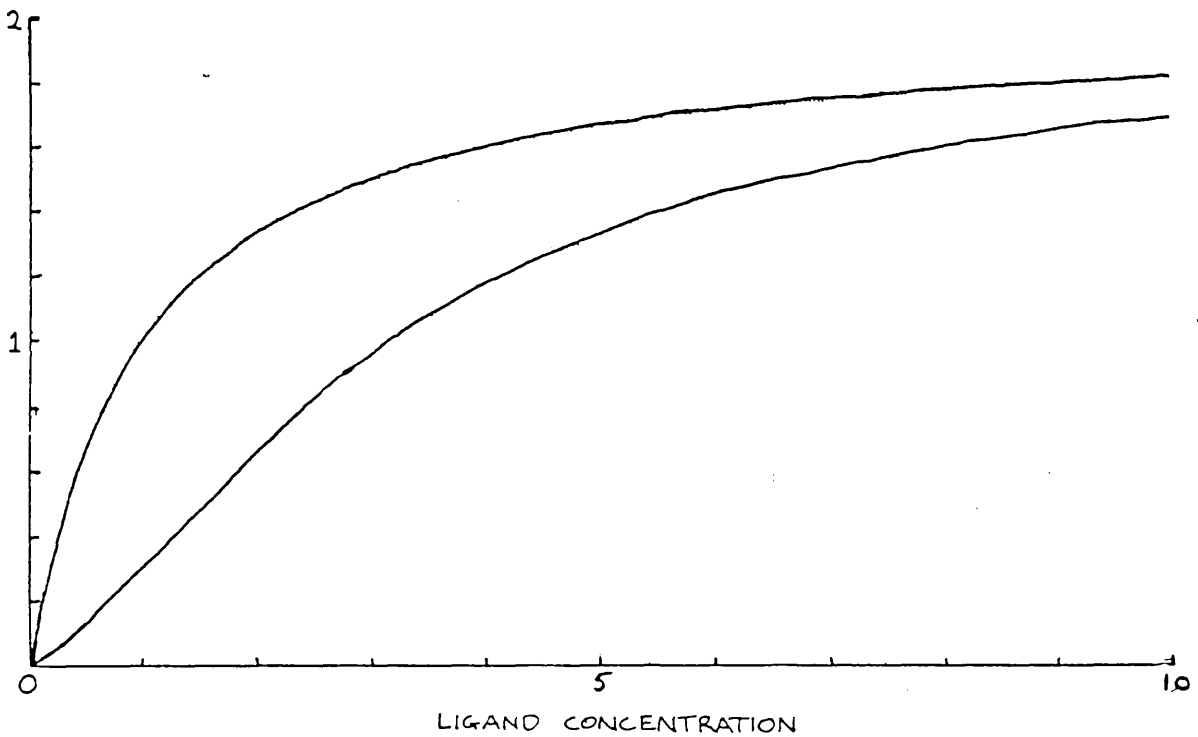


Fig. 2.1 Comparison of binding curves for non-cooperative (upper curve) and cooperative binding in an enzyme system with two binding sites. In the upper curve the dissociation constants are equal to 1. In the lower curve the first dissociation constant is ten times the second dissociation constant of 0.1.

Negative cooperativity gives a hyperbolic graph so other representations of binding data are required to spot this form of allostery. Koshland (1970) covers a wide variety of graphical representations including the widely used Hill and Scatchard plots which display  $\log\left(\frac{Y}{1-Y}\right)$  versus  $\log S$  and  $\left(\frac{X_B}{E_T X_F}\right)$  versus  $\frac{X_B}{E_T}$  respectively, where  $Y$  is the fraction of sites occupied,  $S$  is the total ligand concentration,  $X_B$  and  $X_F$  are the concentrations of bound and free ligands and  $E_T$  is the total enzyme concentration. The slope of the linear Hill plot determines the type of cooperativity, this slope being greater than 1 for positive cooperativity, less than 1 for negative and equal to 1 for non-cooperative, independent, sites. The Scatchard plot is linear for non-cooperative systems, concave downward for positive systems and concave upwards for systems displaying negative cooperativity.

Experimental data plotted in these ways can be fitted to theoretical curves, allowing the association constant for binding to the various liganded states of the protein to be calculated.

The association constants for multiple ligand binding can be defined either as macroscopic binding constants or as intrinsic binding constants and it is very important to state what form is being used as large errors can result.

The macroscopic (stoichiometric) association constants for binding ligand  $X$  to protein  $P$  are defined as

$$K_1 = \frac{[PX]}{[P][X]} \text{ for binding the first ligand}$$

$$K_2 = \frac{[PX_2]}{[PX][X]} \text{ for binding the second}$$

$$K_n = \frac{[PX_n]}{[PX_{n-1}][X]} \text{ for binding the } n\text{th}$$

where the concentrations are equilibrium concentrations, so that [P] and [X] are the amounts of free protein and ligand at equilibrium, not the initial conditions and [PX]<sub>n</sub> is the concentration of protein with n ligands bound.

The intrinsic association constants which take into account the number of ways the protein-ligand complexes can associate or dissociate using a statistical factor, can be written, if the total number of binding sites, N, is known, as

$$K'_{J+1} = \frac{J+1}{N-J} \frac{[PX_{J+1}]}{[PX_J][X]}$$

$$= \frac{J+1}{N-J} K_{J+1}$$

= intrinsic association constant for the J + 1 th ligand

where the subscript J runs from 0 to N-1.

Cooperativity results when the intrinsic association constants are not equal (Perlmutter-Hayman, 1986).

i.e.  $K'_{J+1} \neq K'_J$  or  $\frac{K'_{J+1}}{K'_J} \neq 1$

and this implies for the macroscopic association constants that

$$\frac{J+1}{N-J} K_{J+1} \neq \frac{J}{N-J-1} K_J$$

$$\Rightarrow \frac{K_{J+1}}{K_J} \neq \frac{J(N-J)}{(J+1)(N-J-1)}$$

Positive cooperativity results when the inequality is "greater than" and negative cooperativity when the inequality is "less than".

A most useful quantity to calculate is the fractional saturation of the ligand binding sites or in other words the average number of ligands bound to each protein,  $\bar{n}$ , at equilibrium.

$$\bar{n} = \frac{[PX] + 2[PX_2] + \dots + J[PX_J] + \dots + N[PX_N]}{[P] + [PX] + [PX_2] + \dots + [PX_J] + \dots + [PX_N]}$$

$$= \frac{\text{(total concentration of liganded protein)(weighting factor)}}{\text{total protein concentration}}$$

It is this quantity, which is plotted against free ligand concentration in Figure 2.1. Substitution of the macroscopic association constants gives:

$$\bar{n} = \frac{K_1[X] + 2K_1K_2[X]^2 + \dots + J \cdot K_1K_2 \dots K_J[X]^J + \dots + N \cdot K_1 \dots K_N[X]^N}{1 + K_1[X] + K_1K_2[X]^2 + \dots + K_1 \cdot K_2 \dots K_J[X]^J + \dots + K_1 \cdot \dots \cdot K_N[X]^N}$$

The denominator is called the binding polynomial, a term first used by Wyman (1968), and the numerator is the derivative of this polynomial with respect to  $\ln([X])$ . This expression can also be written using the intrinsic association constants which after a little manipulation can be written as:

$$\bar{n} = \frac{\sum_{J=0}^N J \binom{N}{J} K_0 \dots K_J [X]^J}{\sum_{J=0}^N \binom{N}{J} K_0 \dots K_J [X]^J}$$

with  $K_0 = 1$

$$\text{and } \binom{N}{J} = \frac{N!}{(N-J)! J!}$$

The fraction of protein with J ligands bound can be calculated by writing

$$\bar{n} = \sum_{J=0}^N f(J) J$$

where

$$f(J) = \frac{\binom{N}{J} K_0 \dots K_J [X]^J}{\sum_{J=0}^N \binom{N}{J} K_0 \dots K_J [X]^J}$$

is the required fraction. This is the fraction of protein molecules which have J ligands bound in any distribution among the binding sites. The fraction of protein with J ligands bound in a particular configuration among the sites is a much more complicated parameter to calculate and the quality of experimental results can rarely justify this more detailed treatment. The calculation of these binding site dependent functions is discussed in Klotz & Hunston (1979).

The curve defined by  $\bar{n}$  or some function of  $\bar{n}$  can be fitted to experimental data by a computer and the association constants calculated. Most experimental data, however, is not good enough to give unambiguous results when fitted with the N variable parameters in the function  $\bar{n}$  if  $N > 4$ , therefore assumptions are usually made about the nature of the ligand binding, which reduce the number of variable parameters to more manageable numbers.

The two most widely used models of allostery are the "concerted, all or nothing" model proposed by Monod, Wyman & Changeux (1966) and the "sequential" model proposed by Koshland, Nemethy & Filmer (1966). The "concerted" model assumes that the

protein is oligomeric with the subunits arranged symmetrically about at least one axis of symmetry. The protein can exist in only two states, T (tense) and R (relaxed), which bind the ligands with low and high affinity respectively. The major assumption is that all the subunits with or without ligand bound are in either the T or R state and that there are no states with a mixture of T and R subunits, hence the term "all-or-nothing" is sometimes used to describe this model. This cuts down the number of states required to describe ligand binding, which can be described by only 3 parameters; the allosteric constant, L, which is the equilibrium constant for interconversion of the unliganded R and T states, and  $K_T$  and  $K_R$  the dissociation constants for each site in the T and R states respectively. This model can only give rise to positive cooperativity, the extent of which is controlled by the position of the R to T equilibrium. This equilibrium can be shifted by the binding of allosteric inhibitors and effectors. An inhibitor increases the amount of the low affinity T state present by preferentially stabilising this form and making the transition to the R state more difficult. An allosteric effector has the opposite effect and in some cases is so effective that cooperativity is abolished as the concentration of the T state tends to zero. The ligands then bind to the R state subunits in a normal sequential manner obeying Michaelis-Menten kinetics. Fersht (1977) gives several examples of this process.

The sequential model assumes binding of a ligand to a

subunit changes the interactions between that subunit and one or more of the other subunits changing the equilibrium binding constants of the affected subunits to give either positive or negative cooperativity. It is also assumed for simplicity that the number of different kinds of interactions are limited. Koshland et al (1966) gave several examples of the way four kinetically identical, as opposed to structurally identical subunits could interact with each other giving varying numbers of intermediate states. They derived the binding equations for the average number of ligands bound,  $\bar{n}$ , as a function of ligand concentration, for each of their models using only four "equilibrium constants", two for defining the interactions between subunits and two for their binding affinities. These equations gave rise to positive, negative and half of the sites reactivity and it was also shown how the binding equations for non-identical subunits could be derived using more parameters.

The haemoglobin oxygen binding data used by Monod, Wyman & Changeaux (1966) could be fitted equally well by the sequential model of Koshland et al., (1966) indicating that experimental binding data for allosteric systems needs to be very accurate if a choice between the two models is to be made (see for example Niekamp et al., 1977), and that other information, such as x-ray structure changes on binding, is also required to understand allosteric proteins.

A general thermodynamic model covering ligand binding and temperature and pressure effects using multiple conformational

states of proteins has been given by Gill et al., (1985). Allosteric effects as well as thermodynamic effects were regarded as generalised binding phenomena and this allowed data from various calorimetric and ligand binding experiments to be analysed.

It should also be noted that the above models apply to systems at or near equilibrium which may be an unlikely state for an allosteric system to be in. The fact that haemoglobin functions at equilibrium and is the most well studied system has probably led to nonequilibrium effects being neglected. Catalytic allosteric systems must, on the other hand, operate away from equilibrium to produce a net chemical flow. One such model system due to Go & Anan (1977) which may be particularly applicable to enzyme systems in vivo placed an enzyme obeying the concerted model inside a semi permeable membrane which maintained the substrate and product at concentrations far from equilibrium due to their slow diffusion rates through the membrane. Their results showed that under certain conditions several stationary states of the system could exist allowing the enzyme to be switched sharply between catalytically reactive and non-reactive states; an extreme case of cooperativity. In fact, a similar model applied to a Michaelis-Menten system also showed multiple states (Bunow, 1974). Experimental evidence for this kinetic cooperativity as opposed to equilibrium cooperativity has accumulated over the years and recently a review covering this and the methods of analysis has been published (Ricard & Cornish-

Bowden, 1987). The unusual steady state kinetics of some enzymes has led to the proposal of the mnemonical enzyme and hysteresis effects, where certain of the reaction steps are controlled by relaxation of the enzyme structure. The enzyme is considered to exist in two or more conformations which interact with substrates at different rates. The different conformations of the enzyme interconvert at rates which are slow compared to other steps in the reaction mechanism. This hysteresis effect becomes particularly simple if only the free enzyme undergoes these slow transitions where on release of the product from the reaction site the enzyme retains the conformation stabilised by the product for sometime before relaxing to another conformation. Such an enzyme is termed "mnemonical" and it can be recognised by the presence of transient phases in the kinetics before the steady state is reached. These transients have been studied extensively in the reactions of hexokinases. Structural studies of hexokinase, a bi-lobed enzyme, have indicated the importance of the hinge bending motion closing the two domains around the active site. This sort of motion may be involved in the slow relaxations postulated for mnemonical enzymes.

The importance of protein dynamics in these systems is obvious. The postulate that only the free enzyme undergoes slow relaxations for instance, would imply that the probability distribution function for the protein energy is broader allowing many large fluctuations while substrate binding would narrow the distribution allowing only one predominant conformation.

In the next section the importance of protein dynamics even in equilibrium cooperative behavior is demonstrated with a statistical mechanical theory and a simple visual model.

## 2.2 Protein Dynamics and Equilibrium Allosteric Interactions:

### A General Theory

All the standard models of equilibrium allosteric effects postulate that the protein exists in different "states" which reflect the liganded state of the protein. It is almost invariably assumed that these states are different conformational states where the protein has a different 3-dimensional equilibrium conformation depending on the presence or absence of different ligands at different sites. This assumption is not necessary and neither of the mathematically simple MWC or KNF models, which describe experimental observations so successfully, are dependent upon any assumptions regarding the nature of the "states" involved.

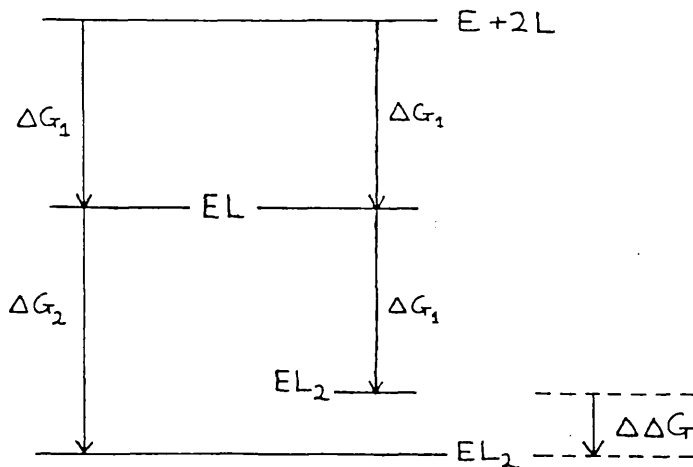
The concept of ligand induced conformational change is well established and, in some cases, has strong experimental support. However, there are several other ligand induced physical changes which could play a role in allosteric and other properties of proteins.

Allostery is concerned with the transfer of information about the occupancy of binding sites from one part of the protein to another. This could be accomplished in a trivial way without

any change in the protein conformation by long range electrostatic interactions between charged ligands. The effect is likely to be small because of the inverse square distance dependence and is not considered further here. A much more interesting possibility involves changes in the protein dynamics promoting the allosteric interaction. These changes could affect the equilibrium positions of atoms or groups of the protein but importantly, they will change the frequency and amplitudes of the dynamic motions about these positions. As will be shown below, such changes can be responsible for changes in ligand binding affinities in a calculable way, with magnitudes in reasonable agreement with observed effects. These dynamic changes can also control the nonequilibrium kinetics of ligand binding and release.

This section develops a statistical mechanical theory of cooperative interactions which explicitly considers the role of protein dynamics which is the main aim of this thesis. The simplest example of allostery would be the binding of two identical ligands to identical binding sites on a monomeric protein. Each binding step must have a negative free energy change to be favourable and can be represented as (Figure 2.2).

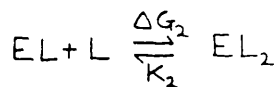
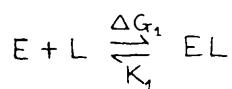
Fig. 2.2. Typical free energy changes involved in positive cooperativity.



where the protein  $E$  binds ligand  $L$  with a standard amount of free energy to form  $EL$ , which then binds the second ligand with a different free energy change. The difference between the free energy of binding both ligands independently  $2\Delta G_1$  and that of binding them cooperatively  $\Delta G_1 + \Delta G_2$  is the cooperative free energy  $\Delta\Delta G$  which measures the coupling strength between the two sites. If  $\Delta\Delta G$  is negative then binding of the second ligand is more favourable than binding the first, which is termed positive cooperativity, while if  $\Delta\Delta G$  is positive then binding of the second ligand is unfavourable leading to negative cooperativity.

Typical values of  $\Delta\Delta G$  vary from  $+ 2.5\text{Kcal mol}^{-1}$  to  $-2.5\text{Kcal}$

$\text{mol}^{-1}$ , while typical  $\Delta G$  values range from  $\sim -25\text{kcal mol}^{-1}$  to  $\sim 0\text{kcal mol}^{-1}$  (see Weber, 1975). The free energy change is the sum of various contributions such as bond formation, electrostatic, vibrational, translational, and rotational enthalpy and entropy changes and conformational changes whether static or dynamic. These terms are not always separable. For binding to be favourable the free energy change must be negative. This is often the case when bond formation occurs since this term is large and negative. These free energy changes can be written in terms of the equilibrium constants of the two binding reactions, and then standard statistical mechanical expressions can be used to calculate the magnitudes of the various contributions to  $\Delta\Delta G$ . It should be noted that the published version of this work (Cooper & Dryden, 1984) contains several trivial algebraic mistakes which are corrected here. A copy of the published work is given in appendix 3. The binding reactions and their association constants can be written as



where  $K_1$  and  $K_2$  are the association constants and

$$\Delta G_1 = -kT \ln K_1$$

$$\Delta G_2 = -kT \ln K_2$$

where  $k$  is the gas constant and  $T$  the temperature.

This gives for the cooperative free energy:-

$$\begin{aligned} \Delta\Delta G &= -kT \ln K_2 + kT \ln K_1 \\ &= -kT \ln \left( e^{-\frac{\Delta G_2^{\text{bond}}}{kT}} \cdot \frac{Q_2}{Q_1 Q_L} \right) + kT \ln \left( e^{-\frac{\Delta G_1^{\text{bond}}}{kT}} \cdot \frac{Q_1}{Q_0 Q_L} \right) \\ &= \Delta G_2^{\text{bond}} - \Delta G_1^{\text{bond}} - kT \ln \frac{Q_0 Q_2}{Q_1^2} \end{aligned}$$

where  $\Delta G_i^{\text{bond}}$  is the free energy change due to bond formation as ligand  $i$  binds, where  $i = 1$  or  $2$  and  $Q_0$ ,  $Q_1$  and  $Q_2$  are the molecular partition functions of E, EL and  $EL_2$  enzyme complexes.  $\Delta G_2^{\text{bond}}$  and  $\Delta G_1^{\text{bond}}$  can be set equal to zero since we are considering identical ligands binding to well separated identical binding sites.

$$\Rightarrow \Delta\Delta G = -kT \ln \frac{Q_0 Q_2}{Q_1^2}$$

The molecular canonical partition function  $Q = \sum_i e^{-\frac{E_i}{kT}}$ , where the summation is over all states  $i$ , with energy  $E_i$ , can be written as the product of partition functions of the various contributions to the free energy (Hill, 1960)

$$Q = q_{\text{trans}} \cdot q_{\text{rotn}} \cdot q_{\text{vib}} \cdot q_{\text{elect}} \cdot q_{\text{conf}}$$

$q_{\text{trans}}$  and  $q_{\text{rotn}}$  are the partition functions for translation and rotation of the whole molecule and are given by the following expressions.

$$q_{\text{trans}} = \left( \frac{2\pi M kT}{h^2} \right)^{3/2} V$$

$$q_{\text{rotn}} = \frac{\pi^{1/2}}{\sigma} \cdot \left( \frac{8\pi^2 kT}{h^2} \right)^{3/2} \cdot (I_A I_B I_C)^{1/2}$$

where  $M$  = mass of molecule,  $I_A$ ,  $I_B$  and  $I_C$  are the moments of inertia of the molecule about its 3 principle axes and  $\sigma$  is a symmetry number to account for repeated counting of indistinguishable states.

The translational and rotational contributions to the cooperative free energy are therefore:

$$\Delta\Delta G_{\text{trans}} = -\frac{1}{2} kT \ln \frac{M_0 M_2}{M_1^2}$$

$$\Delta\Delta G_{\text{rotn}} = -\frac{1}{2} kT \ln \frac{(I_A I_B I_C)_0 \cdot (I_A I_B I_C)_2}{(I_A I_B I_C)_1^2}$$

These contributions to  $\Delta\Delta G$  will usually be very small and positive since typical ligands are usually small compared to the enzyme thus binding will produce negligible changes in mass and moments of inertia. The individual free energy changes  $\Delta G_{1,2\text{trans}}$  and  $\Delta G_{1,2\text{rotn}}$  will typically be large and positive, because of the restrictions placed on the small mobile ligand molecule by binding, and small and positive respectively, so that for binding to be favourable, the free energy of binding must be more negative than their sum.

The contribution to the free energy of the electronic partition functions will be negligible since only the ground electronic state is significantly populated at physiological

temperatures.

### 2.2.1 The Vibrational Contribution to Dynamic Allostery

The partition function for a harmonic oscillator of frequency  $\nu_i$  with quantised energy levels  $n h \nu_i$  ( $n=0,1,2,\dots$ ) is

$$q_{\text{vib}}(\nu_i) = \frac{e^{-\frac{h\nu_i}{2kT}}}{1 - e^{-\frac{h\nu_i}{kT}}}$$

which in the classical limit  $kT \gg h\nu_i$  becomes

$$q_{\text{vib}}(\nu_i) = \frac{kT}{h\nu_i}$$

The complete vibrational partition function for each molecular species is the product of all the  $q_{\text{vib}}(\nu_i)$  for each normal mode:

$$q_{\text{vib}} = \prod_i q_{\text{vib}}(\nu_i)^{g(\nu_i)}$$

where  $g(\nu_i)$  is the degeneracy of modes of frequency  $\nu_i$ .

Substituting this into the equation for  $\Delta \Delta G_{\text{vib}}$  gives

$$\begin{aligned} \Delta \Delta G_{\text{vib}} &= -kT \sum_{\nu} \ln \left( \frac{q_{0\text{vib}}^{g(\nu)} q_{2\text{vib}}^{g(\nu)}}{q_{1\text{vib}}^{2g(\nu)}} \right) \\ &= -kT \sum_{\nu} \left( -2g_1(\nu) \ln q_{1\text{vib}} + g_0(\nu) \ln q_{0\text{vib}} + g_2(\nu) \ln q_{2\text{vib}} \right) \\ &= \sum_{\nu} \left\{ -g_1(\nu) h\nu_1 + \frac{1}{2} g_0(\nu) h\nu_0 + \frac{1}{2} g_2(\nu) h\nu_2 \right\} \\ &\quad + kT \sum_{\nu} \left\{ -2g_1(\nu) \ln \left( 1 - e^{-\frac{h\nu_1}{kT}} \right) + g_0(\nu) \ln \left( 1 - e^{-\frac{h\nu_0}{kT}} \right) + g_2(\nu) \ln \left( 1 - e^{-\frac{h\nu_2}{kT}} \right) \right\} \end{aligned}$$

= ground vibrational states term + excited states term

If ligand binding does not change the vibrational density of states of the protein,  $g(\nu)$ , then  $\Delta\Delta G_{\text{vib}} = 0$ . Similarly if only high frequency modes with  $h\nu \gg kT$  are affected then  $\Delta\Delta G_{\text{vib}}$  will be essentially zero since any frequency change caused by ligand binding will only be a small fraction of the actual frequency resulting in a negligible contribution from the ground states term while the contribution from the excited states tends to zero as exponential terms become negligible.

Low frequency protein modes with  $h\nu \leq kT$  will give sizeable contributions to  $\Delta\Delta G$ . Ligand binding to enzymes often changes their conformation to some extent; associated with this, though rarely considered explicitly, will be a change in the dynamics of the enzyme. High frequency vibrations of amino acid groups may be affected but their contribution to the energetics will be negligible as shown above, but low frequency vibrations involving large parts or even the whole of the enzyme are very likely to be changed by ligand binding. For example glyceraldehyde-3-phosphate dehydrogenase, an allosteric enzyme, has shown heat capacity changes on ligand binding which are consistent with a stiffening of the enzyme structure as a large number of low frequency modes are converted to higher frequencies (Velick *et al.*, 1977; Sturtevant, 1977).

If ligand binding were to convert a single low frequency mode to slightly higher frequencies,  $\nu_0 \rightarrow \nu_1 \rightarrow \nu_2$ , as each ligand binds then

$$\Delta\Delta G_{vib} = -kT \left( \ln q_{0vib} + \ln q_{2vib} - 2 \ln q_{1vib} \right)$$

for this one mode. If the frequency shifts are small then the classical partition function can be used, giving:

$$\Delta\Delta G_{vib} \approx -kT \ln \frac{\nu_1^2}{\nu_0 \nu_2}$$

as the contribution of this mode to the cooperative free energy.

Positive cooperativity will be obtained when  $\nu_1^2 > \nu_0 \nu_2$

and negative cooperativity when  $\nu_1^2 < \nu_0 \nu_2$ . Increases in the

frequency of say 10% at each binding step, which would be of the

order 10 to 20  $\text{cm}^{-1}$  at 25 °C, would give  $\Delta\Delta G_{vib}$  of the order

$\sim 0.01kT$  per mode. Proteins, being large molecules, possess

hundreds of low frequency modes (Go et al., 1983; Brooks &

Karplus, 1983; Levitt et al., 1985) which, if they were all

affected by ligand binding, could contribute several  $\text{kJmol}^{-1}$  to

$\Delta\Delta G$ . Typical  $\Delta\Delta G$  values measured (Weber, 1975, gives examples)

are of this order.

Larger frequency shifts may also be possible which require a

quantum mechanical treatment. One can imagine situations where a

low frequency large collective motion of an enzyme could be

"frozen" on ligand binding and converted to a much higher

frequency. An example might be the proposed hinge bending mode

of lysozyme involving relative motions of the enzyme's two lobes

(Brooks et al., 1985; McCammon et al., 1976). A ligand binding

in the active site between the lobes could "jam" the hinge and

convert the vibration from a low frequency "soft" mode to a

higher frequency "hard" mode. This picture is supported by

neutron inelastic scattering experiments on lysozyme (Bartunik et al., 1980; Middlendorf, 1984) and on hexokinase (Jacrot et al., 1982) where a loss of low frequency modes is seen on ligand binding. A computer normal mode simulation of hexokinase with and without ligand bound also shows a loss of low frequency modes on ligand binding (Harrison, 1984). If a mode such as this connects two ligand binding sites then binding of one ligand could affect the other binding site by restricting it to low amplitude high frequency motions around the optimal binding configuration. This would give positive cooperativity while the reverse situation of negative cooperativity is also possible. Considering such a mode; the frequencies would be  $\nu_2 \approx \nu_1 \gg \nu_0$ . If  $\nu_0$  was a typical low frequency mode of  $50 \text{ cm}^{-1}$  which converted to higher frequencies ( $500 \text{ cm}^{-1}$  say) on binding then using the quantum mechanical expression for  $\Delta\Delta G_{\text{vib}}$  one obtains  $\sim -1\text{kT}$  and  $\sim -1.4\text{kT}$  for the contributions to  $\Delta\Delta G_{\text{vib}}$  from the ground state term and the excited state term respectively, though the ground state term is perhaps better absorbed into the bond formation and ground electronic state terms discussed earlier.

$-1.4\text{kT}$  corresponds to about  $2.1\text{kJ mol}^{-1}$  of cooperative interaction energy at room temperature, so one or two such modes could easily account for the interaction energies typically found in proteins. The free energy for a single mode can also be separated into enthalpy and entropy contributors using the following formulae and considering the excited states contribution only.

$$\Delta\Delta G_{vib} = \Delta\Delta H_{vib} - T\Delta\Delta S_{vib}$$

$$\begin{aligned}\Delta\Delta H_{vib} &= \Delta\Delta G_{vib} - T \left( \frac{\partial \Delta\Delta G_{vib}}{\partial T} \right)_p \\ &= \frac{h\nu_0}{U_0} e^{-\frac{h\nu_0}{kT}} + \frac{h\nu_2}{U_2} e^{-\frac{h\nu_2}{kT}} - \frac{2h\nu_1}{U_1} e^{-\frac{h\nu_1}{kT}}\end{aligned}$$

where  $U_i = \left( 1 - e^{-\frac{h\nu_i}{kT}} \right)$

and 
$$\begin{aligned}\Delta\Delta S_{vib} &= -\frac{\Delta\Delta G_{vib}}{T} + \frac{\Delta\Delta H_{vib}}{T} \\ &= k \ln \left( \frac{U_1^2}{U_0 U_2} \right) + \frac{\Delta\Delta H_{vib}}{T}\end{aligned}$$

Calculating the enthalpy contribution for the 50cm<sup>-1</sup> mode described above one finds that  $\Delta\Delta H$  is positive and is  $\sim 0.6kT$  which implies that the entropy effect is larger and also positive. Binding of the first ligand is therefore more exothermic than the favourably bound second ligand. In the classical limit,  $\Delta\Delta H_{vib}$  will tend to zero because the classical equipartition of energy theorem does not depend on frequency, and the vibrational cooperative effect will be entirely entropic. These changes can also be explained by the "freezing" of the low frequency mode.

Binding of the first ligand, which converts the highly thermally excited low frequency enzyme mode into a higher

frequency mode which is much less excited, results in a large decrease of vibrational entropy which more than compensates for the exothermic contribution to binding of the ligand. The second ligand produces a much smaller change in the vibrational energy level population of the enzyme mode because of the Boltzmann factor resulting in a small entropy change which still, however, compensates for the enthalpy of binding of the second ligand. This enthalpy change will be less exothermic than the first because the enzyme with one ligand bound already, will be more stable.

These arguments are applicable to all the low frequency modes in the enzyme. Sturtevant (1977) shows that a decrease in the number of low frequency modes leads to a negative change in the entropy, which is in agreement with the above example where both  $\Delta S_1$  and  $\Delta S_2$  are negative.  $\Delta S_1$  is more negative than  $\Delta S_2$  resulting in a positive  $\Delta\Delta S$ , since there is a smaller loss of low frequency modes on binding the second ligand. The effects of anharmonicity and damping on the low frequency modes of enzymes should also be considered.

Anharmonicity of the low frequency vibrations of proteins does not affect the general conclusions that ligand binding which leads to a stiffening of the enzyme structure can give significant contributions to cooperative ligand binding. Normal mode calculations for proteins which can only give harmonic modes compare favourably with more complex molecular mechanics simulations which calculate anharmonic effects explicitly

(Brooks & Karplus, 1983; Levitt et al., 1985).

Damping of the global vibrations of the protein by viscous drag of the solvent also does not change the conclusions reached above. The solvent as well as damping the motion of the protein, continually excites the vibrations of the protein by molecular collisions so that at equilibrium the rate of damping is equal to the rate of excitation. The motion then consists of continuous random motion of the protein. Peticolas (1979) has shown that this random motion, if described by a Langevin equation for a damped harmonic oscillator with a random term added, still follows the trajectories of the motion that would be mapped out by the harmonic normal modes in the absence of damping. In this way, the protein maintains its structure and function and does not move in a completely random manner. It will be shown later that dynamic allosteric effects are not restricted to harmonic or quasi-harmonic motions within the protein (see next section).

The theory presented here is based on semi-classical harmonic oscillator theory, in which quantum mechanics is introduced only to quantise the energy levels. The rigorous quantum mechanical treatment of damped harmonic oscillators is complicated and not fully developed but Greenberger, (1979a,b) has shown that the energy of an initially excited harmonic oscillator decays exponentially until the oscillator reaches equilibrium with its surroundings. It is then subject to the fluctuations of its surroundings continually changing its energy in a similar manner to the classical damped oscillator

discussed by Peticolas. Consequently the semi-classical approach used here is unlikely to involve any serious approximations.

### 2.2.2 The Dynamic Conformational Contribution

The thermally induced motion of atoms and groups in a protein will rarely be completely harmonic because of the frictional and anharmonic effects discussed above. The resolution of many x-ray structures of proteins is improved on ligand binding. As well as gross conformational changes, many atoms show a reduction in their thermal motion equivalent to a narrowing of the atom's positional distribution function (see Ringe & Petsko, 1985 for review). The sort of motion reflected by these structural studies is likely to be random, stochastic motion about the equilibrium position rather than correlated harmonic motions. It is the purpose of this section to show that changes induced in the statistical distributions of atoms about their equilibrium position can still give rise to long range allosteric interactions. These ligand induced changes are usually "stiffening" effects and, once again, can occur in the absence of any conventional "conformational change" in the mean atomic coordinates.

The contribution of this stiffening of the structure on ligand binding to the cooperativity of the enzyme was first calculated by Alan Cooper using classical statistical mechanics.

$$\Delta\Delta G_{\text{conf}} = -kT \ln \left( \frac{q_0 q_2}{q_1^2} \right)_{\text{conf}}$$

The partition functions are defined as

$$q = \sum_{\text{all } R} e^{-\frac{E(R)}{kT}}$$

where  $E(R)$  is the potential energy of the protein as a function of the conformation  $R$  of the protein.  $R$  has  $3n$  components which represent the positions of all  $n$  atoms of the protein. This function  $E(R)$  is too complicated to be calculated exactly, but by assuming that each partition function is a product of  $3n$  individual atomic coordinate partition functions, one can write

$$\Delta \Delta G_{\text{conf}} = -kT \sum_i^{\text{All Coords}} \ln \left( \frac{q_0 q_2}{q_1^2} \right)_i$$

The summation is over all atomic coordinates of the different liganded forms and the partition functions are for each atomic coordinate. This assumption implies that all the atomic motions are uncorrelated with their neighbours and is the exact opposite to the assumption in the previous section that the vibrations of the protein are harmonic implying correlated motions of the atoms. This assumption, while being unrealistic, has the advantage that anharmonic motions, transitions between conformational substates and random events can be more easily studied. Molecular mechanics simulations of protein dynamics (Levitt, 1983a,b) show that proteins move in a non-periodic fashion between the various slightly different conformational substrates, which are caused by multiple minima on the multidimensional potential energy surface.

For the case of ligand binding at two identical sites the coordinates of which are related by molecular symmetry (e.g. a dimer of two identical monomers) one can write that for each atom  $i$  on one monomer and its equivalent atom  $i'$  on the other monomer,

that 
$$\Delta\Delta G_i = -kT \ln \left[ \left( \frac{q_0 q_2}{q_1^2} \right)_i \left( \frac{q_0 q_2}{q_1^2} \right)_{i'} \right]$$

For cooperativity to occur, binding at site  $i$  which changes  $q_0(i) \rightarrow q_1(i)$  must also change  $q_0(i') \rightarrow q_1(i')$ , similarly binding of the second ligand which changes  $q_1(i') \rightarrow q_2(i')$  must also change  $q_0(i) \rightarrow q_1(i)$ . If this does not occur then binding occurs independently and  $\Delta\Delta G_{conf}$  is zero, in other words binding of the first ligand has to be communicated in some way to the other binding site.

To calculate the magnitude of this effect when ligand binding changes the extent of fluctuations of the atom about its mean position without changing the mean position (i.e. no conventional conformational change), one assumes that the atomic fluctuations of atom  $i$  fit a Gaussian distribution function with width  $\sigma_i$ . The partition function for a Gaussian distribution is proportional to its width, which can be shown in the following approximate way:

Let  $p(x) = e^{-\frac{x^2}{2\sigma^2}}$ , an unnormalised Gaussian function symmetrical about the origin  $x = 0$ , then the partition function is

$$\begin{aligned} q &= \sum_x p(x) = \int_{-\infty}^{\infty} p(x) dx \\ &= 2 \int_0^{\infty} p(x) dx \\ &= 2 \int_0^{\infty} e^{-\frac{x^2}{2\sigma^2}} dx \end{aligned}$$

Making the substitution  $a^2 = \frac{1}{2\sigma^2}$  and using a standard integral  $\int_0^\infty e^{-ax^2} dx = \frac{\sqrt{\pi}}{2a}$  one obtains

$$q = 2 \cdot \frac{\sqrt{\pi}}{2a} \\ = \sigma \cdot \sqrt{2\pi}$$

partition function  $q \propto$  width  $\sigma_{\text{conf}}$

Substituting this result into  $\Delta\Delta G_{\text{conf}}$  leads to

$$\Delta\Delta G_i = -2kT \ln \left[ \frac{\sigma_0 \cdot \sigma_2}{\sigma_1(i) \cdot \sigma_1(i')} \right]$$

where  $\sigma_0$  and  $\sigma_2$  are the root mean square fluctuations of coordinate  $i$  in the unliganded and fully liganded enzyme, while  $\sigma_1(i)$  and  $\sigma_1(i')$  are the fluctuations when only one binding site is occupied. The most extreme case of cooperativity imaginable is the case where all the dynamic conformational changes occur when the first ligand binds forcing the empty binding site into the optimal configuration for accepting the second ligand. If the changes in the fluctuations are small then they can be written in terms of fractional changes from the unliganded Gaussian width.

i.e.  $\sigma_1(i) \approx \sigma_0 (1 - \delta_1)$  and  $\sigma_1(i') \approx \sigma_0 (1 - \delta_1')$ , but if the protein is symmetrical and there is full cooperativity then  $\delta_1 = \delta_1'$ . Full cooperativity also implies that there is no further change on binding the second ligand so that  $\sigma_2 \approx \sigma_0 (1 - \delta_1)$  as well.

$$\text{This gives } \Delta\Delta G_i \approx -2kT \delta_1.$$

for each atomic coordinate affected. This contribution could amount to 1 or 2  $\text{kJmol}^{-1}$ , even for shifts of the order of 1%, if

a large part of the enzyme is affected. The contribution is entropic only, because of the use of classical mechanics.

### 2.2.3 Discussion of the Theory

The preceding two sections have demonstrated that cooperative effects observed in proteins can be explained in terms of changes in the protein dynamics whether or not a gross change in the protein structure is also involved in the cooperativity. The two different approaches involving correlated global low frequency vibrations and uncorrelated changes in atomic positional fluctuations can give cooperative interaction free energies of the same order as those found experimentally, and they can also be studied experimentally.

Low frequency motions ( $< 200\text{cm}^{-1}$ ) of proteins can be studied directly by Raman, far infra-red and inelastic neutron scattering spectroscopy, and indirectly by thermodynamic measurements of heat capacity changes (Sturtevant, 1977) and possibly by low temperature spin relaxation of heavy atoms in proteins (Wagner et al., 1985). Computer normal mode simulations of protein ligand complexes may also support the model (see Brooks & Karplus, 1983 for possible effects of trypsin binding on the low frequency modes of a large polypeptide inhibitor).

Uncorrelated atomic fluctuations can be studied using the atomic temperature factors derived from protein structures with and without ligands bound (Ringe & Petsko, 1985) which usually show a decrease in atomic motion on ligand binding in agreement

with the model. Molecular mechanics simulations also study these uncorrelated motions and a recent simulation of lysozyme with and without substrate bound showed significant changes in the size of fluctuations (Post et al., 1986).

Both sorts of motion contribute to the cooperative free energy mainly via entropy changes with binding of the second ligand being more favourable because of a less negative  $\Delta S$ . These thermodynamic changes are in agreement with experimental results for ligand binding to the allosteric protein, glyceraldehyde 3-phosphate dehydrogenase, (Niekamp et al., 1977) and for binding to an allosteric organic model compound (Onan et al., 1983). The cooperativity displayed by these two molecules is investigated in terms of the above model for dynamic allostery in Chapters 3 and 5.

Finally, one should say that the above model, which was presented in terms of one species of ligand and two identical binding sites, to simplify the algebra, could be generalised to more complicated systems and with suitable choices of parameters the effects of activation, inhibition, positive and negative cooperativity could be simulated.

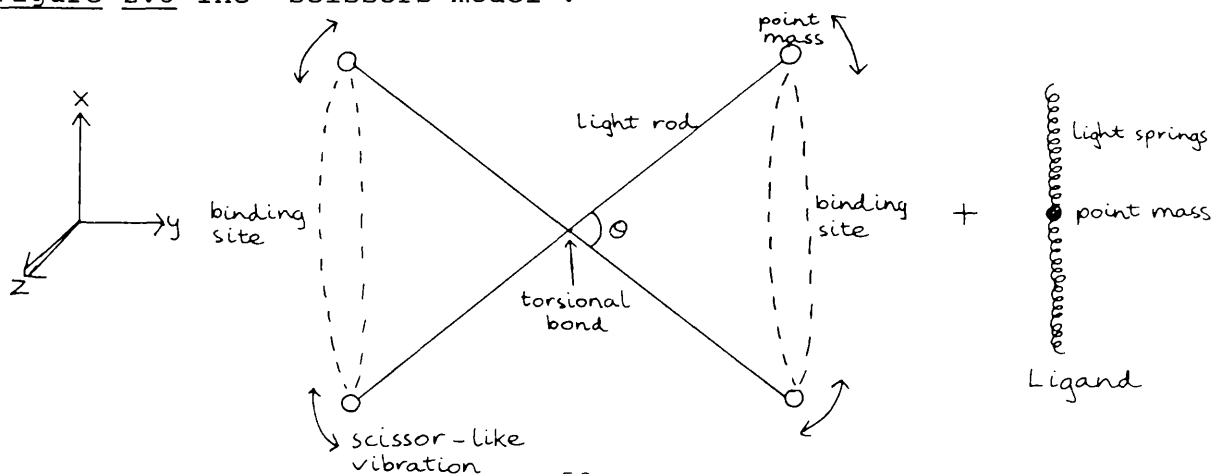
#### 2.2.4 A Simple Model of Allostery using Low Frequency Vibrations of Proteins

In this section a simple mechanical model of an allosteric protein which possesses 2 well separated identical ligand binding

sites is developed. The model is not intended to be a realistic picture of an enzyme, but rather to illustrate clearly the general features of the dynamic allostery theory. Despite this, it bears considerable resemblance to a class of synthetic organic allosteric model compounds discussed in Chapters 3 and 5. The normal modes of the system are calculated and the effect of binding on a particular low frequency mode which connects the 2 binding sites is studied using the thermodynamic expressions developed in the last section.

The enzyme model is considered to be four point masses placed at the ends of 2 massless rods which are joined together at their centre by a torsional bond about which they vibrate harmonically. The two binding sites are between the two opposite pairs of point masses. The ligands are considered to be point masses which bind to the enzyme with two springs which connect to the enzyme masses on either side of the binding site. A sketch of the model, which was dubbed the "scissors model" is shown in Figure 2.3.

Figure 2.3 The "scissors model".



The assumptions used for this model are rather drastic but using bulk masses which would give the model more shape and using more realistic interactions would greatly increase the complexity of the calculations while hardly effecting the results.

This model could perhaps be thought of as only modelling that part of the enzyme which is responsible for allosteric communication, with the rest of the enzyme surrounding the model but playing no part in the binding reactions. It is also not important what sort of protein secondary structural features are involved in the normal modes of the system be they  $\alpha$  helices,  $\beta$  sheets or whole domains.

The mass of the enzyme is  $M_E$  making each point mass of weight  $1/4 M_E$ . The light rods are of length  $L$ , bisect at angle  $\theta$  and vibrate about the torsional bond which obeys Hookes law and has a spring constant  $k$ . The ligand of mass  $M_L$  binds by forming two bonds with force constant  $k_L$  to give a total system mass of  $M_{EL}$  when one ligand is bound and  $M_{EL_2}$  when two are bound. Motion of the enzyme masses or of the ligands in the  $y$  or  $z$  directions is assumed to be negligible.

All the normal modes of the liganded and unliganded models were calculated by solving simultaneous differential equations derived using Lagrange's equation.

$$\frac{\partial}{\partial t} \left( \frac{\partial L}{\partial \dot{q}} \right) - \frac{\partial L}{\partial q} = 0 \quad \text{for all } q$$

where  $q$  is a normal coordinate of the system,  $\dot{q}$  is its time

derivative and  $L$  = Lagrangian = kinetic energy of the system - potential energy.

The solution of this equation for all the normal coordinates is long and tedious and is therefore relegated to Appendix 1.

The most important normal mode in the 3 systems is the scissors mode of the enzyme. This can be visualised as a global low frequency vibration of the enzyme which is responsible for cooperativity between the two binding sites. The expressions for the scissors normal mode frequency found for the model enzyme E and its two complexes EL and  $EL_2$  are.

$$\nu_E^{sc} = \frac{1}{2\pi} \sqrt{\frac{16k}{M_E L^2}}$$

$$\nu_{EL}^{sc} = \nu_E^{sc} \sqrt{1 + \frac{k_L L^2 (1 + \cos \Theta)}{16k}}$$

$$\nu_{EL_2}^{sc} = \nu_E^{sc} \sqrt{1 + \frac{k_L L^2 (1 + \cos \Theta)}{8k}}$$

which can be rewritten if  $k_L$ , the natural ligand bond force constant is substituted for a ligand bond frequency  $\nu_L = \frac{1}{2\pi} \sqrt{\frac{k_L}{M_L}}$  and  $k$  is substituted by  $\nu_E^{sc}$  to give

$$\nu_E^{sc} = \frac{1}{2\pi} \sqrt{\frac{16k}{M_E L^2}}$$

$$\nu_{EL}^{sc} = \nu_E^{sc} \sqrt{1 + \frac{\nu_L^2 M_L}{2 \nu_E^{sc^2} M_E} (1 + \cos \Theta)}$$

$$\nu_{EL_2}^{sc} = \nu_E^{sc} \sqrt{1 + \frac{\nu_L^2 M_L}{\nu_E^{sc^2} M_E} (1 + \cos \Theta)}$$

where it is assumed that there is no gross conformational change of the enzyme caused by ligand binding, in other words  $\phi$  remains constant.

Using these frequencies, the other normal mode frequencies and the standard statistical mechanical expressions for partition functions, the thermodynamic parameters can also be calculated.

$$\Delta G_1 = -kT \ln K_1 = -kT \ln \frac{Q_{EL}}{Q_E Q_L}$$

$$= \Delta G_1^{\text{bond}} - kT \ln \left( \frac{q_{EL}}{q_E q_L} \right)_{\text{conf}} - kT \ln \left( \frac{h^2 M_{EL}}{2\pi kT M_E M_L} \right)^{3/2} \\ - kT \ln \left( \frac{(I_A I_B I_C)_{EL}}{(I_A I_B I_C)_E} \right)^{1/2} - kT \ln \left( \frac{U_E^{\text{sc}}}{U_{EL}^{\text{sc}} U_{EL}^{\text{damp}}} \right) + \frac{h}{2} (\nu_{EL}^{\text{sc}} + \nu_{EL}^{\text{damp}} - \nu_E^{\text{sc}})$$

= translational + rotational + vibrational terms ignoring the first two terms.

Similarly

$$\Delta G_2 = \Delta G_2^{\text{bond}} - kT \ln \left( \frac{q_{EL_2}}{q_{EL} q_L} \right)_{\text{conf}} - kT \ln \left( \frac{h^2 M_{EL_2}}{2\pi kT M_{EL} M_L} \right)^{3/2} - kT \ln \left( \frac{(I_A I_B I_C)_{EL_2}}{(I_A I_B I_C)_{EL}} \right)^{1/2} \\ - kT \ln \left( \frac{U_{EL}^{\text{sc}} U_{EL}^{\text{damp}}}{U_{EL_2}^{\text{sc}} U_{EL_2}^{\text{damp}} U_{EL_2}^x} \right) + \frac{h}{2} (\nu_{EL_2}^{\text{sc}} + \nu_{EL_2}^{\text{damp}} + \nu_{EL_2}^x - \nu_{EL}^{\text{sc}} - \nu_{EL}^{\text{damp}})$$

where  $U_i = 1 - e^{-\frac{h\nu_i}{kT}}$

The vibrational enthalpy and entropy changes only are of interest in this discussion. The enthalpy changes are given below from which the entropy changes can be calculated.

$$\Delta H_1 = \frac{h}{2} (\nu_{EL}^{sc} + \nu_{EL}^{damp} - \nu_{EL}^{sc})$$

$$+ h \left( \frac{\nu_{EL}^{sc} (1 - U_{EL}^{sc})}{U_{EL}^{sc}} + \frac{\nu_{EL}^{damp} (1 - U_{EL}^{damp})}{U_{EL}^{damp}} - \frac{\nu_E^{sc} (1 - U_E^{sc})}{U_E^{sc}} \right)$$

$$\Delta H_2 = \frac{h}{2} (\nu_{EL2}^{sc} + \nu_{EL2}^{damp} + \nu_{EL2}^x - \nu_{EL}^{sc} - \nu_{EL}^{damp})$$

$$+ h \left( \frac{\nu_{EL2}^{sc} (1 - U_{EL2}^{sc})}{U_{EL2}^{sc}} + \frac{\nu_{EL2}^{damp} (1 - U_{EL2}^{damp})}{U_{EL2}^{damp}} + \frac{\nu_{EL2}^x (1 - U_{EL2}^x)}{U_{EL2}^x} \right.$$

$$\left. - \frac{\nu_{EL}^{sc} (1 - U_{EL}^{sc})}{U_{EL}^{sc}} - \frac{\nu_{EL}^{damp} (1 - U_{EL}^{damp})}{U_{EL}^{damp}} \right)$$

It can be seen that the enthalpies consist of a ground state term plus an excited state term and that calculating the ground state entropy changes from  $\Delta G - \Delta H$  gives zero as one would expect.

Magnitudes of the translational, rotational and vibrational contributions can be calculated by defining the following parameters

Temperature = 298K

Enzyme mass  $M_E = 25000$  daltons typical of a small globular protein

Ligand mass  $M_L = 250$  daltons typical of a small organic substrate

Length of rods  $L = 30\text{\AA}$  giving the enzyme a reasonable size

Scissor angle  $\Theta = 1$  radian. This has little effect on the calculations

The free enzyme scissor frequency was varied from  $3\text{cm}^{-1}$  to  $1000\text{cm}^{-1}$  and the ligand to enzyme bond strength was defined to give a frequency typical of a C-H stretch i.e.  $3000\text{cm}^{-1}$  though a lower frequency only reduces the magnitude of the effect but does not change the conclusions.

The magnitudes of the translational and rotational contributions to the cooperativity will be calculated first to show that they have a negligible effect.

#### Translational component

$$\Delta G_{\text{trans}1} = 6309\text{cm}^{-1}$$

$$\Delta G_{\text{trans}2} = 6308.5\text{cm}^{-1}$$

This shows that although binding causes an unfavourable free energy change as the small mobile ligand's freedom is restricted, the contribution to the cooperative free energy interaction of  $-0.5\text{cm}^{-1}$  is negligible.

#### Rotational component

The moments of inertia of the enzyme model about the x, y and z axes are easily calculated using the formula

$$I_{\alpha i} = \sum m_i d_i^2 \quad \text{where } \alpha \text{ is the moment axis}$$

and subscript i runs over all the point masses  $m_i$  at a perpendicular distance  $d_i$  from the axis.

It is then found that

$$\Delta G_{\text{rotn}1} = 2.06\text{cm}^{-1}$$

$$\Delta G_{\text{rotn2}} = 2.04 \text{cm}^{-1}$$

$$\Delta \Delta G_{\text{rotn}} = -0.02 \text{cm}^{-1}$$

where one can see that binding of the small ligand has a negligible effect on the rotational energy of the large enzyme and hence a negligible effect on the cooperativity.

### Vibrational component

The thermodynamic changes,  $\Delta G$ ,  $\Delta H$  and  $\Delta S$  for both the ground and excited vibrational state terms were calculated using a short BASIC programme on an Apple microcomputer. A listing of the programme is given in Appendix 1.

Very large changes occur on binding the first ligand if  $\nu_E^{\text{sc}}$  is low enough, while changes on binding the second ligand are much smaller and not as dependent on  $\nu_E^{\text{sc}}$ . Shown in Table 2.4 is a set of results for a free enzyme scissor frequency of  $25 \text{cm}^{-1}$ .

The large number of numerical results obtained are shown on the following set of graphs. These show

- i. Enzyme scissor frequency of  $EL$  and  $EL_2$  complexes versus free enzyme scissor frequency  $\nu_E^{\text{sc}}$  (Figure 2.5).
- ii. Ground state free energy changes versus  $\nu_E^{\text{sc}}$  (Figure 2.6).
- iii. Excited state free energy changes versus  $\nu_E^{\text{sc}}$  (Figure 2.7).
- iv. Excited state, enthalpy changes versus  $\nu_E^{\text{sc}}$  (Figure 2.8).
- v. Excited state, entropy changes versus  $\nu_E^{\text{sc}}$  (Figure 2.9):

remembering that the ground state free energy changes equal the ground state enthalpy changes and that there are no ground state entropy changes.

Table 2.4 A typical set of results for the scissors<sub>1</sub> model using a free enzyme scissor frequency of 25 cm<sup>-1</sup>.

TEMPERATURE= 298  
ENZYME ANGLE(RDMS)= 1  
SITE SEPARATION(ANGSTROMS)= 30  
  
ENZYME MASS(A.M.U)= 25000  
LIGAND MASS(A.M.U)= 250  
  
ENZYME SCISSOR FREQ.(HZ)= 7.495E+11  
LIGAND-ENZYME BOND FREQ.(HZ)= 9E+13  
  
EL SCISSOR FREQ.=7.93372508E+12  
EL DAMP. FREQ.=9.03459033E+13  
  
EL2 SCISSOR FREQ.=1.11949202E+13  
EL2 DAMP. FREQ.=9.06904873E+13  
EL2 UNDAMP. FREQ.=9E+13  
  
GROUND STATE ENTHALPY CHANGES  
Y.Z MOTION OF LIGANDS IGNORED  
  
GRND. STATE VIBRATION FREE ENERGIES  
  
DG1=DH1=1626.65625  
DG2=DH2=1561.20399  
DDG=DDH=-65.45226  
  
ZERO ENTROPY CHANGE IN GRND STATE  
  
VIBR. ENERGY CHANGES  
  
FREE ENERGIES  
  
DG1=382.625504  
DG2=30.3520313  
DDG=-352.273473  
  
ENTHALPIES  
  
DH1=-92.6299937  
DH2=-28.5458575  
DDH=64.0841362  
  
ENTROPIES  
  
DS1=-1.59481711  
DS2=-.197643922  
DDS=1.39717319  
  
ENTROPY\*TEMP.  
  
T\*DS1=-475.255498  
T\*DS2=-58.8978668  
T\*DDS=416.357609

SCISSOR  
FREQUENCY  $\text{sec}^{-1}$

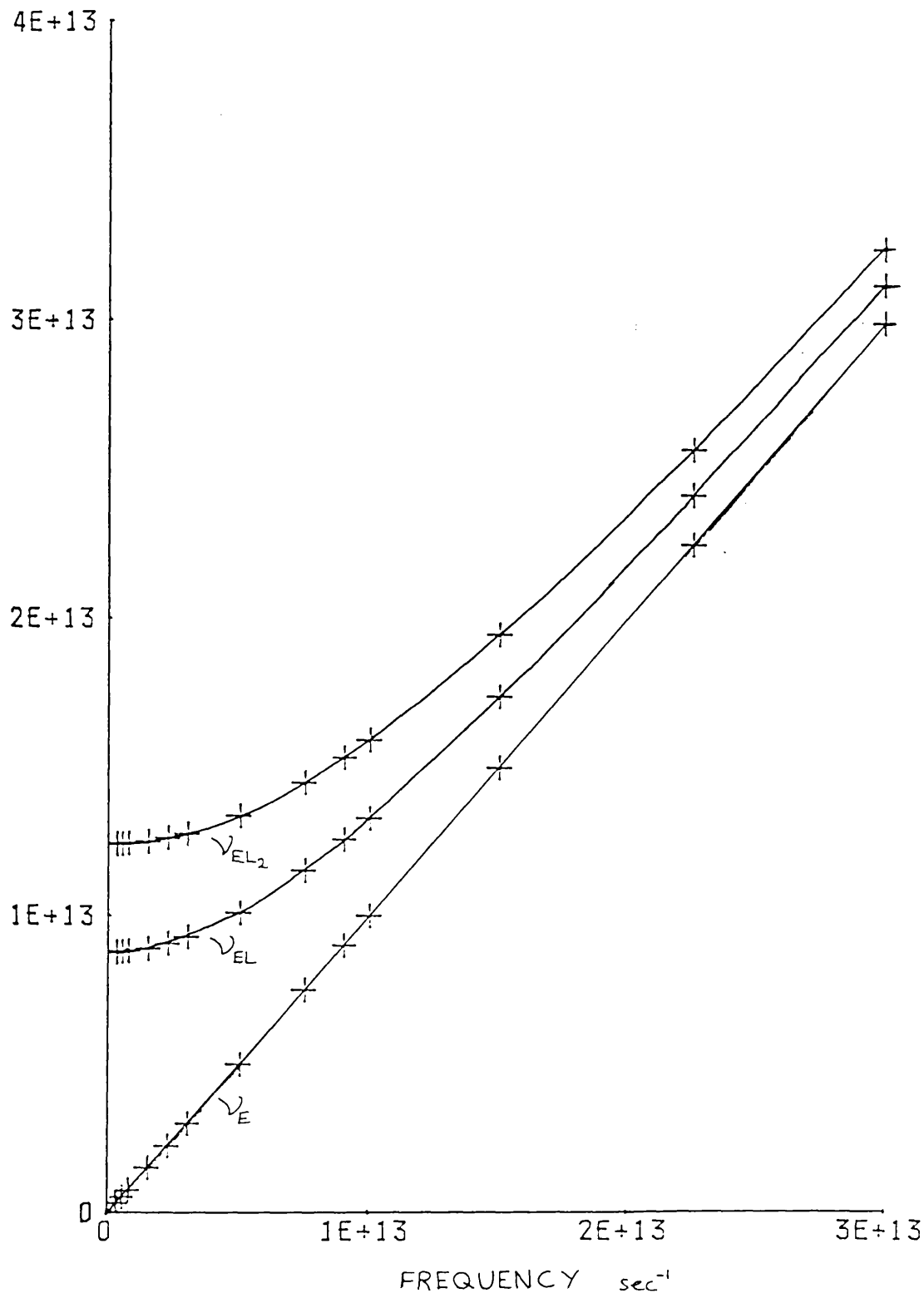


Fig. 2.5 A graph of the scissors frequency of the enzyme-ligand complexes versus unliganded scissor frequency.

FREE  
ENERGY  
CHANGE  
 $\text{cm}^{-1}$

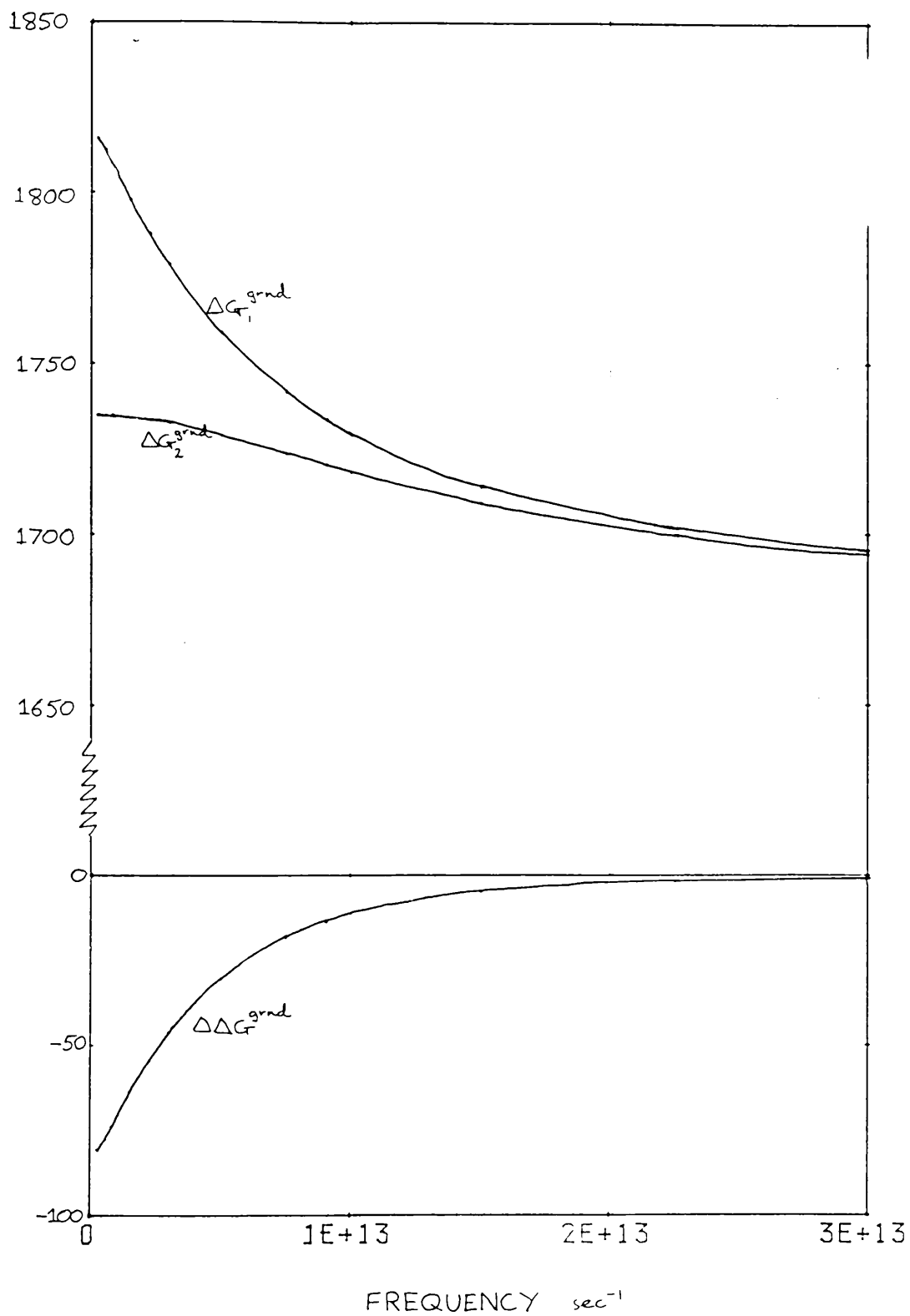


Fig. 2.6 Free energy changes in ground vibrational states on binding ligands against unliganded sensor frequency.

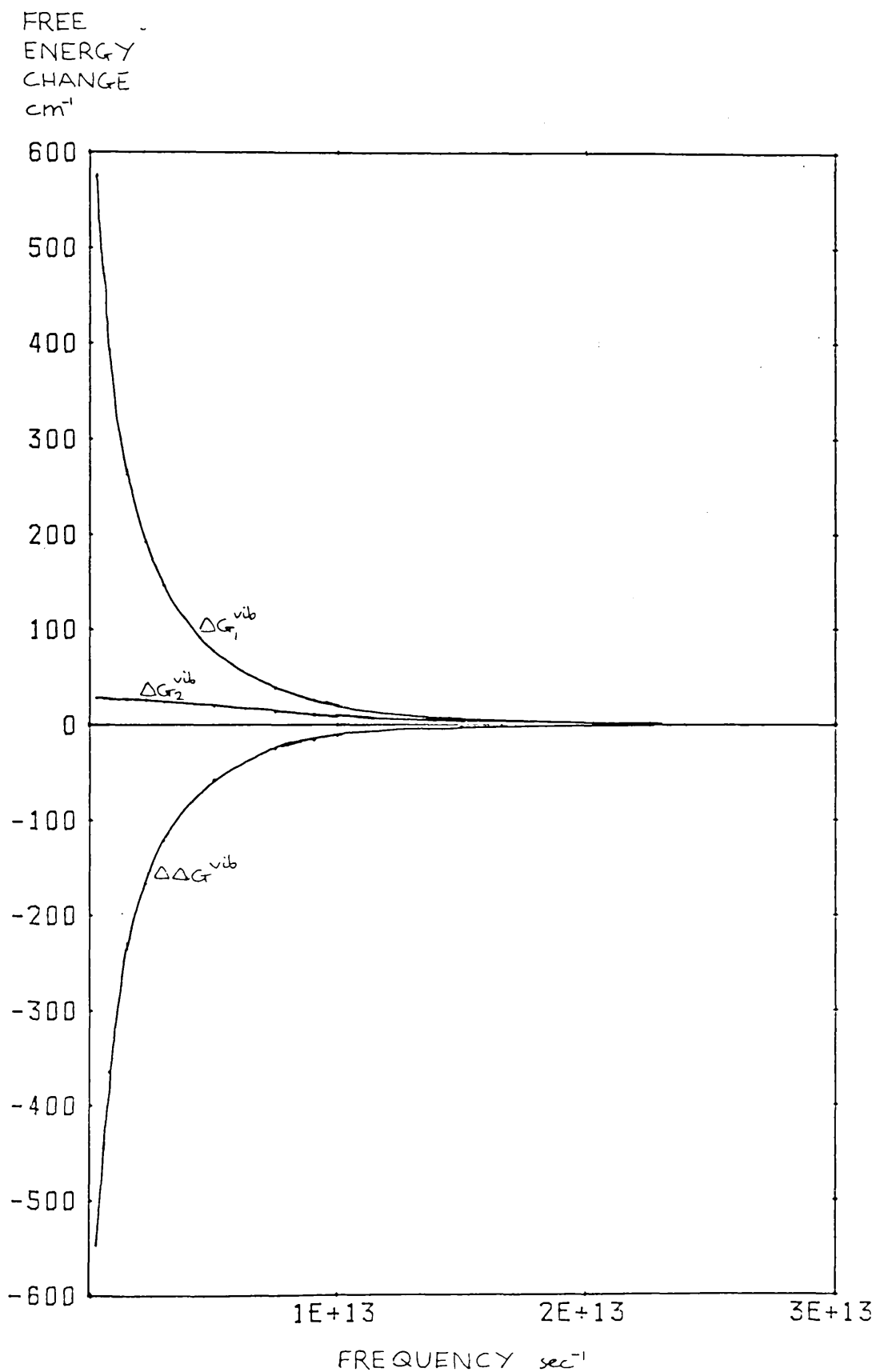


Fig. 2.7 Free energy changes in excited vibrational states against unliganded scissor frequency.

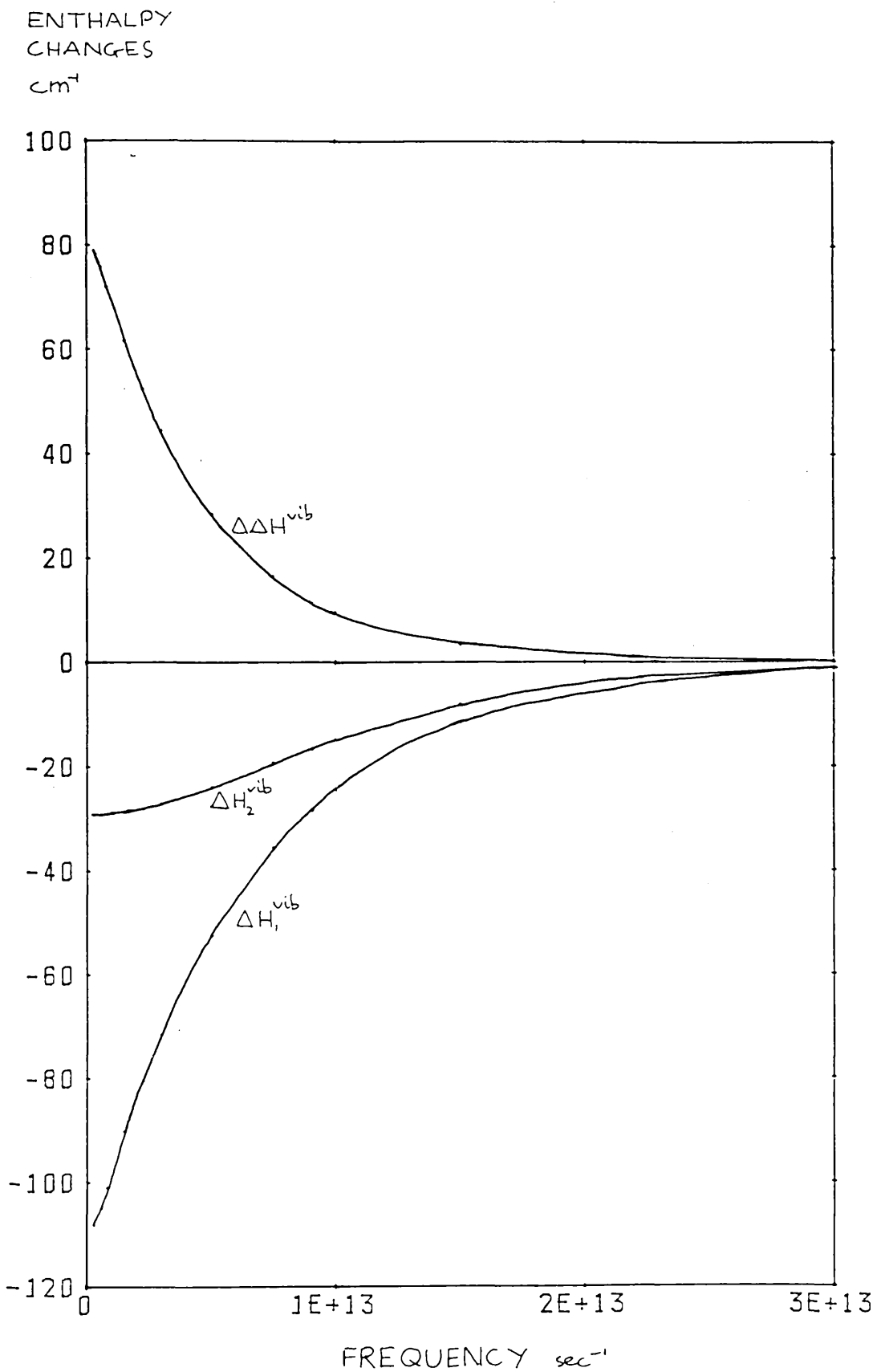


Fig. 2.8 Enthalpy changes in excited vibrational states against unliganded scissor frequency.

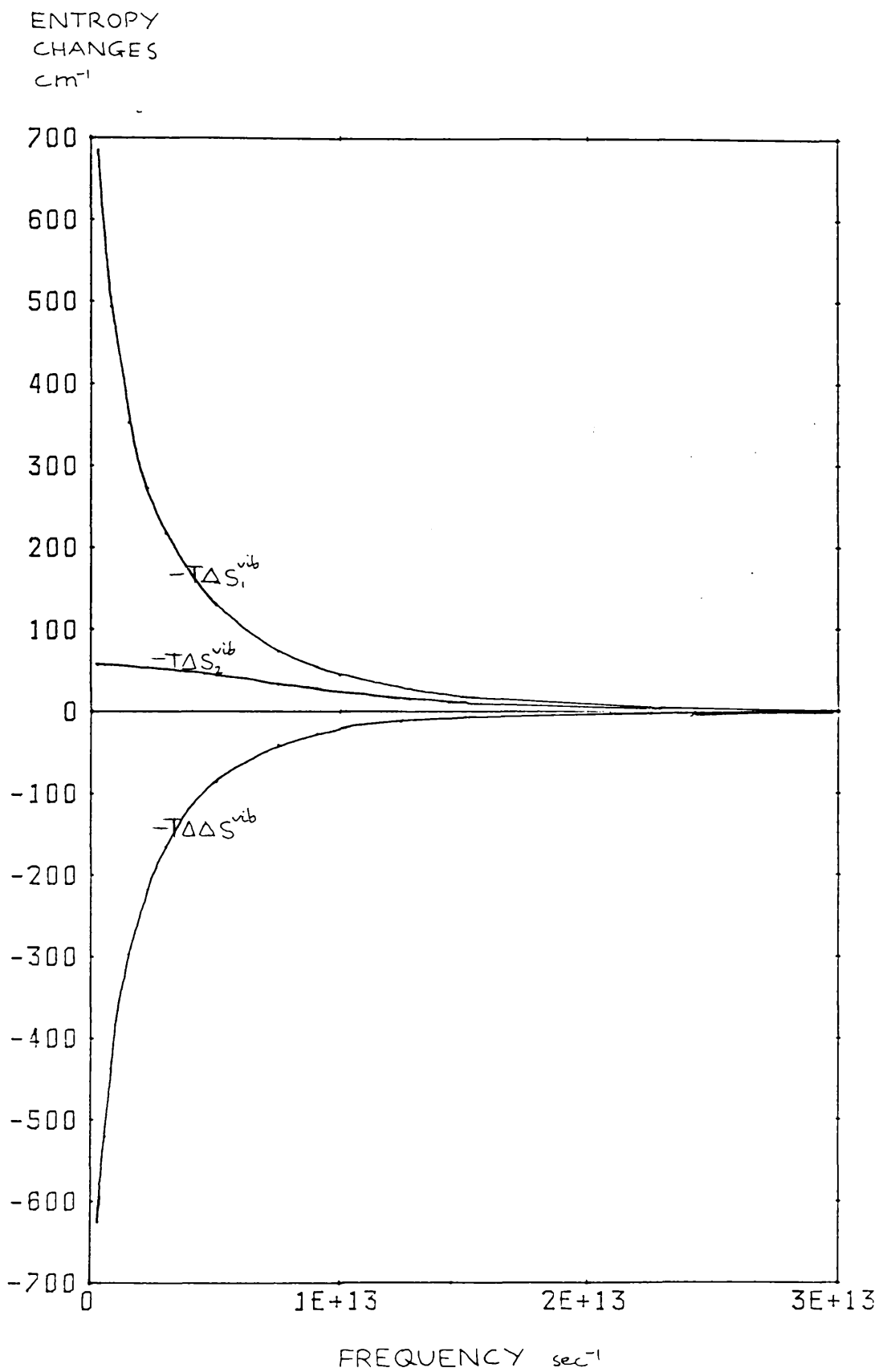


Fig. 2.9 Entropy changes in excited vibrational states against unliganded scissor frequency.

From these graphs it can be seen that the largest cooperative effects occur for free enzyme scissor frequencies of less than  $\sim 200\text{cm}^{-1}$ , in other words only for thermally excited vibrations.

The first graph (Figure 2.5) shows the scissor frequency of the liganded enzymes, EL and EL<sub>2</sub>, versus the free enzyme scissor frequency. On binding the first ligand, the frequency of the thermally excited low frequency scissor mode increases dramatically in frequency with a collapse of the excited states population into the ground state and a release of thermal energy. The binding of the second ligand produces a much smaller increase in the scissor frequency. One can imagine the free enzyme vibrating at low frequency with a large amplitude due to the highly excited states, encountering the ligand which binds without changing the mean conformation, as measured by the angle  $\theta$ , but which restricts the amplitude of the scissor motion severely.

This also reduces the scale of motion in the other binding site which is now held closer to the structure to which the second ligand prefers to bond. This ligand then finds it easier to bind with a consequent reduction in the thermodynamic parameters  $\Delta G$ ,  $\Delta H$  and  $\Delta S$ .

The free energy, enthalpy and entropy changes for the binding of each ligand shown in Figures 2.6 to 2.9, are positive, negative and negative respectively, but these apparently unfavourable changes will be more than compensated by the energy

released by formation of the enzyme - ligand bonds and hence the two binding reactions can be made to be favourable. The quantities  $\Delta\Delta G$ ,  $\Delta\Delta H$  and  $\Delta\Delta S$  however, are independent of this bond formation energy, which will be the same for each ligand because the two binding sites are identical, and are of the correct size.

$\Delta\Delta G$  is increasingly negative for lower scissor frequencies and shows that this simple model exhibits positive cooperativity between its two binding sites. The magnitude of the effect is such that one or two of these modes in a real enzyme could account for the interaction free energies observed in allosteric proteins. Comparison of the  $\Delta\Delta G$  values for the ground vibrational state and for the excited states shows that the excited vibrational states are responsible for the major part of the cooperative interaction energy.

The change in enthalpies,  $\Delta\Delta H$ , is much smaller and positive indicating that binding of the first ligand is more exothermic than binding of the second due to the conversion of the highly excited low frequency scissor mode into a non-excited high frequency mode with a consequent release of heat.

The entropy change,  $\Delta\Delta S$ , more than compensates for the effect of enthalpy and is responsible for the higher binding affinity of the second ligand despite the fact that the first ligand binds more exothermically. The change is positive because  $\Delta S_1$  is much more negative than  $\Delta S_2$ . These unfavourable negative entropy changes caused by the depopulation of excited vibrational

energy levels can be assumed to be compensated by other entropy changes, having approximately equal magnitude for binding each ligand, which would occur in a real enzyme - ligand system.

This very simple system therefore supports the predictions of the general dynamic allostery model presented in the previous sections. The nature of the low frequency mode which connects the two binding sites could be a global mode such as a hinge bending mode which would bear the closest similarity to the scissor mode discussed, the stretching of an  $\alpha$  helix or, the twisting of  $\alpha\beta$  sheet, the frequency of which could change if the ligand became bound to the secondary structure.

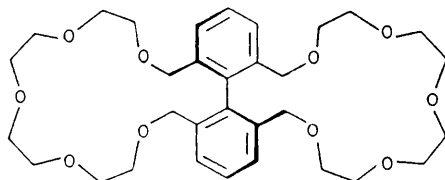
## CHAPTER 3

### 3.1 The Structure and Dynamics of an Allosteric Model Organic Compound

Recently an organic molecule of small molecular weight (590 a.m.u.) has been synthesised by Prof. J. Rebek Jr. and co-workers which possesses positive cooperativity between its two identical ligand binding sites. Two recent summaries of this and related work have been published (Rebek, 1984, Rebek et al., 1985).

The molecule is a macrobicyclic polyether of the structure shown in Figure 3.1 which binds the mercury atom of mercuric cyanide,  $\text{Hg}(\text{CN})_2$ , in the centre of each ether ring.

Figure 3.1. Molecular structure of Rebek's compound



Prof. Rebek kindly supplied samples of the unliganded and fully liganded compound for this study.

Rebek's studies initially showed that the first ligand binds with an association constant of  $10\text{M}^{-1}$  close to the  $13\text{M}^{-1}$  found with a monocyclic counterpart and that binding of the second ligand was enhanced, once statistical factors were taken into

account, by an order of magnitude to  $100M^{-1}$  (Rebek et al., 1981). The ligand binding rates were sufficiently slow for a n.m.r. lineshape analysis of the populations of unliganded, singly liganded and fully liganded molecules present under varying ligand concentrations to be performed. These populations could also be calculated by using the equations given by Weber (1975) and the association constants. The results are shown in Figure 3.2 which indicate that the maximum percentage of singly liganded complex obtainable is 37% occurring at a free ligand concentration of 31.6mM (Rebek et al., 1985). It was suggested that the cooperativity was caused by a restriction of the possible conformations of the unliganded ether ring on binding of a ligand to the other ring. This restriction would be communicated through the biphenyl group. This was recently confirmed when the x-ray structure of the fully liganded complex was published, see Figure 3.3 (Onan et al., 1983).

The mercury atom formed bonds with all five oxygen atoms in the ring which fixed the orientation of the two phenyl rings relative to each other thereby restricting the possible conformations of the other ether ring. This also explained the lack of cooperativity found with a similar macrobicyclic polyether possessing an extra ether group in each ring (Rebek et al., 1980). It was found that an oxygen atom adjacent to the biphenyl group in a monocyclic counterpart with six ether groups did not form a bond with the ligand with the result that the flexibility of the biphenyl group was not restricted, see Figure 3.4.

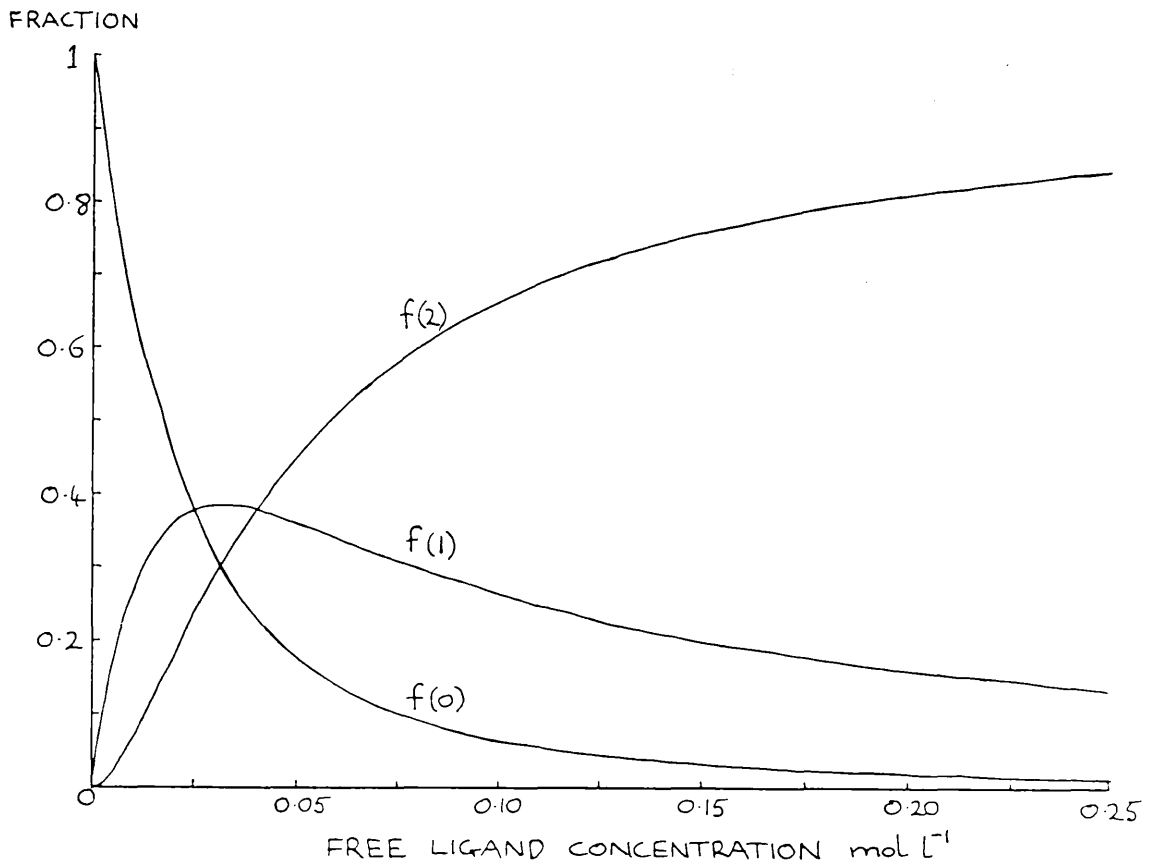


Fig. 3.2 The fraction of the ether with 0,1 or 2 ligands bound as a function of ligand concentration using the experimental association constants.

Fig. 3.3 The X-ray structure of the macrobicyclic ether with two ligands bound. Hydrogen atoms are omitted. (from Onan et al, 1983)

Fig. 3.4 The X-ray structure of a monocyclic ether with a larger ether ring showing the unliganded oxygen atom, number 16. (from Onan et al, 1983)



The resemblance of the macrobicyclic ether to the theoretical scissors model discussed earlier can be seen if the biphenyl group is considered to be the torsional hinge of the scissors. The thermodynamic behaviour of the molecule was determined by studying the temperature behaviour of the ratio of the two association constants. This led to the conclusion that the cooperativity was entropic in origin with  $\Delta S_2 - \Delta S_1 = \Delta\Delta S = -18.5 + 16.5 = + 2$  e.u. and that the enthalpies of binding the two ligands were identical with  $\Delta H_1 = \Delta H_2 = -7.3$  kcal mol<sup>-1</sup>. This gives a value of  $\Delta\Delta G_{tot}$  at 290K of  $-0.580$  kcal mol<sup>-1</sup>. This behaviour is exactly that expected in the dynamic allostery model from a classical mechanics viewpoint where vibrational modes increase slightly in frequency and the range of atomic thermal motion decreases upon ligand binding.

There will be a favourable contribution to the cooperativity from the conformational restrictions imposed by ligand binding where the width of the probability distribution of the atomic positions in the ether rings will be reduced, with or without a shift in the mean positions. This could be most easily verified by a comparison of the Debye & Waller thermal parameters of the unliganded and liganded x-ray crystal structures, unfortunately this data exists only for the liganded form but this still shows smaller uncertainty in the position of the oxygen atoms and the biphenyl group than in the ether carbon atoms. The stiffer structure of the liganded form could also be hinted at by the different physical forms of the unliganded and liganded compounds. The first of which is a waxy solid while the second is a crystalline, hard solid. Thermal parameters do exist,

however, -for the monocyclic ether ring containing 6 ether groups which bind  $\text{Hg}(\text{CF}_3)_2$  with the x-ray crystal structure shown in Figure 3.4.

One of the benzylic oxygen atoms does not bond to the mercury atom with the result that it and the adjacent carbon atoms have a much larger range of movement perhaps similar to that of the unliganded bicyclic polyether rings.

Plots of the isotropic temperature factors in the two x-ray structures are shown in Figure 3.5. The isotropic temperature factors are the averages of the three anisotropic temperature factors for each atom obtained from Onan *et al.*, (1983).

It can be seen that the smaller compound has larger temperature factors than the bicyclic compound which may be due to different crystal structures and static disorder, however, the general trends are the same with the biphenyl groups having smaller thermal motions and the oxygen atoms bound to the ligand having small temperature factors than the adjacent carbon atoms. The unbound oxygen atom and its two adjacent carbon atoms shown starred in the graph of the monocyclic compound, have much larger thermal motions than the equivalent atoms on the opposite side of the ether ring. These larger motions may be typical of those found in the unliganded bicyclic compound, which would confirm that ligand binding causes a stiffening of the bicyclic structure.

It is difficult to make a quantitative estimate of the conformational contribution but if the changes in the thermal parameters shown in Figure 3.5 between the unbound carbons and oxygen of the monocyclic ether and the fully liganded compound are meaningful, then decreases of 5% to 10% in the thermal motion, if

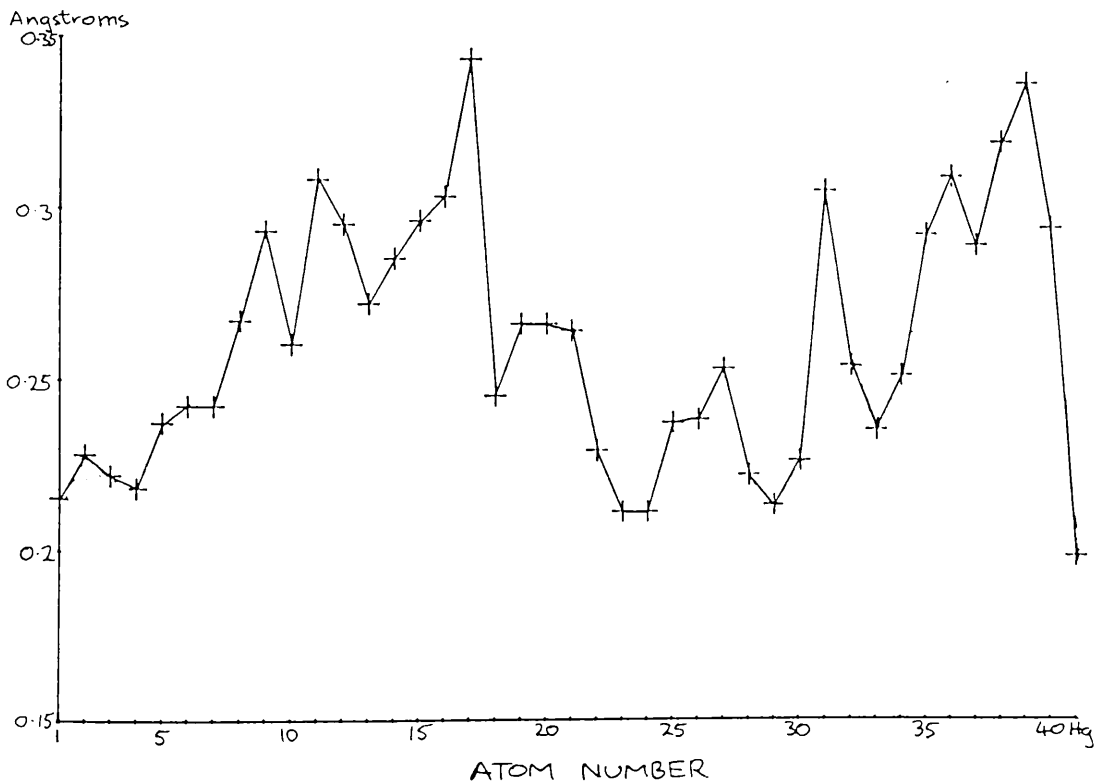
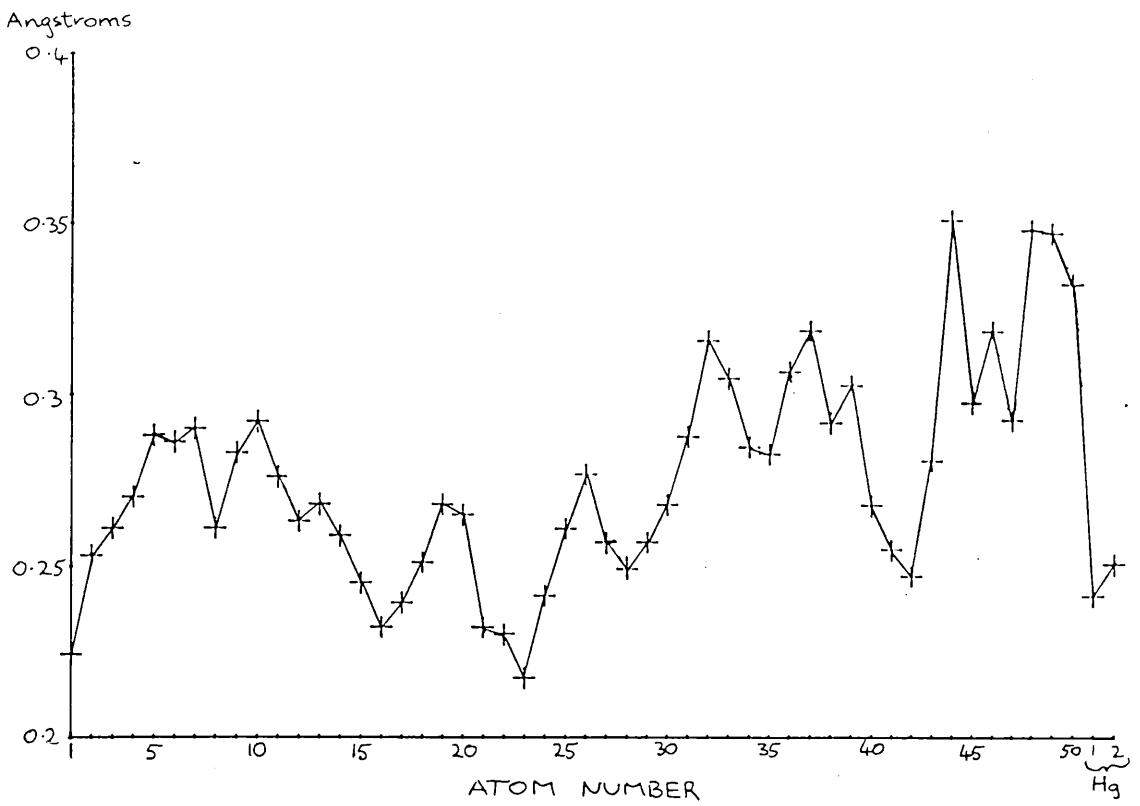


Fig. 3.5 The X-ray temperature factors for the molecules in figures 3.3 and 3.4. The numbering of the atoms is as in the earlier figures. (from Onan et al, 1983)

summed over all the oxygen atoms in the ether rings (5 atoms) would give a sizeable contribution to the cooperative free energy  $\Delta\Delta G_{\text{Total}}$ .

Since  $\Delta\Delta G_{\text{Total}} = -2.427 \text{ kJmol}^{-1}$  at 290K for the bicyclic compound and from Chapter 2  $\Delta\Delta G_i = 2kT \delta_i$ , where  $\delta_i$  is the fractional change in the thermal motion, in the singly liganded molecule, of atom  $i$  and its equivalent atom  $i'$  in the other binding site, then for a fractional change of 0.05 in all the oxygen atoms one finds that

$$\begin{aligned} \Delta\Delta G_{\text{oxygen atoms}} &= 5 \times -2 \times 8.314 \times 290 \times 0.05 \\ &= 1205 \text{ J mol}^{-1} \\ &= 49\% \text{ of } \Delta\Delta G_{\text{tot}} \end{aligned}$$

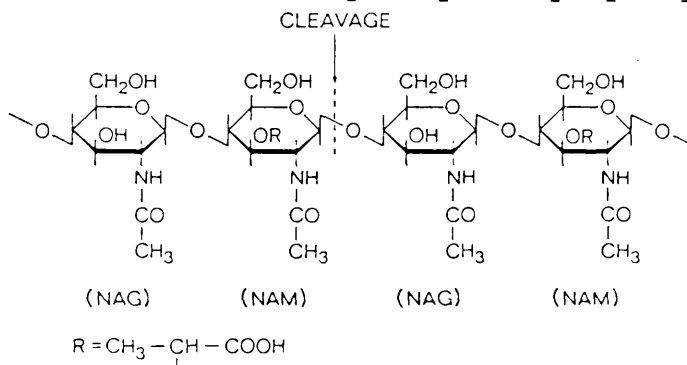
This shows that the dynamic conformational contribution could play a substantial part in the cooperativity of this molecule.

The vibrational contribution to the cooperativity of the bicyclic ether where global low frequency modes of vibration spanning both binding sites would be converted into higher frequency vibrations was studied by Raman and infra red spectroscopy of the unliganded and fully liganded compounds. Several complexes were also prepared with intermediate ligand concentrations for Raman spectroscopy to see if any singly liganded complex could be detected. These results are given in Chapter 5.

### 3.2 Introduction to the Structure and Dynamics of Lysozyme

Hen white lysozyme is a small globular enzyme of molecular weight 14600 a.m.u. composed of a single chain of known sequence consisting of 129 amino acid residues. Its function is to break up polysaccharides consisting of  $\beta(1-4)$  linked alternating N-acetyl-glucosamine (NAG) monomers and N-acetyl-muramic acid (NAM) monomers typically found in bacterial cell walls by hydrolysis of the  $\beta(1-4)$  linkage as shown in Figure 3.6.

Figure 3.6. The structure of the polysaccharide typically found in bacterial cell walls and hydrolysed by lysozyme.



The crystal structure was first solved in 1965 by Blake et al., for a crystal with tetragonal unit cell. The structure of lysozyme with the specific inhibitor tri-N-acetyl glucosamine (tri NAG) bound was solved by the same group, Blake et al., in 1967 again for a crystal with tetragonal symmetry. It was found that the tri NAG bound along one half of a cleft which ran across the lysozyme effectively creating a bilobed enzyme. This cleft was lined with non polar side chains of residues which bound with non polar regions of the substrates, and hydrogen bonding sites for the acylamino and hydroxyl groups. This cleft can be divided into 6 binding sites A-F each of which is associated with a particular monosaccharide of the polymer. Site A is near the

disordered loop of residues 69 to 74 along the top of one domain. NAM can only bind in sites, B, D and F whilst NAG can bind in any site. The hydrolysis reaction occurs between sites D and E by formation of a carboxonium ion followed by general acid catalysed expulsion of the alcohol involving the carboxyl group of Glu35. The ionised carboxyl group of Asp52 stabilises the carboxonium ion. The initial x-ray studies suggested that the glucopyranose ring in site D was distorted into a sofa configuration; however it is now believed that the strain in this site is electrostatic in nature and not conformational. Controversy still exists over the correct mechanism for catalysis with a recent computer simulation by Post and Karplus (1986) suggesting an alternative route. The cleft was found to close slightly ( $<1\text{\AA}$ ) when the inhibitor was bound and a loop consisting of residues 69 to 74 along the top of one domain, hardly visible in the free enzyme, became ordered when the ligand bound.

This loop has been found to have various conformations which it can take up depending on the symmetry of the crystal. In the triclinic crystal a different conformation is found (Moult et al., 1976). There are also significant changes in the main chain and side chain structure of residues on the surface of enzyme due to the more compact triclinic packing of the protein in the crystal lattice. This affects the temperature factors and the ability to form crystals with inhibitor bound. Kurachi et al., (1976) found that oligomers larger than (NAG)<sub>2</sub> could not form crystals with the enzyme. Lysozyme crystals of all symmetries so far discovered (the above two plus monoclinic) convert to an orthorhombic form at physiological temperatures (40°C) (Berthou

et al., 1983) where several groups become better ordered due to crystal packing effects. Substrate binding is still hindered in this structure. The temperature factors which describe thermal motion of the atoms change considerably at the transition temperature from one structure to another, and this has been ascribed to either a crystal packing effect or as "a change in a major vibrational mode of the lysozyme molecule" causing the crystal packing to change to accommodate it.

The residues which become ordered in the orthorhombic crystal Trp62 and Pro70, and indeed the whole disordered loop residues 67 to 94 have been found in several computer simulations, to be heavily involved in a large low frequency vibration of the two domains about the active site cleft termed "hinge bending". This hinge bending motion could account for the closing of the cleft on binding of tri NAG and the obstruction of this mode by the crystal packing would explain the difficulty in binding tri NAG in this crystal. The first simulation of the hinge bending mode (McCammon et al., 1976) treated the enzyme as two lobes which moved according to the Langevin damped oscillator equation. The motion was found to be overdamped with a frequency of  $4.2\text{cm}^{-1}$  when relaxation of the structure was taken into account, and it was suggested that the motion might become under-damped in the presence of a substrate. A more sophisticated calculation of all the torsional normal modes has recently been performed (Levitt, 1985) which shows that;

- i. 60 normal modes out of the 471 calculated occur below  $20\text{cm}^{-1}$ ,
- ii. the lowest 8 modes account for 70% of the total enzyme motion and
- iii. the lowest frequency  $2.98\text{cm}^{-1}$  shows clearly the hinge

bending motion, Figure 3.7.

Another calculation of this hinge bending mode by a different method (Brooks & Karplus, 1985) gives an almost identical motion at a frequency of  $3.6\text{cm}^{-1}$ . These calculations both show particularly large motions for residues on the surface of the enzyme, such as numbers 67 - 94, and also for residues 101 - 105 which lie in the other domain along the lip of the cleft. Molecular mechanics calculations (Post et al., 1986) on lysozyme with and without hexa-NAG bound, show that the possible motions of enzyme atoms change on ligand binding, particularly along the active site where they are smaller, and in the loop of residues 67-88 which move significantly more in the presence of hexa-NAG. The effect of binding then is to reduce motion of atoms in the active site while those on the surface move more so as to close the hinge on the substrate.

What experimental evidence is there for a, low frequency (undamped) or slow (overdamped) large motion in lysozyme and b, for their involvement in enzyme catalysis?

Raman spectroscopy shows two low frequency bands at  $25\text{cm}^{-1}$  and  $75\text{cm}^{-1}$  in crystalline lysozyme, the lower of which disappears in solution due to overdamping (Genzel et al., 1976; Peticolas, 1979). These bands will be a superposition of a large number of protein normal modes. The  $75\text{cm}^{-1}$  band may still be visible in solution because it is composed of more localised vibrations, such as stretches of helices, which would not be damped as much by the solvent. Inelastic neutron scattering has also shown modes at  $25\text{cm}^{-1}$ ,  $75\text{cm}^{-1}$ ,  $112\text{cm}^{-1}$  and  $140\text{cm}^{-1}$  in a polycrystalline sample (Bartunik et al., 1982) with the  $75\text{cm}^{-1}$  band

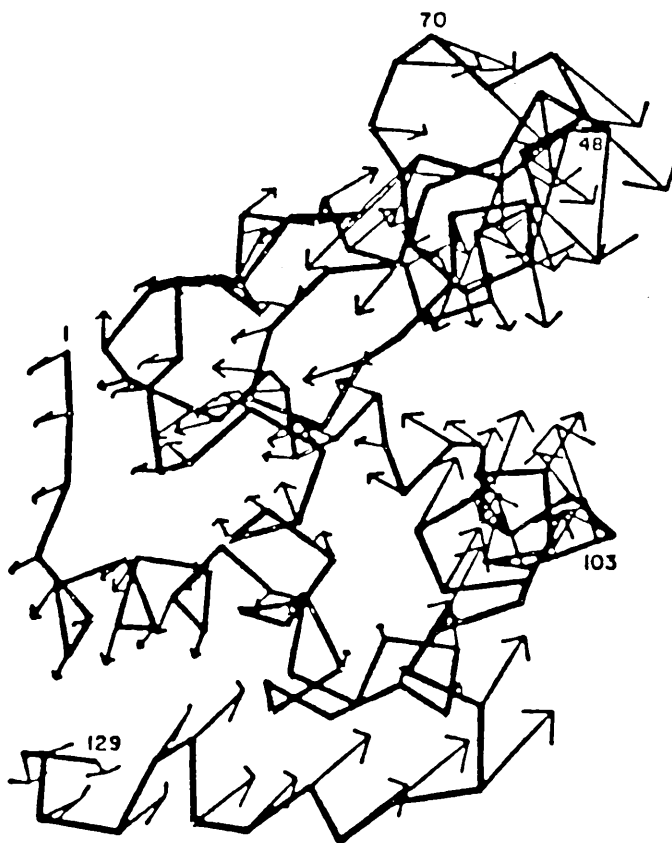


Fig. 5.7 The backbone structure of lysozyme and the hinge bending mode calculated by normal mode analysis. (from Levitt et al, 1985)

being particularly broad. This band was assigned to longitudinal accordian-like motions of  $\alpha$ -helices. Below  $50\text{cm}^{-1}$  it is also stated that there is a "clear dependence on whether the enzyme is in solution or in the polycrystalline form, and on binding of the NAG inhibitor". Unfortunately no spectra or further details of this phenomenon are given in the paper.

Several non-spectroscopic techniques have shown a stiffening of the lysozyme structure with a consequent change in its dynamic properties when a ligand is bound. Proton exchange rates of tryptophan residues near the active sites are slowed by binding of NAG (Cassels et al., 1978). Studies of the compressibility of lysozyme crystals with and without tri-NAG bound (Morozova & Moroyou, 1982) show a 40% reduction in compressibility when the ligand is bound, most of which is attributed to a more compact, stiffer structure. Finally the closure of the active site cleft on ligand binding seen by x-ray crystallography implies changes in the dynamics and their involvement in catalysis.

As well as structural and dynamic studies of ligand binding by lysozyme, there have been many experiments on the energetics of binding of tri NAG which have yielded approximate binding energies of NAG and NAM to each of the sites A to F. The most favourable sites for tri-NAG to bind in are sites A, B and C as found in the crystal structure. Kuhara et al., (1982) showed that theoretically 98% of the bound NAG will be in these 3 sites. Dahlquist et al., (1966) found that there was very little hydrolysis of tri-NAG by lysozyme but that larger oligomers were extensively hydrolysed because they overlapped site D. The thermodynamics of binding of tri-NAG to lysozyme have been well

studied over the years. The following table summarises the data (Figure 3.8).

The high value of  $K^{assoc}$  of approximately  $1.2 \times 10^5 \text{ M}^{-1}$  makes tri-NAG a suitable molecule for binding to lysozyme to ascertain if there are any dynamic changes caused by binding. Bjurulf & Wadso (1972) found that the change in heat capacity on binding was approximately zero. Any decrease in the low frequency vibrations of the lysozyme would be revealed by a negative  $\Delta C_p$  (Sturtevant, 1977), however this could be offset by the decrease in exposure of hydrophobic groups and charged groups along the active cleft when the ligand shields them from the solvent, which would give a positive contribution to  $\Delta C_p$ .

Thermal and chemical denaturation of lysozyme is more difficult in the presence of tri-NAG (Pace & McGrath, 1980). Binding of the inhibitor stabilises the structure reducing the size of fluctuations, and shields many groups from the chemical denaturant guanidine hydrochloride slowing the denaturation.

TABLE 3.8 Thermodynamics of Lysozyme-TriNAG Binding

Association Constant $M^{-1}$	Free Energy Change $\Delta G$ $kJmol^{-1}$	Enthalpy Change $\Delta H$ $kJmol^{-1}$	Entropy Change $\Delta S$ $JK^{-1}mol^{-1}$	Ionic Strength	pH	Temperature	Reference
$1.52 \times 10^5$				0.1M	5	Room Temp.	Dahlquist et al (1966)
	-28.8	-56.8	-94.9	0.1M	5	25°C	Bjurulf & Wadso (1972)
$1.16 \times 10^5$					6.58	25°C	Schindler et al (1977)
	-29.6	-57.7	-92.9	0.1M	5.2		Banerjee et al (1975)
$1.1 \times 10^5$	-20.06				5.4	25°C	Chipman et al (1967)
	-30.25	-59.8	-99.6	0.1M	5.3	25°C	Banerjee & Rupley (1973)
		-50.2			5	23°C	Stasiv et al (1973)
$1.01 \times 10^5$				0.3M	7.5	25°C	Ikeda & Hamaguchi (1976)



system increases the nucleophilic strength of this group by a factor of  $10^3$ . This involves the ionised carboxylate group of Asp102 being hydrogen bonded to the imadazole ring of His57 which is in turn hydrogen bonded to the hydroxyl group of Ser 195. This has the effect of drawing the hydroxyl proton away from Ser 195, through His 57 causing the hydroxyl group of Ser 195 to be a stronger nucleophile. The hydroxyl proton is then lost to the imidazole nitrogen as the hydroxyl group attacks the carbonyl carbon of the substrate to form the tetrahedral intermediate. The x-ray crystallographic structure shown in Figure 3.10 has the residues involved in the charge relay system marked.

Trypsin is exceptionally strongly inhibited by a small polypeptide first isolated by Kunitz called basic pancreatic trypsin inhibitor (BPTI), consisting of 56 residues, with a molecular weight of 5,600. This inhibitor binds to trypsin with one of the largest association constants ever found. Several experimental results are given in Figure 3.12. The association constant and the enthalpy of formation are strongly pH dependent  $K_{\text{assoc}}$  and  $\Delta H_{\text{form}}$  both decreasing. It has also been found that 100% inhibition of the active trypsin in a solution occurs at a mole ratio of 1.07 moles inhibitor for 1 mole of active trypsin, indicating almost complete association to form the 1:1 complex (Keil-Dlouha et al., 1971).

The x-ray crystal structures of trypsin, BPTI and trypsin - BPTI complex have all been solved to high resolution (Rigbi, 1971; Ruhlmann et al., 1973) and the results help explain the very high association constant. The structure of BPTI is shown in Figure 3.11. The narrow end of the pear shaped inhibitor

Fig. 3.10 The backbone X-ray structure of trypsin.  
(from Fersht, 1977)

Fig. 3.11 The backbone X-ray structure of BPTI.  
(from Karplus & McCammon, 1977)

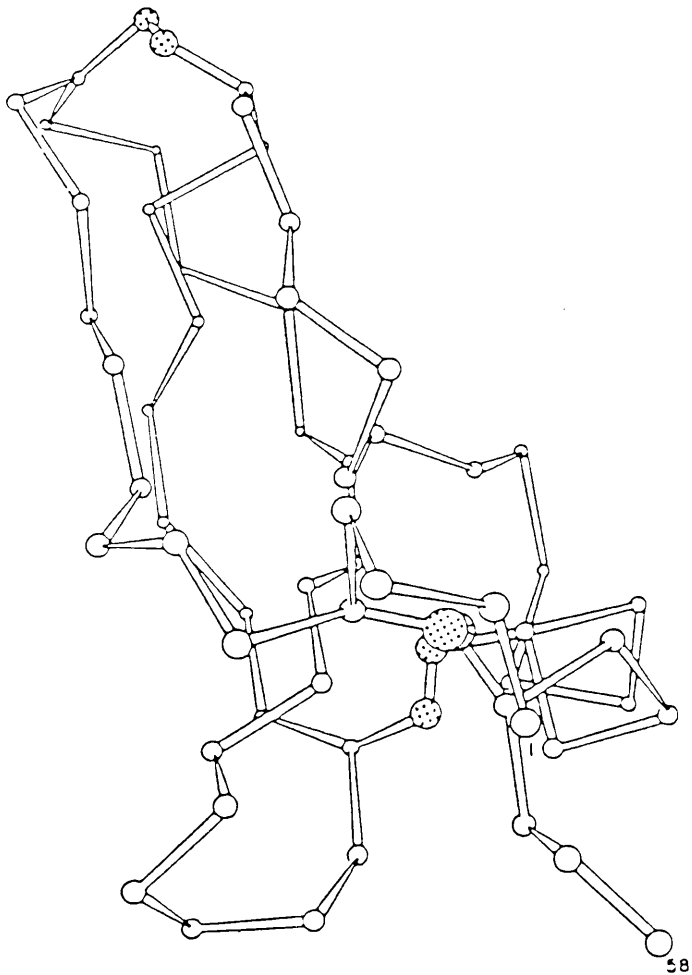
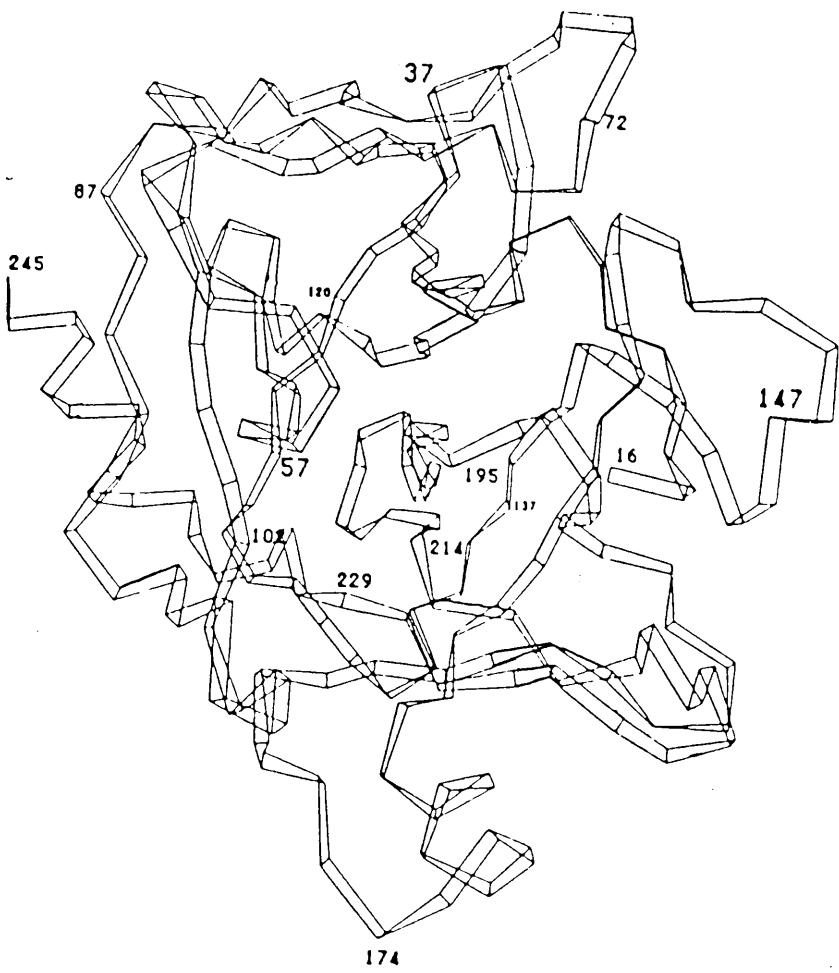


TABLE 3.12

Association Constants for Trypsin and BPTI

Association Constant ( $M^{-1}$ )	pH	Temperature	Ionic Strength	Reference
$1.667 \times 10^{13}$	8	$25^{\circ}C$		Vincent and Lazdunski (1972)
$1.04 \times 10^{10}$	8	$21^{\circ}C$	0.1M	Antonini et al (1983)
$1.8 \times 10^{12}$	7.6	$25^{\circ}C$		Golikov et al (1975)

molecule fits exactly into the hydrophobic pocket of the active site in essentially the same conformation as a bound substrate. The enzyme inhibitor complex is bound together by a covalent bond between the carbonyl carbon of Lys 15 in the inhibitor and the oxygen of Ser 195 to form the tetrahedral complex seen in the third step of the reaction mechanism Figure 3.9. Numerous hydrogen bonds are formed throughout the interface area between the trypsin and the inhibitor further stabilising the complex. Even if hydrolysis of Lys 15 does occur the released amine cannot escape from the active site because of the bulk of the inhibitor. Hydrolysis of the inhibitor can only occur if its stability is reduced by cleaving a disulphide bond in its structure. This removes the conformational constraints in the active site and hydrolysis occurs (Wilson & Laskowski Sr., 1971).

The dynamics of trypsin, BPTI and trypsin-BPTI complex have been extensively studied by hydrogen exchange techniques while BPTI has also been the subject of numerous molecular mechanics and normal mode simulations primarily due to its small size.

A review covering the early molecular mechanics simulations of BPTI which showed small high frequency vibrations about the x-ray structure with the appearance of slower collective motions as the simulations increased in length, is given by McCammon & Karplus (1983). The 132psec simulation by Levitt (1983a,b) showed the existence of multiple conformational minima on the potential energy surface of BPTI in which the molecule would perform localised high frequency vibrations as found in the shorter simulations, before jumping over some energy barrier to a

different - minima and conformation were it vibrated about a slightly different conformation. This behaviour would be expected in Frauenfelders conformational substates model of protein dynamics. Swaminathan et al., (1982) analyse the motions of atoms, residues and groups of residues with the damped Langevin harmonic oscillator equation (Chandrasekhar, 1943), and find collective motions of large amplitude occurring with periods of 1 to 10 psec ( $3-30\text{cm}^{-1}$ ). The clearest picture of motions in BPTI from the computational viewpoint comes from the recent normal mode simulations where it is assumed that all atoms are moving in a harmonic potential (Brooks & Karplus, 1983; Go et al., 1983; Levitt et al., 1983; Levitt et al., 1985).

It was found that ignoring anharmonicities in the atomic potential had little affect on the atomic motions (Brooks & Karplus, 1983; Go et al., 1983). The lowest frequency mode found by Levitt et al., (1985) is shown in Figure 3.13. No simulations of trypsin-BPTI complex have been performed but one would expect that the low frequency motions of BPTI and presumably those of trypsin to be drastically affected.

The hydrogen exchange experiments on BPTI and on the inhibitor complex are supported by the computer simulations despite the fact that the H exchange experiments are studying processes on a much longer time scale than the simulations. This is because although the overall exchange rate itself may be small, the actual exchange and any motions required for it to take place can be very fast. BPTI H exchange has been studied by n.m.r. spectroscopy which allows individual hydrogen/deuterium exchange rates to be found for all exchangeable amide (N-H)

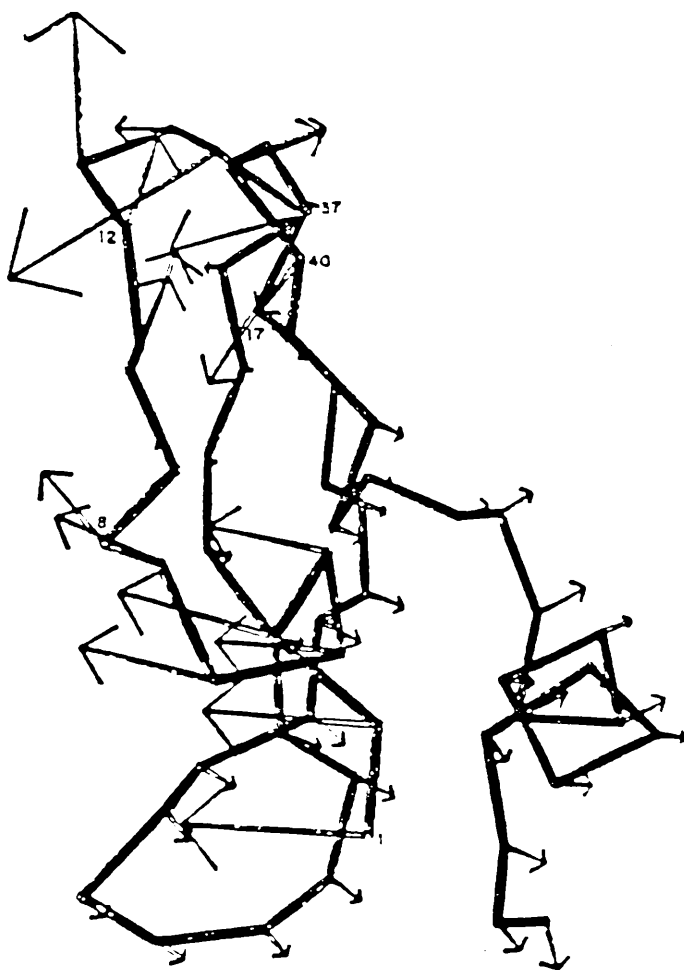


Fig. 3.13 One of the low frequency normal modes of BPTI. (from Levitt et al, 1985)

protons. - It is found that amide protons in the central stretch of the  $\beta$ sheet are very slow to exchange while those at each end of the sheet are much faster, though not as fast as those protons in other parts of the molecule. Attempts to explain this data have used either a global unfolding model where the protein structure opens up considerably allowing the solvent free access to the amide protons (Wagner & Wuthrich, 1979a,b) with the slowest exchange rates being correlated with the most infrequent fluctuations, or by a diffusion or "mobile defect" model whereby solvent molecules diffuse into the protein at rates which depend on the occurrence of small localised fluctuations of the protein structure (Matthew & Richards, 1983), the slowest rates then being found for "buried" protons.

These two models have both been used in a recent study of BPTI (Roder et al., 1985) under a wide range of pH and temperature. They conclude that solvent diffusion and global fluctuations both occur but their relative importance changes with experimental conditions. The  $\beta$  sheet core protons which exchange very slowly have a high activation energy and require large unfoldings, while protons with a low activation energy exchange quickly from positions which deviate little from the native structure. Solvent diffusion and small fluctuations of the protein structure account for the exchange rate of these protons. Different sections of the distribution of internal motions of the protein, as determined by the proton exchange rates, are sampled as the time window studied by the experiment changes. Salemne (1982) proposed that secondary structure features of BPTI can explain the very slow rate of exchange of the  $\beta$  sheet

core protons. A model of the  $\beta$  sheet in BPTI is shown to be able to undergo very large twisting and stretching motions without breaking any of the hydrogen bonds in the sheet, with the result that the amide protons are unable to react with solvent molecules unless an exceptionally large fluctuation occurs which overcomes the activation energy barrier for breaking the hydrogen bonds. Conformational restrictions at the ends of the  $\beta$  sheet in BPTI can explain why the amide protons in these regions exchange more quickly than those in the central portion. One could say that the  $\beta$  sheet can "soak up" a large amount of thermal energy in the form of collective motions before any hydrogen bonds have to break. These cooperative oscillations would correspond to thermally excited low frequency modes which contribute favourably to the entropy component of the molecule's stabilisation free energy (Sturtevant, 1977). The computer simulation by Levitt (1983b) supports this model, even though the time scales are so very different, by showing that hydrogen bonds in the  $\alpha$  helices and the ends of the  $\beta$  sheet break far more frequently than bonds in the central portion of the sheet. Collective motions of the  $\beta$  sheet are also apparent in the simulation.

The importance of secondary structure in determining the exchange rates is also apparent in a neutron diffraction study of the extent of hydrogen exchange in a crystal of trypsin which had been soaked in D<sub>2</sub>O for a year (Kossiakoff, 1982). Almost all the unexchanged amide protons were in  $\beta$  sheet structures implying that their activation energy for exchange is much larger than typical fluctuations in energy. The depth to which an exchangeable proton was buried inside the protein was found to be

not as important as expected, with 27% of exchanged protons being more than 4Å from the protein surface. Interior cavities in the protein which exchanged solvent with the exterior solution freely, were largely responsible for this effect. More importantly than this depth effect is the effect of secondary structure.  $\beta$  sheet structures are so resistant to exchange that in one instance a well defined D<sub>2</sub>O molecule was found to be hydrogen bonded to peptide oxygens adjacent to two unexchanged amide hydrogens. For protons most resistant to exchange it is clear that the effect of solvent diffusion and small atomic fluctuations are negligible when compared to structural effects and larger collective fluctuations.

The x-ray temperature factors which are related to small atomic fluctuations show no correlation with the extent of proton exchange with most exchanged and unexchanged groups having low temperature factors. This implies that these factors can give no information on large collective motions of the protein, which would be infrequent occurrences giving negligible x-ray scattering, and which could be crucial to the function of the enzyme. Similarly a study by Sternberg et al., (1979) of the temperature factors of lysozyme gave no indication of any hinge bending motions which are presumably present, though rare, since the hinge closes when a ligand binds.

The effect of trypsin binding to BPTI on hydrogen exchange rates of the inhibitor's  $\beta$  sheet amide protons was investigated by Simon et al., (1984). It was found that the core protons of the  $\beta$  sheet were only slightly slower to exchange but that the exchange of the amide proton of Tyr 35 at the end of the  $\beta$  sheet,

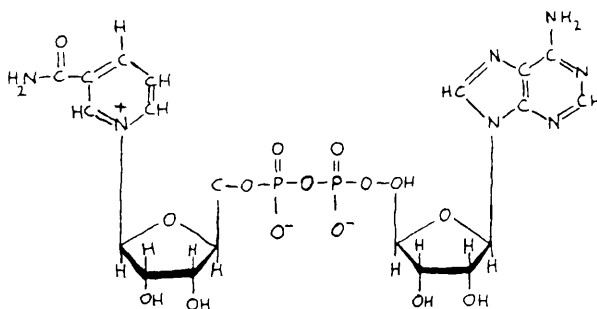
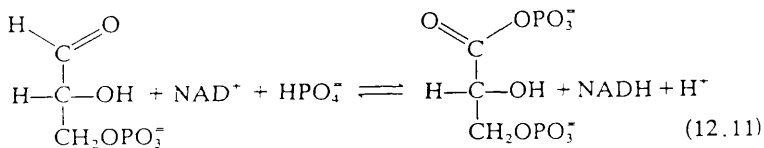
which binds in the trypsin active site, was slowed by a factor of more than  $10^3$ . This implies that the accessibility of this proton to the solvent is drastically reduced, and that the scale of fluctuations felt by Tyr 35 is reduced. It is suggested that this selective slowing is due to the damping out of one or a few low frequency collective modes of the  $\beta$  sheet of the type considered by Salemme (1982), which would reduce the size of fluctuations around Tyr 35 and remove a lot of the strain of the hydrogen bonded structure, thus making it more stable and resistant to hydrogen exchange.

This loss of low frequency modes may possibly be observed by Raman spectroscopy if the large number of other low frequency modes do not conceal them. The only low frequency Raman spectrum published so far of a serine protease is that of  $\alpha$ -chymotrypsin which is structurally very similar to trypsin (Brown et al., 1972). This showed a well resolved low frequency band at  $30\text{cm}^{-1}$  whose shape depended on the method of sample preparation and which disappeared in the denatured protein. One would expect the spectrum of trypsin to be very similar.

### 3.4 Introduction to the Structure and Dynamics of Glyceraldehyde 3-Phosphate Dehydrogenase

Glyceraldehyde-3-phosphate dehydrogenase (GAPDH) is a much larger enzyme than lysozyme or trypsin, composed of 4 identical pseudo-symmetrically arranged subunits each containing 331 amino acid residues giving a total molecule weight of 146,000 (for a review see Harris & Waters, 1976). The enzyme catalyses the oxidation and phosphorylation of D-glyceraldehyde 3-phosphate to 1,3 diphosphoglycerate once the coenzyme nicotinamide adenine dinucleotide (NADH) is bound, by the following reaction:

Figure 3.14. The reaction catalysed by GAPDH and the structure of the cofactor NAD.



Each subunit is composed of two domains, one which binds NAD<sup>+</sup> and the other which binds the substrate, and all four subunits are catalytically active. It has been found that NAD<sup>+</sup>

binding shows positive cooperativity in the yeast enzyme whereas the enzyme isolated from rabbit or pig muscle exhibits negative cooperativity.

The residue sequence of the domains in the rabbit muscle, pig muscle and yeast enzymes have been compared by Jones & Harris (1976) who found that 60% of the residues occur in identical positions in the three species. Similarly, over 50% of the sequence is conserved between lobster muscle enzyme and GAPDH from the bacterium T. aquaticus (Hocking & Harris, 1976).

The three dimensional structure of yeast GAPDH has not yet been solved, however considering the major similarity in sequence and physical properties between the yeast and muscle enzymes, it is reasonable to assume that the crystallographic structures are almost identical. The highest resolution structures of GAPDH so far obtained are those of lobster muscle (see Harris & Waters, 1976 for references) and of the bacterium B. stearothermophilus (Biesecker et al., 1977; Leslie & Wonacott, 1984). These show that NAD<sup>+</sup> binds in an extended conformation, to one of the domains (residues 1-149) in each subunit. This domain consists mainly of a 6 stranded parallel  $\beta$  sheet with several  $\alpha$  helices arranged around the sheet as shown in Figure 3.15. The NAD<sup>+</sup> when bound can interact with adjacent subunits via a section of antiparallel sheet (residues 179-200) in the catalytic domain.

The catalytic domain consists of residues 149-334, lobster muscle GAPDH having 3 more residues per subunit than the yeast enzyme, is shown in Figure 3.16. This consists of a 9 stranded antiparallel  $\beta$  sheet which forms the main inter-subunit contact region and 3  $\alpha$  helices, the last of which (residues 313-

Fig. 3.15 A sketch of the structure of the NAD binding domain of one of the monomers of GAPDH showing the NAD bound. (from Harris & Waters, 1976)

Fig. 3.16 A sketch of the structure of the catalytic domain of one of the monomers of GAPDH. (from Harris & Waters, 1976)



334) projects back into the NAD<sup>+</sup> binding domain. The lobster enzyme has been crystallised in the apo enzyme form (no NAD<sup>+</sup> bound) as well as the holo form shown above, while the B. stearothermophilus has been crystallised in the holo, apo and single NAD<sup>+</sup> bound forms. In the lobster enzyme, little difference between the two forms has been found, except for some minor changes in the NAD<sup>+</sup> binding site and in the antiparallel sheet in the catalytic domain which is in contact with adjacent subunits. Movements of up to 1.7 Å in this region could be important factors in the cooperativity (Murthy et al., 1980). The bacterial enzyme shows rather larger motions with the coenzyme domain rotating by about 4° relative to the catalytic domain, shielding the NAD<sup>+</sup> from the solvent (Leslie & Wonacott, 1984).

Comparison of the 3 structures of the bacterial enzyme, apo, single NAD<sup>+</sup> and holo provide evidence for ligand induced sequential conformational changes, since the enzyme with one NAD<sup>+</sup> bound shows 3 subunits with approximately the apo structure and the subunit with NAD<sup>+</sup> bound shows the holo structure. The lobster enzyme may show smaller, similar changes if the single bound NAD structure could be crystallised, since there is a large amount of chemical evidence (see Harris & Waters, 1986; Grau, 1982 for example) for negative cooperativity of NAD<sup>+</sup> binding occurring via a sequential mechanism (Koshland et al., 1966) in both the lobster and bacterial enzymes. In this model the fully symmetric apo enzyme changes conformation as successive NAD<sup>+</sup> molecules bind, with a consequent change in the affinity for binding the next NAD<sup>+</sup> molecule.

The yeast enzyme on the other hand, shows positive cooperativity between all four NAD<sup>+</sup> binding sites. This cooperativity has been analysed with both the sequential model and the concerted model of Monod et al., (1965). In the concerted model, two symmetric forms of the enzyme exist, one of low binding affinity, the other of high affinity which interconvert at a slow rate. Each tetramer in this model would have 4 equivalent binding sites unlike the sequential model. The concerted model for the yeast enzyme is supported by most experiments that have been done (Harris & Waters, 1976). In all experiments, no cooperativity is seen at 20<sup>o</sup> or at approximately pH 7.5 or below. Positive cooperativity appears as either the temperature or pH are raised becoming particularly obvious at 40<sup>o</sup> and pH 8.5.

Small angle x-ray scattering from solutions of GAPDH containing varying amounts of NAD<sup>+</sup> (Durchschlag et al., 1971; Simon, 1971) show that the enzyme volume contracts by 7% on going from the apo to the holo enzyme and that the radius of gyration also decreases from 32.1Å (Durchschlag et al.,) 32.5Å (Simon) to 31.7Å (Durchschlag et al., & Simon). Durchschlag et al., (1971) show that the volume contraction with increasing saturation of NAD<sup>+</sup> binding sites is not linear which would be indicative of a sequential model. The concerted model is the simplest model which can fit this data.

Jaenicke and Gratzer (1969) used hydrodynamic and spectroscopic techniques to study NAD<sup>+</sup> binding at pH 8.5 and found that this was non-cooperative at 20<sup>o</sup> but, at 40<sup>o</sup> C it was cooperative and fitted the concerted model. A plot of concentration of the

high affinity form of the enzyme versus saturation of NAD binding sites was non linear which again cannot be due to a sequential mechanism. The temperature behaviour of the cooperativity could be explained if the activation barrier between the inactive and active forms is high or if the relative affinities of the two forms for NAD<sup>+</sup> binding change with temperature.

Sloan and Velick (1973) showed that the protein volume decreased by 6.3% on going from the apo to the holo enzyme, by using buoyant density measurements. They also found a corresponding decrease in the extent of hydration of the protein on coenzyme binding. In other words NAD<sup>+</sup> binding expels a large number of water molecules from within the enzyme. They found essentially the same contraction whether at 25 °C, pH 7.4 where binding is noncooperative or at 25 °C, pH 8.5 where binding is cooperative. They state that this pH affect is due to a change in the affinity of the active form of the enzyme for NAD<sup>+</sup> rather than being associated with the allosteric transition from inactive to active form.

This is also consistent with two detailed studies of the thermodynamics of NAD<sup>+</sup> binding to yeast GAPDH (Velick et al., 1971; Neikamp et al., 1977). Velick et al., found that binding at pH 7.3 remained noncooperative even at 40 °C which implies that the activation energy for the allosteric transition in the concerted model is not responsible for the appearance of cooperativity at high temperature. The appearance of cooperativity is therefore due to a strong dependence of the association constants on pH. Niekamp et al., (1977) show that cooperativity does not appear at pH 6.5 either, while they

analyse their binding data at pH 8.5 where cooperativity is clear, in terms of both a sequential model and a concerted model. The two models fit their results equally well. They find that saturation of the enzyme with  $\text{NAD}^+$  causes a large negative heat capacity change as the temperature increases at all pH's studied which implies a strong temperature dependence of  $\Delta H$  and  $\Delta S$ . The negative changes in  $\Delta C_p$  are attributed to a general stiffening of the structure, with the expulsion of water molecules, a decrease in exposure of hydrophobic groups to the solvent and a large decrease in the number of thermally excitable vibrational modes. The first two contributions give positive entropy changes while the third one gives a negative entropy contribution. Since the experimental entropy changes are negative, the third vibrational contribution must be the most important. These changes in heat capacity and entropy are analysed further in Sturtevant (1977).

Equilibrium dialysis results for  $\text{NAD}^+$  binding, due to Cook and Koshland (1970) were found to fit a sequential model of the cooperativity at pH 8.5 and  $40^\circ\text{C}$  rather than a concerted model.

Whether or not the positive cooperativity displayed by yeast GAPDH at high pH can be explained by a sequential model where  $\text{NAD}^+$  binding induces consecutive conformational and dynamic changes or by a concerted model where the enzyme exists in high and low affinity forms is still an open question, though most of the experimental results are in favour of a concerted model.

If the  $\text{NAD}^+$  binding does cause a loss of low frequency vibrational modes of the protein as well as the gross conformational change, then this may be observable with Raman

spectroscopy. As far as I am aware no Raman spectroscopic studies of GAPDH have been reported in the literature.

## CHAPTER 4

### EXPERIMENTAL METHODS

#### 4.1 Introduction

Vibrational modes of low frequency ( $< 200\text{cm}^{-1}$ ) are most easily studied by Raman spectroscopy of solids. Infra-red spectra and inelastic neutron scattering spectra in this region are difficult to obtain, whereas Raman spectra of low and high frequency regions can be obtained easily on one spectrometer. Solutions are difficult to study at low frequency with Raman spectroscopy because of the broad intense Rayleigh wing extending out from the laser excitation line at  $0\text{cm}^{-1}$  to more than  $100\text{cm}^{-1}$ . This scattering is mainly due to the random rotational motion of the solvent molecules, which is absent in solid samples allowing spectra to be recorded to within  $10\text{cm}^{-1}$  of the exciting line.

Four molecules, one organic allosteric model compound, two enzymes which bind one ligand each and an enzyme which binds up to four ligands cooperatively, were studied in various states of ligation to determine if there were any changes in the low frequency spectra which would indicate a protein dynamics contribution to binding and allostery. The three enzymes studied were lysozyme, a small bi-lobed globular enzyme which binds an inhibitor tri-N-acetyl glucosamine between the two lobes possibly affecting the relative motion of the lobes; trypsin, a small globular protein which binds a large natural polypeptide inhibitor with one of the largest association constants known;

and glyceraldehyde-3-phosphate dehydrogenase, a large enzyme composed of four subunits which shows positive cooperativity under some conditions when binding the coenzyme nicotinamide adenine dinucleotide.

#### 4.2 Theory of the Raman Effect

Raman spectroscopy is the study of light inelastically scattered by the electronic distribution of molecules. The scattering process changes the frequency of the light and the shift in frequency corresponds to the frequency of an electronic, vibrational or rotational energy level of the molecule. The effect was first seen by Raman and Krishnan (1928) and independently by Landsberg and Mandelstam (1928). This study is only concerned with vibrational energy levels. Using a monochromatic light source and measuring the changes in the frequency caused by the scattering process a vibrational spectrum showing the frequencies of all Raman active normal modes of the molecule can be obtained.

When the incident light wave interacts with the electrons of the molecule, the electromagnetic field of the light exerts a force on the electrons and displaces them. The Raman effect is only observed when these displacements result in a change in the electronic dipole moment  $\mu$ , in the molecule. Under most conditions it is reasonable to assume that  $\mu$  is proportional to the electric field strength

$$\mu = \alpha \cdot E$$

where  $\alpha$  is the electric polarizability tensor. Writing in all the x, y and z components of  $\mu$ ,  $\alpha$ , and  $E$  gives 3 equations

$$\mu_x = \alpha_{xx} E_x + \alpha_{xy} E_y + \alpha_{xz} E_z$$

$$\mu_y = \alpha_{yx} E_x + \alpha_{yy} E_y + \alpha_{yz} E_z$$

$$\mu_z = \alpha_{zx} E_x + \alpha_{zy} E_y + \alpha_{zz} E_z$$

If the light is monochromatic of frequency  $\omega$ , and plane polarised in say the Z direction, then only  $E_z$  is not zero

$$E_z = E_z^0 \cos \omega t$$

By using the normal coordinates of the molecule to define the displacements of electrons involved in a particular molecular vibration,  $\omega_{vib}$ , which can be written as

$$\Delta r(t) = \Delta r_{max} \cos \omega_{vib} t$$

and expressing the time dependent polarisability of the electrons involved in this vibration in the form of a Taylor series

$$\alpha_{zz}(t) = \alpha_{zz}^0 + \left( \frac{\partial \alpha_{zz}}{\partial r} \right)_0 \Delta r_{max} \cos \omega_{vib} t$$

where the 0 subscript indicates the equilibrium position, it is

easy to show that  $\mu_z(t)$  has three components

$$\begin{aligned} \mu_z(t) = & \alpha_{zz}^0 E_z^0 \cos \omega t + \frac{1}{2} \left( \frac{\partial \alpha_{zz}}{\partial r} \right)_0 \Delta r_{max} E_z^0 \cos(\omega + \omega_{vib})t \\ & + \frac{1}{2} \left( \frac{\partial \alpha_{zz}}{\partial r} \right)_0 \Delta r_{max} E_z^0 \cos(\omega - \omega_{vib})t \end{aligned}$$

The first component is the Rayleigh scattering component where the induced dipole radiates energy at the same frequency as the incident light. In other words the light has been scattered elastically.

The second component shows that some scattered light has a frequency higher than the incident light by an amount corresponding to a vibration of the molecule while the third component shows that light is also scattered at a frequency lower than the incident light. These are termed Anti-Stokes and Stokes

scattering-respectively.

From a quantum mechanical viewpoint these three components correspond to vibrational transitions from within the ground electronic state. Rayleigh scattering corresponds to a transition from the ground vibrational level to itself via a very short lived high energy intermediate state, while Stokes scattering corresponds to a transition from the ground vibrational level to the 1st excited vibrational level with the emission of a photon with lower frequency than the incident photon. Anti-Stokes scattering is the reverse of Stokes scattering and one can see that the intensity of Anti Stokes scattering will be lower than the Stokes scattering because of the lower population of the excited states as determined by the Boltzmann distribution. The classical theory given above does not predict this intensity difference.

The quantum mechanical theory of Raman scattering starts with the definition of a real transition electric dipole moment between two molecular states  $m$  and  $n$  with wave functions  $\psi_m e^{-i\omega_m t}$  and  $\psi_n e^{-i\omega_n t}$

$$(\mu_\alpha)_{mn} = \langle m' | \mu_\alpha | n' \rangle + \langle m' | \mu_\alpha | n' \rangle^*$$

where  $*$  means complex conjugate and  $|m'\rangle$  and  $|n'\rangle$  are the molecular wavefunctions perturbed by the radiation field. See Barron (1982) for a full detailed discussion of the theory of Raman scattering. These wavefunctions are written as the sum of the original unperturbed wavefunction and a weighted sum of all other molecular wavefunctions.

$$\text{eg. } |n'\rangle = \left[ |n\rangle + \sum_{j \neq n} (a_{jn} e^{-i\omega_j t} + b_{jn} e^{i\omega_j t}) |j\rangle \right] e^{-i\omega_n t}$$

Using the time dependent Schrodinger equation, with the perturbed Hamiltonian  $H' = H^{\circ} - \frac{1}{2} \mu_{\beta} E_{\beta}^{\circ} (e^{i\omega t} + e^{-i\omega t})$  where  $H^{\circ}$  is the

Hamiltonian in the absence of the radiation field ( $\tilde{E}_{\beta} = E_{\beta}^{\circ} (e^{i\omega t} + e^{-i\omega t})$ ), the coefficients  $a_{jn}$  and  $b_{jn}$  can be calculated to give

$$|n'\rangle = \left[ |n\rangle + \frac{1}{2\hbar} \sum_{j \neq n} \left\{ \frac{\langle j | \mu_{\beta} | n \rangle}{(\omega_{jn} - \omega)} E_{\beta}^{\circ} e^{-i\omega t} + \frac{\langle j | \mu_{\beta} | n \rangle}{(\omega_{jn} + \omega)} E_{\beta}^{\circ*} e^{i\omega t} \right\} |j\rangle \right] e^{-i\omega_n t}$$

where  $\omega_{xy} = \omega_x - \omega_y$

$|m'\rangle$  and the complex conjugates are calculated in a similar fashion.

$\langle m' | \mu_{\alpha} | n' \rangle$  and  $\langle m' | \mu_{\alpha} | n' \rangle^*$  can then be calculated in a straightforward fashion and if terms in  $E_{\beta}^{\circ 2}$  are ignored then one obtains:

$$\begin{aligned} (\mu_{\alpha})_{mn} &= \langle m | \mu_{\alpha} | n \rangle e^{i\omega_{mn}t} \\ &+ \frac{1}{2\hbar} \sum_{j \neq n} \left[ \frac{\langle m | \mu_{\alpha} | j \rangle \langle j | \mu_{\beta} | n \rangle}{\omega_{jn} - \omega} E_{\beta}^{\circ} e^{-i(\omega - \omega_{mn})t} \right. \\ &\quad \left. + \frac{\langle m | \mu_{\alpha} | j \rangle \langle j | \mu_{\beta} | n \rangle}{\omega_{jn} + \omega} E_{\beta}^{\circ*} e^{i(\omega + \omega_{mn})t} \right] \\ &+ \frac{1}{2\hbar} \sum_{j \neq n} \left[ \frac{\langle m | \mu_{\beta} | j \rangle \langle j | \mu_{\alpha} | n \rangle}{\omega_{jm} - \omega} E_{\beta}^{\circ*} e^{i(\omega + \omega_{mn})t} \right. \\ &\quad \left. + \frac{\langle m | \mu_{\beta} | j \rangle \langle j | \mu_{\alpha} | n \rangle}{\omega_{jm} + \omega} E_{\beta}^{\circ} e^{-i(\omega - \omega_{mn})t} \right] \end{aligned}$$

+ complex conjugate terms calculated from  $\langle m' | \mu_{\alpha} | n' \rangle^*$

The first term and its complex conjugate describes spontaneous radiation of frequency  $\omega_{mn}$  from an excited state  $n$  to a lower state  $m$ . Terms with a frequency dependence  $(\omega + \omega_{mn})$  describe induced emission of two photons, of frequency  $\omega + \omega_{mn}$  and  $\omega$  from an excited state  $n$  to a lower state  $m$  and are not discussed

further. - The terms with frequency dependence  $(\omega - \omega_{mn})$  give rise to Rayleigh scattering when  $m = n$ , Stokes Raman scattering when  $m > n$  and anti-Stokes Raman scattering when  $m < n$ .

Therefore the transition dipole moment giving Raman scattering can be written as:

$$(\mu_\alpha)_{mn} = \frac{1}{2\hbar} \sum_{j \neq n, m} \left[ \frac{\langle m | \mu_\alpha | j \rangle \langle j | \mu_\beta | n \rangle}{\omega_{jn} - \omega} + \frac{\langle m | \mu_\beta | n \rangle \langle j | \mu_\alpha | n \rangle}{\omega_{jm} + \omega} \right] E_\beta^0 e^{-(\omega - \omega_{mn})t}$$

+ complex conjugate

By rearranging this expression, using the properties of complex numbers, into real and imaginary parts and an identity due to Barron (1982) one can then write

$$(\mu_\alpha)_{mn} = (\alpha_{\alpha\beta})_{mn} E_\beta(\omega - \omega_{mn}) + \frac{1}{\omega - \omega_{mn}} (\alpha'_{\alpha\beta})_{mn} \frac{\partial}{\partial t} (E_\beta(\omega - \omega_{mn}))$$

where  $E_\beta(\omega - \omega_{mn}) = E_\beta^0 (e^{-i(\omega - \omega_{mn})t} + e^{i(\omega - \omega_{mn})t})$

and  $(\alpha_{\alpha\beta})_{mn} = \frac{1}{2\hbar} \sum_{j \neq m, n} \frac{1}{(\omega_{jn} - \omega)(\omega_{jm} + \omega)}$

$$\times \left[ (\omega_{jn} + \omega_{jm}) \operatorname{Re} (\langle m | \mu_\alpha | j \rangle \langle j | \mu_\beta | n \rangle + \langle m | \mu_\beta | j \rangle \langle j | \mu_\alpha | n \rangle) \right. \\ \left. + (2\omega + \omega_{nm}) \operatorname{Re} (\langle m | \mu_\alpha | j \rangle \langle j | \mu_\beta | n \rangle - \langle m | \mu_\beta | j \rangle \langle j | \mu_\alpha | n \rangle) \right]$$

$$(\alpha'_{\alpha\beta})_{mn} = \frac{1}{2\hbar} \sum_{j \neq m, n} \frac{1}{(\omega_{jn} - \omega)(\omega_{jm} + \omega)}$$

$$\times \left[ (\omega_{jn} + \omega_{jm}) \operatorname{Im} (\langle m | \mu_\alpha | j \rangle \langle j | \mu_\beta | n \rangle + \langle m | \mu_\beta | j \rangle \langle j | \mu_\alpha | n \rangle) \right. \\ \left. + (2\omega + \omega_{nm}) \operatorname{Im} (\langle m | \mu_\alpha | j \rangle \langle j | \mu_\beta | n \rangle - \langle m | \mu_\beta | j \rangle \langle j | \mu_\alpha | n \rangle) \right]$$

The first terms in  $\alpha_{\alpha\beta}$  and  $\alpha'_{\alpha\beta}$  are symmetric with respect

to interchange of subscripts while the second terms are antisymmetric. The symmetric parts give normal Rayleigh and Raman scattering while the antisymmetric parts, which are usually zero, can give rise to anomalous intensity ratios between polarised and depolarised bands.

The intensity of light of frequency  $\omega$  scattered from a molecule which is much smaller than the wavelength of the light is proportional to  $\omega^4$  as determined by the Rutherford scattering formula for the scattering of small particles.

The Raman intensity can therefore be written

$$\text{Scattered Intensity} = C (\omega \pm \omega_{mn})^4 I_0 \sum_{\alpha, \beta} |(\alpha_{\alpha\beta})_{mn} - i(\alpha'_{\alpha\beta})_{mn}|^2$$

where C is a constant and  $I_0$  is the incident light intensity.

The use of the above theory and the analysis of Raman spectra of biochemical compounds is fully described by Carey (1982).

### Raman Spectrometer

A sketch of the main experimental components used for recording Raman spectra is shown in Figure 4.1.

The Spectra Physics 171 argon ion laser emits an intense monochromatic, plane polarised light<sup>beam</sup> at several useful visible wavelengths with considerable power. The two strongest lines at 488nm and 514.5nm were used throughout. The laser beam is guided through a plasma line filter which removes the large number of weaker laser emissions which are present alongside the main laser beam. The filter consists of a sandwich of several different quartz filters and a different filter is required for each laser line. The 488nm filter successfully removed all but the 2 lowest

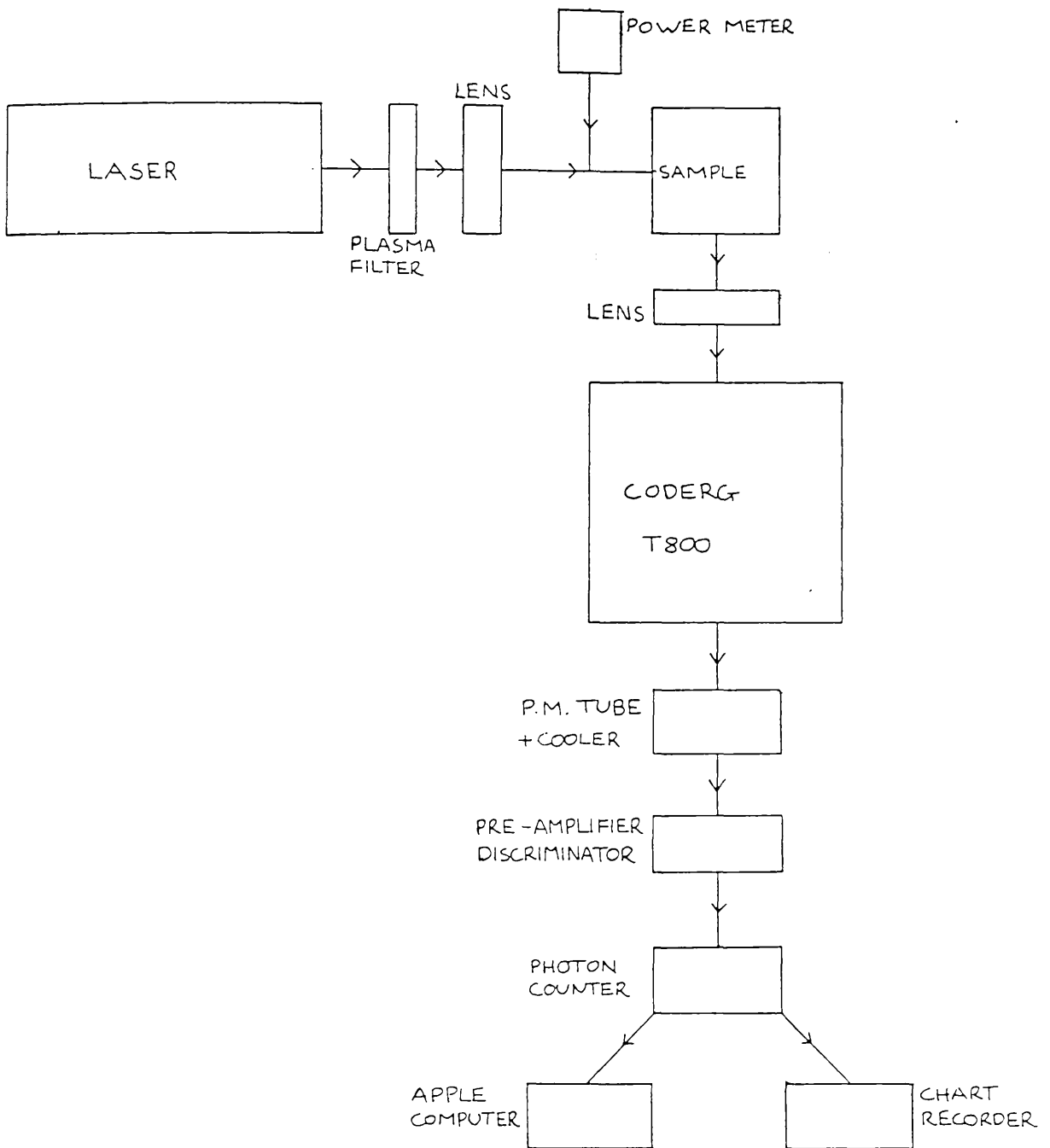


Fig. 4.1 A block diagram of the apparatus used for recording Raman spectra.

frequency- Stokes plasma lines at 37 and 103cm<sup>-1</sup>, while the 514.5nm filter suppressed all the Stokes plasma lines. Neither filter removed the anti-Stokes plasma lines, however the lines at -60 and -136cm<sup>-1</sup> in the 488nm spectra did not interfere with the anti-Stokes protein spectra. The line at -17cm<sup>-1</sup> in the 514.5nm spectra made recording of anti-Stokes protein spectra impossible. The laser beam is then focussed onto the solid sample by a short focal length lens. The power of the laser beam at this point could be measured with a Spectra-Physics power meter and was usually between 30 to 50m watts.

The most convenient way of mounting the samples, which were all powders, was found to be packing them into the ends of small Allen bolts. The bolts were then attached to a rod mounted on a moveable platform with the surface of the powder at a 45° angle to the laser beam and to the collecting lens. The samples could then be changed easily and positioned consistently. The moveable platform was adjusted until the maximum signal as shown on the photon counter was obtained.

In many systems the scattered light passes through a polaroid sheet before going through the collecting lens. This allows depolarisation studies to be performed. However, powder samples usually destroy the polarisation of the beam and in this case the polariser would only reduce the amount of Raman signal reaching the detector. The polaroid was removed to increase the amount of light going through the collecting lens into the spectrometer and hence most of the spectrum shown later are unpolarised. The lens focuses the scattered light onto the narrow entrance slit of the Coderg T800 triple monochromator.

The path followed by the light inside the spectrometer is shown in Figure 4.2.

The three monochromators are arranged so that the dispersion of the light from each diffraction grating adds together, while the four adjustable slits cut down the amount of stray light in the spectrometer that can reach the detector. The diffraction gratings can rotate at various set rates such that the dispersed light is scanned over the slits and the detector at a rate which is linear in wavenumbers. The width of the slits controls the "bandpass" and resolution of the instrument. The spectral resolution in  $\text{cm}^{-1}$  is the full width at half height of an infinitely sharp line as recorded by the spectrometer and gives the minimum separation between Raman bands necessary for them to be resolved individually. The resolution can be determined from a chart showing scanning rate, slitwidth and laser line supplied with the instrument.

The dispersed light then passes out of the Coderg onto the photosensitive front of an EMI 9594B photomultiplier enclosed in a Products for Research thermoelectric cooled chamber. When a photon strikes the photosensitive cathode an electron is emitted inside the tube which is accelerated by a strong electric field down the tube towards the anode. The electron strikes a number of positively charged anodes made of CsSb which then emit secondary electrons. In a very short time a cascade of electrons is produced which when it reaches the anode at the end of the tube produces a measurable electric pulse. The cooler operating at  $-40^{\circ}\text{C}$  is necessary to reduce the thermal noise of the PM tube to negligible levels which normally prevents weak signals from being

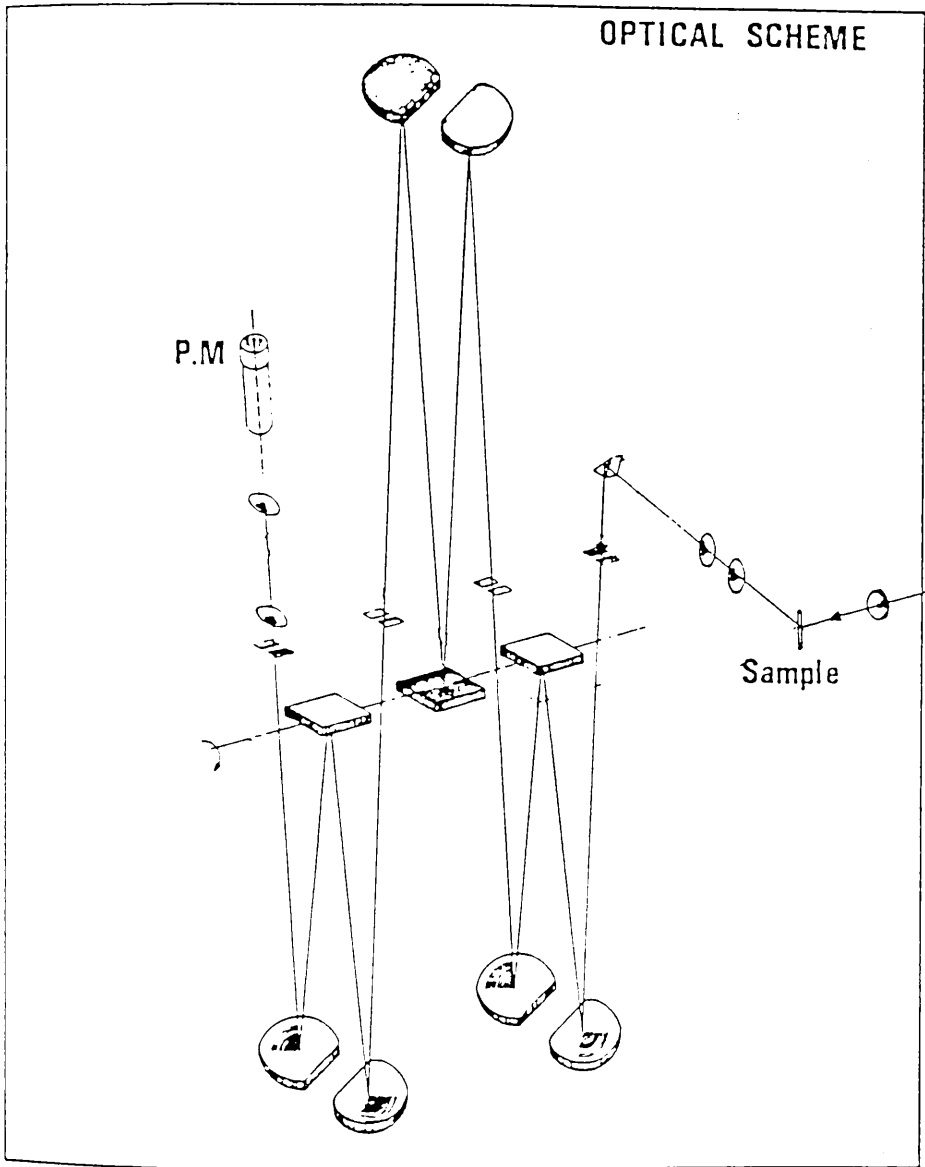


Fig. 4.2 A diagram of the lightpath through the Coderg T800 spectrometer.

detected.- The noise level in the tube used in this work was reduced by 3 orders of magnitude by the cooler. The electric pulse is then amplified by a SSR Instrument Co. Model 1120 preamplifier discriminator before reaching the SSR Instr. Co. Model 1110 Digital Synchronous photon counter. This small computer integrates the amplified pulses received in a preset time to give a measure of the intensity of the scattered light. The preset time is chosen so as to obtain a good signal to noise ratio taking into account the scanning rate and resolution of the Coderg. A simple empirical formula for choosing this time is given in Carey (1982).

$$\frac{\text{preset time (sec)} \times \text{scan speed (cm}^{-1}\text{/sec)}}{\text{spectral resolution (cm}^{-1}\text{)}} \leq 0.25$$

The signal from the photon counter is then recorded on an Oxford Instruments 3000 series chart recorder and on an Apple II Europlus 8 bit microcomputer. The Apple computer stored the 16 bit signal from the photon counter as two 8 bit numbers by using a circuit board built by Dr. K. Tyler, which was then analysed and stored later using software written by Dr. A. Cooper.

Due to the excellent resolution and high stray light rejection characteristics of the Coderg, Stokes Raman spectra should have been obtainable as close as  $10 \text{ cm}^{-1}$  from the exciting line, however, a broad spurious band was found at  $\sim 25 \text{ cm}^{-1}$ , in the same region as the expected low frequency protein bands. This band did not appear on the anti Stokes side of the exciting line and was visible in several unrelated compounds such as lysozyme, magnesium oxide and n-acetyl-glucosamine. It seems most likely that this ghost band is due to small errors on the diffraction

gratings -(Richardson, 1969). The position of the band and the fact that it appears on one side of the exciting line only suggests that it is due to random changes in the spacing of the diffraction grating. These errors produce extra, sharp lines called "satellites" which, if they are numerous, can merge together to form the broad low frequency ghost found in this spectrometer. The ghost did not interfere with the spectra of the allosteric model compound which was much more intense and had no bands in the same region as the ghost, but it made recording of low frequency Stokes spectra of proteins impossible, so the anti-Stokes low frequency spectra of the proteins were recorded instead. The intensity differences at low frequencies between Stokes and anti-Stokes bands due to the Boltzmann factor are small up to  $\sim \pm 100\text{cm}^{-1}$ , but any Raman bands at higher frequencies up to  $\pm 200\text{cm}^{-1}$  might not be visible in the anti Stokes spectrum. Stokes spectra of the proteins between  $+100\text{cm}^{-1}$  and  $+200\text{cm}^{-1}$  however showed no features that were not also seen in the anti Stokes spectra.

### 4.3 Protein Sample Preparation

Hen egg white lysozyme, bovine trypsin, yeast glyceraldehyde-3-phosphate dehydrogenase (GAPDH), bovine pancreatic trypsin inhibitor (BPTI), tri-N-acetylglucosamine (tri-NAG), micrococcus lysodieticus dried cells, p-nitrophenol-p'-guanidinobenzoate, (NPGB) sodium barbital (veronal) and nicotinamide adenine dinucleotide (NAD) were all purchased from the Sigma Chemical Company and were stored, with the exception of veronal, desiccated below 0 °C. All reagents used were analytical grade and distilled water was used throughout.

UV spectra and assays were recorded on a Pye-Unicam SP1800 spectrophotometer. Protein solutions were frozen with liquid nitrogen and then freeze dried for 6 to 8 hours on a vacuum line connected to an Edwards rotary pump.

#### 4.3.1 Lysozyme and Lysozyme-Tri-NAG preparation

50mg of lysozyme was dialysed to remove the sodium salts by dissolving it in 5ml of 0.1M ammonium acetate buffer, pH 5 - 5.25, contained in a length of presoaked dialysis tubing which was then immersed in a large stirred volume of the buffer for approximately 4 hours. If left for too long, the lysozyme, being fairly small, would start to diffuse through the tube and be lost in the large buffer volume. The dialysed solution was recovered and freeze dried.

The 1:1 lysozyme-tri-NAG complex was prepared by taking 1mg of tri-NAG and 20mg of the dialysed freeze dried lysozyme, thus ensuring a slight excess of inhibitor, and dissolving them in 0.3ml of the acetate buffer. The sample was freeze dried for 8

hours giving a dry white powder which was stored below 0 °C in a dessicator.

The enzymatic activity of the dialysed, freeze dried lysozyme, the lysozyme-tri-NAG complex and of the lysozyme as supplied was determined by measuring the initial rate of change of absorbance at 450nm when an aliquot of the enzyme was added to a suspension of *Micrococcus Leisodeikticus* cells. The assay was performed by dissolving the enzyme or enzyme complex in 0.066M phosphate buffer pH 6.24 to obtain a concentration of about 0.2mg/ml. 0.1ml of this solution was then mixed rapidly with 2.5.ml of the lysodiekticus suspension, having an optical density at 450nm of between 0.6 and 0.7, in a 1 cm path length cuvette. The absorption change was then measured for several minutes against a reference cell containing phosphate buffer only. The initial rate of change was estimated by drawing a line through the first part of the curve and extrapolating it to find the change in absorbance in 1 minute. This figure was multiplied by 1000 to give the number of units of enzyme activity in the 0.1 ml sample. To determine the activity in units per mg of protein, the exact concentration of the 0.2mg/ml solution was found by measuring the absorbance of the enzyme solution at 280nm where the absorption coefficient is 26.5 per mmole (Cooper, 1974) and calculating the concentration using the Beer-Lambert Law. The absorption spectra of the lysozyme samples are shown in Figure 4.3.

### Results

The uv absorption spectra at 450nm used for the assays are shown in Figure 4.4 and the results are tabulated in Figure 4.5.

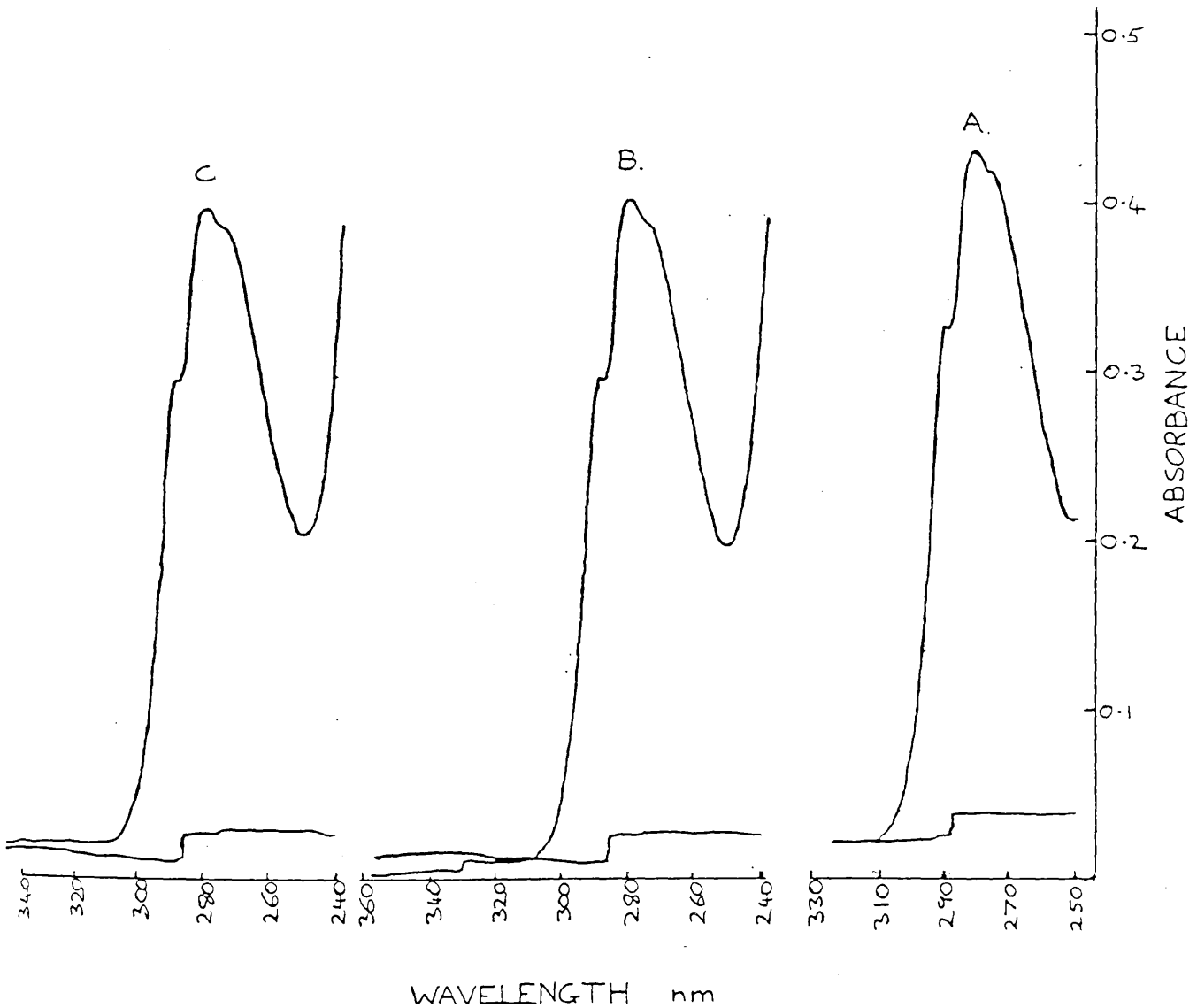
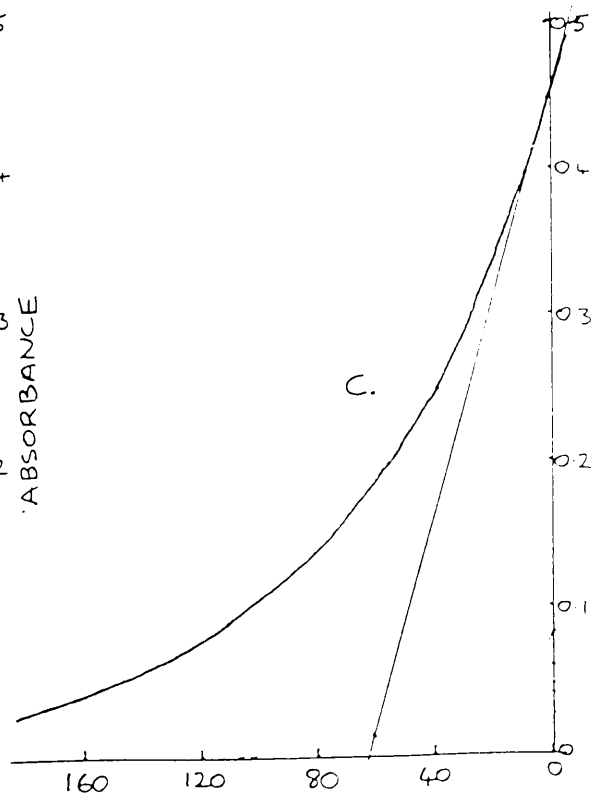
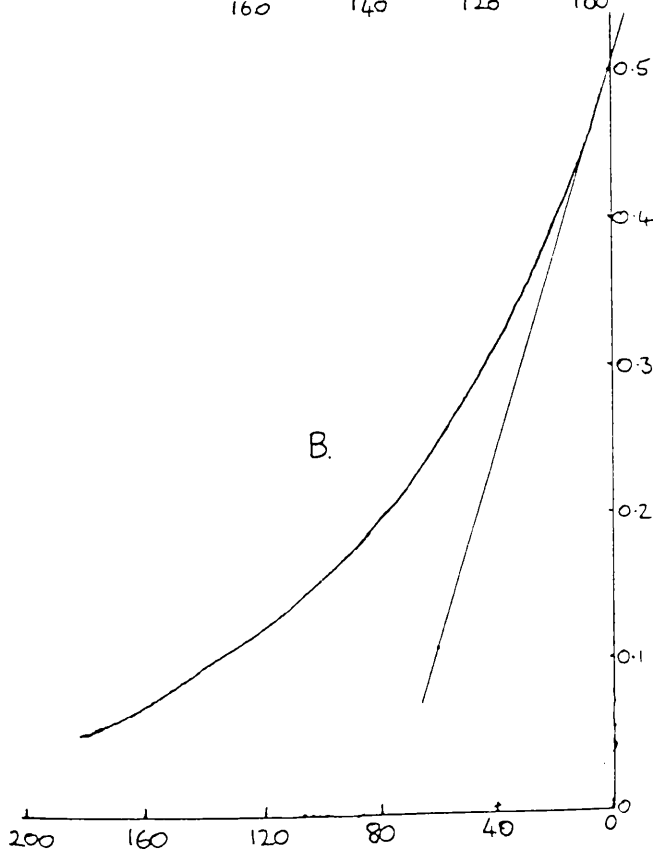
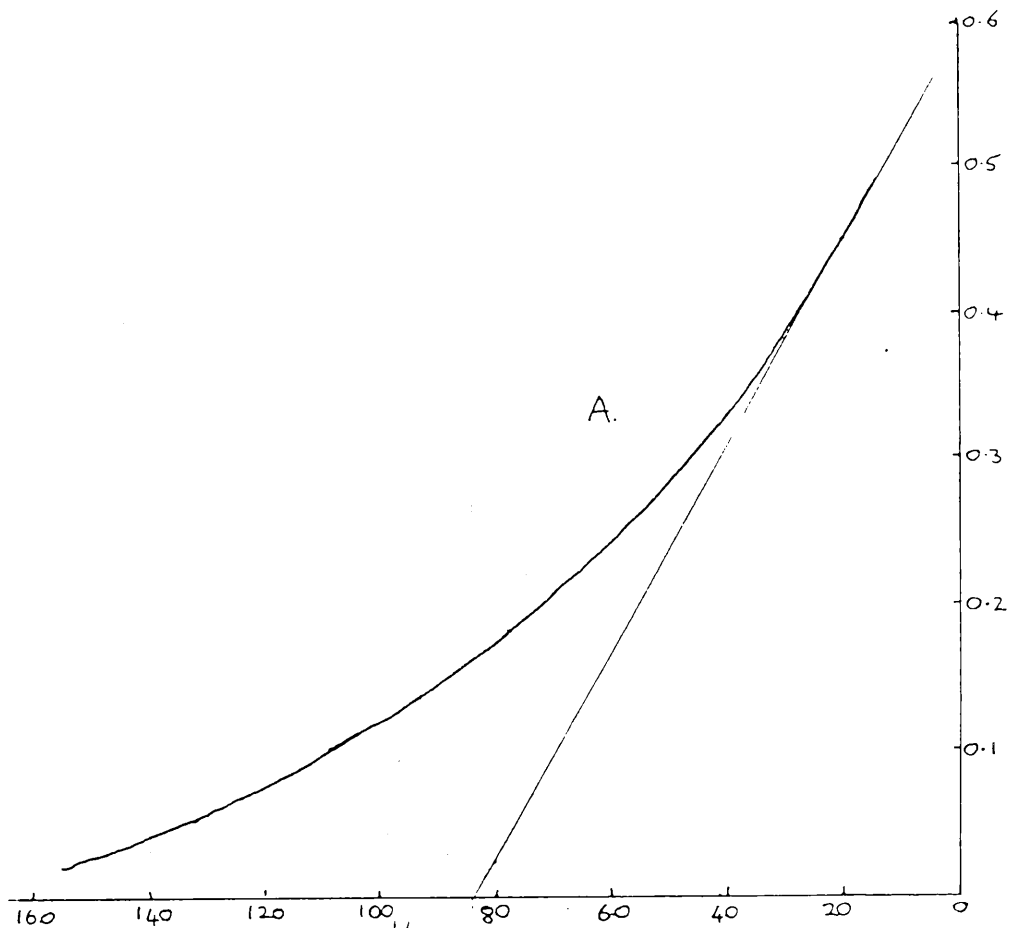


Fig. 4.3 U.V. absorption spectra of dilute lysozyme solutions in 0.1M ammonium acetate buffer pH5.

- a. lysozyme as supplied
- b. lysozyme after freeze drying
- c. lysozyme-tri-NAG complex after freeze drying.

Fig. 4.4 Absorption changes in a dilute suspension of *Micrococcus Lysodeikticus* cells on addition of lysozyme as described in the text,  
a. lysozyme as supplied  
b. lysozyme after freeze drying  
c. lysozyme-tri-NAG complex after freeze drying.

*Details on page 118*



TIME seconds

TABLE 4.5

## Lysozyme and Lysozyme-TriNAG Assays

	Absorption at 280nm	Lysozyme Conc. (mM)	Change in Absorption per minute at 450nm	Activity *
Lysozyme (as supplied)	0.399	0.015	0.424	19000
Lysozyme (freeze dried)	0.371	0.0143	0.390	19000
Lysozyme-TriNAG (freeze dried)	0.379	0.0140	0.435	20000

$$*Activity = \frac{\Delta A_{450}^{1min} \times 10000}{Lys.conc. \times Lys.molec.wt}$$

The accuracy of these activity values are very low because of the rather arbitrary way in which the O.D. at 450nm is measured. However it can be seen from the shape of the complete absorption curves that rates of reaction are similar for all 3 samples, showing that the dialysis and freeze drying of the lysozyme has not affected its properties. The high activity obtained for the lysozyme tri-NAG complex and the lack of inhibition by the tri-NAG is due to the very low concentrations of inhibitor present in the reaction cuvette. This leads to negligible formation of the enzyme-inhibitor complex under the assay conditions leaving the enzyme almost fully available for hydrolysing the lysodeikticus. However, the lysozyme-tri-NAG complex will form under the conditions of higher concentration used for making the Raman samples. Freeze drying will not remove the tri-NAG because of its high molecular weight.

#### 4.3.2 Trypsin and Trypsin-BPTI Preparation

10 mg of trypsin was dissolved in 0.2ml of 0.1M ammonium acetate, pH 8.09 and freeze dried. It was not thought to be necessary to add a small amount of  $\text{CaCl}_2$  to the solution to limit the extent of auto digestion of the trypsin which reduces the solutions activity because the solution was frozen immediately after its preparation. The  $\text{CaCl}_2$  would not have been removed in the freeze drying process and may have interfered with the Raman spectra. The results of the activity assay (see later) show only a small loss of activity on freeze drying.

1.7mg of BPTI and 7.7mg of trypsin, which gives approximately a 1:1 molar ratio, were dissolved in 0.2ml of ammonium acetate solution as described for trypsin. The very large association constant for trypsin-BPTI binding assures almost complete association with the high protein concentrations used.

The method of Chase, Jnr. and Shaw (1967) was used to measure the activity of the freeze dried trypsin and trypsin-BPTI preparations in solution relative to the activity of a sample of trypsin as supplied by Sigma. This method measures the amount of p-nitrophenol released by the hydrolysis of NPGB by trypsin which is directly related to the concentration of active trypsin. A solution of veronal buffer was prepared by making a 0.1M solution of veronal which was then adjusted to pH 8.3 by addition of concentrated HCL. A solution of 0.001M HCL and 0.02M  $\text{CaCl}_2$  and a solution of 0.01M NPGB in dimethyl formamide were also prepared,. The assay was performed by taking enough trypsin or trypsin BPTI complex to make a  $5 \times 10^{-5}$  M solution when dissolved in 0.98ml

buffer and 10ul of the HCL/CaCl<sub>2</sub> solution. This required 1.2mg of trypsin and 1.5mg of the trypsin-BPT1 complex. This solution was placed in a 1 ml cuvette of 1 cm pathlength. The reference cell in the spectrometer contained 0.98ml buffer, 10ul HCL/CaCl<sub>2</sub> and 10ul NPBG in dimethyl formamide. A reference base line at 410nm was recorded using the protein solution and the reference solution. 10ul of the NPBG solution was then added to the cuvette holding the protein solution, mixed rapidly and placed in the spectrometer. The absorbance at 410nm which measures the amount of the red p-nitrophenol molecule released on hydrolysis of the colourless NPBG ester, was recorded for several minutes. Essentially all the p-nitrophenol is released in a fast initial burst during the mixing to give a jump in the absorbance followed by a further slow increase in absorbance due to other slow hydrolysis processes which can be ignored. No extrapolation of absorbance to zero time was felt to be necessary due to the very small change in absorbance after the initial burst.

#### Results for Trypsin and Trypsin BPT1

The UV absorption changes at 410nm found when NPBG was added to solutions of trypsin as supplied, freeze dried trypsin and freeze dried trypsin-BPT1 are shown in Figure 4.6. The concentration (molar) of active trypsin in the 50uM protein solutions is calculated by measuring the optical density from the baseline to initial point after the burst of nitrophenol production and multiplying this figure by  $6.025 \times 10^{-5}$ . The results are summarised in Table 4.7.

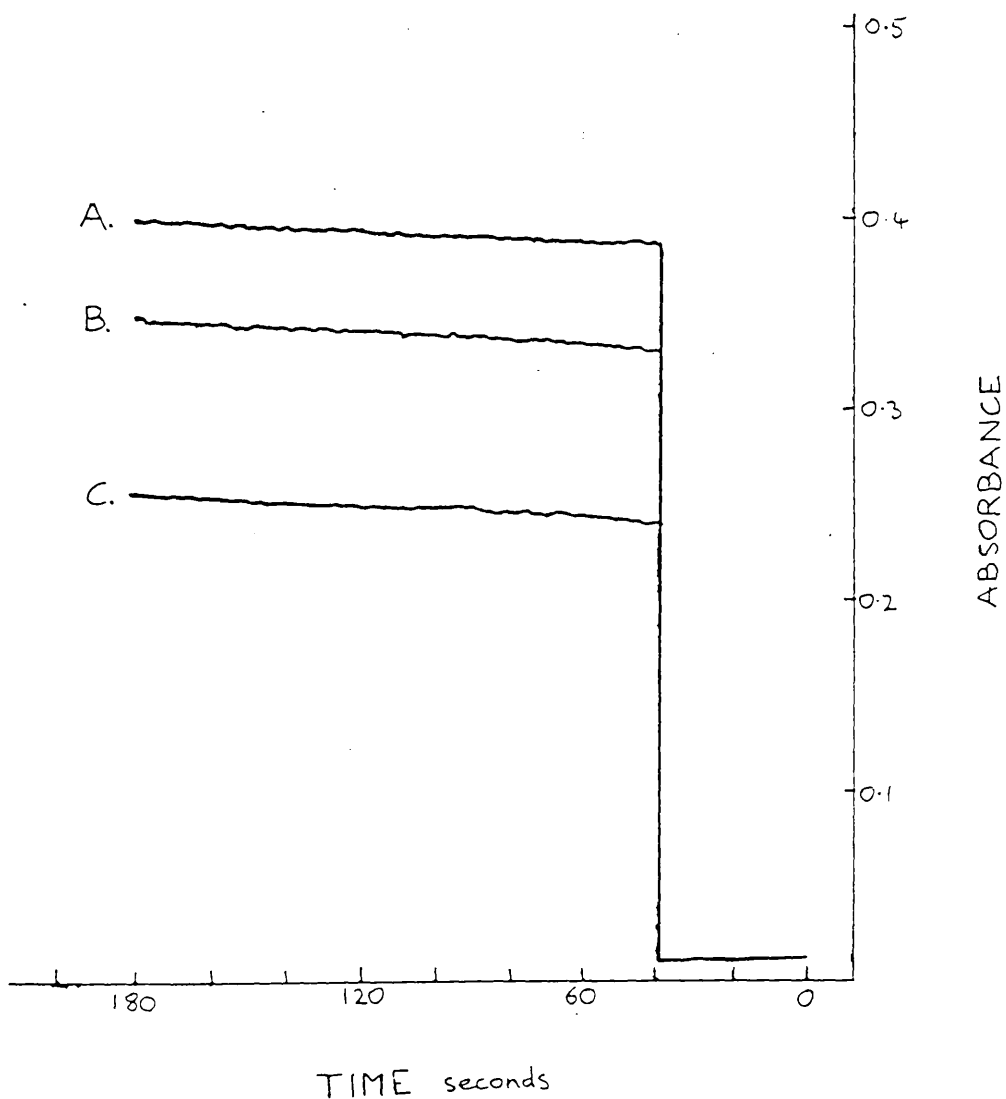


Fig. 4.6 Absorption changes caused by the addition of NPGB to trypsin solutions.  
 a. trypsin as supplied  
 b. trypsin after freeze drying  
 c. trypsin-BPTI complex after freeze drying.

*Details on page 122*

TABLE 4.7

## Trypsin and Trypsin-Inhibitor Complex Assays

	Absorption	Active Trypsin Conc. mol l <sup>-1</sup>	% activity
Trypsin (as supplied)	0.38	$2.29 \times 10^{-5}$	100
Trypsin (freeze dried)	0.32	$1.93 \times 10^{-5}$	84
Trypsin-BPTI (freeze dried)	0.232	$1.40 \times 10^{-5}$	61

From these results one can see that the trypsin is being inhibited by BPTI and that the activity of the freeze dried complex is approximately 70% of that of the freeze dried trypsin in solution. This indicates that perhaps not quite enough BPTI was added to the trypsin to produce a 1:1 mixture when freeze dried or that it has partially dissociated under the assay conditions. However the results do show that the inhibitor is bound to, rather than just mixed with, the trypsin in the freeze dried sample.

#### 4.3.3 GAPDH and GAPDH-NAD Preparation

10mg of the enzyme was dissolved in 2ml of 0.1M ammonium acetate, pH 6.95, and placed in dialysis tubing which had been softened in distilled water. This solution was dialysed against a large volume of ammonium acetate solution for approximately 4 hours, in order to remove the citrate salts. The enzyme solution was then recovered and placed in a flask. The solution was

frozen, attached to the vacuum line and freeze dried for 7 hours. The white solid recovered was used immediately for Raman spectroscopy.

The dehydrogenase -(NAD)<sup>4</sup> complex was formed by dissolving 5mg of undialysed dehydrogenase and 1mg of NAD<sup>+</sup> in 0.3ml of 0.1M ammonium acetate, pH 6.94. The amount of NAD added was sufficient to give a ten fold excess for each binding site on the enzyme, which should ensure that essentially all the enzyme molecules have at least one NAD<sup>+</sup> molecule bound if the association constant is of the order of  $2 \times 10^5 \text{ M}^{-1}$  (Velick et al., 1971). If the concerted model of allostery is appropriate for this enzyme then the largest conformational and dynamic changes should be seen when the first NAD<sup>+</sup> molecule binds. This solution was then frozen and freeze dried for 9 hours to give an "off-white" solid.

UV absorption spectra of 2.6mg of undialysed dehydrogenase and 1.6mg of GAPDH-NAD<sup>+</sup> complex, each dissolved in 0.5ml of 0.1M ammonium acetate, pH 6.95, were recorded on the Pye Unicam SP-1800 spectrophotometer. Figure 4.8 shows the uv absorption spectra of GAPDH as supplied by Sigma, and of the freeze dried GAPDH-NAD<sup>+</sup> complex, each dissolved in 0.5ml 0.1M ammonium acetate, pH 6.95.

GAPDH shows a large peak at 280nm typical of tryptophan and tyrosine absorptions. The ratio of absorbance at 280nm to that at 260nm should be 2:1 if there is no residual NAD<sup>+</sup> bound to the enzyme. In this case the ratio measured from the baseline is 1.78 to 1 indicating that some NAD<sup>+</sup> is present in the preparation supplied by Sigma. This ratio could have been improved by

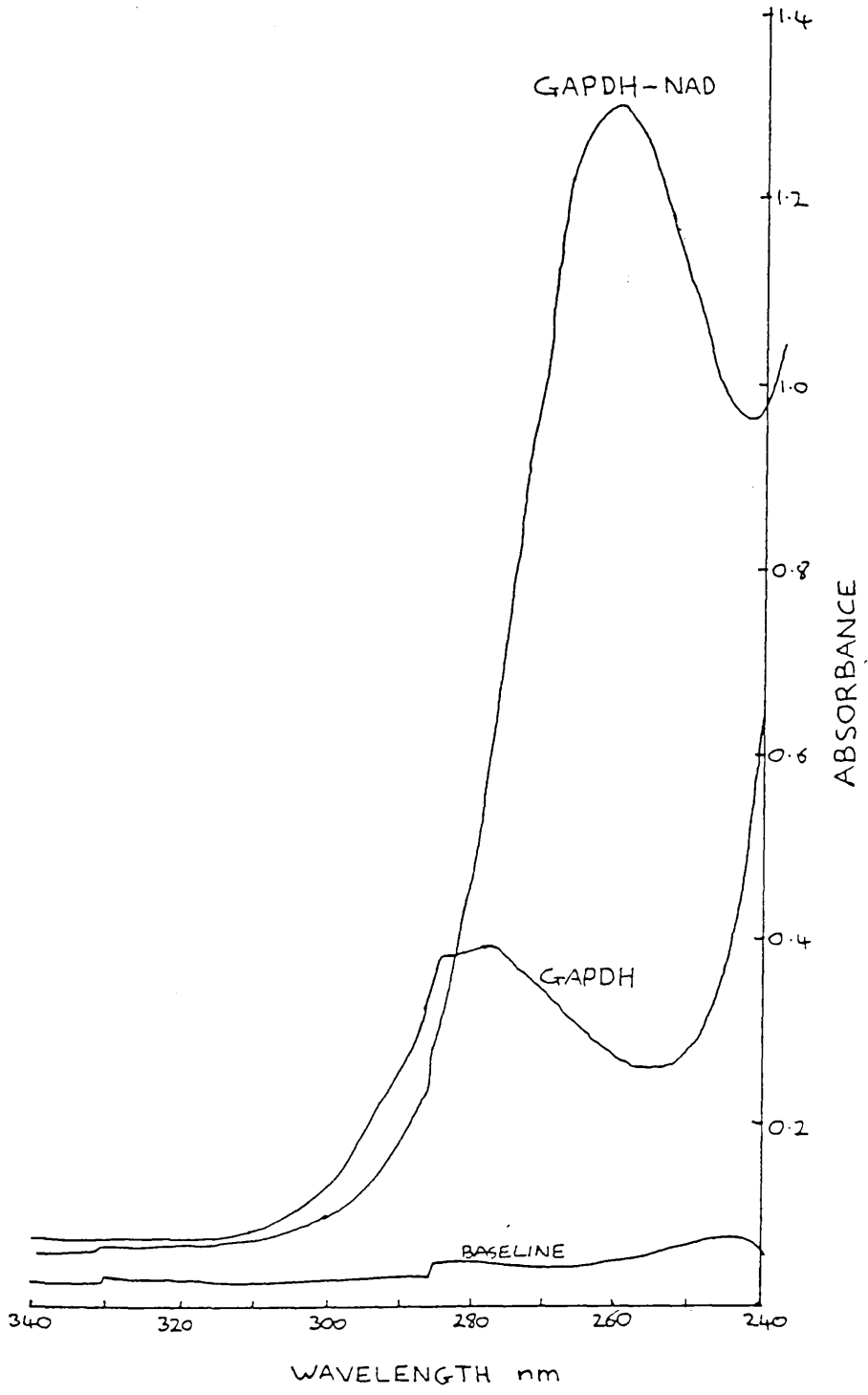


Fig. 4.8 U.V. Absorption spectra of GAPDH as supplied and after the addition of NAD.

chromatographic separation if more sample had been available. Cook and Koshland (1970), however used a sample of GAPDH with a ratio of only 1.8 to 1 and still obtained satisfactory results.

Binding of NAD<sup>+</sup> to GAPDH produces a characteristic shift in the absorbance maximum to 260nm, which is unique among the family of dehydrogenases.\* This shows clearly in the spectrum and indicates that the sample used for the Raman study is GAPDH with NAD<sup>+</sup> bound.

#### 4.3.4 Preparation of Partially Ligand Allosteric Bicyclic Crown Ethers

Small amounts of the unliganded and fully liganded samples supplied by Prof. Rebek were prepared in KBr discs and their infra red spectra recorded on a Perkin-Elmer I.R. spectrophotometer between 200 and 4000 cm<sup>-1</sup>. Raman spectra of samples ground to a fine powder and packed in glass capillaries or Allan bolts were recorded from 10 to 1700 cm<sup>-1</sup>. These spectra were recorded before the photomultiplier cooling unit was fitted and only the 200 to 1700 cm<sup>-1</sup> spectrum of the unliganded compound was of a better quality than those recorded with the cooled PM tube.

The remaining unliganded sample was used to make several partially liganded samples to see if a spectrum of the singly liganded complex could be obtained. Ligand to macrobicycle ratios of 0.5:1, 1:1, 1.5:1 were prepared, as well as a fully liganded 2:1 sample and an unliganded 0:1 control sample.

42.8mg of Hg(CN)<sub>2</sub> was dissolved in 5ml of Aldrich Gold Label spectroscopic methanol. 0.5ml of this solution contained enough

\* NAD gives this characteristic absorption at 260nm.

ligand to fill 25% of the binding sites of a 20mg sample of the unliganded polyether. The various ligand to polyether ratios were obtained by adding the appropriate amount of the ligand solution to 20mg of the unliganded ether and making up to 2ml total volume with more methanol. These solutions were left for approximately 10 minutes to allow equilibrium to be reached then they were frozen by immersing the flask in liquid nitrogen and attached to a vacuum line with a liquid nitrogen cold trap and a Gene-Vac rotary vacuum pump. The pressure in the line could be checked with a Pirani gauge. If the sample was not frozen before exposing it to a vacuum, very rapid boiling would occur with a possible loss of sample in the vacuum line, as the liquid to vapour equilibrium was reached. The methanol and any other volatile impurities evaporated in about one hour leaving a thick oil for the 0:1 and 0.5:1 samples and a white solid for the other samples. The thick oil would solidify to give a waxy solid if it was scraped with a spatula. A small amount of ( 1ml) of Analar Ethyl Acetate (Aldrich) was then added to the samples. When this was vacuumed off and then repeated a white, slightly waxy, solid was recovered for the 0:1 and 0.5:1 samples and a white crystalline powder for the other samples.

When the samples were ground up and placed in an Allen nut sample holder in the spectrometer it was found that they all fluoresced strongly,. This decreased with time to a negligible level with the 1:1, 1.5:1 and 2:1 samples but persisted with the 0:1 and 0.5:1 samples, Raman spectra of these last two samples were of poor quality above 200cm<sup>-1</sup> particularly the 0:1 spectrum hence the spectrum of the original unliganded compound is shown.

## CHAPTER 5

### Raman and Infra-Red Spectroscopy of the Allosteric Model Compound

#### 5.1 General notes on the Spectra of the Unliganded and Fully Liganded Compound

The macrobicyclic ethers will be referred to by their state of ligation i.e. 0/1 for the unliganded molecule and 2/1 for the fully liganded molecule with two mercury cyanide ligands bound. The intermediate ligand/ether molecules prepared will be referred to as 0.5/1, 1/1 and 1.5/1.

Figure 5.1 shows the low frequency Stokes Raman spectra of all the bicyclic ethers supplied or prepared as described in section 4.4. Figure 5.2 shows the high frequency Raman spectra ( $\approx 2000 \text{ cm}^{-1}$ ) of the 0/1 compound as supplied by Prof. Rebek and of the 2/1 compound prepared in section 4.4. Figure 5.3 gives the high frequency Raman spectra of the 0.5/1, 1/1 and 1.5/1 samples and Figure 5.4 the infra-red spectra of the 0/1 and 2/1 compounds. The vibrational frequencies of all the Raman and infra-red bands of the 0/1 and 2/1 samples are given in Figure 5.5.

The bands seen are approximately assigned by comparing them with spectra of biphenyl, 18-crown-6 with and without a ligand coordinated in the centre of the crown ring and with general information on vibrations of organic molecules (Dollish *et al.*, 1974; Bree *et al.*, 1971; Takeuchi *et al.*, 1981; Pouchert, Dale, 1957; Fouassier & Lassegues, 1978; McLachlan, 1974; Wulfsberg & Weiss, 1977; Nyquist & Kogel, 1971; Jones, 1957; Melson, 1979).

Accurate assignments would only be possible if a series of macrobicyclic compounds or the isotopically substituted compound were available for study or if a computer normal mode calculation was available.

The Raman spectra of the 2 molecules are completely different below about  $450\text{cm}^{-1}$  which is the region where vibrations are thermally excited and involve large parts of the molecule thus allowing the possibility of communication between the two binding sites by frequency changes on ligand binding. At higher frequencies the normal modes will involve motions of smaller groups of atoms and one might expect ligand binding to simplify the high frequency spectra, particularly of vibrations of the two crown rings, by restricting the modes of coupling between groups. Modes involving the biphenyl group should be relatively insensitive to ligand binding as no bonds are formed between the ligand and the biphenyl, whereas modes due to the crown  $\text{CH}_2$  groups coupling to each other through the intervening oxygen atoms will become decoupled. This causes the two coupled modes to move closer together in frequency towards their natural frequencies. If these natural frequencies are the same then the two peaks in the 0/1 compound will merge to become one. This is particularly evident in the I.R. spectra where several doublets and the multiple bands around  $1120\text{cm}^{-1}$  in the 0/1 molecule become single bands in the 2/1 complex. The Raman spectra show changes in the relative intensities of several groups of bands. The bands are tentatively assigned to group modes predominantly of the crown ring  $\text{CH}_2$  and  $\text{COC}$  groups.

2

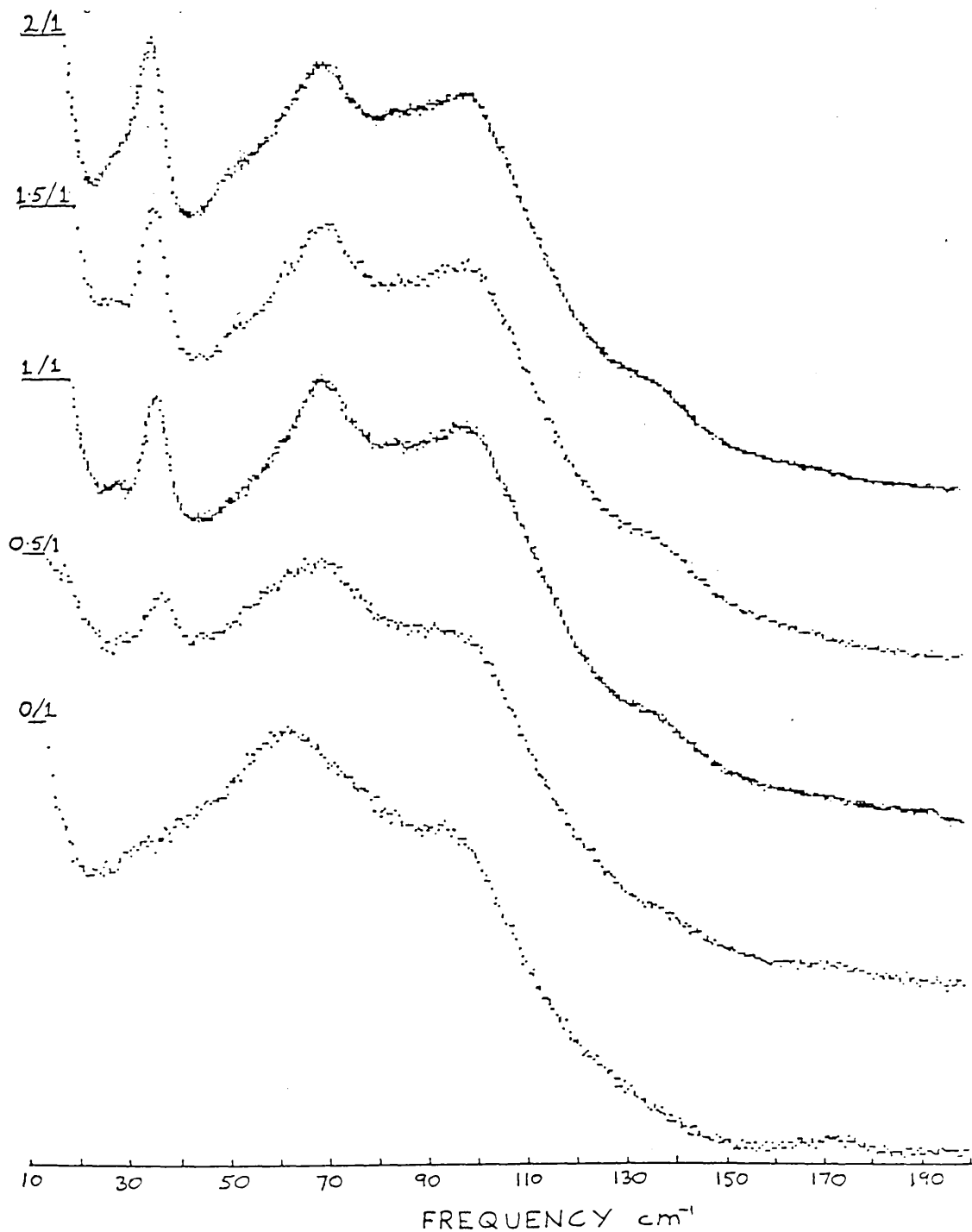


Fig. 5.1 Low frequency ( $10\text{-}200\text{ cm}^{-1}$ ) Raman spectra of the  $0/1$ ,  $0.5/1$ ,  $1.5/1$  and  $2/1$  macrobicyclic ether compounds. Recorded with  $20\text{-}45\text{ mW}$  of  $514.5\text{ nm}$  radiation,  $250\text{ micron}$  slitwidths at  $10\text{ cm}^{-1}/\text{min}$  with time constants of  $1.2$  or  $3$  seconds.

Fig. 5.2 High frequency (200-1650  $\text{cm}^{-1}$ ) Raman spectra of the 0/1 and 2/1 compounds. Recorded with 380 and 200 mW of 614.5 nm radiation, 500 micron slitwidths at 50  $\text{cm}^{-1}/\text{min}$  and 25  $\text{cm}^{-1}/\text{min}$  with time constants of 1 and 2 seconds.

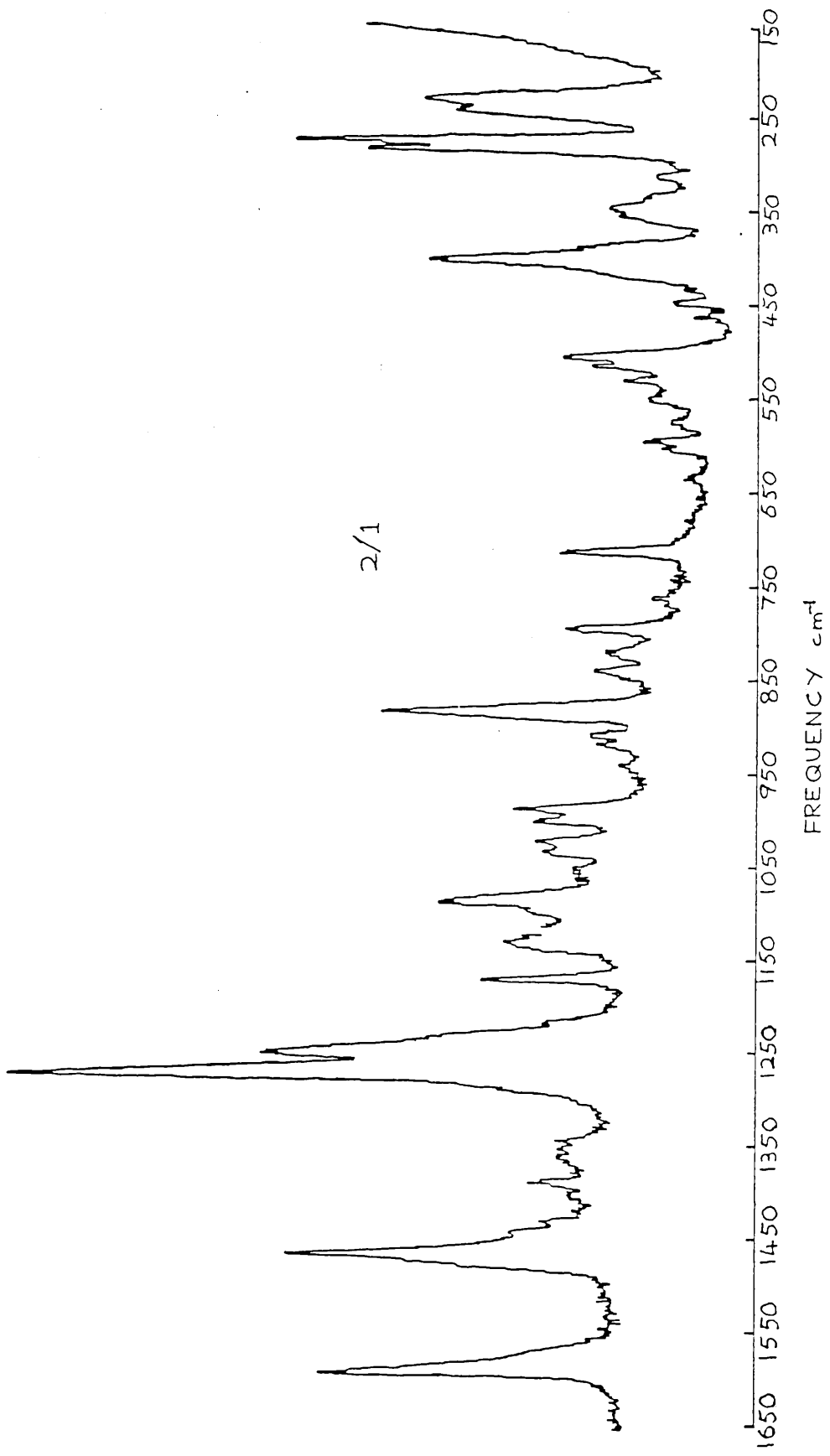
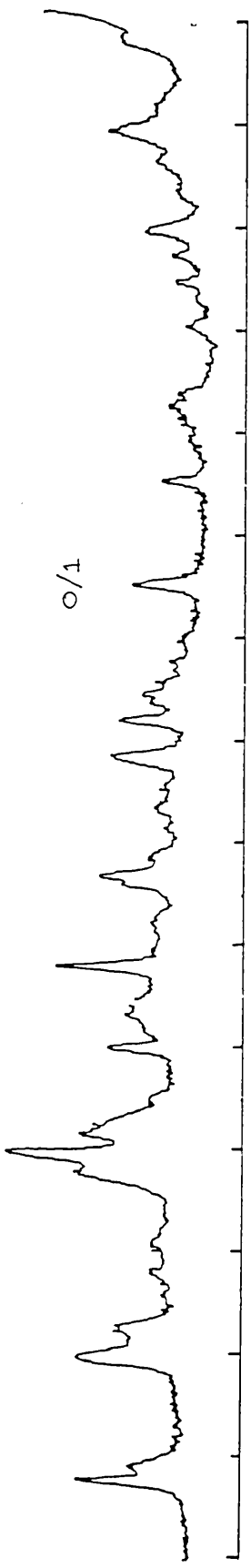


Fig. 5.3 High frequency (200-1650  $\text{cm}^{-1}$ ) Raman spectra of the 0.5/1, 1/1 and 1.5/1 compounds. Recorded with 200,200 and 30 mW of 514.5 nm radiation, 500 micron slitwidths at 25,50 and 25  $\text{cm}^{-1}/\text{min}$  with 2,1 and 3 second time constants.

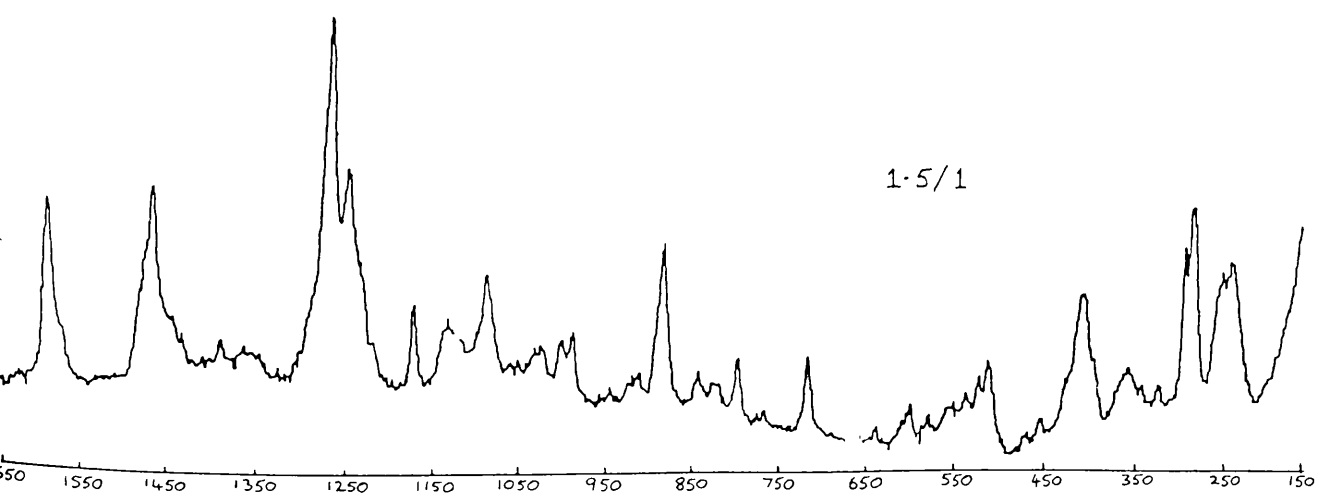
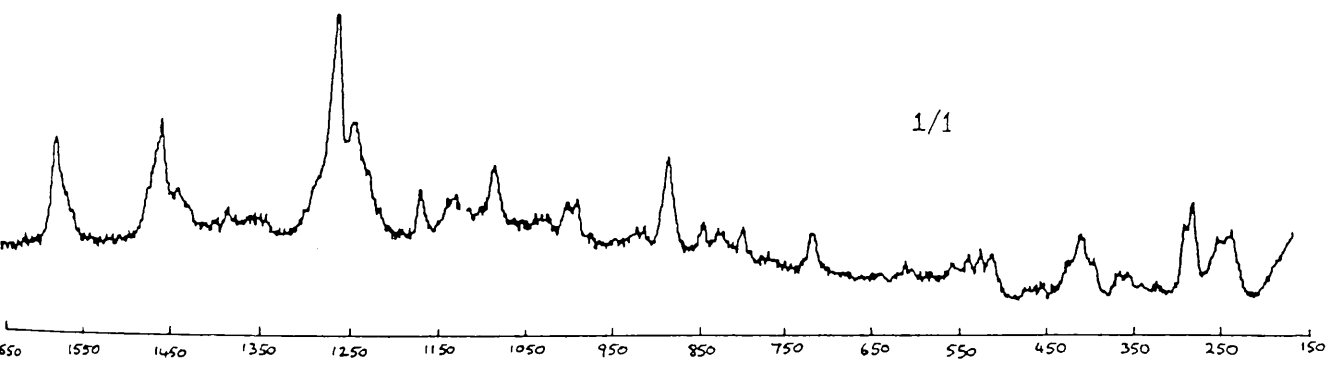
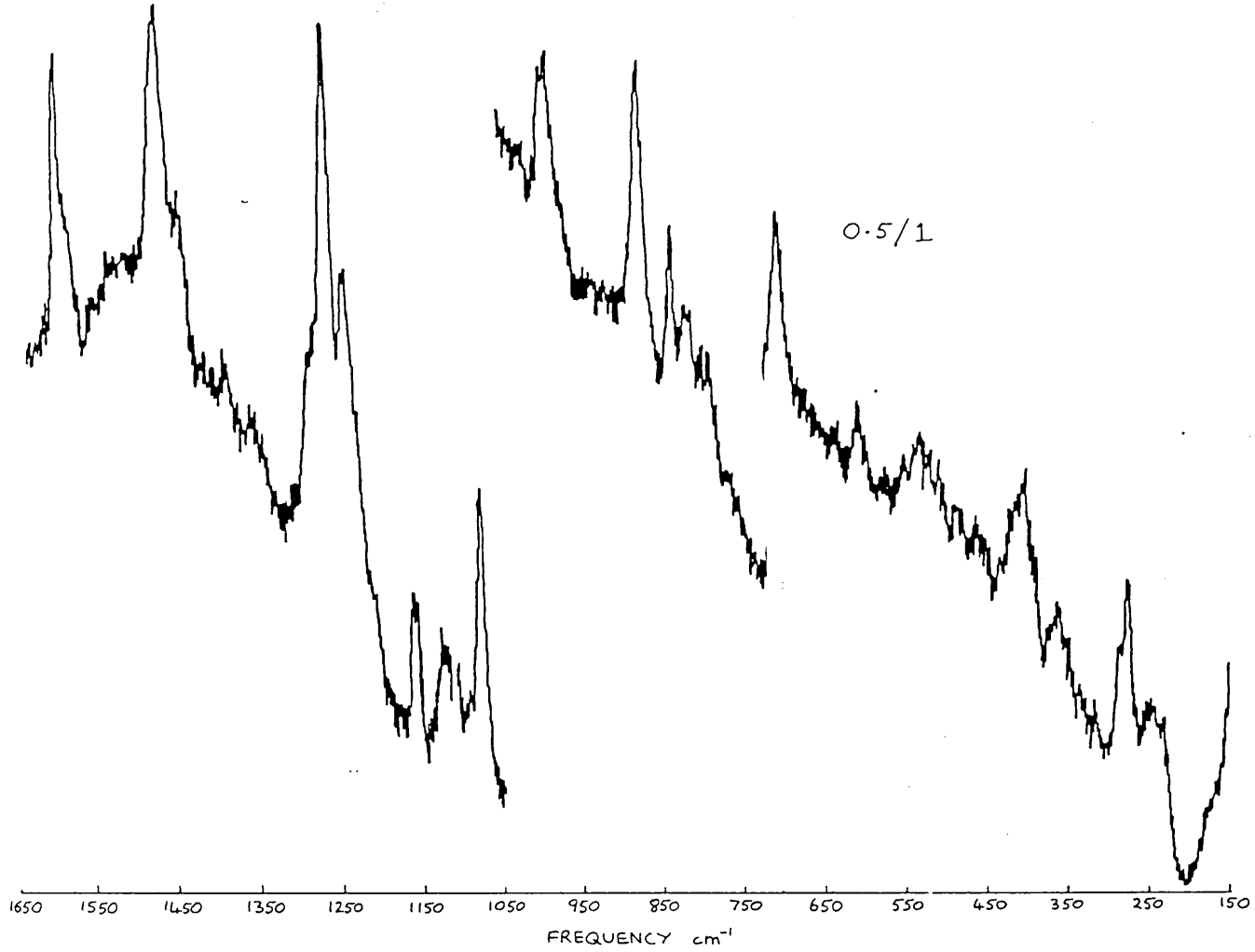


Fig. 5.4 The infra red spectrum of the 0/1 and 2/1 compounds from 200 to 1300  $\text{cm}^{-1}$ .

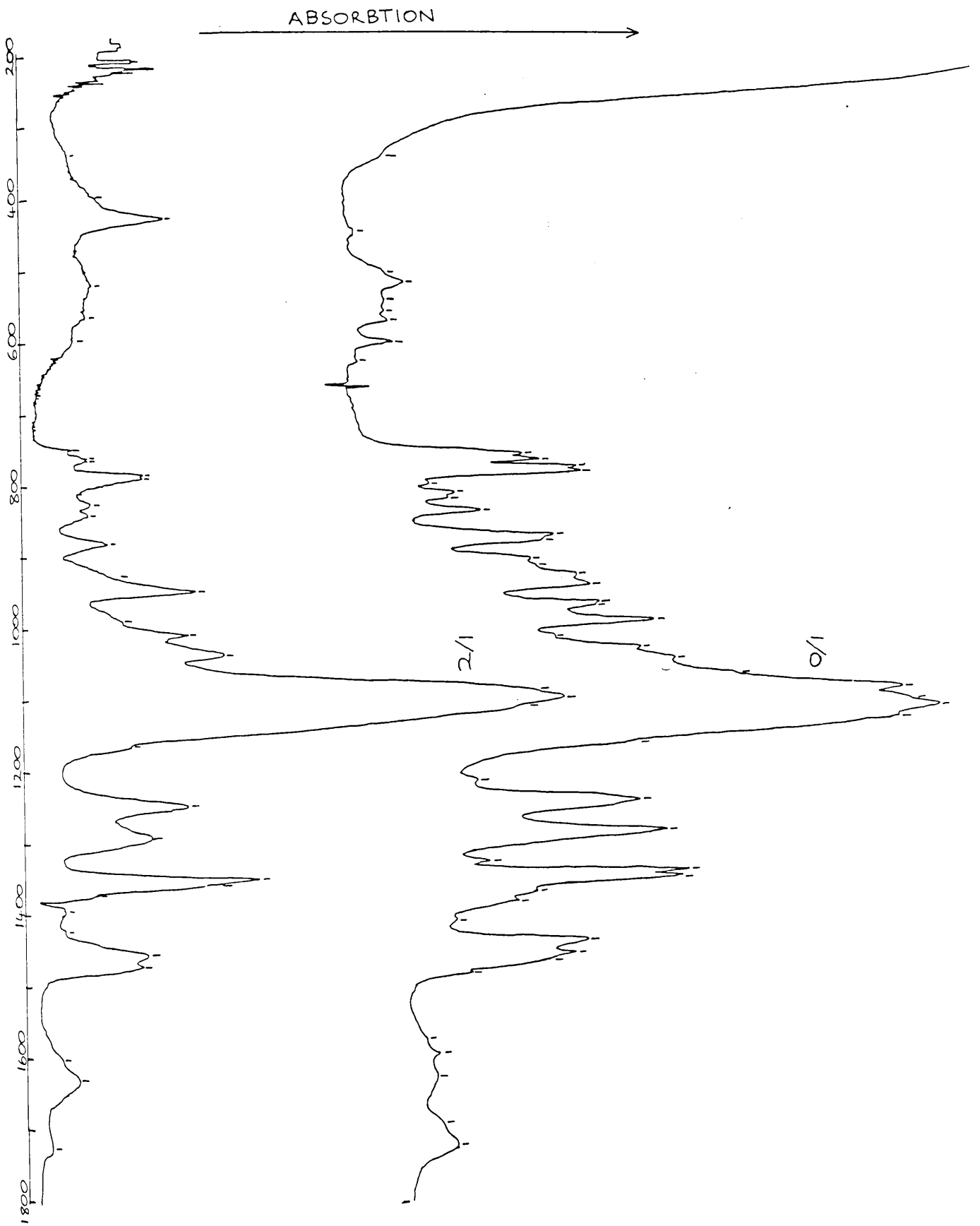


Table 5.5

Vibrational frequencies of Raman and infra-red bands for the unliganded and fully liganded macrobicyclic ether

Unliganded (cm <sup>-1</sup> )		Liganded		Unliganded		Liganded	
1722	I.R.	1722	I.R.			889	
1690	I.R.			880	I.R.	880	I.R.
1627	I.R.	1627	I.R.	878			
1599		1598	I.R.	874	I.R.		
1595	I.R.	1592		842		847	
1586				839	I.R.	840	I.R.
1573	I.R.	1574		824		825	I.R.
1482	I.R.			820	I.R.	824	
1474		1478		817			
1469	I.R.	1468	I.R.	812	I.R.		
		1466		804		801	
		1450	I.R.	800	I.R.		
1445		1447		793		790	I.R.
1442	I.R.			785	I.R.	785	I.R.
		1432		784			
1410	I.R.			779	I.R.		
1390		1390		768	I.R.	768	
1385	I.R.	1390	I.R.	763		765	I.R.
1373	I.R.	1370	I.R.	760	I.R.	760	I.R.
1360		1355				750	I.R.
1355	I.R.	1353	I.R.	710	I.R.	718	
1347	I.R.	1346	I.R.	708			
1291		1292				641	
1290	I.R.	1288	I.R.	629	I.R.		
1275		1269		605		609	
1253		1250		604	I.R.	601	
1248	I.R.	1245	I.R.			597	I.R.
1243		1234		574	I.R.	580	
1218		1220		565		565	I.R.
1215	I.R.			548			
1167		1174		545	I.R.		
1165	I.R.	1160	I.R.	531		535	
1149				521	I.R.	523	I.R.
1137	I.R.			518		518	
1134		1135		508	I.R.	511	
1120	I.R.					467	
1110	I.R.	1110	I.R.	452		451	
		1100		450	I.R.		
		1100	I.R.			432	I.R.
1094	I.R.	1092		427		430	
1086		1088	I.R.	408		406	
1070	I.R.					400	I.R.
		1060				392	
1048	I.R.			383			
1042		1040		357		354	
1032	I.R.	1035	I.R.	345	I.R.	342	I.R.
		1028				338	
1015	I.R.	1008	I.R.	319		316	
1004		1006		289		287	
996		991				277	
995	I.R.	987	I.R.	258			
973	I.R.					244	
970	I.R.			235		234	
949		946		173			
943	I.R.	945	I.R.			137	
929		925		93		100	
917	I.R.	925	I.R.	62		70	
908						52	
908	I.R.					36	
				~ 30-50?			

## 5.2 Assignments of Raman and I.R. Bands for the 0/1 and 2/1 compounds

0-450cm<sup>-1</sup>

Both the 0/1 and 2/1 compounds possess two intense, very broad bands at 62cm<sup>-1</sup> and 93cm<sup>-1</sup> and at 70cm<sup>-1</sup> and 100cm<sup>-1</sup> respectively. These bands may be composed of several vibrational modes as well as rotational and translational vibrations of the whole molecule in the crystal lattice. The broad sloping shoulder in the 0/1 molecule may be converted to the more well defined shoulder at 52cm<sup>-1</sup> in the 2/1 molecule and the long shallow tail of the 93cm<sup>-1</sup> band may mask a band which becomes the 137cm<sup>-1</sup> band in the 2/1 compound. This band becoming visible when the structure is stiffened on ligand binding. These bands of the 0/1 and 2/1 molecules are impossible to assign to any particular inter or intramolecular mode. They will mainly be intramolecular vibrations spanning the whole molecule as seen in other large organic molecules (Vergoten et al., 1978).

There are various rigid body motions of the molecules within the crystal lattice unit cell which may also contribute. There are  $3m$  rotations about the axes of inertia and  $3(m-1)$  translational modes where  $m$  is the number of molecules per unit cell, which is 4 in the 2/1 complex. Assuming that  $m=4$  for the 0/1 unit cell as well then there will be 12 rotations and 9 translations. Rotations about two of the axes of inertia will be hindered because of a large moment of inertia and consequently be of very low frequency, while rotation about the axis joining the two binding sites may well be easier and give rise to a visible

band. There will be 4 rotational modes in the unit cell about this molecular axis but they will probably be degenerate giving only one band. These rotations will shift in frequency only a negligible amount on ligand binding because the heavy mercury atoms bind along the axis of inertia thus not contributing anything to the moment of inertia. Since all the bands seen in this region do shift on ligand binding one concludes that these rotational modes are too weak to be seen. The 9 translational modes are likely to be of very low frequency or weak because of the large mass of the molecule and the weak nature of intermolecular interactions in organic molecules. This implies that the low frequency modes, except the  $36\text{cm}^{-1}$  in the 2/1 complex to be discussed next are intramolecular long range global vibrations of the molecular skeleton which are the sort of modes required for dynamic allostery. The shifts of  $8\text{cm}^{-1}$  on ligand binding will contribute favourably to the cooperative free energy  $\Delta\Delta G$ . The sharp intense peak at  $36\text{cm}^{-1}$  in the 2/1 complex is assigned to a vibration of the ligand perpendicular to and through the plane of the crown rings. That this mode is due to the ligand is supported by the low frequency spectra of the partially liganded complexes where this mode increases in intensity as the ligand concentration increases. The nature of the mode is suggested by several studies of ion and ligand binding in the centre of 18-crown-6, (Fouassier et al., 1978; Melson et al., 1979) where the frequency of this sort of mode was found to depend on the weight of the ligand but not on the solvent. If it is assumed that the vibrations are harmonic, that the bond strengths are equal and that the different number of

bonds involved (6 for the 18-crown-6, 5 for the Rebek molecule), does not influence the result, than a plot of wavenumber versus (ligand mass)<sup>-1/2</sup> should be a straight line. Such a plot shown in Figure 5.6 is in fact remarkably good considering the crudity of the assumptions and supports the assignment of this mode in the 2/1 complex.

Above 150cm<sup>-1</sup> the 0/1 molecule shows strong bands at 173, 258 and 357cm<sup>-1</sup> with other less intense bands at 235, 289, 319, 383, 408, 427 and 452 cm<sup>-1</sup>. These are all assigned to deformation modes of the crown rings with the modes becoming more localised as their frequency increases. The lower frequency modes particularly may be involved in the allosteric effect. These modes are assigned to the crown rings because 18-crown-6 and its complexes show several modes in this region while biphenyl only has two weak bands in this region.

The 2/1 complex shows strong bands at 234, 244, 277, 287 and 406 cm<sup>-1</sup> in the Raman spectrum and a strong I.R band at 432 cm<sup>-1</sup>. There are medium to weak bands at 316, 338, 354, 392, 430, 451 and 467 cm<sup>-1</sup>. The especially sharp bands at 277 and 287 cm<sup>-1</sup> and the I.R. band at 432 cm<sup>-1</sup> are probably ligand bends and a stretch respectively since Hg(CN)<sub>2</sub> alone shows strong I.R. bands at 276 and 442 cm<sup>-1</sup> while 18 crown 6 and biphenyl show nothing. The other bands are again probably crown ring deformations with vibrations of the ligand now mixed in. The doublet like appearance of the 234, 244 and 277, 287 cm<sup>-1</sup> bands may be due to an increase in the coupling of the vibrations involved in one crown ring with the similar vibrations in the other ring, as discussed in the general notes. The more localised the modes

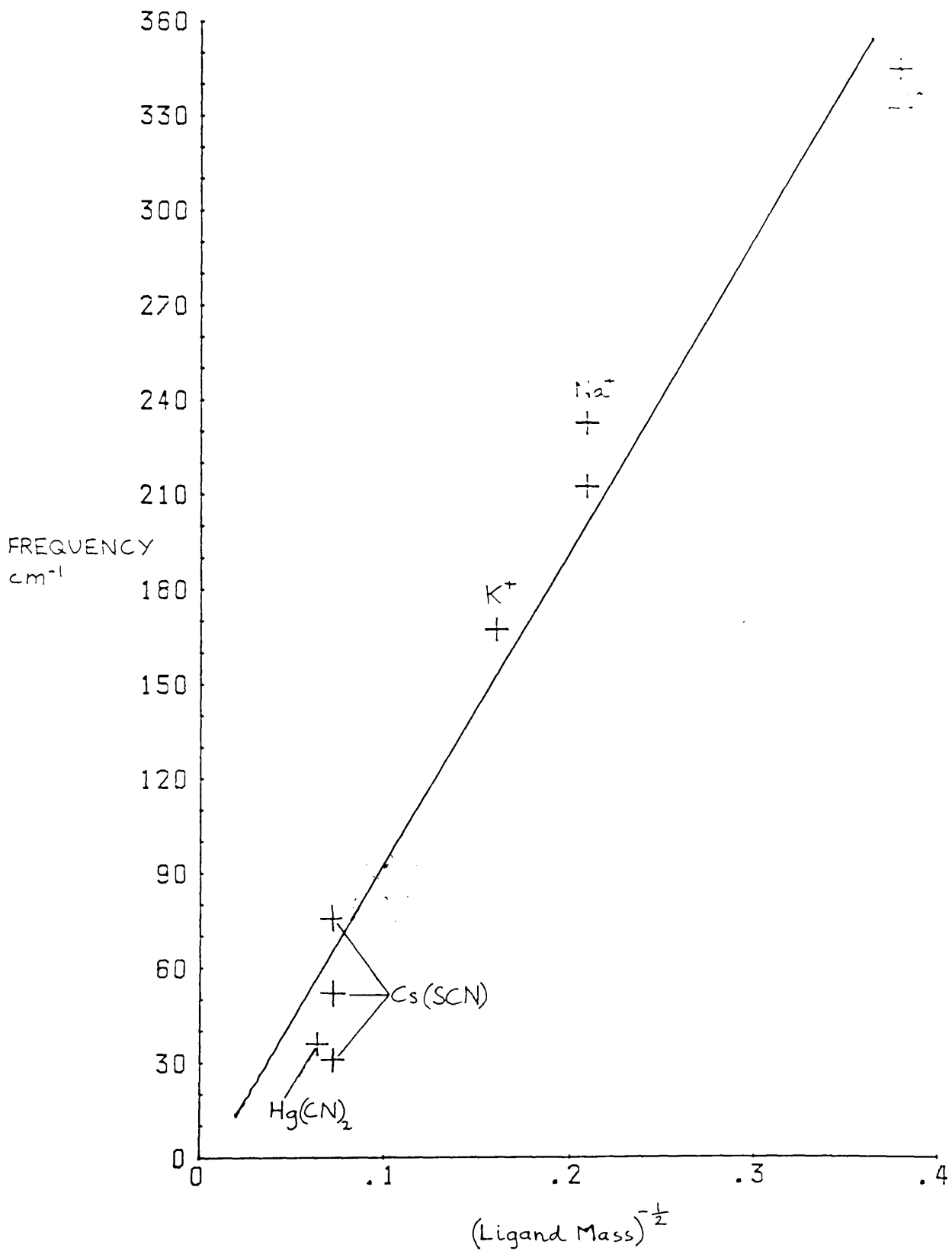


Fig. 5.6 Ligand-crown ether low frequency vibrations for various sizes of ligand.

become the more likely is a decrease in the coupling on ligand binding.

#### 450-650cm<sup>-1</sup>

The 0/1 spectra show several medium to weak bands at 518, 531, 548, 565 and 605 cm<sup>-1</sup> in the Raman and 508, 521, 545, 560, 574 and 604 cm<sup>-1</sup> in the I.R spectrum. These bands may involve bending of C-OC and O-C-C groups of the crown rings coupled to C-C in-plane deformations of the biphenyl group. 18-crown-6 shows no bands in this region but biphenyl shows a sharp band at 610cm<sup>-1</sup> and biphenyl substituted with a methyl group next to the bridge bond, shows this mode as well as several others between 450 and 600cm<sup>-1</sup>. These bands are therefore likely to arise from the biphenyl group and the nearest ether groups.

Ligand binding broadens the I.R. bands so that only 3 remain at 523, 565 and 597cm<sup>-1</sup> but gives rise to more modes in the Raman spectrum at 511, 518, 535, 554 and 580 cm<sup>-1</sup> which decrease in intensity from the medium strength 511cm<sup>-1</sup> peak to the weak 580cm<sup>-1</sup> peak. The 605cm<sup>-1</sup> peak in the 0/1 spectrum becomes a weaker doublet at 601 and 609 cm<sup>-1</sup>. This splitting may be due to the ligands increasing the coupling between modes on either side of the biphenyl groups as discussed earlier.

#### 650-750cm<sup>-1</sup>

The only band present in either the 0/1 or 2/1 spectra is a medium strength sharp Raman band at 708cm<sup>-1</sup> in the 0/1 and 718cm<sup>-1</sup> in the 2/1 molecules. 18-crown-6 shows nothing in this region but biphenyl shows a band of similar shape at about 730cm<sup>-1</sup>. This band is likely to be a benzene ring vibration affected by the substitution pattern of groups on the ring.

750-900cm<sup>-1</sup>

The Raman spectrum of the 0/1 sample shows a succession of bands of increasing intensity starting from a weak band at 753cm<sup>-1</sup>, through 784, 793, 804, 817 and 824cm<sup>-1</sup> to a medium strength band at 842cm<sup>-1</sup>. At 878cm<sup>-1</sup> there is another medium strength band. The 2/1 complex shows a weak band at 768cm<sup>-1</sup>, a medium band at 801cm<sup>-1</sup>, followed by two weaker bands at 824cm<sup>-1</sup> and 847cm<sup>-1</sup> and a strong band at 889cm<sup>-1</sup>.

There are similar large changes in the I.R. spectra, where the two strong doublets at 760, 768cm<sup>-1</sup> and 779, 785cm<sup>-1</sup> become the weaker pair at 760, 765cm<sup>-1</sup> and 785, 790cm<sup>-1</sup> on binding. The weak bands at 800, 812, 820 and 839cm<sup>-1</sup> become the 825 and 840cm<sup>-1</sup> bands and the strong doublet at 874, 880cm<sup>-1</sup> becomes the weak singlet at 880cm<sup>-1</sup>.

The bands below 800cm<sup>-1</sup> in the I.R. are likely to be biphenyl C-C deformation modes due to the ring substitution pattern and hence one would not expect ligand binding to change the coupling pattern by much.

Above about 800cm<sup>-1</sup>, biphenyl shows no I.R. or Raman modes, but 18-crown-6 shows 3 strong Raman bands at about 810, 850 and 870cm<sup>-1</sup> and a broad I.R. band around 850cm<sup>-1</sup>. These have been approximately assigned to CH rock in the crown ring for the modes between 800cm<sup>-1</sup> and 850cm<sup>-1</sup> while the large band(s) between 850 and 900cm<sup>-1</sup> are C-O-C symmetric stretches in the crown rings. These stretches would be little affected by ligand binding because of their symmetry.

900-950cm<sup>-1</sup>

The Raman spectrum of the 0/1 compound shows 3 weak bands at 908, 929 and 949cm<sup>-1</sup> which become 914, 925 and 946cm<sup>-1</sup> on ligand binding. The 914 and 925cm<sup>-1</sup> bands become stronger and sharper. The 0/1 I.R. spectrum shows well defined medium strength bands at 908, 917, 929 and 943 cm<sup>-1</sup> which change dramatically on binding to give a medium strength band at 945cm<sup>-1</sup> and a weak shoulder at 925cm<sup>-1</sup>. 18-crown-6 shows a very weak Raman band and a strong I.R. band in this region while biphenyl shows no bands. These bands are therefore assigned to methylene rocks of the crown rings, the effect of ligand binding being to reduce coupling between CH groups and reduce the number of bands.

950-1200cm<sup>-1</sup>

The 0/1 I.R. spectrum shows a large number of medium to strong bands in this region most of which disappear in the 2/1 spectrum. The 0/1 spectrum shows peaks at 970, 973 and 995cm<sup>-1</sup> which become a weak shoulder at about 987cm<sup>-1</sup> in the 2/1. Similarly in the Raman spectrum where the 978cm<sup>-1</sup> band disappears. The I.R. spectrum of the 0/1 molecule then shows a strong broad band made up of many components at 1015, 1032, 1048, 1070, 1094, 1110, 1120, 1137 and 1165cm<sup>-1</sup> with the maximum absorbance at 1120cm<sup>-1</sup>. Binding simplifies this dramatically leaving two medium strength peaks of 1008, and 1035cm<sup>-1</sup> and a very strong peak consisting of poorly resolved components at 1088, 1100 and 1110cm<sup>-1</sup> and a weak shoulder at 1160cm<sup>-1</sup>. The Raman spectrum on the other hand, becomes more complicated on binding with the medium strength doublet at 996, 1004cm<sup>-1</sup> becoming better resolved at 991, 1006cm<sup>-1</sup>.

and the weak  $1042\text{cm}^{-1}$  band becoming a well resolved doublet of medium strength at  $1028, 1040\text{cm}^{-1}$ . A weak band at  $1160\text{cm}^{-1}$  also appears on binding. The strong sharp  $1086\text{cm}^{-1}$  band weakens and shifts to  $1092\text{cm}^{-1}$  with a shoulder at  $1100\text{cm}^{-1}$  while the weak broad bands at  $1134\text{cm}^{-1}$  and  $1149\text{cm}^{-1}$  become a medium strength band at  $1135\text{cm}^{-1}$ . The medium strength  $1167\text{cm}^{-1}$  band shifts to  $1174\text{cm}^{-1}$  and remains as strong.

The Raman spectrum of biphenyl shows 3 strong bands at  $1000, 1040$  and  $1170\text{cm}^{-1}$ , the first two of which split into doublets in the methyl substituted biphenyl. 18-crown-6 however only shows two medium strength peaks around  $1050\text{cm}^{-1}$ . The I.R. of biphenyl shows two bands at  $1010\text{cm}^{-1}$  and  $1040\text{cm}^{-1}$ . These biphenyl modes are all ring breathing modes and the Raman bands at  $991, 1006, 1028, 1040$  and  $1174\text{cm}^{-1}$  in the 2/1 and  $996, 1004, 1042$  and  $1167\text{cm}^{-1}$  in the 0/1 molecule are assigned to these modes. The I.R. bands at  $1008, 1035$  and  $1160\text{cm}^{-1}$  in the 2/1 and  $1015, 1032$  and  $1165\text{cm}^{-1}$  in the 0/1 molecule are probably the infra red equivalents of these Raman bands. All the other I.R. and Raman bands in this region are assigned to C-O-C antisymmetric stretches of the crown rings since the very strong I.R. peak around  $1100\text{cm}^{-1}$  is characteristic of crown ethers and the Raman spectrum of 18-crown-6 shows some strong bands here as well. The antisymmetric stretch, unlike the symmetric C-O-C stretch, will be affected by the presence of the ligand because the ligand-oxygen bond will restrict the oxygen movement and decouple vibrations of neighbouring groups resulting in a simpler I.R. spectrum and reducing the intensity of the Raman antisymmetric stretch relative to the symmetric stretch.

1200-1310cm<sup>-1</sup>

The 0/1 Raman spectrum shows shoulders to the strong 1253cm<sup>-1</sup> band at 1218cm<sup>-1</sup> and 1243cm<sup>-1</sup>. There is a shoulder of equal strength to the 1253cm<sup>-1</sup> band at 1291cm<sup>-1</sup> on the very strong sharp Raman band at 1275cm<sup>-1</sup>. In the 2/1 complex, there are shoulders at 1220cm<sup>-1</sup> and 1234cm<sup>-1</sup> to the strong 1250cm<sup>-1</sup> band which maintains its intensity relative to the very strong band at 1269cm<sup>-1</sup> while the shoulder at 1292cm<sup>-1</sup> loses intensity.

The 0/1 I.R. spectrum shows a weak band at 1215cm<sup>-1</sup> and two strong bands at 1248cm<sup>-1</sup> and 1290cm<sup>-1</sup>, the higher frequency band being stronger. On binding the 1288cm<sup>-1</sup> band loses intensity and becomes weaker than the 1245cm<sup>-1</sup> bands as in the Raman spectra. These bands are the I.R. equivalent to the 1253, 1291cm<sup>-1</sup> bands in the 0/1 Raman spectrum and the 1250, 1291cm<sup>-1</sup> bands in the 2/1 Raman spectrum.

Biphenyl shows no I.R. bands and one very strong Raman band at 1275cm<sup>-1</sup>, while 18-crown-6 shows two characteristic I.R. bands at 1250cm<sup>-1</sup> and 1300cm<sup>-1</sup> and 4 medium strength Raman bands from about 1220cm<sup>-1</sup> to 1300cm<sup>-1</sup>.

Consequently the 1275cm<sup>-1</sup> band in the 0/1 and the 1269cm<sup>-1</sup> band in the 2/1 complex are assigned to the C-C stretch between the two benzene rings of the biphenyl while all the other bands are assigned to CH<sub>2</sub> twists of the crown rings.

1310-1400cm<sup>-1</sup>

The Raman spectra of both compounds show weak Raman bands at 1360cm<sup>-1</sup> and 1390cm<sup>-1</sup> and at 1355cm<sup>-1</sup> and 1390cm<sup>-1</sup> in the 0/1 and 2/1 compounds respectively. These bands are associated with much stronger I.R. bands.

The 0/1 I.R. spectrum shows a weak band at  $1328\text{cm}^{-1}$ , and a strong doublet at  $1347, 1355\text{cm}^{-1}$  with two medium strength shoulders at  $1371\text{cm}^{-1}$  and  $1385\text{cm}^{-1}$ . The 2/1 complex shows only a strong band at  $1346\text{cm}^{-1}$  with a strong poorly resolved band at  $1351\text{cm}^{-1}$ . Ligand binding has again decoupled the modes and simplified the 2/1 molecule's spectrum.

The I.R. of biphenyl shows weak bands at  $1325\text{cm}^{-1}$  and  $1380\text{cm}^{-1}$  which will probably correspond to the weak band at  $1328\text{cm}^{-1}$  and the shoulders at  $1373\text{cm}^{-1}$  and  $1385\text{cm}^{-1}$  in the 0/1 compound and the  $1370\text{cm}^{-1}$  shoulder in the 2/1 complex and no Raman bands.

18 crown 6 shows some weak Raman bands and a strong I.R. band at  $1350\text{cm}^{-1}$ , assigned to CH<sub>2</sub> wags. Therefore the strong I.R. doublets at  $1347, 1346, 1355\text{cm}^{-1}$  in the 2/1 molecules are CH<sub>2</sub> wagging modes of the crown rings.

#### 1400-1500cm<sup>-1</sup>

The 0/1 compound shows two strong Raman bands at  $1445\text{cm}^{-1}$  and  $1477\text{cm}^{-1}$ , the higher frequency peak being the stronger. The I.R. also show strong peaks of approximately equal intensity at  $1442\text{cm}^{-1}$  and  $1460\text{cm}^{-1}$  with shoulders at  $1469\text{cm}^{-1}$  and  $1482\text{cm}^{-1}$ . The 2/1 complex shows a strong Raman band at  $1466\text{cm}^{-1}$  with poorly resolved shoulders at  $1432, 1447\text{cm}^{-1}$  and  $1478\text{cm}^{-1}$  and two broad medium strength I.R. bands at  $1450\text{cm}^{-1}$  and  $1468\text{cm}^{-1}$ .

Biphenyl shows no Raman bands but two strong I.R. bands at  $1430\text{cm}^{-1}$  and  $1490\text{cm}^{-1}$  while 18-crown-6 shows strong Raman bands at  $1435, 1460$  and  $1475\text{cm}^{-1}$  and strong I.R. bands at  $1450$  and  $1470\text{cm}^{-1}$ .

The Raman bands are assigned to CH<sub>2</sub> in-plane deformation

modes of the crown rings while the I.R. bands will probably be a superposition of these modes with C-C stretches of the biphenyl group.

1500-1750cm<sup>-1</sup>

The 0/1 compound shows strong Raman bands at 1586cm<sup>-1</sup> and 1599cm<sup>-1</sup> and very weak broad I.R. bands at 1573, 1595, 1625, 1690 and 1722cm<sup>-1</sup>, while the 2/1 complex shows a strong Raman band at 1592cm<sup>-1</sup> with a shoulder at 1571cm<sup>-1</sup> and weak, broad I.R. bands at 1598, 1627 and 1722cm<sup>-1</sup>.

Biphenyl shows a strong Raman doublet with bands of equal intensity at 1590cm<sup>-1</sup> and 1670cm<sup>-1</sup> while the methyl substituted biphenyl shows a strong peak at 1600cm<sup>-1</sup> with a weaker band at 1580cm<sup>-1</sup>, which is more similar to those bands seen in the Rebek compounds. There are no I.R. bands visible above a broad background in this region. 18-crown-6 shows no Raman or I.R. bands in this region so the bands seen in the 0/1 and 2/1 compounds are assigned to C-C stretches of the aromatic rings in the biphenyl group.

### 5.3 Raman spectra of Partially Liganded Macrobicyclic Compounds

Raman spectra of several partially liganded samples and of the liganded and fully liganded samples are shown in Figures 5.1 and 5.3. The low frequency spectra have been scaled by the computer to have approximately the same intensity and then superimposed while the high frequency spectra have been traced from the chart recorder output.

It can be seen from the high frequency spectra that the 0.5/1 spectrum is most like the 0/1 spectrum showing all the 0/1

bands above  $500\text{cm}^{-1}$  with the same relative intensities except those at  $1445\text{cm}^{-1}$  and  $1291\text{cm}^{-1}$  which are less well defined possibly because of the poor quality of this spectrum. From  $200\text{cm}^{-1}$  to  $500\text{cm}^{-1}$ , there are both 0/1 and 2/1 bands present. The sharp doublet due to the ligand at  $277, 287\text{cm}^{-1}$  is present while the bands at  $234, 244\text{cm}^{-1}$  are not, instead the 0/1 band at  $258\text{cm}^{-1}$  is present. The  $406\text{cm}^{-1}$  of the 2/1 molecule is clearly visible while the  $357\text{cm}^{-1}$  band of the 0/1 molecule has weakened. The  $319\text{cm}^{-1}$  and  $289\text{cm}^{-1}$  weak bands in the 0/1 molecule are not visible, possibly due to the large amount of noise.

The 1/1 sample on the other hands shows bands mostly seen in the 2/1 molecule though with some differences in relative intensity. The  $200-500\text{cm}^{-1}$  region shows only bands also seen in the 2/1 complex but bands at  $511\text{cm}^{-1}$ ,  $801\text{cm}^{-1}$ ,  $1028\text{cm}^{-1}$  and  $1040\text{cm}^{-1}$  are weaker relative to neighbouring bands than in the 2/1 spectrum.

The addition of more ligand to form the 1.5/1 compound gives a Raman spectrum identical to the 2/1 spectrum.

The low frequency spectra clearly show an increase in the intensity of the  $36\text{cm}^{-1}$  band with increasing ligand concentration supporting its assignment as a vibration of the whole ligand within the crown ring. The 2 broad bands between  $60-70\text{cm}^{-1}$  and  $90-100\text{cm}^{-1}$  gradually shift from the 0/1 positions to the 2/1 positions. The 0.5/1 spectrum shows particularly broad bands probably indicating a mixture of the 0/1 and 2/1 molecules while by the time the ligand/ether ratio is 1/1 the bands are virtually identical to the fully liganded bands. The shoulders at  $52\text{cm}^{-1}$  and  $137\text{cm}^{-1}$  in the 2/1 molecule become increasingly

visible as the ligand concentration increases from 1/1 and 0.5/1 respectively while the  $173\text{cm}^{-1}$  band of the 0/1 molecule disappears as the ligand/ether ratio reaches 1/1.

From all these spectra one can see that the transition from the 0/1 spectrum to the 2/1 spectrum is practically complete when the ligand to ether ratio reaches 1/1 and that no new bands due to a molecule with only one ligand bound can be seen. This implies that the 2/1 molecule gives a more intense spectrum than the 0/1 molecule, and either that there is so little singly liganded compound present that it is not visible or that the conformational restrictions placed on the molecule by the single ligand cause it to vibrate at the same frequencies as the fully liganded molecule and thereby only add some intensity to the 2/1 bands already present.

To clarify the situation the relative intensities of the low frequency bands were compared as a function of ligand concentration. To do this, it was assumed that the intensity of the  $36\text{cm}^{-1}$  ligand band was proportional to the concentration. The height of the band was measured at  $36\text{cm}^{-1}$  from an estimated background taking into account the Rayleigh wing and the broad bands to higher frequency. The distance from the baseline of the spectrum (taken to be the lowest point) to this background was also measured.

These distances were then scaled to match the distance from the baseline of the 0/1 spectrum to the point at  $36\text{cm}^{-1}$ . Once this was done the peak heights of the  $36\text{cm}^{-1}$  band and of all the other bands could be multiplied by the scale factor and plotted against ligand to ether ratio. The heights and scale factors

used are shown in the following table (5.7) and Figure 5.8 shows the relative intensities of all low frequency bands as a function of ligand to ether ratio.

It can be seen that the intensity of the  $36\text{cm}^{-1}$  peak is approximately proportional to the ligand concentration. The intensity at  $62\text{cm}^{-1}$  decreases initially as the amount of unliganded molecule decreases but then climbs again because of the broad tail of the  $70\text{cm}^{-1}$  band of the 2/1 molecule. The  $70\text{cm}^{-1}$  band increases steadily as ligand is added in a similar fashion to the  $100\text{cm}^{-1}$  band also typical of the 2/1 molecule. The relative intensity of the unliganded molecule's band at  $93\text{cm}^{-1}$  falls with respect to the  $100\text{cm}^{-1}$  band as the amount of ligand increases.

This graph indicates that the fully liganded compound does give a more intense Raman spectrum particularly of the  $70\text{cm}^{-1}$  band when compared to the  $62\text{cm}^{-1}$  band in the unliganded compound. The fairly linear increase in intensity of the bands due to the 2/1 complex indicates that there is a negligible amount of singly liganded ether present even if it has the same spectrum as the 2/1 complex as one would expect from an a molecule showing positive cooperativity. If there was a lot of the 1/1 complex with the same spectrum as the 2/1 complex then the intensity of the  $70\text{cm}^{-1}$  and  $100\text{cm}^{-1}$  bands would level off after the 1/1 ratio was reached since the addition of more ligand would not create more of these global vibrations. If there was a lot of the 1/1 complex with a different spectrum from either the 0/1 or 2/1 compounds then the approximately linear increase in intensity of the 2/1 bands would not be seen, instead their intensity would

Table 5.7      Scaling factors for low frequency Raman spectra

Sample Liquid: ether ratio	Intensity from Baseline to Background scatter at 36 cm <sup>-1</sup>	Conversion factor to scale the background level
0:1	42.5	1
0.5:1	43.2	0.984
1:1	37.8	1.124
1.5:1	36.5	1.164
2:1	32.4	1.312

Scaling of measured Raman intensities using conversion factors above

Sample	Raman Intensities (mm)	Peak cm <sup>-1</sup>							
		36	52	62	70	94	99	137	173
0:1	measured	42.5	51.7	56.4	51.7	43.7	40.7	7.2	3.2
	scaled	42.5	51.7	56.4	51.7	43.7	40.7	7.2	3.2
0.5:1	measured	52.0	50.2	53.7	56.2	46.9	45.7	11.7	3.7
	scaled	51.2	49.4	52.8	55.3	46.2	45.0	11.5	3.6
1:1	measured	54.1	42.6	48.8	56.1	49.8	50.8	13.6	3.5
	scaled	60.8	47.9	54.8	63.0	56.0	57.1	15.3	3.93
1.5:1	measured	55.5	41	47.8	53.9	48.3	49	15.8	2.5
	scaled	64.6	47.7	55.6	62.7	56.2	57.0	18.4	2.9
2:1	measured	55.9	40.6	45.9	53.2	48.5	49.7	14.5	2.5
	scales	73.5	53.4	60.3	69.9	63.7	65.3	19.0	3.3

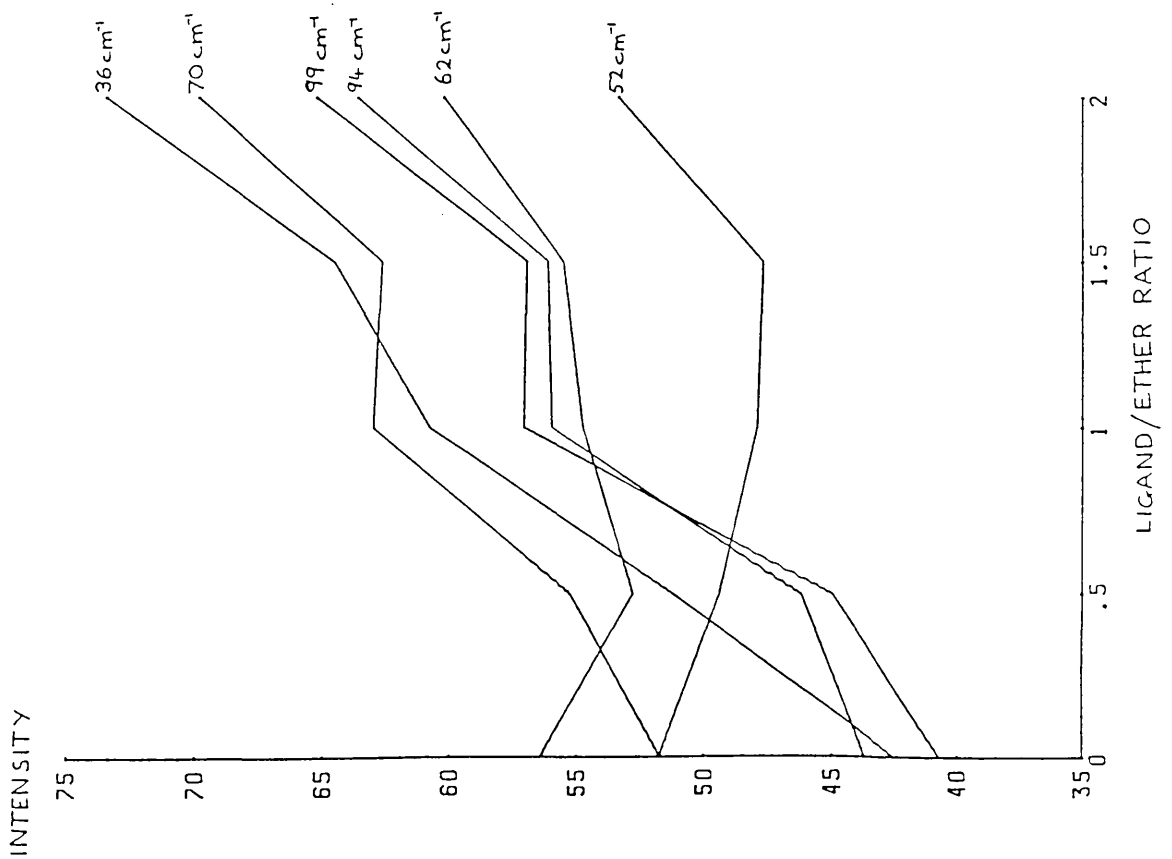
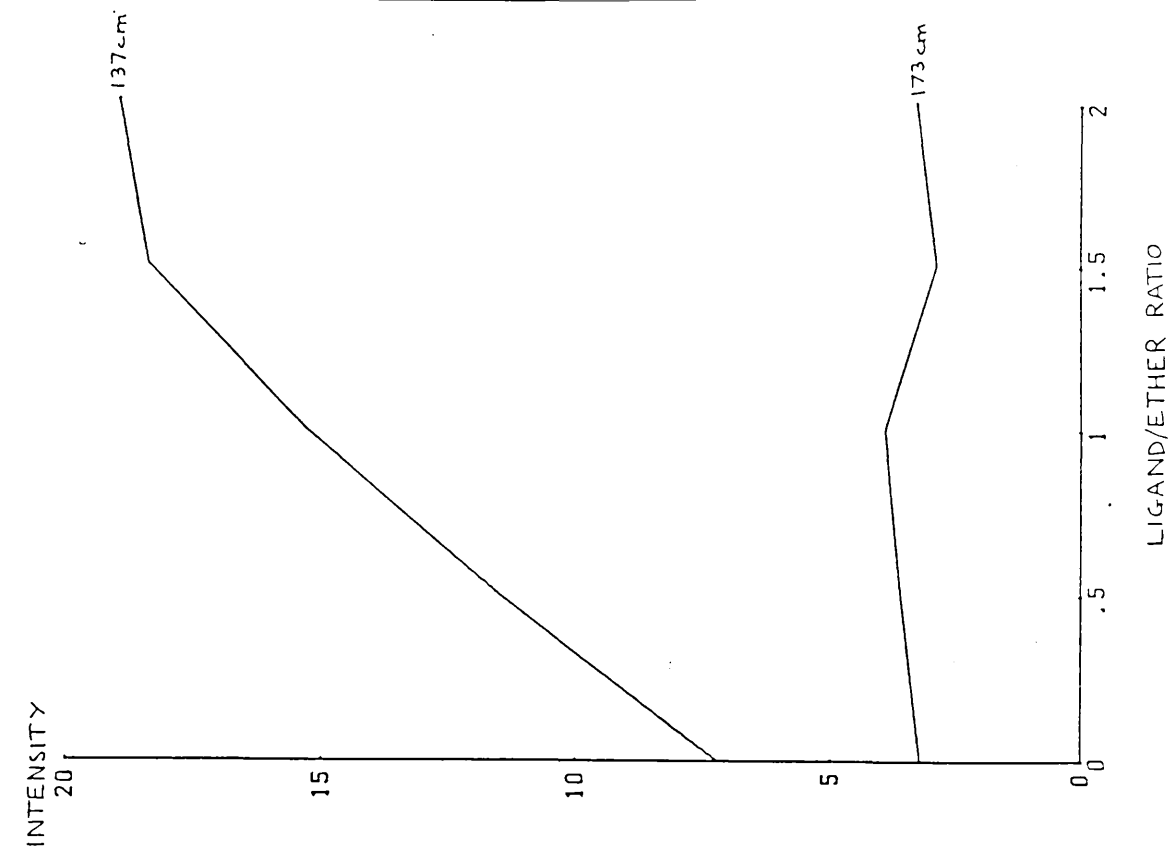


Fig. 5.3 Change in scaled low frequency Raman bands as a function of ligand concentration.

only start to increase once the 1/1 ratio had been exceeded and more fully liganded molecules were formed. If one assumes that the low frequency modes of the singly liganded complex are intermediate between those of the 0/1 and 2/1 compounds and are nearer in frequency to those of the 2/1 complex since it is unlikely that binding of the second ligand will lower the frequency of a mode, then small positive contributions to the allosteric effect in this molecule are possible if  $\nu_{1/1}^2 > \nu_{0/1} \nu_{2/1}$  the maximum amount being obtained if  $\nu_{1/1} = \nu_{2/1}$ . For example the  $8\text{cm}^{-1}$  shift of the  $52\text{cm}^{-1}$  band in the 0/1 molecule to  $70\text{cm}^{-1}$  in the 2/1 would contribute a maximum of 12% of the cooperative free energy if  $\nu_{1/1} = \nu_{2/1} = 70\text{cm}^{-1}$ .

From section 2.3 the cooperative free energy for one vibrational mode is

$$\begin{aligned} \Delta\Delta G_{\text{vib}} &= -kT \ln \frac{\nu_{1/1}^2}{\nu_{0/1} \nu_{2/1}} \\ &= -8.314 \times 290 \times \ln \frac{70}{62} \\ &= -292.6 \text{ J mol}^{-1} \end{aligned}$$

Also for the  $94\text{cm}^{-1}$  band which shifts to  $100\text{cm}^{-1}$  on ligand binding

$$\begin{aligned} \Delta\Delta G_{\text{vib}} &= -8.314 \times 290 \times \ln \frac{100}{94} \\ &= -149.2 \text{ J mol}^{-1} \end{aligned}$$

which contribute 12% and 6% respectively to the total  $\Delta\Delta G$  calculated earlier in section 3.1

Further contributions to  $\Delta\Delta G$  may arise from low frequency modes not visible by Raman spectroscopy or the Raman bands observed may be a superposition of several overlapping vibrations.

These and other positive contributions will be partially offset by the contributions to the vibrational free energy of the new low frequency modes at  $36\text{cm}^{-1}$  and  $54\text{cm}^{-1}$  in the fully liganded molecule.

#### Summary of Dynamic Conformational and Vibrational Contributions to the Positive Cooperativity

The analysis of the x-ray temperature factors has shown that a substantial part of the cooperativity observed in this molecule can be explained by a stiffening of the structure on ligand binding. The binding of the first ligand restricts the possible torsion angles of the biphenyl group and of, at least, the nearest groups of the second crown ring to values optimal for binding of the next ligand.

The Raman spectra of the macrobicyclic ether in various states of ligation have shown that as well as the dynamic conformational mechanism, a vibrational mechanism contributes to the allosteric effect in the molecule. Long range, low frequency modes connecting both binding sites are increased in frequency when the first ligand is bound thereby affecting all the motion of the other binding site without producing a conformational change.

In the following chapter several enzymes with and without ligands bound will be studied with Raman spectroscopy to determine if any vibrational changes occur at low frequency, on ligand binding, which may be involved in the function of the enzyme.

## CHAPTER 6

### Raman Spectroscopy of Lysozyme, Trypsin and Glyceraldehyde 3-Phosphate Dehydrogenase

#### 6.1 High frequency Raman spectra

Figure 6.1 shows the high frequency Raman spectra of lysozyme as supplied, after dialysis and freeze drying to remove salts and of the freeze dried lysozyme-tri-NAG complex. Comparison of the lysozyme spectra shows no changes caused by the dialysis and freeze drying and both compare favourably with the published spectrum of solid lysozyme (Lord & Yu, 1970). Their assignments of the vibrational bands are shown on the figure. Binding of the tri-NAG produces no noticeable changes in the high frequency region as would be expected since tri-NAG is bound noncovalently so that the vibrations of residues in the binding site will be little affected. No bands due to tri-NAG itself are seen because the inhibitor is only a small fraction of the total sample.

The Raman spectra of the trypsin as supplied and after further freeze drying are shown in Figure 6.2. The signal to noise ratio of these spectra is slightly poorer than that of the published spectrum of solid trypsin (Chen & Lord, 1980) but all except the weakest bands are clearly visible. Binding of the trypsin inhibitor produces several small changes which are marked on the figure. Two bands at  $409\text{cm}^{-1}$  and  $434\text{cm}^{-1}$  are better resolved in the complex though their origin is not clear. The "tyrosine doublet" bands,  $832\text{cm}^{-1}$  and  $854\text{cm}^{-1}$ , change intensity

Fig. 6.1 High frequency ( $200-1750\text{ cm}^{-1}$ ) Raman spectra of, from top to bottom, lysozyme as supplied, lysozyme after freeze drying and lysozyme tri-NAG complex after freeze drying. Recorded with 50 mW of 488 nm radiation, 500 or 750 micron slitwidths at  $25\text{ cm}^{-1}/\text{min}$  with 2 second time constants.

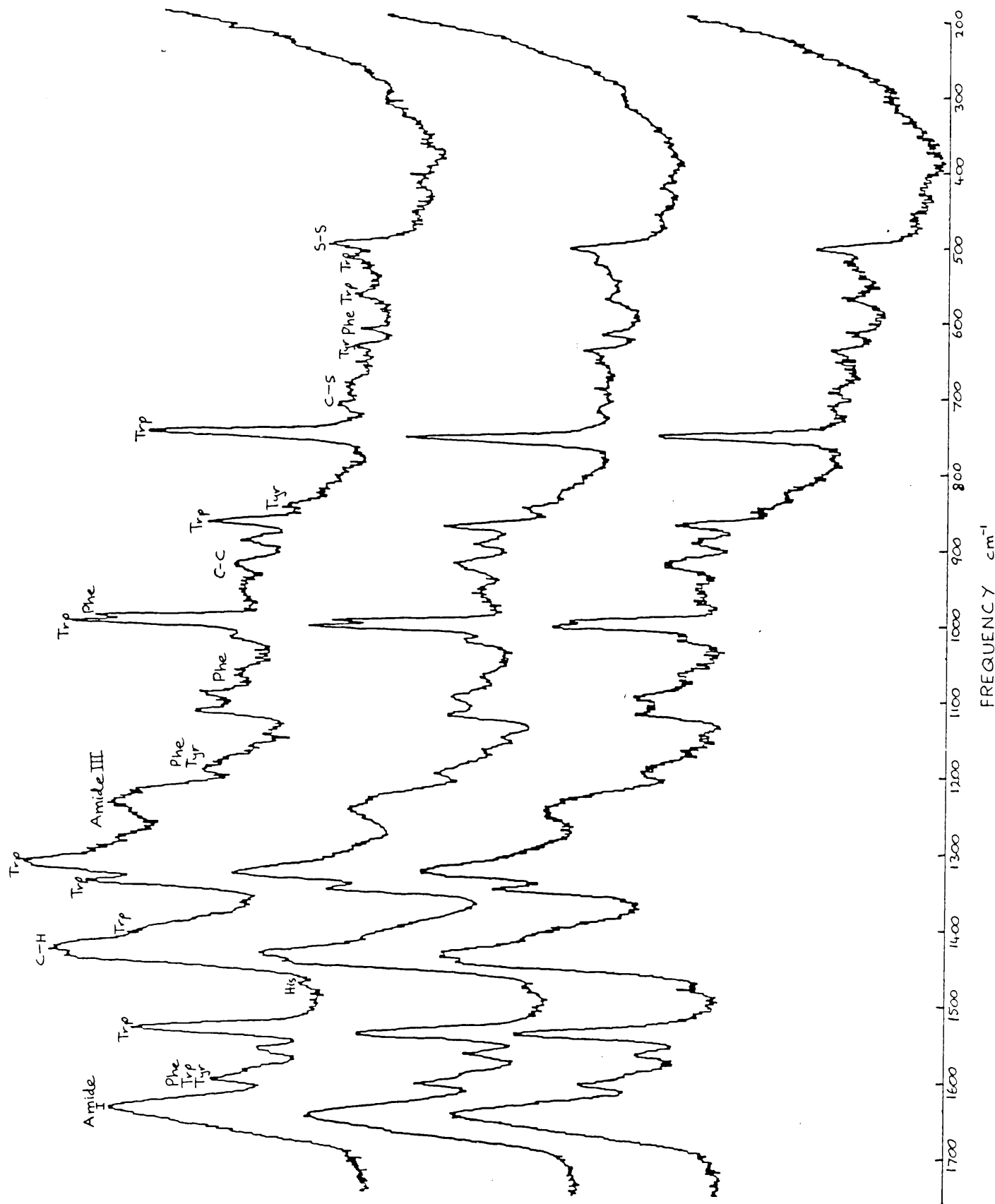


Fig. 6.2 High frequency (200-1750  $\text{cm}^{-1}$ ) Raman spectra of, from top to bottom, trypsin as supplied, after freeze drying and trypsin-BPTI complex after freeze drying. Recorded with 45 mW of 488 nm radiation, 500 or 750 micron slitwidths at 25  $\text{cm}^{-1}/\text{min}$  with time constants of 2 seconds.

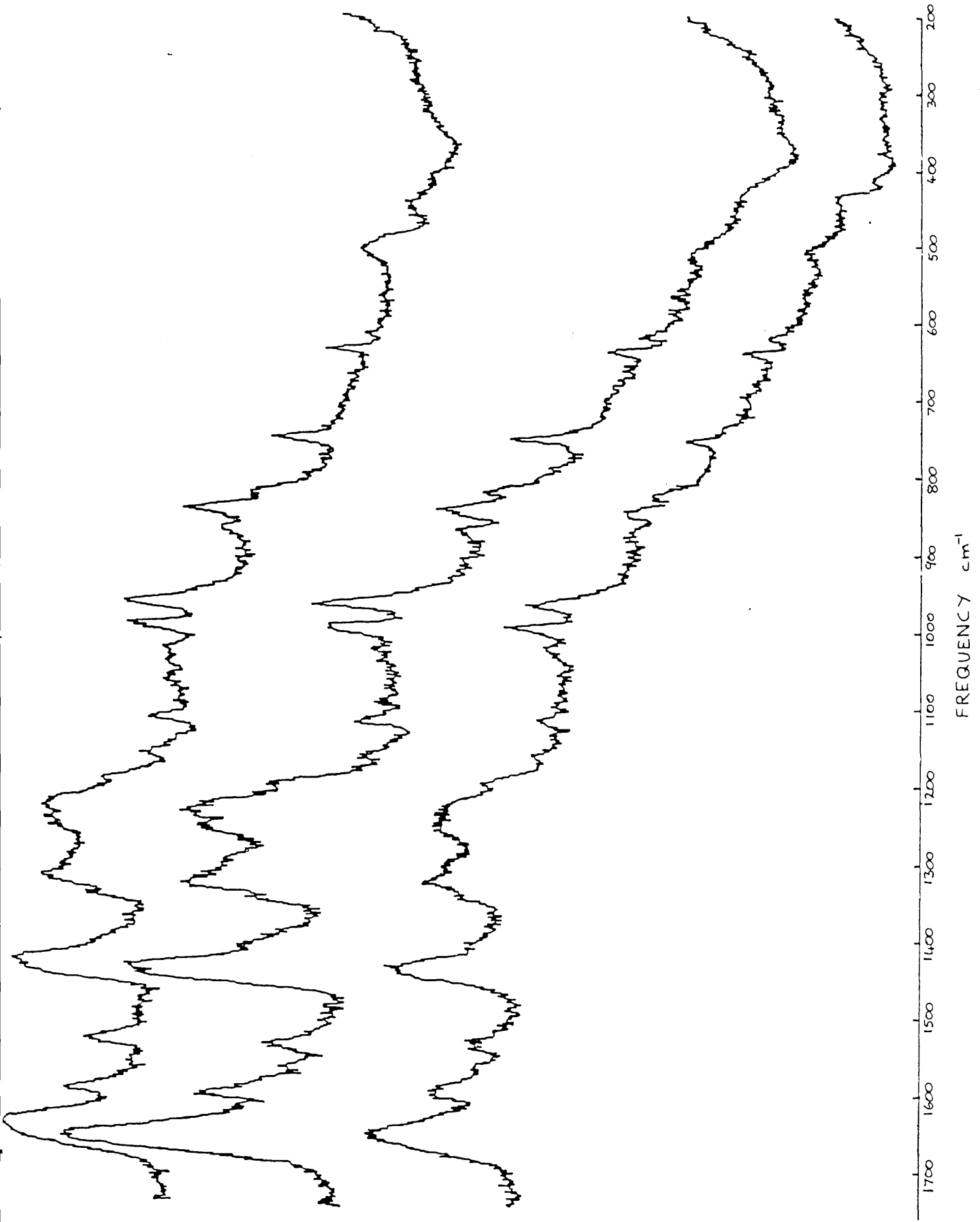
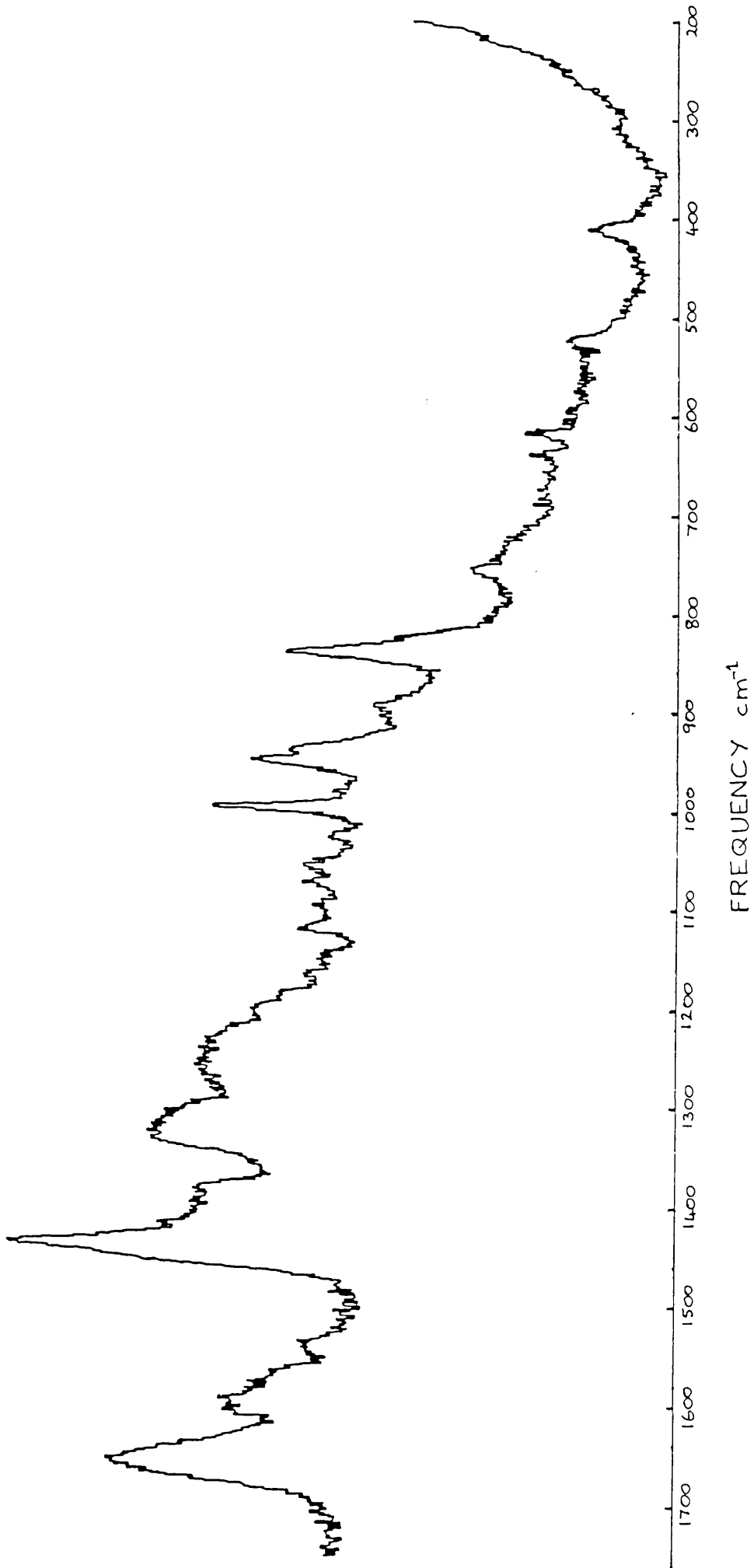


Fig. 6.3 High frequency (200-1750  $\text{cm}^{-1}$ ) Raman spectra of GAPDH as supplied. Recorded with 50 mW of 488 nm radiation, 750 micron slitwidths at 25  $\text{cm}^{-1}/\text{min}$  with a 5 second time constant.



relative to each other which indicates that some tyrosines are being shielded from the external environment by inhibitor binding (Chen & Lord, 1980). None of the ten tyrosines in trypsin are in the binding site though long range effects such as a stiffening of the structure might restrict their accessibility. A more likely source of the change in intensity could be Tyr35 in BPT1 which will be trapped in the trypsin binding site. Simon et al (1984) in their hydrogen exchange experiment showed that Tyr35 is much less accessible when bound to trypsin which would lead to a weakening of the  $854\text{cm}^{-1}$  band relative to the lower frequency band. The  $976\text{cm}^{-1}$  band is most probably due to sulphate ions bound to the protein, the concentration of which may vary from sample to sample. The partially resolved bands at  $1318\text{cm}^{-1}$  and  $1338\text{cm}^{-1}$  are due to C-H deformations while the band at  $1358\text{cm}^{-1}$  has been assigned to tryptophan residues. The small changes in this region may be due to changes in the relative numbers of these groups when the inhibitor is bound.

Glyceraldehyde-3-phosphate dehydrogenase as supplied gave the Raman spectrum shown in Figure 6.3. The freeze dried sample possessed such a strongly sloping fluorescence background that it is not shown, though all the major bands were visible. This background was even stronger in the GAPDH-NAD complex and no high frequency spectrum could be obtained. The assignments of the bands were estimated by comparison with the known bands in lysozyme (Lord & Yu, 1970) and trypsin (Chen & Lord, 1980) and are shown on the figure. The strong peak at  $839\text{cm}^{-1}$  with a possible shoulder at  $825\text{cm}^{-1}$  should be the tyrosine Fermi resonance doublet. The unusual appearance of this band may be

due to the large number of tyrosines in GAPDH. Also of note is the very strong band at  $1433\text{cm}^{-1}$  with a shoulder at  $1454\text{cm}^{-1}$  which are usually assigned to tryptophans and  $\text{CH}_2$  deformations respectively. The tryptophan band is usually weaker than the higher frequency band. Trp193 which is in a section of antiparallel beta sheet contacting the adjacent subunit and which moves considerably on NAD binding, may have a larger than normal polarisability. The amide III band is broad and consists of three poorly resolved components of approximately equal intensity at  $1221$ ,  $1238$  and  $1257\text{cm}^{-1}$  which implies roughly equal proportions of  $\beta$ -sheet, random coil and  $\alpha$ -helical secondary structure in GAPDH in agreement with the structure by x-ray crystallography (Harris & Waters, 1976).

The Raman spectrum of GAPDH in this region clearly deserves a more extensive study.

## 6.2 Low frequency Raman spectra

Of the three proteins studied with and without ligands bound, lysozyme gave the best resolved low frequency band at  $-25\text{m}^{-1}$  in both the free enzyme and the enzyme inhibitor complex (Figure 6.4). Trypsin and its complex with BPTI shown in Figure 6.6 gave a less well resolved band at  $-25\text{cm}^{-1}$ , while GAPDH and its coenzyme complex (Figure 6.7) only showed a broad shoulder on the side of the Rayleigh line.

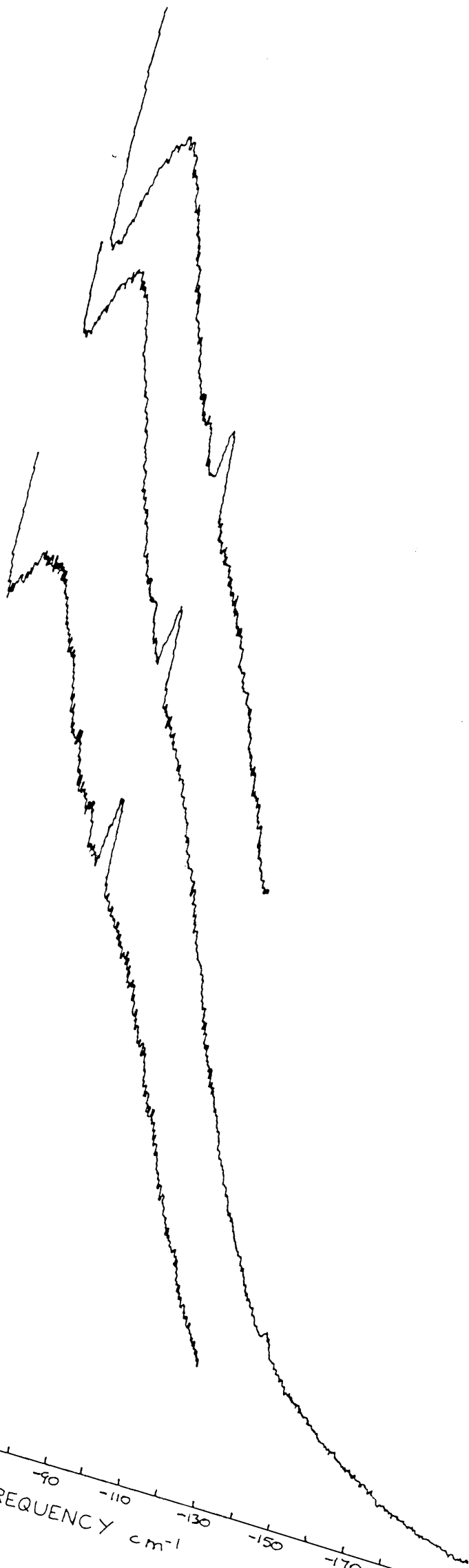
No changes in the low frequency spectra of the proteins on ligand binding could be detected with the given experimental conditions

The lysozyme spectra show that there was a loss of intensity when the samples were freeze dried. This may be due to the sample being less densely packed into the sample holder or being slightly out of alignment. In all the proteins studied, the alignment of the sample had a large effect on the band intensity. Differences in intensity between samples could be compensated by using different scanning rates and integration times. As well as a broad band at  $-25\text{cm}^{-1}$  in lysozyme and its complex with tri-NAG there was also a very broad shoulder centred around  $-75\text{cm}^{-1}$  band which may be equivalent to the  $75\text{cm}^{-1}$  seen in the inelastic neutron scattering study (Bartunick et al., 1982) which was assigned to longitudinal motions of  $\alpha$ -helices. They also suggested that the  $25\text{cm}^{-1}$  band could be due to  $\beta$ -sheet motions. The low frequency Raman results of Genzel et al (1976) on an orthorhombic crystal of lysozyme agree with those presented here though their  $25\text{cm}^{-1}$  band is not fully resolved from the Rayleigh line. The density of vibrational normal modes calculated for lysozyme by Levitt et al (1985) shown in Figure 6.5 bears some resemblance to the overall shape of the Raman band though not all these modes would be equally Raman active.

The trypsin and trypsin-BPT1 samples which gave the high frequency spectra shown earlier also gave the low frequency spectra shown in Figure 6.6. They all show a well resolved broad band at  $-25\text{cm}^{-1}$  with a very broad shoulder around  $-75\text{cm}^{-1}$  similar to that seen in lysozyme. The spectra of the freeze dried trypsin and trypsin-BPT1 complex are virtually identical. This is rather unexpected as BPT1 has many low frequency modes being a large molecule itself, which one might have expected to add onto the

Fig. 6.4 Low frequency ( $-10$  to  $-200\text{ cm}^{-1}$ ) anti-Stokes Raman spectra of, from top to bottom, lysozyme as supplied, lysozyme after freeze drying and lysozyme-tri-NAG complex after freeze drying. Recorded with 50 mW of 488 radiation, 200 micron slitwidths at  $5\text{ cm}^{-1}/\text{min}$  with 3 or 6 second time constants.

-10 -30 -50 -70 -90 -110 -130 -150 -170 -190  
FREQUENCY  $\text{cm}^{-1}$



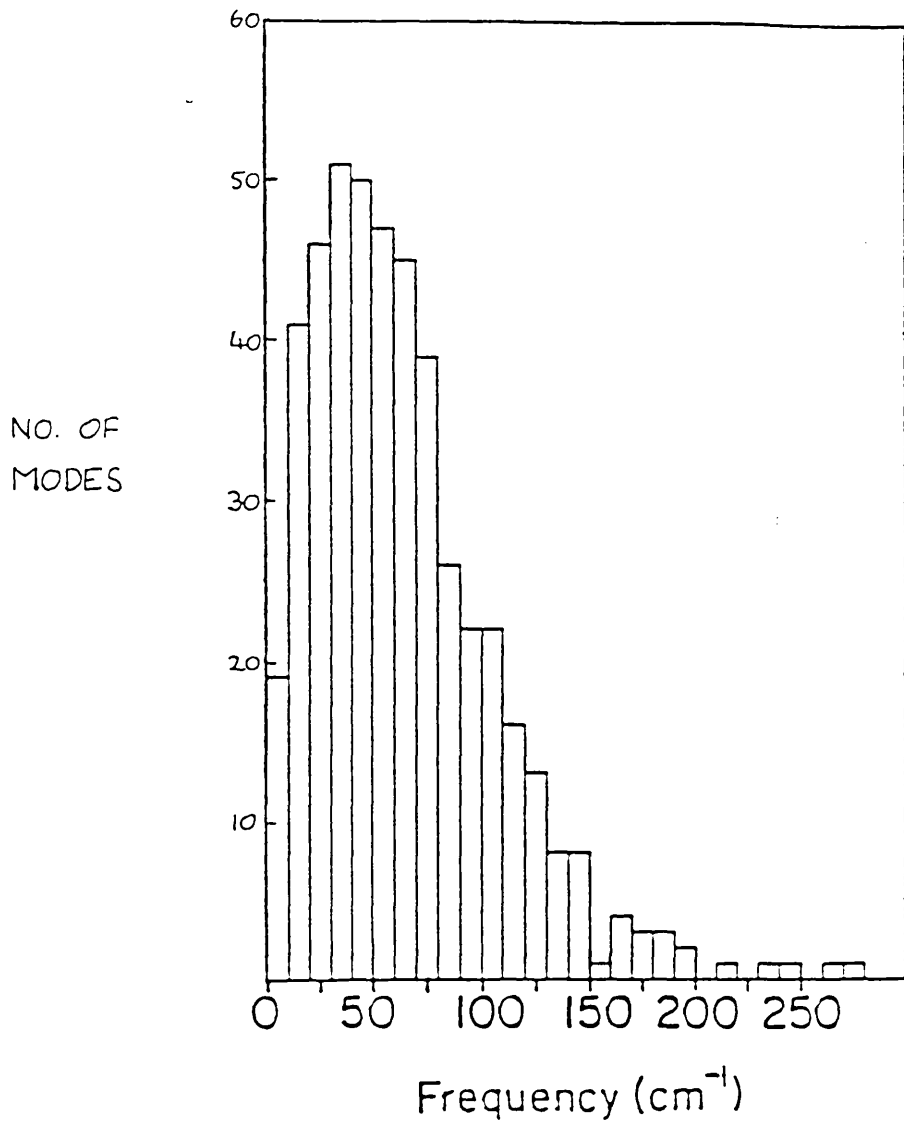
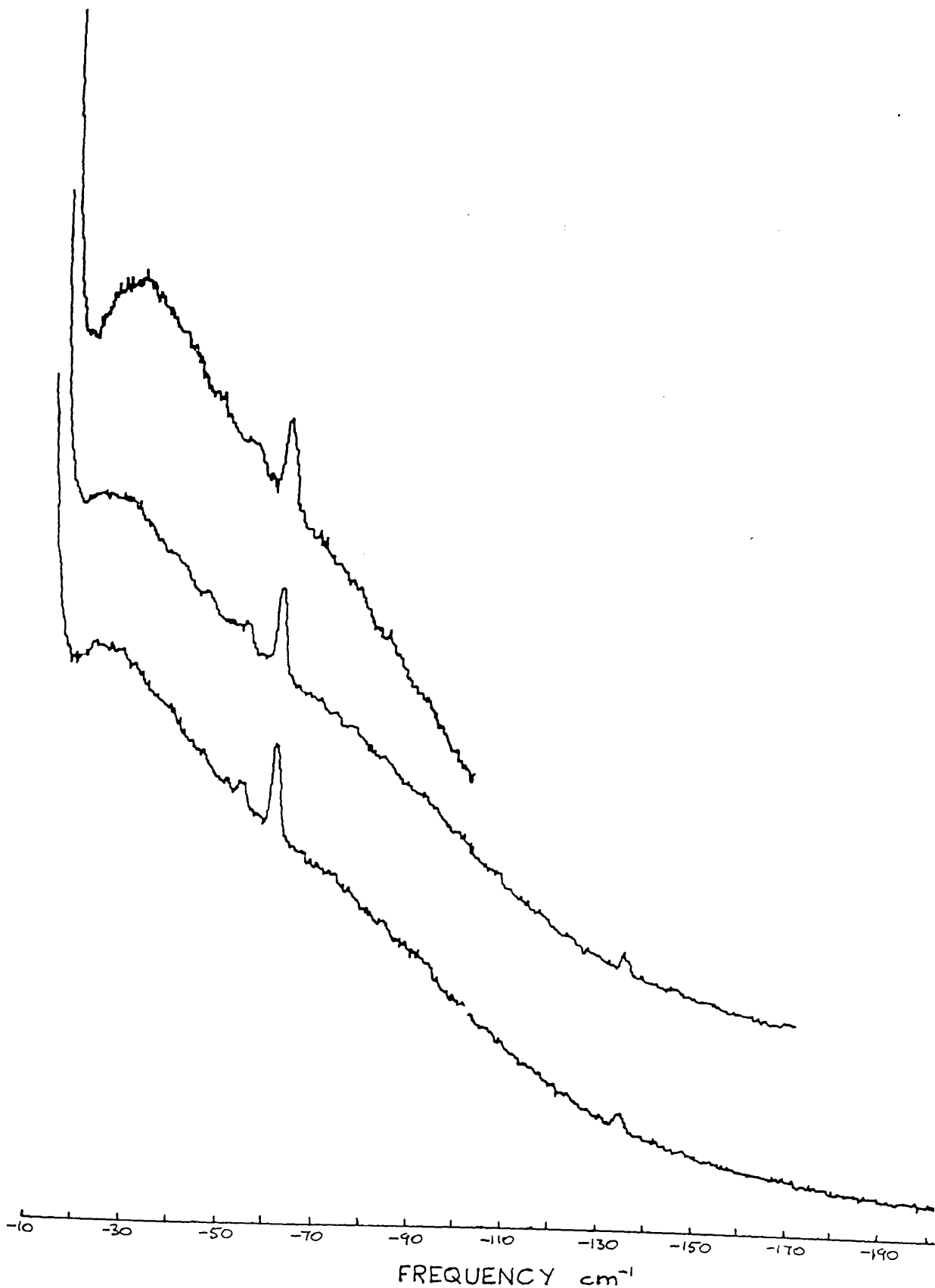


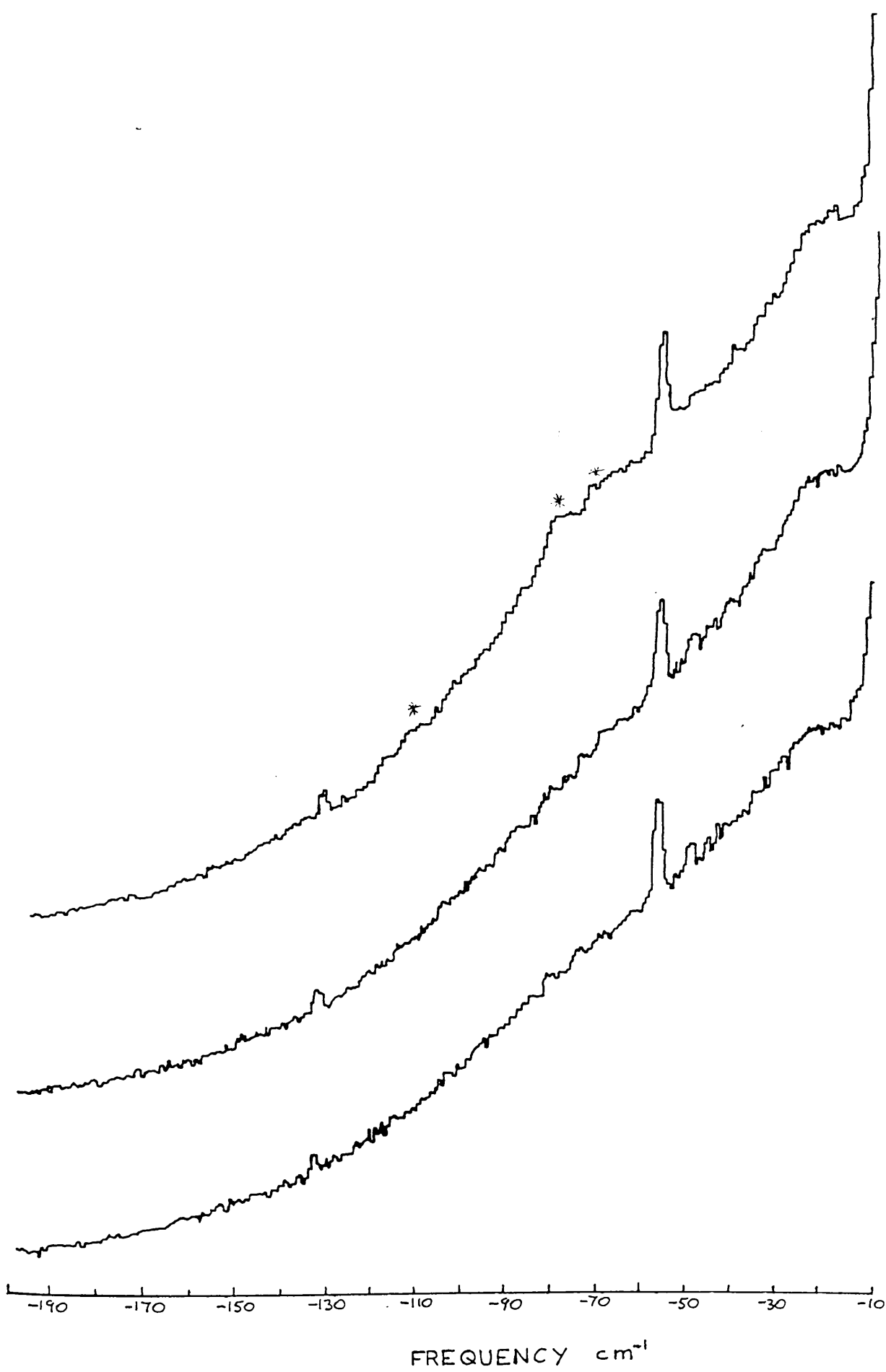
Fig. 6.5 The density of low frequency normal modes of lysozyme as calculated by Levitt et al (1985).

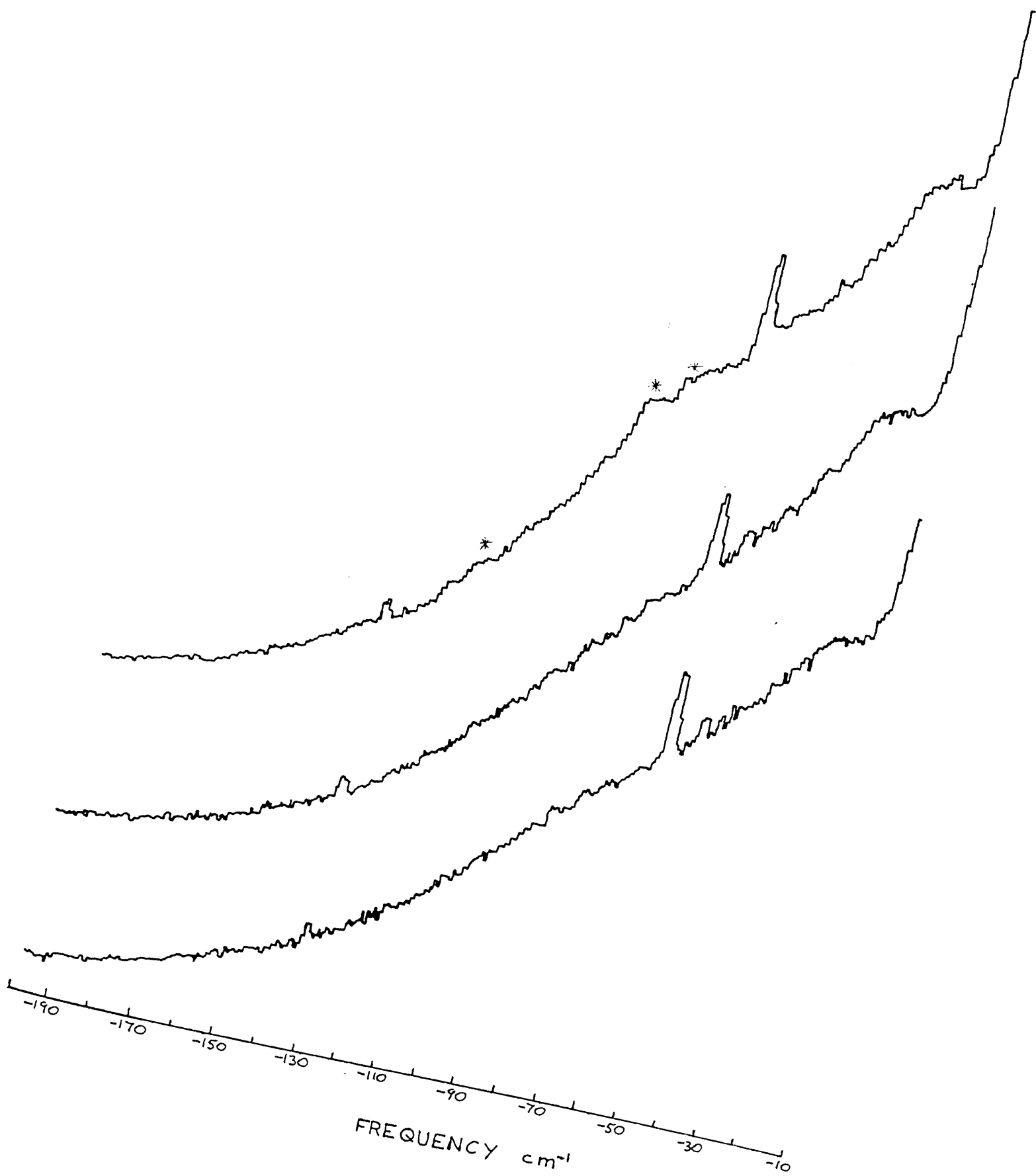
Fig. 6.6 Low frequency ( $-10$  to  $-200$   $\text{cm}^{-1}$ ) anti-Stokes Raman spectra of, from top to bottom, trypsin as supplied, trypsin after freeze drying and freeze dried trypsin-BPTI complex. Recorded with 45  $\mu\text{W}$  of 488 nm radiation, 200 micron slitwidths at 5  $\text{cm}^{-1}/\text{min}$  with 3 second time constants.



trypsin spectrum changing the shape of the band. Brown et al (1972) have presented a spectrum of freeze dried chymotrypsin which is very similar to the ones shown.

Low frequency anti-Stokes Raman spectra are shown in Figure 6.7 of GAPDH as supplied with a large amount of citrate buffer salt present, GAPDH after dialysis and freeze drying and of the GAPDH-NAD complex. Comparison of the two GAPDH spectra shows that dialysis has removed the spurious bands (marked with a \*) which can therefore be attributed to the residual buffer salts. A spectrum of crystalline sodium citrate also shows particularly strong Raman bands at the same frequencies. This leaves a broad shoulder on the Rayleigh line at about  $-22$  to  $-24\text{cm}^{-1}$  and a broad weak shoulder around  $-75\text{cm}^{-1}$ . The spectrum of the GAPDH-NAD complex does not show the spurious lines even though it was not dialysed. This sample shows a broad shoulder around  $-24\text{cm}^{-1}$  and a broad weak band around  $-75\text{cm}^{-1}$ . No differences between this sample and GAPDH alone can be seen but the poor quality of the GAPDH-NAD sample may obscure any differences. Since GAPDH is such a large enzyme it will have many more low frequency modes than lysozyme or trypsin and the conversion of several hundred of these modes to higher frequency, as postulated by Sturtevant (1977) to account for the large negative heat capacity and entropy changes on  $\text{NAD}^+$  binding, may not be noticeable. Sturtevant estimated that there would be approximately 50 normal modes for every 100 daltons of enzyme, which would give over 70,000 normal modes for GAPDH many of which would have low frequencies. One should also note that under the conditions used for preparing the complex the proportion of GAPDH with more than





one NAD molecule bound is low though almost all have one NAD molecule bound. It is possible that the changes produced by binding a single NAD molecule are not sufficiently large to be visible. If this were the case then the effect of binding further NAD molecules would not be noticeable either if the enzyme followed the concerted model of cooperativity since most of the vibrational changes would occur on binding the first ligand (cf dynamic conformational allostery). If NAD binding follows a sequential model in which the vibrational changes would be cumulative, then preparation of a fully liganded complex might show differences in the low frequency Raman spectra.

### 6.3 Summary of low frequency results

If one assumes that the low frequency Raman spectra obtained were not dependent on the sample preparation and that the enzyme - ligand complexes are fully formed then the lack of change seen in the spectra on ligand binding may be explained in various ways.

- i. There are no changes in the vibrations of the enzyme when the complex is formed.
- ii. Any modes affected are not Raman active.
- iii. The bands seen are intermolecular lattice vibrations involving rigid body motions of the whole protein and will be intrinsic in any solid protein sample.
- iv. The bands are due to localised vibrations of the protein which do not involve the ligand binding site.
- v. Too few normal modes are affected to be noticed amongst the large number of other low frequency modes.

vi. The shifts in frequency are small and not visible at the spectral resolution used.

vii. The modes affected by binding are overdamped or at too low a frequency to be seen by the spectrometer or by this technique in general.

i. is unlikely to hold because there is a large amount of experimental evidence, particularly thermodynamic (Sturtevant, 1977) that there are considerable vibrational changes on ligand binding.

If the number of modes affected by ligand binding is large then ii is unlikely to be true. Also, since proteins are large and unsymmetric, Raman exclusion rules are unlikely to apply.

Peticolas (1979) has argued convincingly against the low frequency bands arising from intermolecular vibrations. The results of Painter and colleagues (Painter & Mosher, 1979; Painter et al, 1981; Painter et al, 1982) and those obtained here show no systematic variation of the position of the band with protein molecular weight which might be expected if these bands were due to lattice movements.

If the low frequency bands are due to localised vibrations of the protein structure, for instance of  $\alpha$  helices and  $\beta$  sheets, then ligand binding is unlikely to cause any changes in these vibrations unless it binds closely to these structures. The modes of vibration of the  $\alpha$  helix have been extensively studied (Peticolas 1979 for example) and calculated frequencies are in the 0-100cm<sup>-1</sup> region. However the Raman spectra of  $\alpha$  helices look very different from those of proteins with strong well

defined bands appearing around  $100\text{cm}^{-1}$ . Tipping et al (1984) show low frequency spectra of  $\alpha$  helical poly-L-alanine which has several well defined bands. The protein spectra are therefore not entirely due to localised vibrations of secondary structural features but must contain many contributions from the whole protein to account for the broadness of the spectra. The number of modes affected by ligand binding may be low for some proteins though Sturtevant (1977) has predicted that a large number of modes are affected by ligand binding when large negative heat capacity changes are seen on binding as in the case of GAPDH. He has also discussed positive changes which could offset any vibrational contribution detected via thermodynamic changes. This may be the case for tri-NAG binding by lysozyme were Bjurulf and Wadso (1972) found essentially no heat capacity change on ligand binding even though binding causes global stiffening of the lysozyme structure which would surely affect many low frequency modes.

This leaves the last two explanations which are perhaps the best supported by various published observations and calculations. Normal mode calculations on lysozyme (Levitt et al., 1985; Go et al., 1983; Brooks & Karplus, 1983) indicate that the hinge bending motion if not damped by solvent is of very low frequency, around  $3\text{cm}^{-1}$ , and that a small number ( $\sim 10$ ) of the lowest frequency modes with frequencies of less than  $10\text{cm}^{-1}$  account for about 70% of the global protein motion. If these results are generally applicable to other proteins then this very low frequency range is just outside the range accessible under the experimental conditions used. More recent calculations (Bruccoleri et al., 1986) for the hinge bending mode of

lysozyme indicate that tri-NAG binding causes only a very small increase of approximately  $1\text{cm}^{-1}$  in the hinge bending mode's frequency. Such small increases, even if many modes were affected, would be very difficult to see because of the relatively low resolution of the broad protein band. If these small frequency changes are typical of ligand binding by proteins then they would support the use of classical statistical mechanics of harmonic oscillators as given in Chapter 2.

There is also evidence that some of the global motions of proteins may be overdamped even in the solid state which would cause them to tend to zero frequency as the damping increased (Swaminathan et al., 1982; James, 1985). These overdamped modes would not be visible with Raman spectroscopy though if ligand binding stiffened the structure sufficiently the mode could become visible as the damping would be reduced.

The low frequency Raman spectra of the three proteins studied here are therefore composed of vibrations that involve large sections of the protein giving rise to the band at  $25\text{cm}^{-1}$  with increasingly localised vibrations of structural features such as  $\beta$  sheets and  $\alpha$  helices contributing to the broad scattering up to  $150\text{cm}^{-1}$ . The lowest frequency motions involving the whole protein which would be most affected by ligand binding are at too low a frequency, possibly being damped out, and shift in frequency by too small an amount to be observed with the methods used. A most important extension to these experiments would be to repeat them at liquid  $\text{N}_2$  or  $\text{He}^2$  temperatures where the damping would be frozen out leading to

more harmonic vibrations. Cooling of samples for low frequency Raman spectroscopy also usually increases the frequency of low frequency bands and narrows the Rayleigh wing significantly, which would both lead to an improvement in resolution possibly allowing ligand induced changes to be visible. This effect of cooling is demonstrated in Appendix 2 for an organic compound. The liquid nitrogen cryostat used was unfortunately not available during the protein work.

CHAPTER 7  
CONCLUSIONS

The theory presented earlier for allostery via changes in low frequency motions of proteins has recently been generalised to study the effects of specific interactions on the dynamics and stability against unfolding of proteins (Jackson, 1987). The addition or subtraction of hydrogen bonds, disulphide bridges, charged groups and amino acid residues by chemical modification or site directed mutagenesis will change some of the normal modes of the protein. Removal of interactions will soften the modes while additional interactions, as considered in the allostery model, will increase the vibrational frequencies. Jackson gives free energy changes of about  $0.2\text{kcal mol}^{-1}$  to  $2\text{kcal mol}^{-1}$  for single site perturbations, similar in magnitude to the changes found for ligand binding in the simple scissors model. Mutant forms of lysozyme have shown even larger effects caused by single amino acids changes (Hawkes et al., 1984), implying that the replacement has affected several vibrations of the protein. Mutations of residues some distance away from the catalytic sites of enzymes may produce changes in the reaction by affecting the dynamics of the active site, in contrast to mutations of the active site, to form extra bonds for example, where the reaction mechanism is changed directly (Ackers & Smith, 1985; Leatherbarrow & Fersht, 1986).

Even larger changes in the normal modes of the protein might be expected in systems where ligand binding produces large

conformational changes, such as the hinge bending in hexokinase or domain movement in dehydrogenases, but because of the large number of normal modes the vibrational density of states may not change noticeably. Protein-antibody binding such as for lysozyme (Amit et al., 1986) may not change the crystal structure of either the protein or the antibody but the pattern of normal modes will certainly be affected by the binding.

Experimental studies on the low frequency modes of proteins are few and far between. No Raman or far infra-red spectroscopic studies have compared liganded and unliganded states of the protein and only two inelastic neutron scattering studies on lysozyme and hexokinase with and without ligands have been published, (Middendorf, 1984; Jacrot et al., 1982). Both neutron scattering studies, though not entirely conclusive, showed that ligand binding decreased the intensity of scattering and shifted the vibrational density of states slightly to higher frequencies as expected from the theory.

The results obtained in this thesis on the changes in the low frequency Raman spectrum of Rebek's macrobicyclic allosteric crown ether due to ligand binding provide support for the theory as well, though further studies at low temperature are necessary to study the contribution of intermolecular crystal lattice modes to the observed spectral shifts. The shifts seen are sufficient to provide at least 20% of the cooperative free energy of binding, which combined with a sizeable contribution due to a reduction in magnitude of the uncorrelated thermal motions of the atoms as determined by the dynamic conformational allostery theory, can account for the major part of the cooperativity of

ligand binding seen in this molecule.

If similar changes in some of the low frequency modes of proteins on ligand binding contributed a similar proportion of the cooperative free energy then the attribution of allostery to conformational changes as seen by crystallography would have to be re-examined.

The low frequency Raman spectra presented here of lysozyme, trypsin and glyceraldehyde-3-phosphate dehydrogenase show no changes, within the resolution of the spectrometer, on the binding of ligands, most likely because the modes affected are too few in number or at too low a frequency to be seen as discussed in Section 6.3. The binding of ligands introducing additional constraints on the structure must, however change some of the normal modes of the protein and various experimental changes might allow them to be seen by Raman spectroscopy.

Cooling the solid samples to liquid nitrogen or helium temperatures would reduce any damping of the modes increasing their frequency giving better resolution from the Rayleigh wing. The bandwidth of Raman lines also decrease at lower temperatures which would allow finer details on the broad low frequency band to be observed. The use of protein crystals instead of freeze dried powders might also enhance the quality of the spectrum.

The use of difference spectra for the protein in the presence and absence of ligand in either solid form or in solution may also be useful. A sample holder has recently been described for the recording of low temperature difference spectra of solid samples, (Eng et al., 1985). Although the low frequency

spectra of protein solutions show only a broad, featureless Rayleigh wing, difference spectroscopy could reveal any changes caused by ligand binding. The distortion of low frequency solution spectra by the laser line itself can be suppressed by using a scaling factor,  $R(\bar{\nu})$  which takes into account the thermal population of the vibrational energy levels and also transforms the spectra so that it is directly comparable to far infra-red spectra

$$R(\bar{\nu}) = I(\bar{\nu}) \cdot \bar{\nu} \cdot \left(1 - e^{-\frac{h\bar{\nu}}{kT}}\right) \approx I(\bar{\nu}) \cdot \bar{\nu}^2$$

where  $R(\bar{\nu})$  = scaled spectrum at wavenumber  $\bar{\nu}$  and  $I(\bar{\nu})$  = Raman intensity at wavenumber  $\bar{\nu}$  (Lund et al., 1978; Perrott et al., 1981; Brooker & Perrot, 1981; James, 1985). This scaling factor would allow any changes produced by ligand binding in solution to be studied more easily.

Changes in vibrational modes which are overdamped in solution and hence appear on the Rayleigh line at  $0\text{cm}^{-1}$  or modes at very low frequencies could perhaps be seen by carefully scanning over the Rayleigh line and looking for changes in its width.

Surface enhanced Raman spectroscopy of proteins adsorbed onto silver surfaces or colloids which allows very low concentrations to be studied may also be useful (Moskovits, 1985). However, numerous experiments in this lab using silver colloids have failed to give any reproducible or recognisable protein spectra, though the technique has worked well on small molecules.

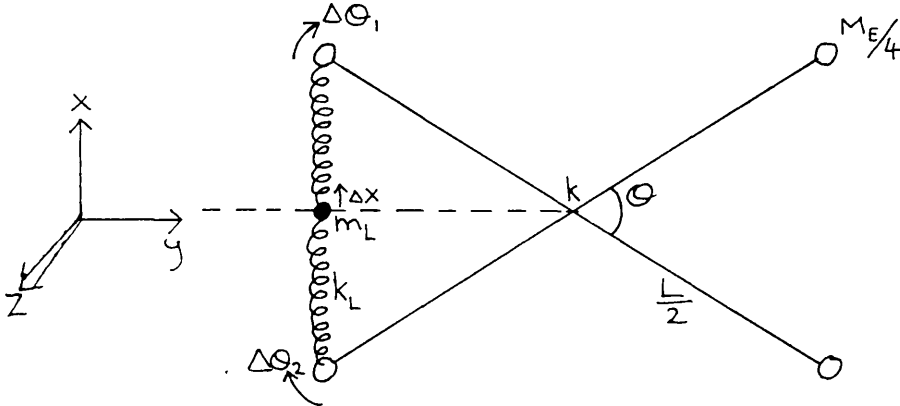
Finally, the use of resonance Raman and time resolved

resonance Raman spectroscopy should become increasingly useful in studying ligand induced changes in vibrations of the polypeptide backbone of the protein and their functional consequences, as ultra-violet lasers become more available. Time resolved resonance Raman spectroscopy of the porphyrin chromophore of heme proteins has already shown many transient changes in the vibrational spectra caused by photodissociation, (Friedman et al., 1982). The iron-histidine stretching vibration at approximately  $200\text{cm}^{-1}$  increases by several wavenumbers upon photolysis and the shifts correlate with changes in other higher frequency bands.

These Raman experiments, combined with further far infra-red and inelastic neutron scattering experiments, should define the role of low frequency motions of protein in catalysis, folding, cooperativity and all other protein functions.

Appendix 1      Details of the scissors dynamic allostery model

The system considered consists of two massless rods of length  $L$  with point masses  $1/4 M$  at each end giving a total mass  $M$ . The rods bisect each other at an angle  $\Theta$ . There are two binding sites between the pairs of masses subtended by the angle  $\Theta$  in which massless springs of force constant  $k$  with masses  $m_L$  at their midpoints, representing the ligand, can be placed. The rods can twist about angle  $\Theta$  in the  $x,y$  plane in a harmonic potential with torsional spring constant  $k$ . Lagrange's equation is used to calculate the normal modes of the model with 0, 1 and 2 springs attached.



Oscillations in the  $y$  and  $z$  directions are assumed to be negligible. No "conformational change" as represented by a change in the angle  $\Theta$  is allowed on binding of the springs, so that dynamic effects only are considered. The angular

displacements  $\Delta\theta_1$  and  $\Delta\theta_2$  are assumed to be small allowing the approximations  $\cos\Delta\theta = 1$  and  $\sin\Delta\theta = \Delta\theta$  to be used.

1. Free "enzyme"

Variables  $\Delta\theta_1, \Delta\theta_2$

$$\text{Potential energy} = V = \frac{1}{2} k (\Delta\theta_1 - \Delta\theta_2)^2$$

$$\begin{aligned} \text{Kinetic energy} &= T = \frac{1}{2} I \Delta\dot{\theta}^2 \\ &= \frac{M_E L^2}{16} (\Delta\dot{\theta}_1^2 + \Delta\dot{\theta}_2^2) \end{aligned}$$

where  $I$  = moment of inertia about the Z axis

$\Delta\dot{\theta}$  = angular velocity

The Lagrangian  $L = T - V$  and Lagranges equation says

$$\frac{\partial}{\partial t} \left( \frac{\partial L}{\partial \dot{q}} \right) - \frac{\partial L}{\partial q} = 0$$

where  $q$  represents each variable in turn.

This gives  $\Delta\theta_1$  and  $\Delta\theta_2$

$$\frac{M_E L^2}{8} \Delta\ddot{\theta}_1 + k(\Delta\theta_1 - \Delta\theta_2) = 0$$

$$\frac{M_E L^2}{8} \Delta\ddot{\theta}_2 - k(\Delta\theta_1 - \Delta\theta_2) = 0$$

Letting  $\Delta\theta_1 = A e^{i\omega t}$  and  $\Delta\theta_2 = B e^{i\omega t}$  gives two solutions for the normal mode frequencies of the system, namely

i.  $\omega = 0$  and  $A = B$  which represents only a translation of the system

ii.  $\omega = \sqrt{\frac{16k}{M_E L^2}}$ ,  $A = -B$

The normal mode here represents the basic scissor like motion of the enzyme model. The scissor frequency  $\nu_E^{sc}$  which shifts to higher frequencies on ligand binding is:

$$\nu_E^{sc} = \frac{1}{2\pi} \sqrt{\frac{16k}{M_E L^2}}$$

2. One ligand bound

Variables  $\Delta\theta_1, \Delta\theta_2, \Delta x$  (motion of mass  $m_L$ )

$$\text{Kinetic energy} = \frac{M_E L^2}{16} (\Delta\dot{\theta}_1^2 + \Delta\dot{\theta}_2^2) + \frac{1}{2} m_L \Delta\dot{x}^2$$

$$\begin{aligned} \text{Potential energy} &= \frac{1}{2} k (\Delta\theta_1 - \Delta\theta_2)^2 \\ &+ \frac{1}{2} k_L \left( \frac{L}{2} \left( \sin\left(\frac{\theta}{2} + \Delta\theta_1\right) - \sin\frac{\theta}{2} \right) - \Delta x \right)^2 \\ &+ \frac{1}{2} k_L \left( \frac{L}{2} \left( \sin\left(\frac{\theta}{2} - \Delta\theta_2\right) - \sin\frac{\theta}{2} \right) + \Delta x \right)^2 \end{aligned}$$

where the second and third terms of the potential energy represent the extension of the spring on either side of the mass  $m_L$ .

Lagrange's equation for the 3 variables gives:-

$$2 m_L \Delta\ddot{x} + 4 k_L \Delta x - k_L L \cos\frac{\theta}{2} (\Delta\theta_1 + \Delta\theta_2) = 0$$

$$M_E L^2 \Delta\ddot{\theta}_1 + (8k + 2k_L L^2 \cos^2\frac{\theta}{2}) \Delta\theta_1 - 8k \Delta\theta_2 - 4k_L L \cos\left(\frac{\theta}{2}\right) \Delta x = 0$$

$$M_E L^2 \Delta\ddot{\theta}_2 + (8k + 2k_L L^2 \cos^2\frac{\theta}{2}) \Delta\theta_2 - 8k \Delta\theta_1 - 4k_L L \cos\left(\frac{\theta}{2}\right) \Delta x = 0$$

Substituting

$$\Delta x = A e^{i\omega t}$$

$$\Delta\theta_1 = B e^{i\omega t}$$

$$\Delta\theta_2 = C e^{i\omega t}$$

gives the three normal modes:-

$$i. \quad B = C = 1, \quad A = \frac{-M_E L}{2 m_L \cos\frac{\theta}{2}} \quad \text{and} \quad \nu_{EL}^{damp} = \frac{1}{2\pi} \sqrt{\frac{2k_L}{m_L} + \frac{2k_L \cos^2\frac{\theta}{2}}{M_E}}$$

$$\text{since } M_E \gg m_L \text{ then the frequency } \nu_{EL}^{damp} \approx \frac{1}{2\pi} \sqrt{\frac{2k_L}{m_L}}$$

which is simply a high frequency vibration of the ligand in the jaws of the binding site rather than the low frequency scissor mode.

$$\text{ii. } \omega^2 = 0, \quad B = C = 1, \quad A = \frac{L}{2} \cos \frac{\theta}{2}$$

This is a translation of the whole system. The unusual amplitude for A is due to the coordinate system.

$$\text{iii. } \omega^2 = \frac{16k + 2k_L L^2 \cos^2 \frac{\theta}{2}}{M_E L^2}, \quad A = 0, \quad B = -C$$

This represents the scissor like motion of the enzyme with one ligand bound. The frequency can be re-written as

$$\begin{aligned} \nu_{EL}^{\text{sc}} &= \frac{1}{2\pi} \sqrt{\frac{16k + 2k_L L^2 \cos^2 \frac{\theta}{2}}{M_E L^2}} \\ &= \frac{1}{2\pi} \sqrt{1 + \frac{k_L L^2 (1 + \cos \theta)}{16k}} \end{aligned}$$

This scissor mode can be seen to increase on ligand binding.

### 3. Two ligands bound

Variables  $\Delta\theta_1, \Delta\theta_2, \Delta X_1, \Delta X_2$

$$\text{Kinetic energy} = \frac{M_E L^2}{16} (\Delta\dot{\theta}_1^2 + \Delta\dot{\theta}_2^2) + \frac{1}{2} m_L (\Delta\dot{X}_1^2 + \Delta\dot{X}_2^2)$$

$$\begin{aligned} \text{Potential energy} &= \frac{1}{2} k (\Delta\theta_1 - \Delta\theta_2)^2 \\ &\quad + \frac{1}{2} k_L \left( \frac{L}{2} (\sin(\frac{\theta}{2} + \Delta\theta_1) - \sin \frac{\theta}{2}) - \Delta X_1 \right)^2 \\ &\quad + \frac{1}{2} k_L \left( \frac{L}{2} (\sin(\frac{\theta}{2} - \Delta\theta_2) - \sin \frac{\theta}{2}) + \Delta X_1 \right)^2 \\ &\quad + \frac{1}{2} k_L \left( \frac{L}{2} (\sin(\frac{\theta}{2} - \Delta\theta_2) - \sin \frac{\theta}{2}) + \Delta X_2 \right)^2 \\ &\quad + \frac{1}{2} k_L \left( \frac{L}{2} (\sin(\frac{\theta}{2} + \Delta\theta_1) - \sin \frac{\theta}{2}) - \Delta X_2 \right)^2 \end{aligned}$$

Lagrange's equation for the 4 variables gives:-

$$2m_L \Delta\ddot{X}_1 + 4k_L \Delta X_1 - k_L L \cos \frac{\theta}{2} (\Delta\theta_1 + \Delta\theta_2) = 0$$

$$2m_L \Delta\ddot{X}_2 + 4k_L \Delta X_2 - k_L L \cos \frac{\theta}{2} (\Delta\theta_1 + \Delta\theta_2) = 0$$

$$M_E L^2 \Delta \ddot{\Theta}_1 + \Delta \Theta_1 (8k + 4k_L L^2 \cos^2 \frac{\Theta}{2}) - 8k \Delta \Theta_2 - 4k_L L \cos \frac{\Theta}{2} (\Delta X_1 + \Delta X_2) = 0$$

$$M_E L^2 \Delta \ddot{\Theta}_2 + \Delta \Theta_2 (8k + 4k_L L^2 \cos^2 \frac{\Theta}{2}) - 8k \Delta \Theta_1 - 4k_L L \cos \frac{\Theta}{2} (\Delta X_1 + \Delta X_2) = 0$$

Substituting

$$\Delta X_1 = A e^{i\omega t}$$

$$\Delta X_2 = B e^{i\omega t}$$

$$\Delta \Theta_1 = C e^{i\omega t}$$

$$\Delta \Theta_2 = D e^{i\omega t}$$

gives the following normal modes:-

$$i. \quad A = B = 1, \quad C = D = \frac{-4 m_L \cos \frac{\Theta}{2}}{M_E L}$$

$$\omega^2 = \frac{2k_L}{m_L} + \frac{4k_L \cos^2 \frac{\Theta}{2}}{M_E} \Rightarrow \nu_{EL_2}^{damp} = \frac{1}{2\pi} \sqrt{\frac{2k_L}{m_L} + \frac{4k_L \cos^2 \frac{\Theta}{2}}{M_E}}$$

This solution represents the two ligands vibrating in phase with each other and the enzyme moving out of phase. The enzyme motion will be damped out in solution and the vibrational frequency, if  $M \gg m_L$ , will be high representing a local vibration of the ligand. This mode is similar to the first solution for the case of one ligand bound.

$$ii. \quad A = -B, \quad C = D = 0, \quad \omega^2 = \frac{2k_L}{m_L} \Rightarrow \nu_{EL_2}^x = \frac{1}{2\pi} \sqrt{\frac{2k_L}{m_L}}$$

This mode represents a stationary enzyme with the ligands vibrating out of phase with each other at the natural frequency of the spring binding the ligand to the enzyme. This mode will be a high frequency local mode.

$$iii. \quad A = B = \frac{L}{2} \cos \frac{\Theta}{2}, \quad C = D = 1, \quad \omega^2 = 0$$

This mode represents a translation of the whole system.

$$iv. \quad A = B = 0, \quad C = -D, \quad \omega^2 = \frac{16k + 4k_L L^2 \cos^2 \frac{\Theta}{2}}{M_E L^2}$$

This represents the scissor like mode of the system with

both ligands stationary. The frequency can be re-written as:-

$$\begin{aligned} \nu_{EL_2}^{sc} &= \frac{1}{2\pi} \sqrt{\frac{16K + 4k_L L^2 \cos^2 \frac{\theta}{2}}{M_E L^2}} \\ &= \nu_E^{sc} \sqrt{1 + \frac{k_L L^2 \cos^2 \frac{\theta}{2}}{8K}} \end{aligned}$$

It can be seen that binding of the second ligand causes a further increase in the scissor frequency.

BLIST

```

10 PRINT "LIGAND BINDING 7"
15 PRINT
20 K = 0.695
30 H = 3.3357E - 11
40 INPUT "TEMP=":T
42 Z = H / (K * T)
45 INPUT "ENZYME ANGLE(RDNS)= ":
    B
50 A = 1 + COS (B)
55 INPUT "SITE SEPARATION(ANGSTR
    OMS)= ":L
60 INPUT "ENZYME MASS(A.M.U)= ":
    ME
65 INPUT "LIGAND MASS(A.M.U)= ":
    ML
70 INPUT "ENZYME SCISSOR FREQ.(H
    Z)= ":VE
75 INPUT "LIGAND-ENZYME BOND FRE
    Q.(HZ)= ":VL
80 PR# 1
83 PRINT "TEMPERATURE= ":T
86 PRINT "ENZYME ANGLE(RDNS)= ":
    B
90 PRINT "SITE SEPARATION(ANGSTR
    OMS)= ":L
92 PRINT
93 PRINT "ENZYME MASS(A.M.U)= ":
    ME
96 PRINT "LIGAND MASS(A.M.U)= ":
    ML
97 PRINT
100 PRINT "ENZYME SCISSOR FREQ.(
    HZ)= ":VE
103 PRINT "LIGAND-ENZYME BOND FR
    EQ.(HZ)= ":VL
105 PRINT
120 V1 = VE * SQR (1 + (ML * VL *
    VL * A / (2 * VE * VE * ME))
    )
130 V2 = VL * SQR (1 + (ML * A /
    (2 * ME)))
140 V3 = VE * SQR (1 + (ML * VL *
    VL * A / (ME * VE * VE)))
150 V4 = VL * SQR (1 + (ML * A /
    ME))
160 V5 = VL
170 PRINT "EL SCISSOR FREQ.=":V1

180 PRINT "EL DAMP. FREQ.=":V2
185 PRINT
190 PRINT "EL2 SCISSOR FREQ.=":V
    3

```

```

200 PRINT "EL2 DAMP. FREQ.=":V4
210 PRINT "EL2 UNDAMP. FREQ.=":V
5
230 PRINT
300 PRINT "GROUND STATE ENTHALPY
    CHANGES"
302 PRINT "Y,Z MOTION OF LIGANDS
    IGNORED"
305 PRINT
310 H1 = 0.5 * H * (V1 + V2 - VE)

320 H2 = 0.5 * H * (V3 + V4 + V5 -
    V1 - V2)
330 DH = H2 - H1
340 PRINT "GRND. STATE VIBRATION
    FREE ENERGIES"
345 PRINT
350 PRINT "DG1=DH1=":H1
360 PRINT "DG2=DH2=":H2
370 PRINT "DDG=DDH=":DH
375 PRINT
380 PRINT "ZERO ENTROPY CHANGE I
    N GRND STATE"
385 PRINT
400 PRINT "VIBR. ENERGY CHANGES"

405 PRINT
410 FE = 1 - EXP (- Z * VE)
420 F1 = 1 - EXP (- Z * V1)
430 F2 = 1 - EXP (- Z * V2)
440 F3 = 1 - EXP (- Z * V3)
450 F4 = 1 - EXP (- Z * V4)
460 F5 = 1 - EXP (- Z * V5)
470 G1 = - K * T * LOG (FE) + K
    * T * LOG (F1) + K * T * LOG
    (F2)
480 G2 = - K * T * LOG (F1) - K
    * T * LOG (F2) + K * T * LOG
    (F3) + K * T * LOG (F4) + K
    * T * LOG (F5)
490 DG = G2 - G1
500 H1 = - H * VE * EXP (- Z *
    VE) / FE + H * V1 * EXP (-
    Z * V1) / F1 + H * V2 * EXP
    (- Z * V2) / F2
510 HA = - H * V1 * EXP (- Z *
    V1) / F1 - H * V2 * EXP (-
    Z * V2) / F2

```

```

514 HB = H * V3 * EXP ( - Z * V3
      ) / F3 + H * V4 * EXP ( - Z
      * V4) / F4 + H * V5 * EXP
      ( - Z * V5) / F5
516 H2 = HA + HB
520 DH = H2 - H1
530 S1 = - (G1 - H1) / T
540 S2 = - (G2 - H2) / T
550 DS = S2 - S1
560 PRINT "FREE ENERGIES"
565 PRINT
570 PRINT "DG1="; G1
580 PRINT "DG2="; G2
590 PRINT "DDG="; DG
595 PRINT
610 PRINT "ENTHALPIES"
615 PRINT
620 PRINT "DH1="; H1
630 PRINT "DH2="; H2
640 PRINT "DDH="; DH
655 PRINT
660 PRINT "ENTROPIES"
665 PRINT
670 PRINT "DS1="; S1
680 PRINT "DS2="; S2
690 PRINT "DDS="; DS
691 PRINT
692 PRINT "ENTROPY*TEMP. "
693 PRINT
694 PRINT "T*DS1="; T * S1
696 PRINT "T*DS2="; T * S2
698 PRINT "T*DDS="; T * DS
699 PRINT
700 PR# 0
800 INPUT "NEW FREQ. (Y/N)?: " Y#
810 IF Y# = "Y" THEN GOTO 40
900 END

```

Appendix 2 Raman spectroscopy at room temperature and 77K of urethane prepared from cycloundecanone and 4-phenylsemicarbazide

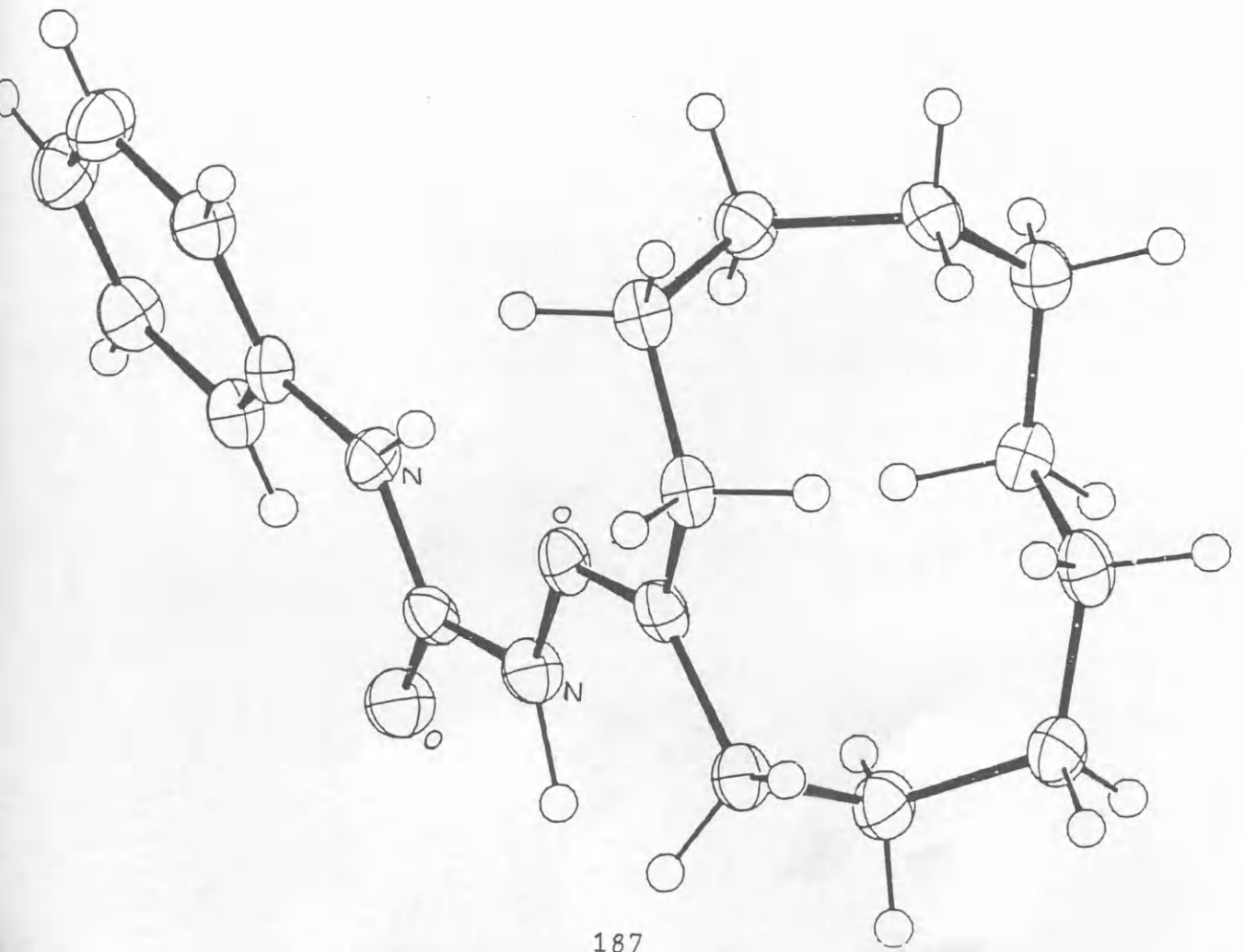
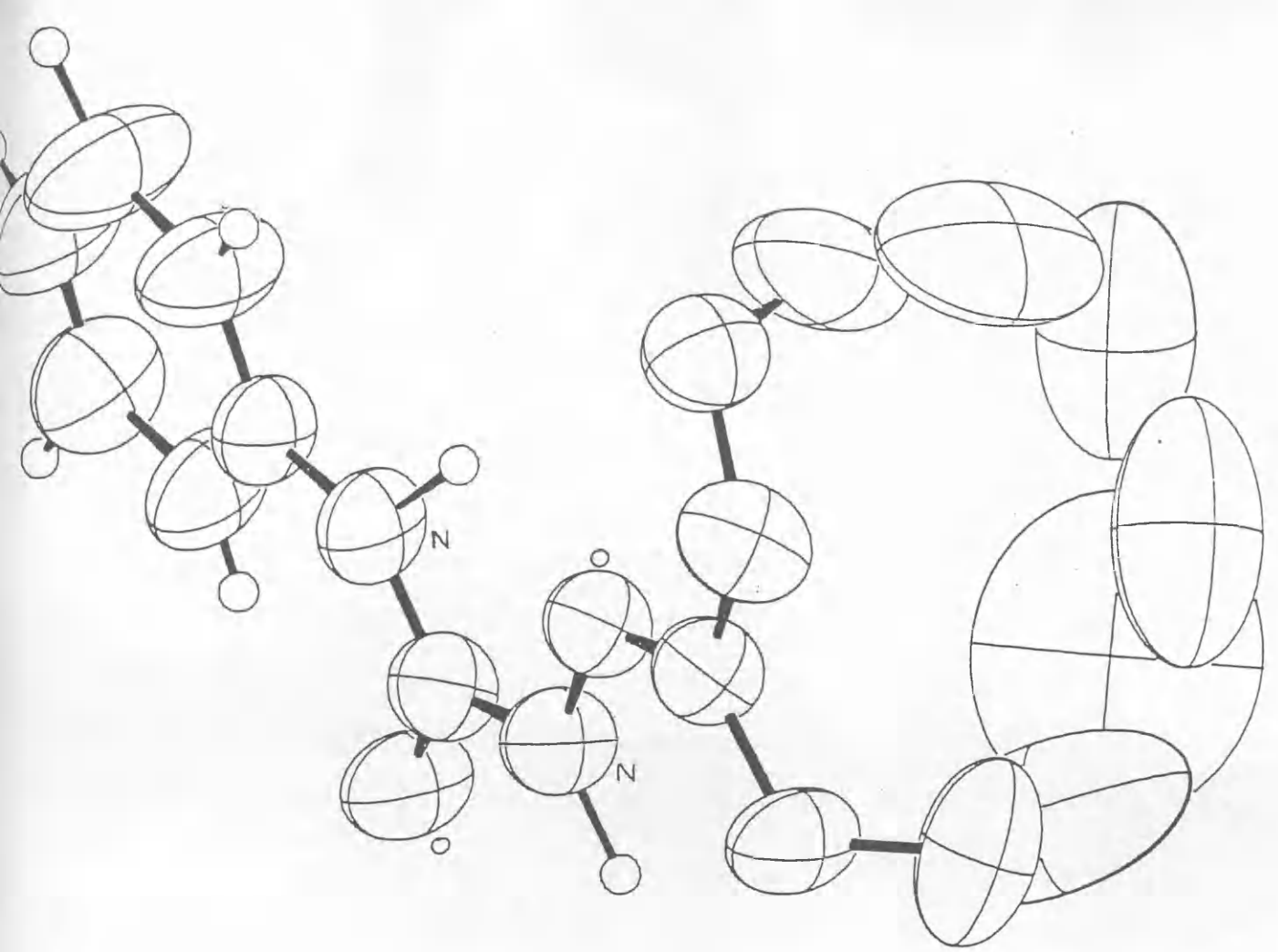
Professor George Sim of this department supplied a crystalline compound formula between cycloundecanone and 4-phenylsemicarbazide which possess different structures at room and liquid nitrogen temperatures as shown in Figures A2.1 and A2.2

The part of the alkane ring furthest from the phenylsemicarbazide group shows very large anisotropic thermal ellipsoids at room temperature indicating a high degree of flexibility which is abolished at low temperature where there is only one well defined structure. At room temperature this part of the ring can probably take up several different conformations which interchange rapidly using thermal energy to cross various potential energy barriers. One of these conformations may be the low temperature structure which becomes more energetically favourable and hence more populated as the temperature is lowered until it is the only structure present.

Depolarised Raman spectra of powdered samples in a sealed glass capillary were recorded at the two temperatures by fixing the capillary to a copper block on the end of the cold finger in a home made glass cryostat. The laser beam and the scattered radiation passed through optical windows set into the sides of the glass outer casing. Insulation of the liquid nitrogen filled cold finger and sample block was provided by evacuating the space between the cold finger and the outer casing. Laser heating of

Fig. A2.1 X-ray structure of the cycloundecanone-phenylsemicarbazide compound at room temperature showing thermal motion ellipsoids for each atom. Unlabelled atoms are carbon.

Fig. A2.2 X-ray structure of the compound at 77K showing much reduced thermal motion and a different conformation.



the sample would cause the sample temperature to be somewhat higher than 77K though this would be minimised by the large copper block conducting heat away efficiently with the result that the sample temperature should be within 10K of the liquid nitrogen temperature.

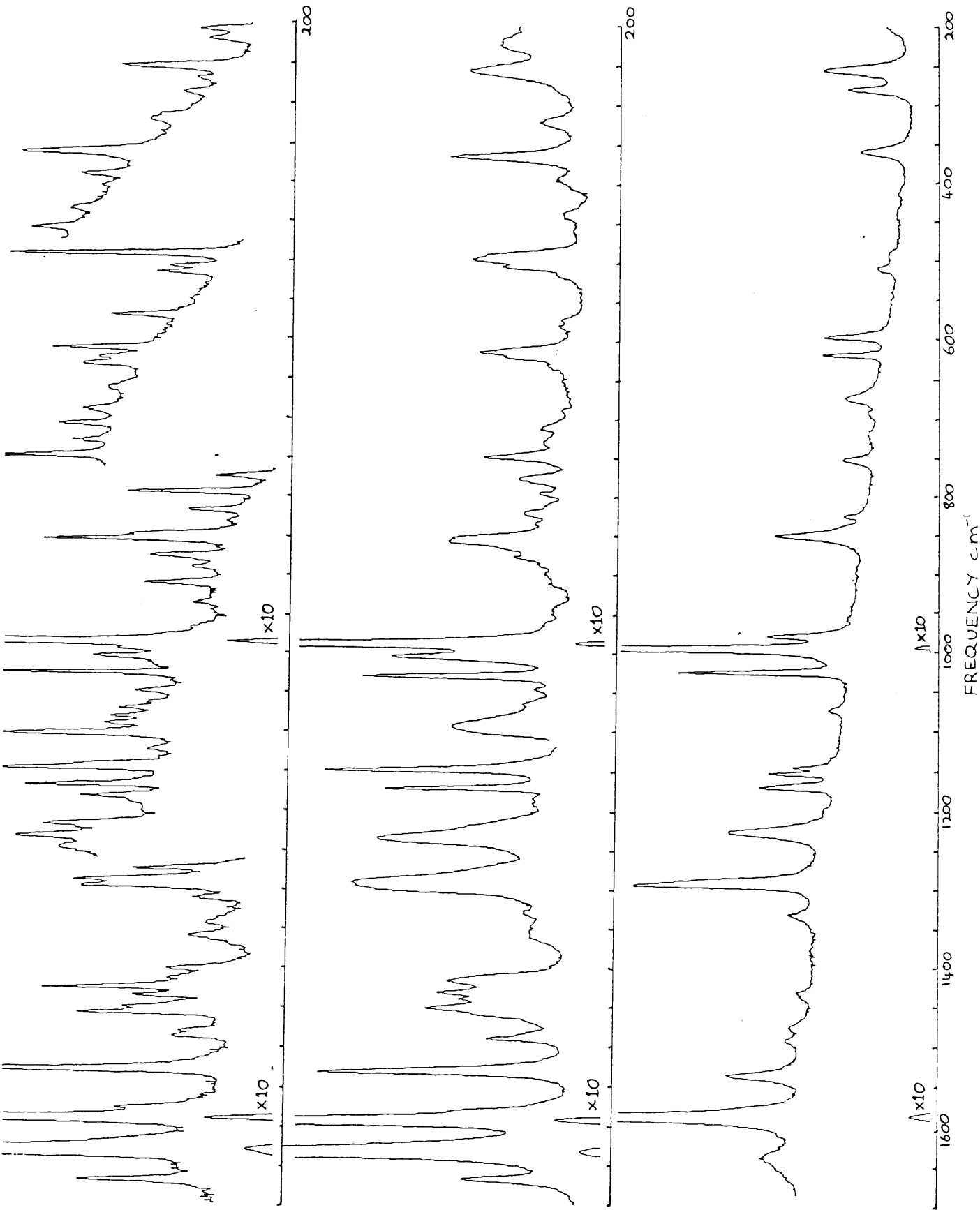
The assignment of the very large number of Raman bands in the high frequency region shown in Figure A2.3 was simplified by recording a room temperature spectrum of 4-phenylsemicarbazide as a powdered solid also shown in Figure A2.3, and using published data on cycloundecane (Sterin et al). The bands were then assigned using information in Dollish, Fateley & Bentley (1974).

The room temperature spectrum of the compound was compared to that of phenylsemicarbazide. Many bands matched up closely indicating that the rest are due to vibrations of the cycloundecane ring and the C=N bond which joins the ligand to the ring.

There are 3 bands in the compound's spectrum which do not match the semicarbazide spectrum but which are very probably due to the semicarbazide:-

i. The intense band at  $495\text{cm}^{-1}$  which increases in strength on cooling and becomes much sharper. This is similar behaviour to that of the other bands at  $365$ ,  $612$ ,  $748$  and  $854\text{cm}^{-1}$  which do match up with semicarbazide bands. This band may be the equivalent of the ligand band at about  $600\text{cm}^{-1}$  which is sharp and of similar intensity.

ii. The 2 broad strong bands at  $1232$  and  $1290\text{cm}^{-1}$  appear in both the semicarbazide spectrum and in the cycloundecane spectrum



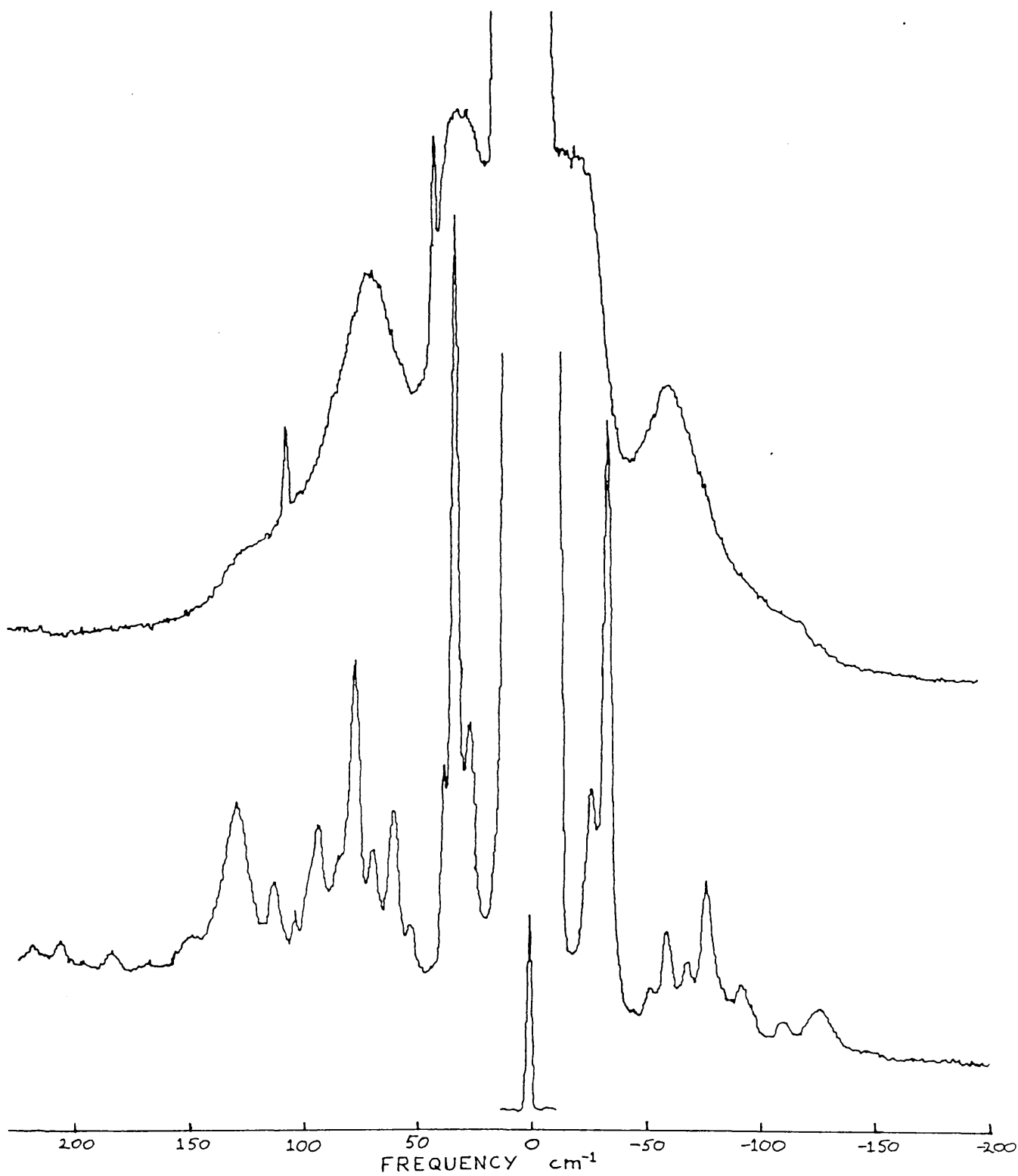
although the lower of the cycloundecane bands is much weaker. These peaks become resolved into several sharper bands on cooling. Two, or possible three of these bands will be due to the semicarbazide and the rest to the cycloundecane ring. There may be coupling between these various modes so determining which bands are due to the semicarbazide and which to the cycloundecane is difficult.

Apart from the usual line narrowing at low temperature, it can be seen that in all cases, except those noted above, that only bands due to the cycloundecane ring change on cooling the complex. By ignoring bands due to the semicarbazide, the cycloundecane bands can be assigned using information on alkanes in Dollish et al. (1974), and the data on cycloundecane.

Bands below about  $550\text{cm}^{-1}$  are CCC skeletal deformation modes. Between  $1000\text{cm}^{-1}$  and  $500\text{cm}^{-1}$  there are numerous  $\text{CH}_2$  rocking and twisting modes. C-C stretches occur between  $1000$  and  $1130\text{cm}^{-1}$  and from  $1150\text{cm}^{-1}$  to  $1360\text{cm}^{-1}$  there are methylene twists and rocks. Above  $1300\text{cm}^{-1}$  these methylene modes are in-phase twists and below this they are out-of-phase rocks, The group of bands between  $1400\text{cm}^{-1}$  and  $1450\text{cm}^{-1}$  are methylene in plane, 'scissor' like deformations. The modes between  $1475\text{cm}^{-1}$  and  $1490\text{cm}^{-1}$  and the band at  $1667\text{cm}^{-1}$  are unassigned.

Figure A2.4 shows the low frequency Stokes and anti-Stokes spectra of the compound.

Fig. A2.4 Low frequency ( $-200$  to  $+200$   $\text{cm}^{-1}$ ) Raman spectra of the compound at room temperature (upper spectrum) and  $77\text{K}$  (lower spectrum). Recorded with  $100$  mW of  $488$  nm radiation,  $250$  micron slitwidths at  $25$   $\text{cm}^{-1}/\text{min}$  with  $1.2$  second time constants.



## Results

On going from low temperature where there is one unique molecular conformation and spectrum, to room temperature where the average conformation of part of the cycloundecane ring is different and very mobile there are several major changes in the compounds Raman spectrum shown in detail in Figures A2.4, A2.5, A2.6 and A2.7.

i. The very complex low frequency spectrum showing a large number of lattice modes, librations and other low frequency intramolecular vibrations at 77K is lost at room temperature where only a few poorly resolved bands are visible.

ii. Several sharp bands of medium intensity at 459, 662, 793, 874, 889 and  $908\text{cm}^{-1}$  become much weaker, some almost disappearing.

iii. Two sharp medium strength bands at  $570\text{cm}^{-1}$  and  $1180\text{cm}^{-1}$  become weak doublets at room temperature.

iv. Several doublets of approximately equal intensity at  $208\text{-}220\text{cm}^{-1}$ ,  $506\text{-}514\text{cm}^{-1}$  and  $623\text{-}631\text{cm}^{-1}$ , become doublets where the lower frequency band increases in intensity at the expense of the higher frequency band.

v. There are large relative intensity changes of bands in the CH scissors region,  $1380\text{-}1470\text{cm}^{-1}$ , coupled with a broadening of the bands. The most intense peaks at room and low temperature are at different frequencies.

vi. Large relative intensity changes in the CH rocks and twists with such large broadening that the individual peaks are unresolved.

vii. In the C-C stretch region there is a large broadening of

peaks with the lower frequency bands increasing in intensity at the expense of the most intense highest frequency band. The most intense peak moves from  $1100\text{cm}^{-1}$  at 77K to  $1093\text{cm}^{-1}$  at room temperature.

### Conclusions

The Raman spectra show clearly that as the temperature is raised the average conformation of the molecule changes. This is particularly noticeably in the C-C strength and  $\text{CH}_2$  scissors regions where the relative intensities of bands change considerably.

The increase in resolution at low temperature could be useful for studying the low frequency modes of proteins. Any low frequency bands would be better resolved from the Rayleigh wing as well as being sharper and shifted to higher frequency due to respectively, a decrease in the anharmonicity of the vibration and a decrease in the damping of the motion.

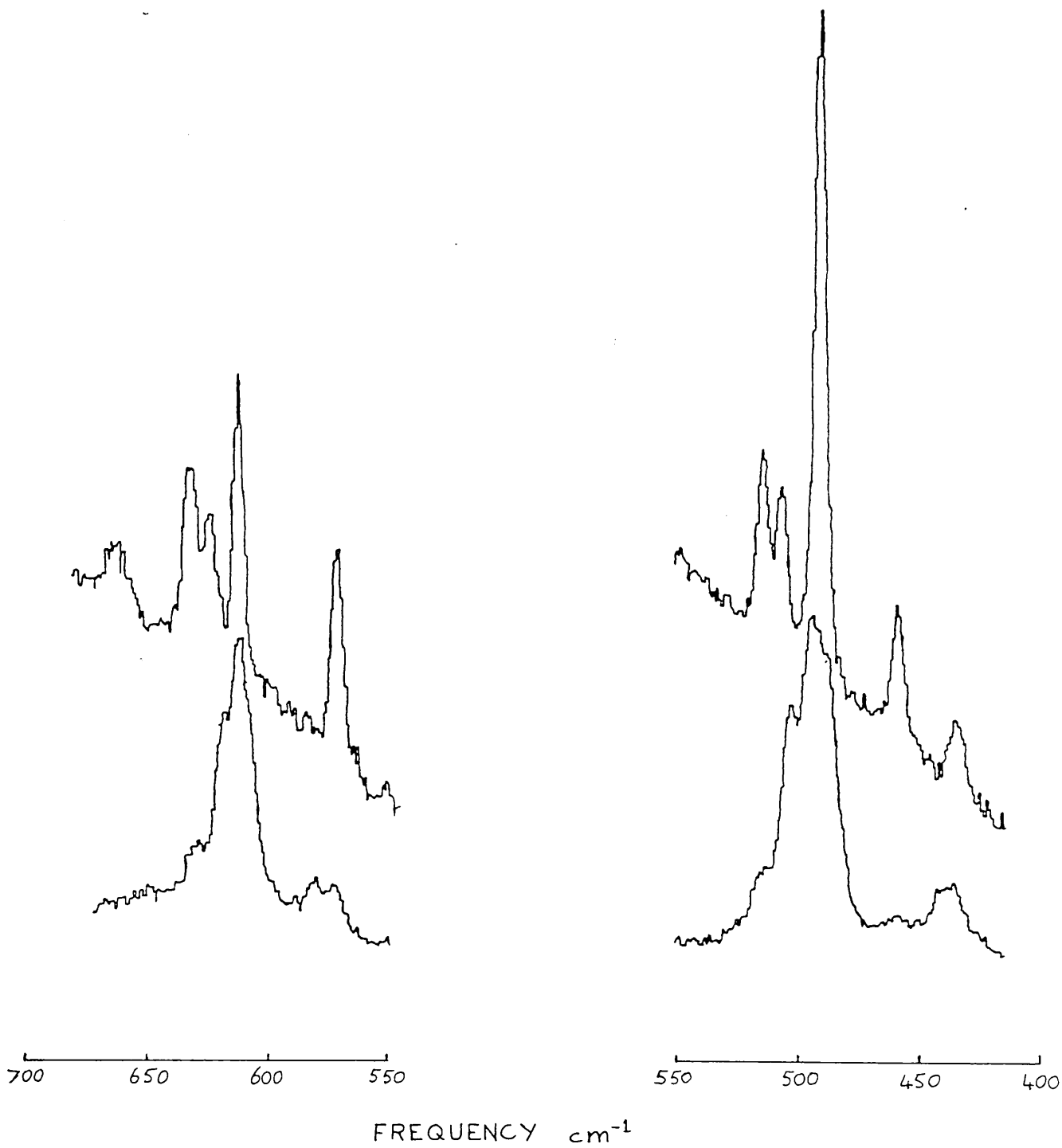


Fig. A2.5 Expanded portion of Fig. A2.3 showing the C-C-C skeletal deformations and  $\text{CH}_2$  rocks and twists. The 77K spectrum is the upper one.

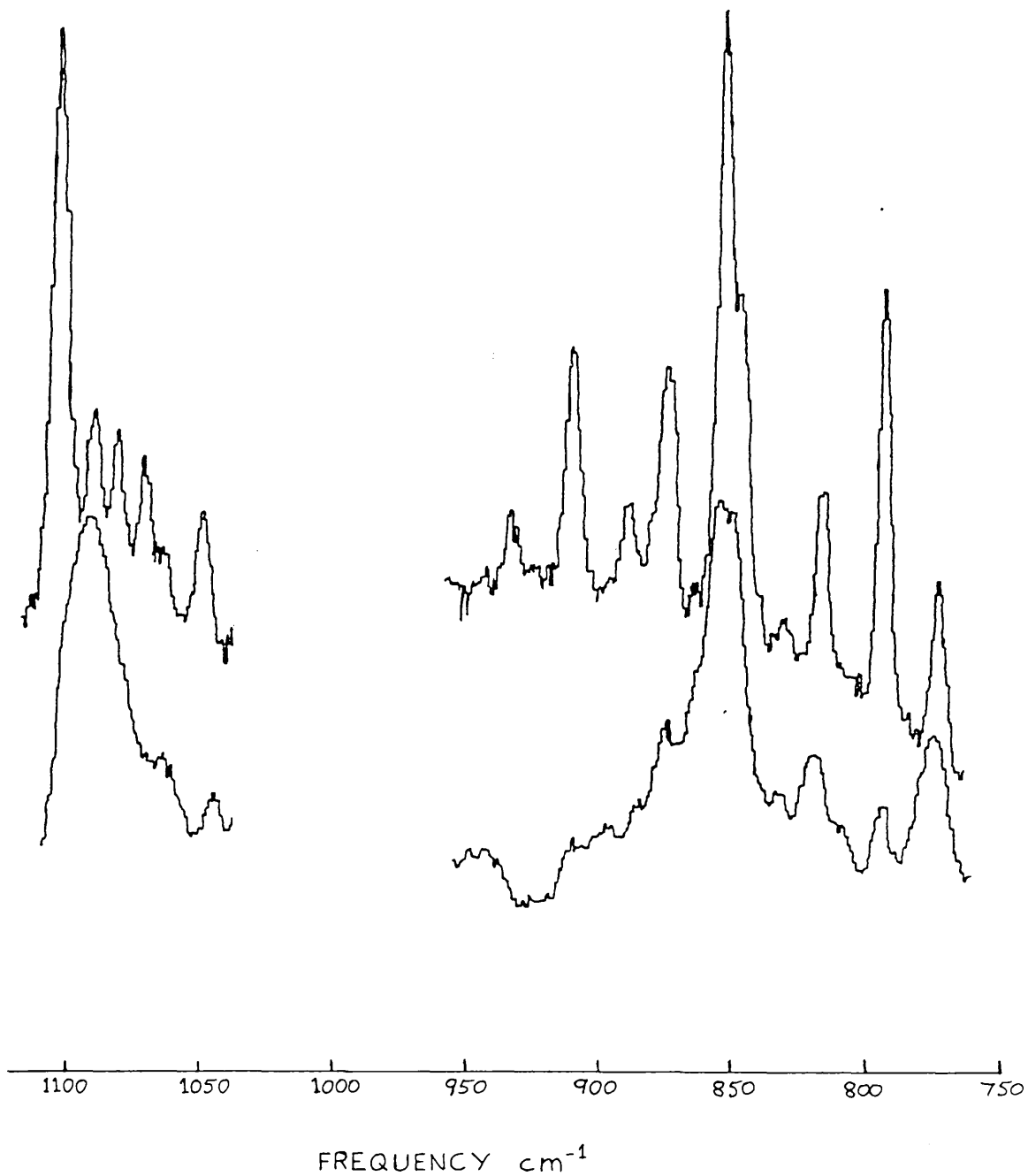


Fig. A2.6 Expanded portion of Fig. A2.3 showing the in-phase  $\text{CH}_2$  rocks, out-of-phase twists and C-C stretches. The 77K spectrum is the upper one.

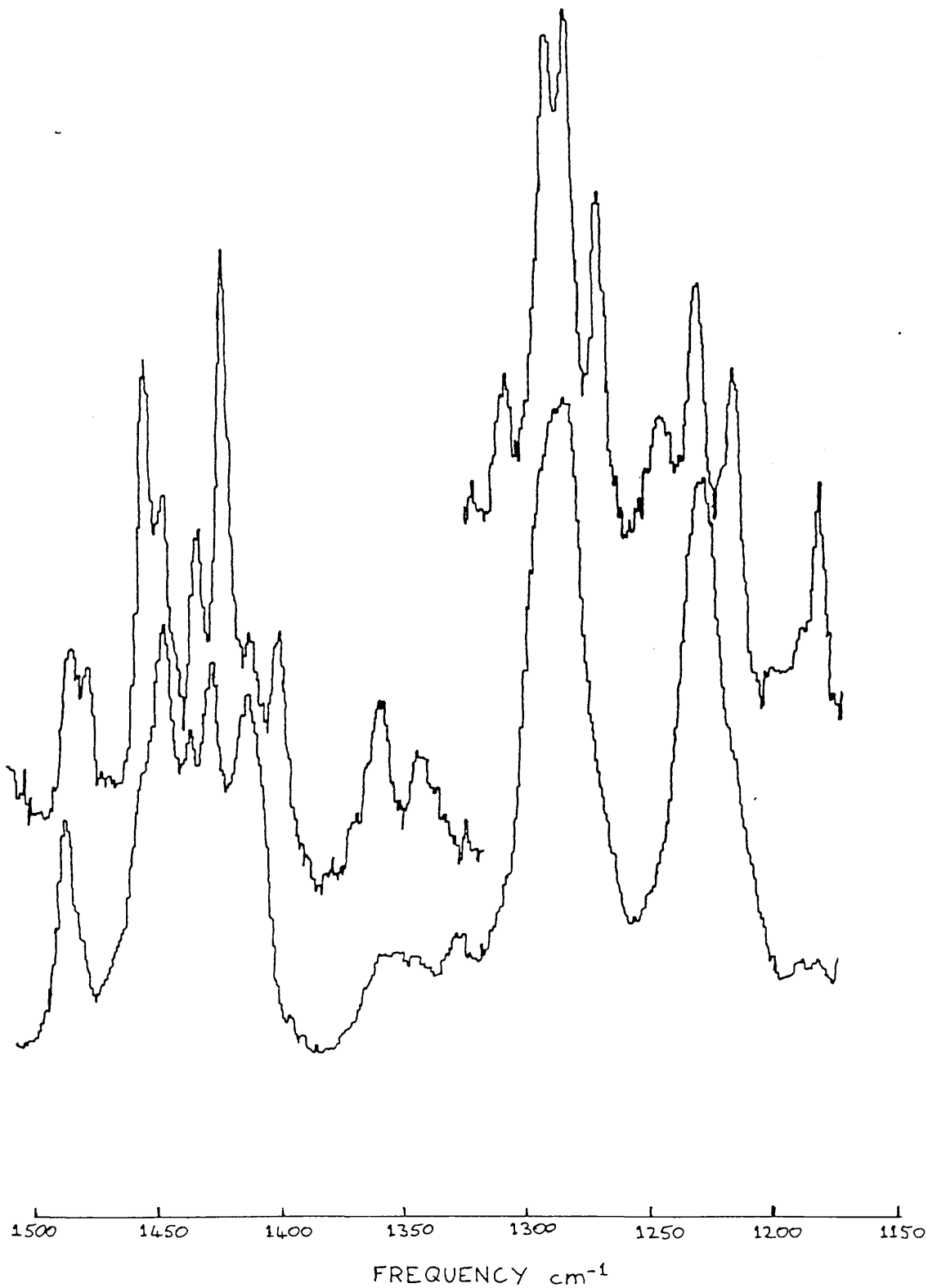


Fig. A2.7 Expanded portion of Fig. A2.3 showing the CH<sub>2</sub> out-of-phase rocks, in-phase twists and scissor-like deformations. The 77K spectrum is the upper one.

# Allostery without conformational change

## A plausible model

A. Cooper\* and D. T. F. Dryden

Chemistry Department, Glasgow University, Glasgow G12 8QQ, Scotland

Received March 2, 1984/Accepted July 6, 1984

**Abstract.** A general model is presented whereby ligand-induced changes in protein dynamics could produce allosteric communication between distinct binding sites, even in the absence of a macromolecular conformational change. Theoretical analysis, based on the statistical thermodynamics of ligand binding, shows that cooperative interaction free energies amounting to several  $\text{kJ} \cdot \text{mol}^{-1}$  may be generated by this means. The effect arises out of the possible changes in frequencies and amplitudes of macromolecular thermal fluctuations in response to ligand attachment, and can involve all forms of dynamic behaviour, ranging from highly correlated, low-frequency normal mode vibrations to random local anharmonic motions of individual atoms or groups. Dynamic allostery of this form is primarily an entropy effect, and we derive approximate expressions which might allow the magnitude of the interaction in real systems to be calculated directly from experimental observations such as changes in normal mode frequencies and mean-square atomic displacements. Long-range influence of kinetic processes at different sites might also be mediated by a similar mechanism. We suggest that proteins and other biological macromolecules may have evolved to take functional advantage not only of mean conformational states but also of the inevitable thermal fluctuations about the mean.

**Key words:** Protein dynamics, fluctuations, allostery, cooperativity

### Introduction

Allosteric effects, involving communication between distant ligand-binding sites on biological macromolecules, are central to many physiological control and

receptor processes. Conventionally, these effects are ascribed to ligand-induced conformational changes transmitted through the macromolecule and across subunit boundaries. Monod et al. (1965) graphically demonstrated how this concept could explain quantitatively many of the observed cooperative and linkage phenomena in proteins – and yet even in this seminal paper it was emphasized that the concept of “conformational transition . . . should be understood in its widest connotation”, and not solely in the strict stereochemical sense that we usually use today. Accordingly, we wish to develop here one of the alternative mechanisms for long-range site-site interaction (Cooper 1980; Salemme 1978) based on current thinking about the dynamic properties of proteins. We will show that it is possible to explain cooperative ligand binding in terms of the frequency and amplitude of atomic motions about fixed mean positions, i.e., without a conformational change in any sense that could be determined structurally.

The conformation of a macromolecule, as defined, for example, by X-ray crystallography, gives the mean atomic positions averaged over a large number of, supposedly, identical molecules and over times which are long compared to typical molecular motions. We now know, however, from fundamental theoretical considerations and from a wide variety of experiments, that individual macromolecules are dynamic objects undergoing various forms of intramolecular motion (for recent reviews, see: Cooper 1980; Gurd and Rothgeb 1979; McCammon and Karplus, 1983; Careri et al. 1979). These fluctuations have been variously described in terms of vibration, libration, or rotation of individual chemical groups, global oscillations of protein domains, “hinge bending”, “breathing”, “local unfolding”, and so on, and can involve relative motion over several angstroms covering the entire time spectrum. Thermally excitable low-frequency vibrations ( $\leq 200 \text{ cm}^{-1}$ ) in globular proteins have been detected experimentally

\* To whom offprint requests should be sent

(Peticolas 1979; Jacrot et al. 1982; Middendorf 1984) and demonstrated by theoretical normal mode analysis to involve cooperative motions spanning entire molecules (Gō 1980, Gō et al. 1983; Brooks and Karplus 1983). Anharmonic and aperiodic motions are predicted by molecular dynamics simulations (McCammon and Karplus 1983; Levitt 1983a, b) and are also indicated by various experimental observations (Cooper 1980; Gurd and Rothgeb 1979). Such dynamic phenomena are not unique to biological macromolecules, being simply a manifestation of heat energy (Cooper 1976), but the thermodynamic fluctuations involved are quite large in these relatively small systems, and we might expect that, during evolution, any useful dynamic phenomena might become part of the repertoire of these systems. For example, in the present context of allostery, since the information content of a macromolecule consists not only of its average conformation but also of the frequencies and amplitudes of fluctuation about this conformation, communication across the molecule could go via changes in these dynamic frequencies and amplitudes, independently or even in the absence of conformation change.

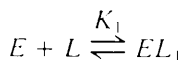
We should emphasize from the start that it is not our intention to deny the existence or significance of conformational changes in protein receptor and control functions – but, rather, to illustrate that equally plausible, quantifiable alternatives do exist.

### Statistical thermodynamics of multiple ligand binding

Sturtevant (1977) has discussed the various factors which contribute to the thermodynamics of protein interactions, emphasizing the significance of dynamic (vibrational) contributions. In reviewing the available data, he notes the almost universal decrease in heat capacity (i.e., negative  $\Delta C_p$ ) associated with protein-ligand binding and points out how this could arise from the loss of many internal, vibrational degrees of freedom. Similar conclusions may be reached by more general treatment of thermodynamic fluctuations (Cooper 1976), which shows that a decrease in heat capacity of a system inevitably implies that the thermal energy fluctuations in the system are reduced. Thus, we can picture the usual effects of ligand-binding to be a “stiffening” of the protein structure, although cases may be imagined in which the reverse is true. We wish to analyse in more detail the thermodynamic consequences of this.

Textbook statistical thermodynamics (e.g., Hill 1960; McQuarrie 1976; Davidson 1962) gives the free energy of molecular association in terms of the

canonical partition functions of the molecular species involved. Thus, for the ligand-binding equilibrium at constant volume:



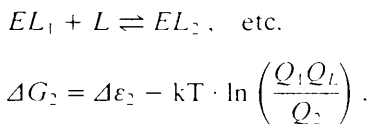
the dissociation constant is given by:

$$K_1 = e^{-\Delta\varepsilon_1/kT} \cdot \frac{Q_0 Q_L}{Q_1},$$

where  $\Delta\varepsilon_1 = \varepsilon_E + \varepsilon_L - \varepsilon_{EL_1}$  is the difference in ground state energies corresponding to the (hypothetical) energy of ligand binding at 0 K in the absence of thermal motion, and  $Q_0$ ,  $Q_1$ , and  $Q_L$  are the partition functions for the free enzyme ( $E$ ), the binary complex ( $EL_1$ ) and the free ligand ( $L$ ), respectively. In the absence of significant volume changes, the Gibbs free energy of reaction is

$$\begin{aligned} \Delta G_1 &= -kT \ln K_1 \\ &= \Delta\varepsilon_1 - kT \cdot \ln \left( \frac{Q_0 Q_L}{Q_1} \right). \end{aligned}$$

Subsequent binding steps (at different sites) can be treated similarly, thus:



where  $\Delta\varepsilon_2 = \varepsilon_{EL_1} + \varepsilon_L - \varepsilon_{EL_2}$ ;  $Q_2$  refers to the ternary complex ( $EL_2$ ); and so on.

The difference  $\Delta\Delta G = \Delta G_2 - \Delta G_1$  in binding free energies is a measure of the cooperativity (allostery) and may be written:

$$\Delta\Delta G = \Delta\varepsilon_2 - \Delta\varepsilon_1 - kT \cdot \ln \left( \frac{Q_1^2}{Q_0 Q_2} \right).$$

If we restrict our attention to the binding of identical ligands to (formally) identical and physically distant binding sites then  $\Delta\varepsilon_2 = \Delta\varepsilon_1$ , since the same molecular contacts are involved in each site, and

$$\Delta\Delta G = -kT \cdot \ln \left( \frac{Q_1^2}{Q_0 Q_2} \right).$$

The canonical partition function of a system is defined as  $Q = \sum_i e^{-E_i/kT}$ , where the summation is taken over all possible states,  $i$ , of the system with energies  $E_i$ . These will include all allowed translational, rotational, vibrational, electronic, and con-

formational states of the protein, or complex, as appropriate. As is conventional, we may assume separability and write

$$Q = q_{\text{Trans}} \cdot q_{\text{Rot}} \cdot q_{\text{Vib}} \cdot q_{\text{Elect}} \cdot q_{\text{Cont}}$$

and examine each contribution in turn. (For simplicity, we will ignore other possible internal modes of motion, such as free rotation of chemical groups, and assume that, at least formally, they may be treated as internal vibrational modes or different conformational substates.) The electronic energy level contributions may be eliminated from the start since they are not significantly excited at normal temperatures, and any changes in ground-state levels due to bond formation in the *EL* complex have already been assumed in the  $\Delta\varepsilon$  terms.

The partition functions representing global translation and rotation of the entire protein molecule,  $q_{\text{Trans}}$  and  $q_{\text{Rot}}$ , are given by standard expressions which depend on the mass and moments of inertia of the molecule, respectively (Hill 1960; Davidson 1962; McQuarrie 1976). If we assume that the ligands are small compared to the enzyme, then these terms are numerically very similar for the different ligated states and effectively cancel in the expression for  $\Delta\Delta G$ .

This leaves:

$$\Delta\Delta G = -kT \cdot \left\{ \ln \left( \frac{q_1^2}{q_0 q_2} \right)_{\text{Vib}} + \ln \left( \frac{q_1^2}{q_0 q_2} \right)_{\text{Cont}} \right\}$$

which identifies two possible sources of cooperativity between the two binding sites. The first term gives rise to a finite  $\Delta\Delta G$  if there are changes induced in the vibrational spectrum of the system by ligand binding. The second term in the equation expresses any effects of conformational change in the conventional sense, plus more subtle dynamic effects which we shall examine later.

### The vibrational contribution

The vibrational partition function of the *i*th. normal mode of a system, with frequency  $\nu_i$ , taking quantized energy levels  $n h \nu_i$  ( $n = 0, 1, 2, \dots$ ) and incorporating the zero-point energy ( $1/2 h \nu_i$ ) into the ground state energy term, is given by

$$q_{\text{Vib}}(\nu_i) = (1 - e^{-h\nu_i/kT})^{-1}$$

which, in the classical limit  $kT \gg h\nu_i$ , becomes

$$q(\nu_i)_{\text{class.}} = \frac{kT}{h\nu}$$

(Hill 1960; Davidson 1962; McQuarrie 1976).

For the complete spectrum of normal modes in the system the total vibrational partition function is given by the product

$$q = \prod_i q(\nu_i)^{g(\nu_i)}$$

where  $g(\nu_i)$  is the spectral density of normal modes and represents the degeneracy (multiplicity) at each frequency.

Thus, in our simple case of sequential binding of two ligands, the vibrational contribution to any differences in site-binding affinity is

$$\Delta\Delta G_{\text{Vib}} = -kT \sum_{\nu} [g_0(\nu) + g_2(\nu) - 2g_1(\nu)] \ln q(\nu),$$

where, as before, the subscripts refer to the different states of ligation of the enzyme and the term  $[g_0(\nu) + g_2(\nu) - 2g_1(\nu)]$  represents any ligand-induced changes in the normal mode spectrum.

In the simplest case where binding of ligands has no effect on normal mode spectra,  $g_0 = g_1 = g_2$  at all frequencies, and there is no difference in binding free energies at each site. Similarly, if only high frequency modes are affected ( $h\nu \gg kT$ ) the (quantum) partition function is essentially unity (i.e., high frequency modes are not thermally excited) and again  $\Delta\Delta G_{\text{Vib}} = 0$ .

More interesting, however, is the case of low-frequency modes. Imagine the situation in which a single thermally excited mode of the free enzyme,  $\nu_0$ , undergoes frequency shifts  $\nu_0 \rightarrow \nu_1 \rightarrow \nu_2$  during the sequential binding process  $E \rightarrow EL_1 \rightarrow EL_2$ . In this case

$$\Delta\Delta G_{\text{Vib}} = -kT \{ \ln q(\nu_0) + \ln q(\nu_2) - 2 \ln q(\nu_1) \}.$$

If the frequency shifts are small, such that they may all be treated classically, then substitution of the appropriate partition functions give

$$\Delta\Delta G_{\text{Vib}} \approx -kT \cdot \ln \left( \frac{\nu_1^2}{\nu_0 \nu_2} \right)$$

so that if, as we anticipate, ligand binding induces a "stiffening" in the protein to give higher normal mode frequencies, then  $\Delta\Delta G$  will indeed be finite and negative - indicating positive cooperativity in ligand binding. (Strictly speaking, the condition for negative  $\Delta\Delta G$  in this classical limit is  $\nu_1^2 > \nu_0 \nu_2$ . It is also feasible that the reverse is true and that  $\Delta\Delta G$  is positive, i.e., negative cooperativity.) The magnitude of the effect can only be guessed at in the absence of detailed normal mode analysis of an appropriate system, but even a modest 10% increase in frequency at each binding step would give  $\Delta\Delta G$  of order  $-0.01$  kT per mode. Bearing in mind that there are several hundred low-frequency modes in any protein of

reasonable size (Sturtevant 1977; Gō et al. 1983; Brooks and Karplus 1983), which might all be affected, it is not difficult to arrive at cooperative free energies of the order of a few  $\text{kJ} \cdot \text{mol}^{-1}$  in this classical limit. ( $kT \approx 2.5 \text{ kJ} \cdot \text{mol}^{-1}$  at room temperature.)

But, in addition to small frequency shifts resulting from an overall stiffening of the protein structure, there are likely to be much larger ligand-induced effects on specific modes of vibration. For example, a soft "hinge-bending" mode involving collective motions of lobes or domains of polypeptide about an active site, such as has been described for lysozyme (McCammon et al. 1976), might well become "frozen" or converted to higher frequency modes by ligand binding at the hinge region. This intuitive picture is supported by the inelastic neutron scattering analysis of lysozyme (Middendorf 1984) and hexokinase (Jacrot et al. 1982) – both of which show an apparent loss of low-frequency modes on ligand binding (though details of the hexokinase experiment are proving difficult to reproduce: S. Cusack, personal communication).

Analysis of simple molecular models (unpublished work) also indicates that thermally excited collective modes strongly coupled to ligand binding sites can be effectively suppressed and converted to non-excited high frequency vibrations by the attachment of small ligands to the equilibrium conformation.

Thermodynamic analysis of this case requires the use of the fully quantized partition function, and gives

$$\Delta\Delta G_{\text{vib}} = -kT \cdot \ln \left( \frac{U_1^2}{U_0 U_2} \right)$$

where

$$U_i = 1 - e^{-h\nu_i/kT}$$

A typical low-frequency global mode, with  $\nu_0 \approx 50 \text{ cm}^{-1}$ , converted to higher frequencies ( $\nu_1, \nu_2 > 500 \text{ cm}^{-1}$ ) on ligation, would provide  $\Delta\Delta G_{\text{vib}} \leq -1.4 \text{ kT}$ , for each such mode affected. This corresponds to cooperative interactions of about  $2.1 \text{ kJ} \cdot \text{mol}^{-1}$  at room temperature. One or two such modes would amply describe the magnitudes of typical cooperative interactions.

Separating the interaction free energy into its enthalpy and entropy components

$$\Delta\Delta G = \Delta\Delta H - T \cdot \Delta\Delta S$$

we obtain:

$$\Delta\Delta H = \frac{h\nu_0}{U_0} \cdot e^{-h\nu_0/kT} + \frac{h\nu_2}{U_2} \cdot e^{-h\nu_2/kT} - \frac{2h\nu_1}{U_1} \cdot e^{-h\nu_1/kT}$$

$$\Delta\Delta S = k \cdot \ln \left( \frac{U_1^2}{U_0 U_2} \right) + \frac{\Delta\Delta H}{T}$$

showing that the cooperative interaction is primarily an entropy effect.  $\Delta\Delta H$  is normally positive ( $\sim 0.6 \text{ kT}$  with the parameters used above), but is offset by the larger, positive entropy contribution. This implies, interestingly, that binding of the first ligand is more exothermic, despite the stronger binding of the second ligand. (Note that in the classical limit  $\Delta\Delta H = 0$ , and the cooperative effect is entirely entropic. This is a consequence of the equipartition theorem in which, without quantization, all oscillators have the same mean internal energy,  $kT$ , regardless of frequency.) The origin of this vibrational contribution to cooperative ligand binding can thus be seen as follows: the free enzyme has a multiplicity of thermally excited, low-frequency vibrational modes, many of which involve motions spanning the entire macromolecule and coupling distant ligand binding sites. On introduction of the first ligand to one of the sites, enzyme-ligand contacts are formed which stabilize the complex and may, or may not, induce a change in conformation of the polypeptide. Concomitantly, the protein structure is stiffened so that some vibrational modes are shifted to higher frequencies where they are less thermally excited. The consequent release of thermal energy is, however, more than cancelled by the loss of vibrational entropy in these modes, and the net effect is to reduce the overall ligand binding free energy. Because of the non-linear nature of the thermodynamics (i.e., the exponential Boltzmann factor) these effects are significantly less for the binding of the second ligand which, therefore, has a higher thermodynamic affinity for its site.

In concluding this section, we should make some mention of the effect of damping since, it might be argued, in the presence of solvent and internal viscosity a protein does not vibrate perpetually like a tuning fork. This is true. But the solvent, as well as acting as a damper on motion, also acts as a source of fluctuations which excite motion by molecular collisions, Brownian motion, and the like. Thus, viewed classically, although harmonic oscillations may be rapidly damped out, they are equally rapidly being excited by solvent collisions, and the actual motion consists of perpetual random excitation and decay of different levels of the different vibrational modes (McCammon et al. 1976). It is precisely the average of this motion which is calculated by statistical thermodynamics. The quantum mechanical treatment of damped harmonic oscillators (Greenberger 1979a, b) leads to essentially the same picture.

## The dynamic conformational contribution

Harmonic oscillations are not, of course, the only form that fluctuations in protein structure might take. The more general view, supported by molecular dynamics simulations (Levitt 1983a, b) is of the protein wandering in a haphazard and non-periodic fashion amongst a multitude of possible conformational states, with any harmonic motions superimposed. The width of the probability distribution of these conformational substates, and the associated partition function, can be viewed as a measure of the "flexibility" of the protein and will determine its average observed properties. The response to ligand binding might be two-fold: firstly, the presence of a ligand may stabilise certain of the conformational substates over others and result in a shift in the mean of the probability distribution, i.e., a conformational change in the conventional sense. Secondly, the *shape* of the distribution might be affected – a narrower distribution representing a "stiffening" of the protein structure due to ligand binding. Both of these effects would be reflected in the thermodynamics of ligand attachment, and the second, due to the change in conformational dynamics, could occur even in the absence of a gross conformational change.

To estimate the magnitude of such effects and to relate them to observable properties of the protein structure, we need to consider the contribution

$$\Delta\Delta G_{\text{Conf}} = -kT \cdot \ln \left\{ \frac{q_1^2}{q_0 q_2} \right\}_{\text{Conf}}$$

where each partition function is of the form of a summation

$$q = \sum_{\text{all } R} e^{-E(R)/kT}$$

and  $E(R)$  represents the generalized potential energy of the protein ( $n$  atoms) as a function of the  $3n$ -dimensional conformation  $R \equiv x_1, y_1, z_1; x_2, y_2, z_2; \dots; x_n, y_n, z_n$ . (We shall assume classical dynamics so that the kinetic energy contributions are identical for each state of ligation and cancel in the expression for  $\Delta\Delta G$ ). An exact calculation would require evaluation of the partition function  $q_0, q_1, q_2, \dots$  for each liganded state, which is beyond our present capabilities. However, we may proceed with the aid of two simplifying assumptions.

Firstly, we will assume that each  $q$  may be written as a product of the  $3n$  individual atomic coordinate partition functions.

$$q \equiv \prod_{i=1}^{3n} q_i.$$

This is equivalent to assuming that the motion of individual atoms, or groups, is uncorrelated, with each moving in a mean field generated by all the others. Although this is unrealistic, it has the virtue of being at the opposite extreme to the highly correlated motions assumed in the analysis of the normal mode vibrational contributions, and allows us to write

$$\Delta\Delta G_{\text{Conf}} = -kT \sum_i \ln \left( \frac{q_i^2}{q_0 q_2} \right)_i,$$

where the summation is over all coordinates and the term in brackets now represents the contribution from each atomic coordinate.

Many of these terms in the summation might cancel because of molecular symmetry. For example, in the case of a system with two identical ligand binding sites (i.e., usually a dimer of symmetry-related monomers), for each atom  $i$  there will be an equivalent atom  $i'$  in an identical molecular environment. (e.g., on the opposite subunit). We must consider the combined effect of symmetry-related pairs of coordinates

$$\Delta\Delta G_i = -kT \ln \left\{ \left( \frac{q_i^2}{q_0 q_2} \right)_i \left( \frac{q_{i'}^2}{q_0 q_2} \right)_{i'} \right\}.$$

From symmetry:

$$q_0(i) = q_0(i')$$

and

$$q_2(i) = q_2(i').$$

If the conformational effects of ligand binding are only short range, then no cooperativity occurs, i.e., binding of the first ligand might affect atom  $i$  [ $q_0(i) \rightarrow q_1(i)$ ], but not  $i'$  [ $q_0(i') = q_1(i')$ ]. Similarly, binding of the second ligand would affect  $i'$  [ $q_1(i') \rightarrow q_2(i')$ ] but not  $i$  [ $q_2(i) = q_1(i)$ ]; all the terms cancel and  $\Delta\Delta G_i = 0$ . This is merely a mathematical statement of what is intuitively expected: that in order to mediate communication between distant ligand sites, any atom must in some way "feel" the presence of ligand at each of the sites. But this effect depends on the thermodynamic partition functions and may result not only from a conformational change in the position of the atom but also from a change in the dynamic fluctuations about its mean position.

To see this, we make our second simplifying assumption: that the fluctuations in atomic coordinates are approximately Gaussian, of width  $\sigma$  (which will be different for each atom). For a Gaussian probability distribution about a fixed mean position (i.e., without conformational change) the atomic

partition function is proportional to the width,  $\sigma$  (see Hill 1960, for example). Thus, using the symmetry arguments for two identical sites:

$$\Delta\Delta G_i = -2kT \cdot \ln \left[ \frac{\sigma_1(i) \cdot \sigma_1(i')}{\sigma_0 \cdot \sigma_2} \right],$$

where  $\sigma_0, \sigma_2$  are the root-mean-square fluctuations of coordinate  $i$  in the unliganded and fully liganded states, respectively;  $\sigma_1(i)$  and  $\sigma_1(i')$  represent the rms fluctuations at  $i$  and  $i'$  when only one ligand site is occupied. This gives the purely dynamic contribution to the interaction between the ligand sites in terms of quantities that may be visualized and, in principle, measured experimentally.

In practice, ligand-induced changes in conformational fluctuations may be small, e.g.,

$$\sigma_1(i) \approx \sigma_0(1 - \delta_i)$$

$$\sigma_1(i') \approx \sigma_0(1 - \delta'_i)$$

$$\sigma_2 \approx \sigma_0(1 - \delta_i - \delta'_i)$$

so that, to approximate first order in the fractional shifts,  $\delta$ ,

$$\Delta\Delta G \approx -2kT \delta_i \delta'_i$$

for each atomic coordinate affected.

Even rms shifts of the order of 1% per atom, scarcely observable with current techniques, if summed over much of the molecule would give cooperative free energies of the order of  $kT$ . Again, in this classical treatment, the effect is entirely entropic.

## Discussion

We have shown how long-range interactions between ligand binding sites on a macromolecule might be produced by purely dynamic processes, over and above any additional effects due to conformational change. With plausible and experimentally verifiable assumptions about the magnitudes of ligand-induced changes in vibrational frequencies or thermal fluctuation amplitudes, allosteric interaction free energies amounting to several  $\text{kJ} \cdot \text{mol}^{-1}$  can be estimated. Moreover, the effect can arise both from highly correlated global oscillations in the protein and from uncorrelated random motion of individual atoms or groups. Although we have concentrated on the simplest case of cooperative interactions between two identical sites in order to simplify the algebra, it is clear that similar arguments apply in the more general cases of allosteric communication and, by appropriate adjustment of dynamic amplitudes and fre-

quencies, all the familiar phenomena of activation, inhibition, positive and negative cooperativity might be reproduced.

Furthermore, the effects might not be limited solely to equilibrium binding parameters. Rate processes such as enzymic catalysis or ligand attachment and dissociation rates, which depend on relatively rare thermal fluctuations ("activation steps"), might also be subject to control via the dynamic processes we have been describing. Such rare fluctuations would not contribute significantly to the thermodynamic ligand-binding affinities, but could give rise to the sort of kinetic allosteric effects seen in some systems (Dixon and Webb, 1979). For example, the rates of attachment or release of a ligand requiring the transient opening of the jaws of the active site (or a "gate" or "channel") might well be increased, or suppressed, if that particular mode of motion were coupled to similarly transient events at other ligand sites. The ramifications in such areas as transmembrane communication and translocation remain to be explored.

Although the concept of dynamically mediated allosteric interaction might appear unfamiliar and hard to visualize, at first, the molecular mechanism is fundamentally the same as in the more familiar process of conformational change. The basic requirement for long-range inter-site communication is the existence of atoms or structural groups dispersed throughout the protein molecule which, directly or indirectly, experience the presence of ligands at each of the sites concerned, and these effects could be either static or dynamic.

In practice ligand-induced changes in *both* the mean conformation and dynamics are to be expected, and even in cases where a gross conformational change can be demonstrated the associated dynamic changes may in fact be the real source of allosteric effects. Experimentally, the situation will be difficult to resolve especially as, given the finite resolution of structural methods, it will always be difficult to rule out "small" (i.e., not observed) conformational changes. But, one advantage of our dynamic formalism is that the interactive free energies are, within the approximations, expressed in terms of quantities which are, in principle, measurable — i.e., changes in normal mode frequencies and/or mean square amplitudes of coordinate fluctuations. Thus quantitative estimates might be made independent of any model of the molecular potential energy surface and the attendant problems of solvation, etc., which would be required to analyse the conformational contribution.

We have shown that dynamically mediated cooperativity should be entropy driven: that is, binding of a second ligand is made thermodynamically more

favourable because of a less negative  $\Delta S^\circ$ . Similarly, with the failure of equipartition due to quantum effects, the enthalpy changes are in the opposite direction, i.e., more exothermic for binding the first ligand. It is also straightforward to show that heat capacity changes ( $\Delta c_p$ ) on ligand binding are expected to be negative (Sturtevant 1977), and more so in this case for the first ligand. Reliable experimental data on relevant systems are, unfortunately, scarce and we are aware of only one detailed study, involving calorimetric measurements of cooperative binding of NAD to glyceraldehyde phosphate dehydrogenase (Niekamp et al. 1977). It is gratifying that the results are in accord with our expectations. But, even with such painstaking experiments, estimation of individual site binding parameters is not trivial and can be influenced by the choice of binding model (Niekamp et al. 1977), and data on other systems are sorely needed.

In conclusion, it is worth drawing attention to recent experiments on the appearance of allosteric effects in non-biological systems, for which dynamic conformational interpretations similar to those presented here are now receiving some consideration (Onan et al. 1983).

*Acknowledgement.* David Dryden is supported by a S.E.R.C. research studentship.

## References

- Brooks B, Karplus M (1983) Harmonic dynamics of proteins: Normal modes and fluctuations in bovine pancreatic trypsin inhibitor. *Proc Natl Acad Sci USA* 80: 6571–6575
- Careri G, Fasella P, Gratton E (1979) Enzyme dynamics: The Statistical physics approach. *Annu Rev Biophys Bioeng* 8: 69–97
- Cooper A (1976) Thermodynamic fluctuations in protein molecules. *Proc Natl Acad Sci USA* 73: 2740–2741
- Cooper A (1980) Conformational fluctuation and change in biological macromolecules. *Sci Prog (Oxford)* 66: 473–497
- Davidson N (1962) *Statistical mechanics*. McGraw-Hill, New York
- Dixon M, Webb EC (1979) *Enzymes*, 3rd edn. Longman, London
- Gō N (1980) Thermodynamics of small-amplitude conformational fluctuations in native globular proteins. *Proc Jpn Acad Ser B* 56: 414–419
- Gō N, Noguti T, Nishikawa T (1983) Dynamics of a small globular protein in terms of low-frequency vibrational modes. *Proc Natl Acad Sci USA* 80: 3696–3700
- Greenberger DM (1979a) A critique of the major approaches to damping in quantum theory. *J Math Phys* 20: 762–770
- Greenberger DM (1979b) A new approach to the problem of dissipation in quantum mechanics. *J Math Phys* 20: 771–780
- Gurd FRN, Rothgeb TM (1979) Motions in proteins. *Adv Protein Chem* 33: 73–165
- Hill TL (1960) *An introduction to statistical thermodynamics*. Addison-Wesley, Reading, Mass
- Jacrot B, Cusack S, Dianoux AJ, Engelman DM (1982) Inelastic neutron scattering analysis of hexokinase dynamics and its modification on binding of glucose. *Nature* 300: 84–86
- Levitt M (1983a) Molecular dynamics of native protein. I. Computer simulation of trajectories. *J Mol Biol* 168: 595–620
- Levitt M (1983b) Molecular dynamics of native protein. II. Analysis and nature of motion. *J Mol Biol* 168: 621–657
- McCammon JA, Gelin BR, Karplus M, Wolynes PG (1976) The hinge-bending mode in lysozyme. *Nature* 262: 325–326
- McCammon JA, Karplus M (1983) The dynamic picture of protein structure. *Acc Chem Res* 16: 187–193
- McQuarrie DA (1976) *Statistical mechanics*. Harper & Row, New York
- Middendorf HD (1984) Biophysical aspects of quasi-elastic and inelastic neutron scattering. *Annu Rev Biophys Bioeng* 13: 425–451
- Monod J, Wyman J, Changeux J-P (1965) On the nature of allosteric transitions: A plausible model. *J Mol Biol* 12: 88–118
- Niekamp CW, Sturtevant JM, Velick SF (1977) Energetics of the cooperative and noncooperative binding of nicotinamide adenine dinucleotide to yeast glyceraldehyde-3-phosphate dehydrogenase at pH 6.5 and pH 8.5. Equilibrium and calorimetric analysis over a range of temperature. *Biochemistry* 16: 436–444
- Onan K, Rebek J, Costello T, Marshall L (1983) Allosteric effects: structural and thermodynamic origins of binding cooperativity in a subunit model. *J Am Chem Soc* 105: 6759–6760
- Peticolas WL (1979) Low frequency vibrations and the dynamics of proteins and polypeptides. *Methods Enzymol* 61: 425–458
- Salemme FR (1978) Protein dynamics, potential regulation and redox coupled conformational changes in cytochromes C. In: Dutton PL, Leigh JS, Scarpa A (eds) *Frontiers of biological energetics*, vol 1. Academic Press, New York, pp 83–90
- Sturtevant JM (1977) Heat capacity and entropy changes in processes involving proteins. *Proc Natl Acad Sci USA* 74: 2236–2240

- Ackers, G.K., Smith, F.R. (1985) *Ann. Rev. Biochem.* 54, 597-629.
- Alben, J.O., Beece, D., Bowne, S.F., Eisenstein, L., Frauenfelder, H., Good, D., Marden, M.C., Moh, P.P., Reinisch, L. (1980) *Phys. Rev. Lett.* 44, 1157-1159.
- Alberding, N., Chan, S.S., Eisenstein, L., Frauenfelder, H., Good, D., Gunsalus, I.C., Nordlund, T.M., Perutz, M.F., Reynolds, A.H., Sorensen, L.B. (1978) *Biochemistry* 17, 43-51.
- Amit, A.G., Mariuzza, R.A., Phillips, S.E.V., Poljak, R.J. (1986) *Science* 233, 747-753.
- Ansari, A., Berendzen, J., Bowne, S.F., Frauenfelder, H., Iben, I.E.T., Sauke, T.B., Shyamsunder, E., Young, R.D. (1985) *Proc. Natl. Acad. Sci. USA* 82, 5000-5004.
- Ansari, A., Berendsen, J., Braunstein, D., Cowen, B.R., Frauenfelder, H., Hong, M.K., Iben, I.E.T., Johnson, J.B., Ormos, P., Sauke, T.B., Scholl, R., Schulte, A., Steinbach, P.J., Vittitow, J., Young, R.D. (1987) *Biophys. Chem.* 26, 337-355.
- Ansari, A., DiIorio, E.E., Dlott, D.D., Frauenfelder, H., Iben, I.E.T., Langer, P., Roder, H., Sauke, T.B., Shyamsunder, E. (1986) *Biochemistry* 25, 3139-3146.
- Antonini, E., Ascenzi, P., Bolognesi, M., Gatti, G., Guarneri, M., Menegatti, E. (1983) *J. Mol. Biol.* 165, 543-558.
- Ataka, M., Tanaka, S. (1979) *Biopoly.* 18, 507-516.
- Austin, R.H., Beeson, K.W., Eisenstein, L., Frauenfelder, H., Gunsalus, I.C., (1975) *Biochemistry* 14, 5355-5373.
- Avarmaa, R.A., Rebane, K.K. (1985) *Spectrochim. Acta* A41, 1365-1380.
- Banerjee, S.K., Rupley, J.A. (1973) *J. Biol. Chem.* 248, 2117-2124.
- Banerjee, S.K., Holler, E., Hess, G.P., Rupley, J.A. (1975) *J. Biol. Chem.* 250, 4355-4367.
- Barron, L.D. (1982) *Molecular Light Scattering and Optical Activity*, Cambridge.
- Bartunik, H.D., Jolles, P., Berthou, J., Dianoux, A.J. (1982) *Biopoly.* 21, 43-50.
- Beece, D., Eisenstein, L., Frauenfelder, H., Good, D., Marden, M.C., Reinisch, L., Reynolds, A.H., Sorensen, L.B., Yue, K.T. (1980) *Biochemistry* 19, 5147-5157.

- Berthou, J., Lifchitz, A., Artymiuk, P., Jolles, P. (1983) Proc. Roy. Soc. Lond. B217, 471-489.
- Biesecker, G., Harris, J.I., Thierry, J.C., Walker, J.E., Wonacott, A.J. (1977) Nature 266, 328-333.
- Bialek, W., Goldstein, R.F. (1985) Biophys. J. 48, 1027-1044.
- Bjurulf, C., Wadso, I. (1972) Eur. J. Biochem. 31, 95-102.
- Blake, C.C.F., Koenig, D.F., Mair, G.A., North, A.C.T., Phillips, D.C., Sarma, V.R. (1965) Nature 206, 757-761.
- Blake, C.C.F., Johnson, L.N., Mair, G.A., North, A.C.T., Phillips, D.C., Sarma, V.R. (1967) Proc. Roy. Soc. Ser. B. 167, 378-388.
- Boxer, S.G., Lockhart, D.J., Middendorf, T.R. (1986) Chem. Phys. Lett. 123, 476-482.
- Bree, A., Yang, C.Y., Rabanek, L. (1971) Spectrochim. Acta 27A, 1293-1298.
- Brooker, M.H., Perrot, M. (1981) J. Chem. Phys. 74, 2795-2799.
- Brooks, B., Karplus, M. (1983) Proc. Natl. Acad. Sci. USA 80, 6571-6575.
- Brooks, B., Karplus, M. (1985) Proc. Natl. Acad. Sci. USA 82, 4995-4999.
- Brown, K.G., Erfurth, S.C., Small, E.W., Peticolas, W.L. (1972) Proc. Natl. Acad. Sci. USA 69, 1467.
- Bruccoleri, R.E., Karplus, M., McCammon, J.A. (1986) Biopoly. 25, 1767-1802.
- Bunow, B. (1974) Bull. Math. Biol. 36, 157-169.
- Campbell, I.D., Dobson, C.M., Moore, G.R., Perkins, S.J., Williams, R.J.P. (1976) FEBS Lett. 70, 96-100.
- Careri, G., Fasella, P., Gratton, E. (1975) CRC crit. Rev. Biochem. 3, 141-164.
- Careri, G., Fasella, P., Gratton, E. (1979) Ann. Rev. Biophys. Bioeng. 8, 69-97.
- Carey, P.R. (1982) Biochemical Applications of Raman and Resonance Raman Spectroscopies, Academic Press.
- Carter, T.P., Small, G.J. (1985) Chem. Phys. Lett. 120, 178-182.

- Cassels, -R., Dobson, C.M., Poulsen, F.M., Williams, R.J.P.  
(1978) Eur. J. Biochem. 92, 81-97.
- Chandrasekhar, S. (1943) Rev. Mod. Phys. 15, 1-89.
- Chase, T. Jr., Shaw, E. (1967) Biochem. Biophys. Res. Commun.  
29, 508-514.
- Chen, M.C., Lord, R.C. (1980) J. Raman Spectr. 9, 304-307.
- Chipman, D.M., Grisaro, V., Sharon, N. (1967) J. Biol. Chem.  
242, 4388-4394.
- Chou, K.-C. (1984) Biophys. J. 45, 881-890.
- Chou, K.-C. (1985) Biophys. J. 48, 289-298.
- Cook, R.A., Koshland, D.E. Jr. (1970) Biochemistry 9, 3337-  
3342.
- Cooper, A. (1974) Biochemistry 13, 2853-2856.
- Cooper, A. (1976) Proc. Natl. Acad. Sci. USA 73, 2740-2741.
- Cooper, A. (1980) Sci. Prog. Oxford 66, 473-497.
- Cooper, A. (1983) Chem. Phys. Lett. 99, 305-309.
- Cooper, A. (1984) Prog. Biophys. Mol. Biol. 44, 181-214.
- Cooper, A., Dryden, D.T.F. (1984) Eur. Biophys. J. 11, 103-109.
- Cotton, T.M., Schultz, S.G., von Duyne, R.P. (1980) J. Am.  
Chem. Soc. 102, 7960-7962.
- Cusack, S. (1984) *personal communication*
- Cusack, S., Smith, J., Finney, J., Karplus, M., Trehella, J.  
(1986) Physica 136B, 256-259.
- Dahlquist, F.W., Jao, L., Raftery, M. (1966) Proc. Natl. Acad.  
Sci. USA 56, 26-30.
- Dale, J. (1957) Acta Chem. Scand. 11, 640-649.
- Debrunner, P.G., Frauenfelder, H. (1982) Ann. Rev. Phys. Chem.  
33, 283-299.
- Demchenko, A.P. (1986) Essays in Biochemistry 22, 120-157.
- Dollish, F.R., Fateley, W.G., Bentley, F.F. (1974)  
Characteristic Raman Frequencies of Organic Compounds, Wiley.
- Durchschlag, H., Puchwein, G., Kratky, O., Schuster, I.,  
Kirschner, K. (1971) Eur. J. Biochem. 19, 9-22.

- Eftink, M.R., Ghiron, C.A. (1976) *Biochemistry* 15, 672-680.
- Elber, R., Karplus, M. (1987) *Science* 235, 318-321.
- Eng, J.F., Czernuszewicz, R.S., Spiro, T.G. (1985) *J. Raman Spectrosc.* 16, 432-437.
- Englander, S.W., Englander, J.J. (1978) *Meth. Enzymol.* XLIX, 24-39.
- Englander, S.W., Kallenbach, N.R. (1984) *Quart. Rev. Biophys.* 16, 521-655.
- Fersht, A. (1977) *Enzyme Structure and Mechanism*, W.H. Freeman & Co.
- Fouassier, M., Lassegues, J.C. (1978) *J. Chim. Phys.* 75, 865-874.
- Fox, R.O., Evans, P.A., Dobson, C.M. (1986) *Nature* 320, 192-194.
- Frauenfelder, H., Petsko, G.A., Tsernoglou, D. (1979) *Nature* 280, 558-563.
- Frauenfelder, H. (1984) *Structure and Dynamics of Nucleic Acids, Proteins and Membranes* (Eds. E. Clementi, R.H. Sarma) Adenine Press.
- Friedman, J.M., Rousseau, D.L., Ondrias, M.R. (1982) *Ann. Rev. Phys. Chem.* 33, 471-491.
- Friedrich, J., Scheer, H., Zickendraht-Wendelstadt, B., Haarer, D. (1981) *J. Am. Chem. Soc.* 103, 1030-1035.
- Friedrich, J., Scheer, H., Zickendraht-Wendelstadt, B., Haarer, D. (1981) *J. Chem. Phys.* 74, 2260-2266.
- Friedrich, J., Haarer, D. (1984) *Angew. Chem. Int. Ed. Eng.* 23, 113-140.
- Gavish, B., Werber, M.M. (1979) *Biochemistry* 18, 1269-
- Gavish, B., Gratton, E., Hardy, C.J. (1983) *Proc. Natl. Acad. Sci. USA*, 80, 750-754.
- Gekko, K., Hasegawa, Y. (1986) *Biochemistry* 25, 6563-6571.
- Genzel, L., Keilmann, R., Martin, T.P., Winterling, G., Yacoby, Y., Frohlich, H., Makinen, M. (1975) *Biopoly.* 15, 219-
- Gill, S.J., Richey, B., Bishop, G., Wyman, J. (1985) *Biophys. Chem.* 21, 1-14.
- Go, N., Anan, Y. (1977) *J. Theor. Biol.* 66, 475-483.

- Go, N., Noguti, T., Nishikawa, T. (1983) Proc. Natl. Acad. Sci. USA 80, 3696-3700.
- Golikov, A.G., Kazanskaya, N.F., Larionova, N.I., Vichutinski, A.A. (1975) Conf. Int. Thermodyn. Chim. 4th 5, 76-82. (Ed. J. Rouquerol, R. Sabbah).
- Grau, U.M. (1982) The Pyridine Nucleotide Coenzymes, Academic Press, p135-187.
- Greenberger, D.M. (1979) J. Math. Phys. 20, 762-770.
- Greenberger, D.M. (1979) J. Math. Phys. 20, 771-780.
- Gurd, F.R.N., Rothgeb, T.M. (1979) Adv. Prot. Chem. 33, 74-165.
- Harris, J.I., Water, M. (1976) The Enzymes 3rd Ed. (Ed. P. Boyer) 13, 1-49. Academic Press.
- Harrison, R.W. (1984) Biopolymers 23, 2943-
- Hawkes, R., Grutter, M.G., Schellman, J. (1984) J. Mol. Biol. 175, 195-212.
- Hill, T.L. (1960) An Introduction to Statistical Thermodynamics, publ. Addison-Wesley.
- Hill, T.L., Chen, Y.-D. (1985) Proc. Natl. Acad. Sci. USA 82, 3654-3657.
- Hocking, J.D., Harris, J.I. (1976) Experientia Suppl. 26, 121-133.
- Ikeda, K., Hamaguchi, K. (1976) J. Biochem. (Tokyo) 79, 237-247.
- Ikegami, A. (1981) Adv. Chem. Phys. 46, 363-413.
- Jackson, M.B. (1987) Biophys. J. 51, 313-321.
- Jacrot, B., Cusack, S., Dianoux, A.J., Engelman, D.M. (1982) Nature 300, 84-86.
- Jaenicke, R., Gratzer, W.B. (1969) Eur. J. Biochem. 10, 158-164.
- James, D.W. (1985) Adv. I.R. and Raman Spectroscopy 12, 311-340. (Eds. R.J.H. Clark, R.E. Hester). Wiley, New York.
- Janin, J., Wodak, S.J. (1983) Prog. Biophys. Mol. Biol. 42, 21-78.
- Jones, G.M.T., Harris, J.I. (1972) FEBS Lett. 22, 185-189.
- Jones, L.H. (1957) J. Chem. Phys. 27, 665-668.

- Karplus, - M., McCammon, J.A. (1983) *Ann. Rev. Biochem.* 53, 263-300.
- Keil-Dlouha, V., Imhoff, J.M., Keil, B. (1971) *Proc. Int. Res. Conf. Proteinase Inhibitors*, p95-104. Ed. H. Fritz, publ. W. de Gruyter.
- Klotz, I.M., Hunston, D.L. (1979) *Arch. Biochem. Biophys.* 193, 314-328.
- Koshland, D.E., Nemethy, G., Filmer, D. (1966) *Biochem.* 5, 365-385.
- Koshland, D.E. (1970) *The Enzymes 3rd Ed.* 1, 341-396.
- Kossiakoff, A.A. (1982) *Nature* 296, 713-721.
- Kramers, H.A. (1940) *Physica* 7, 284-304.
- Krupyanskii, Yu.F., Parak, F., Goldanskii, V.I., Mossbauer, R.L., Gaubman, E.E., Engelmann, H., Suzalalev, I.P. (1982) *Z. Naturforsch.* 37C, 57-62.
- Kuhara, S., Ezaki, E., Fukamizo, T., Hayashi, K. (1982) *J. Biochem. (Tokyo)* 92, 121-127.
- Kurachi, K., Sieber, L.C., Jensen, L.H. (1976) *J. Mol. Biol.* 101, 11-24.
- Lakowicz, J.R., Weber, G. (1973) *Biochemistry* 12, 4171-4179.
- Landsberg, G., Mandelstam, L. (1928) *Naturwiss.* 16, 557-558.
- Lauger, P. (1984) *Biochim. Biophys. Acta* 779, 307-341.
- Leatherbarrow, R.J., Fersht, A.R. (1986) *Protein Engineering* 1, 7-16.
- Lee, B. (1983) *Proc. Natl. Acad. Sci. USA* 80, 622-626.
- Leslie, A.G.W., Wonacott, A.J. (1984) *J. Mol. Biol.* 178, 743-772.
- Levitt, M. (1983a) *J. Mol. Biol.* 168, 595-620.
- Levitt, M. (1983b) *J. Mol. Biol.* 168, 621-657.
- Levitt, M., Sander, C., Stern, P.S. (1983) *Int. J. Qu. Chem., Qu. Biol. Symp.* 10, 181-199.
- Levitt, M., Sander, C., Stern, P.S. (1985) *J. Mol. Biol.* 181, 423-447.

- Levy, R.M., Sheridan, R.P., Keepers, J.W., Dubey, G.S., Swaminathan, S., Karplus, M. (1985) *Biophys. J.* 48, 509-518.
- Linderstrom-Lang, K.U., Schellman, J.A. (1959) *The Enzymes* (eds P.O. Boyer, H. Lardy, K. Myrback), 2nd Edn., Vol. 1, Academic Press.
- Lord, R.C., Yu, N.-T. (1970) *J. Mol. Biol.* 50, 509-524.
- Lumry, R., Rosenberg, A. (1975) *Colloques Internationaux du C.N.R.S. No. 246*, 55-63.
- Lund, P.A., Faurskov Nielsen, O., Praestgaard, E. (1978) *Chem. Phys.* 28, 167-173.
- Mao, B., Pear, M.R., McCammon, J.A. (1982) *Biopoly.* 21, 1979-1989.
- Matthew, J.B., Richards, F.M. (1983) *J. Biol. Chem.* 258, 3039-3044.
- McCammon, J.A., Gelin, B.R., Karplus, M., Wolynes, P.G. (1976) *Nature* 262, 325-326.
- McCammon, J.A., Gelin, B.R., Karplus, M. (1977) *Nature* 267, 585-590.
- McCammon, J.A., Lee, C.Y., Northrup, S.H. (1983) *J. Am. Chem. Soc.* 105, 2232-2237.
- McCammon, J.A., Karplus, M. (1983) *Acc. Chem. Res.* 16, 187-193.
- McCammon, J.A. (1984) *Rep. Prog. Phys.* 47, 1-46.
- McLachlan, R.D. (1974) *Spectrochim. Acta* 30A, 2153-2158.
- Meech, S.R., Hoff, A.J., Wierswa, D.A. (1985) *Chem. Phys. Lett.* 121, 287-292.
- Melson, G.A. (Ed.) (1979) *Coordination Chemistry of Macrocyclic Compounds*, pp 591-592, Plenum Press.
- Mezard, M., Parisi, G., Sourlas, N., Toulouse, G., Virasovo, M. (1984) *Phys. Rev. Lett.* 52, 1156-1159.
- Middendorf, H.D. (1984) *Ann. Rev. Biophys. Bioeng.* 13, 425-451.
- Monod, J., Wyman, J., Changeux, J.-P. (1965) *J. Mol. Biol.* 12, 88-118.
- Montroll, E.W., Shuler, K.E. (1957) *J. Chem. Phys.* 26, 454-464.
- Morgan, J.D., McCammon, J.A., Northrup, S.H. (1983) *Biopoly.* 22, 1579-1594.

- Morozova, T.Y., Morozov, V.N. (1982) J. Mol. Biol. 157, 173-179.
- Moskovits, M. (1985) Rev. Mod. Phys. 57, 783-826.
- Moult, J., Yonath, A., Traub, W., Smilansky, A., Podjarny, A., Rabinovich, D., Saya, A. (1976) J. Mol. Biol. 100, 179-195.
- Murthy, M.R.N., Garavito, R.M., Johnson, J.E., Rossman, M.G. (1980) J. Mol. Biol. 138, 859-872.
- Nabiev, I.R., Sarchenko, V.A., Efremov, E.S. (1983) J. Raman Spectr. 14, 375-379.
- Niekamp, C.W., Sturtevant, J.M., Velick, S.F. (1977) Biochem. 16, 436-444.
- Northrup, S.H., Pear, M.R., McCammon, J.A. (1980) Nature 286, 304-305.
- Northrup, S.H., McCammon, J.A. (1984) J. Am. Chem. Soc. 106, 930-934.
- Nyquist, R.A., Kogel, R.O. (1971) I.R. Spectra of Inorganic Compounds, Academic Press.
- Onan, K., Rebek, J. Jr., Costello, T., Marshall, L. (1983) J. Am. Chem. Soc. 105, 6759-6760.
- Pace, C.N., McGrath, T. (1980) J. Biol. Chem. 255, 3862-3865.
- Painter, P.C., Mosher, L.E. (1979) Biopoly. 18, 3121-3123.
- Painter, P.C., Mosher, L.E., Rhoads, C. (1981) Biopoly. 20, 243-247.
- Painter, P.C., Mosher, L.E., Rhoads, C. (1982) Biopoly. 21, 1469-1472.
- Parak, F., Knapp, E.W. (1984) Proc. Natl. Acad. Sci. USA 81, 7088-7092.
- Perlmutter-Hayman, B. (1986) Acc. Chem. Res. 19, 90-96.
- Perrot, M., Brooker, M.H., Lascombe, J. (1981) J. Chem. Phys. 74, 2787-2794.
- Peticolas, W.L. (1979) Meth. Enzymol. 61, 425-458.
- Post, C.B., Brooks, B.R., Karplus, M., Dobson, C.M., Artymiuk, P.J., Cheetham, J.C., Phillips, D.C. (1986) J. Mol. Biol. 190, 455-479.
- Post, C.B., Karplus, M. (1986) J. Am. Chem. Soc. 108, 1317-1319.

- Pouchert, C.J. The Aldrich Library of I.R. Spectra, 3rd Ed.
- Privalov, P.L. (1979) Adv. Prot. Chem. 33, 167-241.
- Privalov, P.L. (1982) Adv. Prot. Chem. 35, 1-104.
- Raman, C.V., Krishnan, K.S. (1928) Nature 121, 501-502.
- Rebek, J. Jr., Wattley, R.V. (1980) J. Heterocyclic Chem. 17; 749-751.
- Rebek, J. Jr., Wattley, R.V., Costello, T., Gadwood, R., Marshall, L. (1980) J. Am. Chem. Soc. 102, 7398-7400.
- Rebek, J. Jr., Wattley, R.V., Costello, T., Gadwood, R., Marshall, L. (1981) Angew. Chem. Int. Ed. Engl. 20, 605-606.
- Rebek, J. Jr. (1984) Acc. Chem. Res. 17, 258-264.
- Rebek, J. Jr., Costello, T., Marshall, L., Wattley, R., Gadwood, R.C., Onan, K. (1985) J. Am. Chem. Soc. 107, 7481-7487.
- Richardson, D. (1969) Applied Optics and Optical Engineering, Ed. R. Kingslake, vol. 5, p17-46.
- Richarz, R., Nagayama, K., Wuthrich, K. (1980) Biochem. 19, 5189-5196.
- Rigbi, M. (1971) Proc. Int. Res. Conf. Proteinase Inhibitors p74-88. Ed. H. Fritz, Wde Gruyter, Berlin.
- Ringe, D., Petsko, G.A. (1985) Prog. Biophys. Mol. Biol. 45, 197-235.
- Roder, H., Wagner, G., Wuthrich, K. (1985) Biochem. 24, 7396-7407.
- Ruhlmann, A., Kukla, D., Schwager, P., Bartels, K., Huber, R. (1973) J. Mol. Biol. 77, 417-436.
- Salemne, F.R. (1982) Nature 299, 754-756.
- Schindler, M., Assaf, Y., Sharon, N., Chipman, D.M. (1977) Biochem. 16, 423-431.
- Silva, J.L., Miles, E.W., Weber, G. (1986) Biochemistry 25, 5780-5786.
- Simon, I. (1971) J. Appl. Cryst. 4, 317-318.
- Simon, I., Tuchsén, E., Woodward, C. (1984) Biochemistry 23, 2064-2068.
- Ricard, J., Cornish-Bowden, A., (1987) Eur. J. Biochem. 166, 255-272

- Singh, G.P., Schink, H.J., Lohneysen, H.v., Parak, F., Hunklinger, S. (1984) Zeit. Fur. Physik B55, 23-26.
- Sloane, D.L., Velick, S.F. (1973) J. Biol. Chem. 248, 5419-5423.
- Smith, J., Cusack, S., Pezzeca, U., Brooks, B., Karplus, M. (1986) J. Chem. Phys. 85, 3636-3654.
- Stasiv, R.O., Zaun, J.W., Patel, A.B., Brown, H.D. (1973) Int. J. Pept. Prot. Res. 5, 11-17.
- Stein, D.L. (1985) Proc. Natl. Acad. Sci. USA 82, 3670-3672.
- Sterin, Kh.E., Aleksanyan, V.T., Zhizkin, G.N. (1980) Raman Spectra of Hydrocarbons: A Data Handbook, Pergamon Press.
- Sternberg, M.J., Grace, D.E., Phillips, D.C. (1979) J. Mol. Biol. 130, 231-
- Sturtevant, J.M. (1977) Proc. Natl. Acad. Sci. USA 74, 2236-2240.
- Swaminathan, S., Ichiye, T., van Gunsteren, W., Karplus, M. (1982) Biochemistry 21, 5230-5241.
- Szabo, A., Shoup, D., Northrup, S.H., McCammon, J.A. (1982) J. Chem. Phys. 77, 4484-4493.
- Takeuchi, N., Suzuki, S., Dianoux, A.J., Allen, G. (1981) Chem. Phys. 55, 153-162.
- Tipping, M., Viras, K., King, T.A. (1984) Biopoly. 23, 2891-2899.
- van Gunsteren, W.F., Berendsen, H.J.C. (1984) J. Mol. Biol. 176, 559-564.
- Velick, S.F., Baggott, J.P., Sturtevant, J.M. (1971) Biochemistry 10, 779-786.
- Vergoten, G., Fleury, G., Moschetto, Y. (1978) Adv. I.R. Raman. Spectr. 4, 195-269.
- Vincent, J.P., Lozdunski, I.M. (1972) Biochemistry 11, 2967-2977.
- Wagner, G., Wuthrich, K. (1979) J. Mol. Biol. 130, 31-37.
- Wagner, G., Wuthrich, K. (1979) J. Mol. Biol. 134, 75-94.
- Wagner, G. (1983) Quart. Rev. Biophys. 16, 1-57.
- Wagner, G.C., Colvin, J.T., Allen, J.P., Stapleton, H.J. (1985) J. Am. Chem. Soc. 107, 5589-5594.

- Weber, G. (1975) Adv. Prot. Chem. 29, 1-83.
- Welch, G.R., Somogyi, B., Damjanovich, S. (1982) Prog. Biophys. Mol. Biol. 39, 109-146.
- Wemmer, D., Shvo, H., Ribeiro, A.A., Bray, R.P., Jardetzky, O. (1981) Biochem. 20, 3351-3354.
- Westerhoff, H.V., Chen, Y.-D. (1985) Proc. Natl. Acad. Sci. USA 82, 3222-3226.
- Wilson, E.B., Decius, J.C., Cross, P.C. (1955) Molecular Vibrations, McGraw-Hill, New York.
- Wilson, K.A., Laskowski, M. Sr. (1971) J. Biol. Chem. 246, 3555-3561.
- Woodward, C.K., Hilton, B.D. (1979) Ann. Rev. Biophys. Bioeng. 8, 99-127.
- Wulfsberg, G., Weiss, A. (1977) J. Chem. Soc. (Dalton), 1640-1649.
- Wyman, J. (1968) Q. Rev. Biophys. 1, 35-80.
- Xu, G.-J., Weber, G. (1982) Proc. Natl. Acad. Sci. USA 79, 5268-5271.